COMPUTATIONAL AND ANALYTICAL PERSPECTIVES ON THE DRIFT PARADOX PROBLEM IN A FRESHWATER EMBAYMENT

A Dissertation

Presented to the Faculty of the Graduate School

of Cornell University

in Partial Fulfillment of the Requirements for the Degree of

Doctor of Philosophy

by

Virginia Barton Pasour

January 2007

COMPUTATIONAL AND ANALYTICAL PERSPECTIVES ON THE DRIFT PARADOX PROBLEM IN A FRESHWATER EMBAYMENT

Virginia Barton Pasour, Ph.D.

Cornell University 2007

Small, planktonic organisms in a variety of fresh and saltwater environments with primarily unidirectional flow often manage to avoid washout into a larger, often inhospitable body of water, a phenomenon commonly termed the 'drift paradox.' We investigate the drift paradox in the case of vertically migrating zooplankton in a long, narrow embayment emptying into a colder lake by means of a three-dimensional hydrodynamic model, SI3D, along with an accompanying (modified) particle tracking module. Chapter 1 describes tests of SI3D designed to insure that the basic advection and scalar (temperature) transport behave as expected in the embayment regime. Chapter 2 describes simulations using different migration types, zooplankton cloud sizes, start times, and background flow speeds. Largely due to its interaction with exchange flow between lake and embayment, background flow speed emerged as the most important factor influencing the residence time of the zooplankton, with smaller flow speeds, normal migration, and larger zooplankton clouds typically leading to higher residence times. Chapter 3 discusses similar smulations, with the addition of rooted macrophytes, which are represented in SI3D by changing the amount and height of drag in the channel. Flow rate was again the single most important variable, with the interaction between flow and zooplankton cloud size also significant. Chapter 4 describes the results of attempts

to represent the advection of zooplankton undergoing vertical migration by a relatively simple partial differential equation, with the goal of approximating the results of Chapters 2 and 3. The equation contains advective and diffusive terms with the velocity term encompassing the water flow as well as zooplankton vertical position in the embayment. Background water flow, assumed homogeneous in time and longitudinally, is obtained by averaging output velocities from SI3D. A simple distance/rate approximation was also investigated. While the analytical models can be useful in situations involving a simple flow field, when more accuracy is needed, or in case of a vegetated channel, using the full computational model is advisable.

BIOGRAPHICAL SKETCH

Virginia Barton Pasour was born in Raleigh, N.C., on April 8, 1969, where she lived until beginning college at Wake Forest University in Winston-Salem, N.C., in 1987. After receiving a B.S. in Mathematics, she worked as a programmer for IBM for a short time before going to New Zealand on a Rotary Scholarship, where she studied mathematics and engineering for a year at the University of Canterbury. Upon returning to the United States, she enrolled in the Biostatistics program at the University of North Carolina at Chapel Hill. After completing her degree in 1995, she worked as a statistician at Research Triangle Institute in RTP, N.C., before enrolling in the Biomathematics program at North Carolina State University. Virginia transferred from that program to the Center for Applied Mathematics at Cornell University in Ithaca, N.Y., in 1999.

ACKNOWLEDGEMENTS

This work was supported by NSF award OCE-0083625 (Mark Bain, PI) and a 2002 IAGLR scholarship. All errors and omissions are my own.

I would like to thank my adviser, Steve Ellner, for his willingness to supervise a very interdisciplinary PhD project and for his commitment to producing independent researchers, and the other members of my committee – Todd Cowen, Cliff Kraft, and Rick Durrett – for willingly sharing their expertise and their critical comments on this dissertation.

This research could not have been completed without the time, efforts, and resources of Bruce J. Carter. I would also like to thank Suzanne Shontz, Mike Singer, Michael Robinson, Carla Martin, and Nancy Sundell, students with me in the Center for Applied Mathematics, for their friendship and support. In addition, Robyn Miller was a neverending source of encouragement, and Donna Dietz was a great friend with a lot of good advice. Last but not least, I thank my parents for always being there.

TABLE OF CONTENTS

LIST OF TABLES

LIST OF FIGURES

Chapter 1

Verification of a Three-Dimensional Semi-Implicit Shallow Water Code for Use in Embayment-Lake Simulations

1.1 Abstract

We tested SI3D [35, 32], a three-dimensional, semi-implicit, finite difference solver originally developed for lake environments, under a variety of scenarios important for later simulations involving an embayment-lake interface. The three test cases involve simple advection in the embayment, a lock-exchange due to temperature differences between lake and embayment, and a lock-exchange combined with advection. Flow boundary conditions, water surface elevation boundary conditions, and a combination of upstream flow and downstream water surface elevation boundary conditions are considered, as are a variety of values for bottom friction. While oscillations corresponding to the first modes of a seiche were witnessed under simple advection, mixed boundary conditions gave to give the most stable and accurate results when advecting temperature and will be used in future simulations utilizing this software.

1.2 Introduction

Three-dimensional fluid flow models usually require overly simplified bathymetry, boundary forcing and lake/stream/river conditions and often pose a limitation on the time simulated. Rueda [32] considered various three-dimensional models that

solve the shallow water equations and extended the most suitable one, called SI3D, to a 3D numerical model for lake environments that contains appropriate physics, requires minimal tuning and is adaptable to various applications, while containing little numerical damping and dispersion and being computationally efficient. SI3D is a 3D semi-implicit [1] leapfrog-trapezoidal [2] finite difference solver that uses an orthogonal structured grid. The extended version of SI3D can use spatially and temporally variable wind fields and calculate mixing coefficients with a high-order turbulence closure model, and also enables the use of temperature as the active scalar responsible for stratification. In addition, a stand-alone Lagrangian particle tracking model (ptrack) was developed to take advantage of SI3D output to simulate transport of particulate matter and help visualize circulation patterns.

We are interested in a shallow-water code like SI3D for simulating the movement of passive particles in a channel emptying into a larger body of water, with exchange flow due to a temperature difference between the two bodies of water, as well as advection due to background flow, both contributing to the movement of the particles. As SI3D is not a commercial code and had undergone extensive testing

[1] In a semi-implicit scheme only some of the terms in the governing equations (gravity wave and vertical diffusion terms) are treated implicitly, while the others (Coriolis, horizontal friction, advection and baroclinic pressure terms) are treated explicitly. Implicit numerical schemes require the simultaneous solution of a system of algebraic equations because the unknown variables at a given spatial point at a given time depend on the unknown variables at neighboring points at the same time. Alternatively, in explicit numerical schemes, the unknown variables at any spatial point at a given time are calculated directly from known variables at neighboring points at one or more previous times.

[2] SI3D [35] uses a three-level leapfrog-trapezoidal scheme to solve the conservative form of the governing equations for shallow water flow, with second order accuracy in time and space. A leapfrog step is used in the first iteration, followed by as many trapezoidal steps as desired to help remove the computational mode associated with leapfrog discretization [10] and increase the stability of the code [35].

solely for a lacustrine environment, we decided to test aspects of the code relevant to our intended test scenarios before utilizing it extensively in applications. To that end, we present a number of test cases that were used to verify the full SI3D code (and can be used in general in verifying 3D hydrodynamic models of free-surface flows). Analytical solutions are presented and used where possible, but the test cases involving scenarios similar to those desired for biological residence time simulations required the complete forms of the PDE's for 3D shallow water flow without simplification.

The advective and viscous terms were two elements of the shallow water equations that could not be neglected in our simulations. As our ultimate questions concern the amount of time that organisms can spend in a habitat before being washed out, advection of water carrying particles (mediated by behavior of the particles, or zooplankton) was of paramount importance and could not be neglected. In addition, a steady flow environment was desired for testing and could most realistically be achieved in the code by using bed friction/viscosity with water surface elevation boundary conditions, so that viscous forces were also important to test. Furthermore, we suspected that exchange flow at the embayment outlet would likely provide a means of increasing biological retention time, so test cases involve solutions to the advection-diffusion (temperature transport) equation as well as to the hydrodynamic equations.

To accomplish these goals, the suite of tests included three scenarios: steady flow under isothermal conditions to test basic advection, lock-exchange with no flow to test basic scalar transport, and lock-exchange with a background steady flow, to test the intersection of advection and temperature transport. Because no analytical solution exists for the full set of equations, any solution in general can

give only an approximation to the code results.

The format of each test case setup follows that of the "Analytical Test Cases" chapter in [36]. For each test case, the partial differential equations along with boundary and initial conditions are presented. The solution, if possible, or as quantitative a criterion as possible for each test case, is given first, along with any assumptions that allow a simplification of the hydrodynamic/transport equations. The actual test case is defined by a set of physical parameters that determine a particular problem geometry, along with a set of boundary/initial values. Each test was run using a rectangular channel, on a suite of up to three different flow rates and with up to three different values of drag. (Different values of drag were used, in some cases to make the results easier to compare with analytical results, in others to create a more realistic scenario, and in yet others to be able to verify that increasing bottom drag yielded the expected consequences.) In general, any method that could confirm the workings of the code was utilized, including qualitative comparisons, as well as comparing numerical results against predicted results where possible.

1.3 Mathematical Problem

1.3.1 Assumptions, Equations and Boundary Conditions

The equations that form the basis for 3-D circulation models are the mass conservation (or continuity) equation for incompressible fluids, the Reynolds-averaged form of the Navier-Stokes equations for momentum, and the transport equation for active scalar fields such as temperature, salinity and sediment concentration. These equations are supplemented with an equation of state that relates active

scalar concentrations to fluid density [32]. We will only be interested in the active transport of temperature, which can be related to density by an equation of state (1.6).

Two approximations that can be applied to geophysical flows [21] allow us to make major simplifications to the governing equations. The hydrostatic approximation, which assumes an exact equilibrium in the vertical between the pressure gradient force and the gravitational force, is reasonable because basin-scale oscillations in our long, narrow channel should have much longer horizontal than vertical wavelengths. The second approximation is the Boussinesq approximation, which assumes that density differences are small enough to be neglected, except where gravity is involved. (The assumption is that the difference in inertia is negligible, but gravity is an unbalanced force, making the specific weight appreciably different between two fluids.) With these two approximations, we have the following set of equations:

Momentum Conservation

$$\frac{\partial u}{\partial t} + u\frac{\partial u}{\partial x} + v\frac{\partial u}{\partial y} + w\frac{\partial u}{\partial z} - fv = -\frac{1}{\rho_0}\frac{\partial p}{\partial x} + \frac{\partial}{\partial x}\left(K_H\frac{\partial u}{\partial x}\right) + \frac{\partial}{\partial y}\left(K_H\frac{\partial u}{\partial y}\right) + \frac{\partial}{\partial z}\left(K_V\frac{\partial u}{\partial z}\right) \tag{1.1}$$

$$\frac{\partial v}{\partial t} + u\frac{\partial v}{\partial x} + v\frac{\partial v}{\partial y} + w\frac{\partial v}{\partial z} + fu = -\frac{1}{\rho_0}\frac{\partial p}{\partial y} + \frac{\partial}{\partial x}\left(K_H\frac{\partial v}{\partial x}\right) + \frac{\partial}{\partial y}\left(K_H\frac{\partial v}{\partial y}\right) + \frac{\partial}{\partial z}\left(K_V\frac{\partial v}{\partial z}\right) \tag{1.2}$$

$$0 = -\frac{\rho}{\rho_0}g - \frac{1}{\rho_0}\frac{\partial p}{\partial z} \tag{1.3}$$

Mass Conservation

$$\frac{\partial u}{\partial x} + \frac{\partial v}{\partial y} + \frac{\partial w}{\partial z} = 0 \tag{1.4}$$

Scalar Transport

$$\frac{\partial s}{\partial t} + u\frac{\partial s}{\partial x} + v\frac{\partial s}{\partial y} + w\frac{\partial s}{\partial z} = \frac{\partial}{\partial x}\left(D_H \frac{\partial s}{\partial x}\right) + \frac{\partial}{\partial y}\left(D_H \frac{\partial s}{\partial y}\right) + \frac{\partial}{\partial z}\left(D_V \frac{\partial s}{\partial z}\right) + \Delta_s \tag{1.5}$$

Equation of State

$$\rho = \rho(s)$$

In the specific case of temperature, the equation of state becomes

$$\rho(T) = 516(1.939933 + T(5.88599 \cdot 10^{-5} - 1.108539 \cdot 10^{-5} \cdot T)) \tag{1.6}$$

In the above equations, we use a right-handed coordinate system fixed on the earth's surface with horizontal coordinates x (east-west) and y (north-south), and vertical coordinate z. Additionally, u, v, and w are the velocities in the x, y, and z directions, respectively, f is the Coriolis parameter, g is the acceleration of gravity, ρ_0 is the mean density and ρ the variation of density with respect to the mean, s represents the active scalar, T denotes temperature, and p stands for pressure. The coefficients K_H and K_V represent the horizontal and vertical turbulent momentum

transfer coefficients, or eddy viscosities, and D_H and D_V represent the coefficients for the horizontal and vertical turbulent transfer of the active scalar (temperature), or eddy diffusivities. The Boussinesq approximation has been implemented by only including density in the buoyancy term. The last term in the equation for scalar transport, equation 1.5, is a source-sink term representing the divergence of the downward solar irradiance I.

The hydrostatic assumption allows us to reformulate expressions involving pressure in terms of the free surface elevation ζ and density. The pressure gradient terms in the horizontal momentum equations can be rewritten using the hydrostatic equation 1.23 as

$$\frac{1}{\rho_0}\frac{\partial p}{\partial x} = \frac{1}{\rho_0}\frac{\partial p_a}{\partial x} + g\frac{\partial \zeta}{\partial x} + g\frac{1}{\rho_0}\int_z^\zeta \frac{\partial \rho}{\partial x}dz'$$
$$\frac{1}{\rho_0}\frac{\partial p}{\partial y} = \frac{1}{\rho_0}\frac{\partial p_a}{\partial y} + g\frac{\partial \zeta}{\partial y} + g\frac{1}{\rho_0}\int_z^\zeta \frac{\partial \rho}{\partial y}dz'$$

where p_a is the atmostpheric pressure and ζ represents the water surface elevation above a reference level $z = 0$. The integral terms above are called baroclinic pressure terms and connect the solution to the hydrodynamic equations to the scalar transport solution. The terms involving ζ are called barotropic pressure terms and are constant with depth.

Both dynamic and kinematic boundary conditions must be satisfied at both the free surface and at the lower boundary. At the free surface, the dynamic conditions specify the wind stresses (τ_{0x}, τ_{0y}):

$$\rho_0 K_V \left(\frac{\partial u}{\partial z}, \frac{\partial v}{\partial z}\right) = (\tau_{0x}, \tau_{0y}) \tag{1.7}$$

as well as the requirement of no advective fluxes of temperature (or other scalar) through the free surface:

$$H_S = \rho_0 D_V \left(\frac{\partial s}{\partial z} \right) = 0, \tag{1.8}$$

where H_S represents the net effect of the non-penetrating components of the heat flux (evaporation, conduction, and long-wave radiation).

The kinematic boundary condition requires that there be no advective flux through the free surface (i.e., a particle that starts on the free surface stays there):

$$w|_{z=\zeta} = \frac{Dh}{Dt} = \frac{\partial h}{\partial t} + u\frac{\partial h}{\partial x} + v\frac{\partial h}{\partial y} = 0, \tag{1.9}$$

Here h represents the depth of the water. Integrating the continuity equation over the water column and combining it with the kinematic boundary condition gives an equation for ζ:

$$\frac{\partial \zeta}{\partial t} + \frac{\partial}{\partial x}\left[\int_{-H}^{\zeta} u dz\right] + \frac{\partial}{\partial y}\left[\int_{-H}^{\zeta} v dz\right] = 0,$$

where $z = H(x, y)$ is the depth of the bottom boundary measured from the undisturbed free surface $z = 0$. (Thus, $h = H + \zeta$.)

At the lower boundary, we would like to implement a no-slip condition, which means that $u, v = 0$, as we would expect. However, vertical resolution would have to be much greater than desired for the rest of the channel to resolve the

resulting strong velocity gradients in the viscous sublayer [2]. Instead, as velocity at the lower boundary is chiefly important in determining the stress exerted on the boundary, we define the bottom boundary condition in terms of the stress:

$$\rho_o K_V \left(\frac{\partial u}{\partial z}, \frac{\partial v}{\partial z} \right) = (\tau_{bx}, \tau_{by}) \tag{1.10}$$

where the bottom friction stresses (τ_{bx}, τ_{by}) typically depend on the bottom velocities (u_b, v_b) and drag coefficient C_d by way of a quadratic law:

$$(\tau_{bx}, \tau_{by}) = C_d \sqrt{u_b^2 + v_b^2} (u_b, v_b) \tag{1.11}$$

The boundary condition at the bottom for the scalar transport equation is no transport normal to the boundary:

$$\left. \frac{\partial s}{\partial n} \right|_{z=-H} = 0 \tag{1.12}$$

where n is the direction normal to the bottom boundary layer. Similarly, the kinematic boundary condition at the bottom requires no flow normal to the boundary and can be described by the equation

$$w|_{z=-H} = -u \frac{\partial H}{\partial x} - v \frac{\partial H}{\partial y} = 0 \tag{1.13}$$

At the lateral boundaries, a "perfect slip" condition is preferred to either a no-slip requirement or a quadratic stress law condition as horizontal grid sizes are typically much larger than vertical grid sizes and therefore can only very crudely resolve velocities at the lateral boundaries [32]. Thus, water can move freely at the lateral boundaries without any resistance. In addition, no flux of any scalar is allowed across lateral boundaries. At open boundaries, either velocity or water surface elevation is defined, with the type of boundary not necessarily constant for any particular test case.

1.4 Test Cases

In this section, features common to all of the test cases are given. These features include physical parameters giving channel bathymetry, as well as numerical parameters giving cell size, simulation length, and time step. While the bathymetry and cell sizes will be modified for future field simulations, the current values were chosen to give a reasonable balance between accuracy and simulation time and represent a two-dimensional channel of similar numerical resolution to the embayment of interest. At times, the ability to observe flow behavior over more than 64 grid cells is desirable, and for these testing situations, the extended version of the channel is used. The simulation length is consistent with the length of the upcoming studies and corresponds to a conservative estimate of the life span of the organisms whose movement we will be modeling. Moreover, the time step is shown to be adequate to provide stability under the flow regimes used in the tests. In addition, a listing of the test cases with features to be verified is given, along with

a description of error measures for later use in describing discrepancies between model results and anticipated behavior.

The slowest flow speed investigated in the present study is 0.0033 cm/s. Assuming a temperature of 20° C, the Reynolds number Re is bounded below by $Re = \frac{UL}{\nu} \leq \frac{(0.0033)(12)}{1.004E-6} \approx 40,000$, if the height of the channel is taken to be the length scale. This value of Re clearly indicates turbulent flow. While an important consideration is accuracy, almost as important, given the number of simulations required to the desired various aspects of SI3D, is computational efficiency, so that a simple model is preferable. Thus, for the simple, isothermal simulations involved in Test 1 we utilized simple constant coefficients computed as $0.15hu^*$ for horizontal eddy coefficients and $0.067hu^*$ for vertical coefficients, where h denotes the height of the water column in meters and u^* is 10% of $\bar{u}$ [11]. For the lock exchange simulations in Tests 2 and 3, we used the Smagorinsky model to determine horizontal eddy coefficients and the Kantha and Clayson formulation of the original Mellor and Yamada 2.5 second moment closure two-equation model to determine vertical eddy viscosities and diffusivities. More detailed discussion of turbulence models is included in the Appendix.

1.4.1 Physical Parameters

Regular Channel

$$\begin{aligned} \text{length} = L &= 16384 \text{ m} \\ \text{width} = B &= 256 \text{ m} \\ \text{height} = H &= 12 \text{ m} \end{aligned}$$

Extended Channel

$$\begin{aligned} \text{length} = L &= 71424 \text{ m} \\ \text{width} = B &= 256 \text{ m} \\ \text{height} = H &= 12 \text{ m} \end{aligned}$$

1.4.2 Numerical Parameters

$$\begin{aligned} \Delta x &= 256 \text{ m} \\ \Delta y &= 256 \text{ m} \\ \Delta z &= 0.5 \text{ m} \\ T_s &= 7 \text{ days} \end{aligned}$$

A time step of 120 seconds was used, which, for the three different flow rates used for testing, gives steady state gravity wave Courant numbers in the neighborhood of

$$\begin{aligned} 10 \text{ m}^3/\text{s} \Rightarrow (Q/A)\Delta t/\Delta x = 0.0015 << 1 \\ 155 \text{ m}^3/\text{s} \Rightarrow (Q/A)\Delta t/\Delta x = 0.0236 << 1 \\ 300 \text{ m}^3/\text{s} \Rightarrow (Q/A)\Delta t/\Delta x = 0.0458 << 1, \end{aligned}$$

guaranteeing a stable solution for explicit methods.

1.4.3 Test Cases for the Verification of Advection and Scalar Transport in the Full SI3D Model

The three tests for verifying the components of the shallow water equations, as implemented in SI3D, that are especially of interest for future simulations are listed in the table below:

Table 1.1: SI3D test cases, along with the feature(s) to be tested with each

Test Case	Feature(s) Verified
1 - Steady flow under isothermal conditions	advection
2 - Lock-exchange problem with no initial flow	scalar transport
3 - Lock-exchange problem with flow	advection and scalar transport

1.4.4 Quantitative Evaluation of Results

For most of the test cases presented, no analytic solution exists due to the complexity of the problem. However, various aspects of the flow can be examined to detect deviations from expected behavior, and in some cases, approximations to the solution can be given. Where the numerical solution can be quantified and compared with some sort of analytical approximation, we have used one or more of the error measures defined in Table 1.2 to describe the disparity between predicted and numerically obtained results.

1.5 Test Case 1: Steady State Flow under Isothermal Conditions

1.5.1 Description and Objectives

The phenomenon of steady state flow under isothermal conditions tests the discretization and implementation of the advection terms in the momentum equation. It also tests the implementation of the continuity equation, both for the solution of the free-surface position and for the calculation of horizontal and vertical velocities throughout the 3D domain.

Simulations are run for three different levels of bed friction, including $C_d = 0$, $C_d = 0.002$, and $C_d = 0.01$. While assuming no bed friction is not physically realistic, it can make some aspects of the flow easier to test and so is included. Friction values of 0, 0.002, and 0.01 can be viewed as corresponding to, respectively, a smooth bottom, a sandy/muddy bottom and a rougher one, perhaps with macrophytes. Water surface elevation boundary conditions cannot be used to achieve a steady state in the case of inviscid flow, as a constant acceleration is achieved, so flow conditions at both boundaries were implemented for this case ($C_d = 0$), as well as for the tests involving non-zero bed frictions, for consistency (although in general flow-flow boundary conditions are undesirable - see Section 1.7).

1.5.2 Assumptions

- Flow speed constant at boundaries
- Constant temperature (no scalar transport)
- Constant ρ

Table 1.2: Definition of error measures used to evaluate the performance of numerical models. A_n denotes an analytical solution, and N_n denotes a numerical solution, while $'$ denotes deviations from the mean analytical solution. N_{max} is the number of data points.

Error Measures	Definition
Index of agreement (d)	$d = 1 - \frac{\sum_{n=1}^{N_{max}} (A_n - N_n)^2}{\sum_{n=1}^{N_{max}} (\lvert A'_n \rvert - \lvert N'_n \rvert)^2}$
l_1 (relative) error norm	$\ell_1 = \frac{\sum_{n=1}^{N_{max}} \lvert N_n - A_n \rvert}{\sum_{n=1}^{N_{max}} \lvert A_n \rvert}$
l_2 (relative) error norm	$\ell_2 = \frac{(\sum_{n=1}^{N_{max}} (A_n - N_n)^2)^{1/2}}{(\sum_{n=1}^{N_{max}} (A_n)^2)^{1/2}}$
l_∞ (relative) error norm	$\ell_\infty = \frac{\max_n \lvert N_n - A_n \rvert}{\max_n \lvert A_n \rvert}$
Root Mean Square Error (RMSE)	$RMSE = \sqrt{\frac{\sum_{n=1}^{N_{max}} (A_n - N_n)^2}{N_{max}}}$
Error (E_n) for a given node	$E_n = \lvert N_n - A_n \rvert$

1.5.3 Governing Equations

Continuity

$$u_x + v_y + w_z = 0$$

$$\zeta_t + u_x H + v_x H = 0$$

Momentum

$$\frac{\partial u}{\partial t} + u\frac{\partial u}{\partial x} + v\frac{\partial u}{\partial y} + w\frac{\partial u}{\partial z} = -\frac{1}{\rho_0}\frac{\partial p}{\partial x} + \frac{\partial}{\partial x}\left(K_H\frac{\partial u}{\partial x}\right) + \frac{\partial}{\partial y}\left(K_H\frac{\partial u}{\partial y}\right) + \frac{\partial}{\partial z}\left(K_V\frac{\partial u}{\partial z}\right) \tag{1.14}$$

$$\frac{\partial v}{\partial t} + u\frac{\partial v}{\partial x} + v\frac{\partial v}{\partial y} + w\frac{\partial v}{\partial z} = -\frac{1}{\rho_0}\frac{\partial p}{\partial y} + \frac{\partial}{\partial x}\left(K_H\frac{\partial v}{\partial x}\right) + \frac{\partial}{\partial y}\left(K_H\frac{\partial v}{\partial y}\right) + \frac{\partial}{\partial z}\left(K_V\frac{\partial v}{\partial z}\right) \tag{1.15}$$

$$0 = -\frac{\rho}{\rho_0}g - \frac{1}{\rho_0}\frac{\partial p}{\partial z} \tag{1.16}$$

1.5.4 Boundary Conditions

$$\left.\frac{\partial u}{\partial y}\right|_{y=0} = \left.\frac{\partial u}{\partial y}\right|_{y=B} = 0$$

$$u|_{x=0} = u|_{x=L} = Q/A$$

$$\left.\frac{\partial v}{\partial x}\right|_{x=0} = \left.\frac{\partial v}{\partial x}\right|_{x=L} = v|_{y=0} = v|_{y=B} = 0$$

$$\left.\frac{\partial u}{\partial z}\right|_{z=-H} = \left.\frac{\partial v}{\partial z}\right|_{z=-H} = \left.\frac{\partial u}{\partial z}\right|_{z=\zeta} = \left.\frac{\partial v}{\partial z}\right|_{z=\zeta} = 0$$

1.5.5 Initial Conditions

Velocities in all coordinate directions are initially 0 (i.e., $u, v, w|_{t=0} = 0$), although a ramping up parameter brings the flow at the boundaries up to the desired flow rate of Q by $t = 1$ hour.

1.5.6 Results

Flow rates of 10 m^3/s, 155 m^3/s, and 300 m^3/s were imposed, in turn, on both boundaries, under conditions of $C_d = 0$ (no drag), $C_d = 0.002$, and $C_d = 0.01$, in turn. Although steady flow was desired, the imposition of a constant flow rate at the boundaries, even with a 'ramp-up' time of one hour (and even in the case of no bed friction), produced oscillations in the velocity field and in the water surface elevation. Figure 1.1 shows velocities (in cm/s) for three time slices that are a third of an hour apart, using a flow rate of 10 m^3/s and no bed friction. Note that the middle 60 cells (out of 64) are shown in all figures.

Figures 1.2 and 1.3 show velocities at the same three time slices for higher flow rates ($Q = 155$ m^3/s and $Q = 300$ m^3/s). Oscillations are again present and in fact appear virtually identical to those found in the low flow case, although the flow is uniformly faster. With an increase in magnitude of the water surface elevation as flow speed increases (see Figures 1.4, 1.9, and 1.14), an offset in velocity is seen at the top of the water column for the last time period, with the faster flow case showing the greatest effect.

Because of the type of boundary conditions used, we might expect to see oscillations due to a seiche. If so, we should be able to detect at least the first mode, which should have a period of $2L/\sqrt{gh}$, where L is the length of the channel, g is gravity, and h is the depth of the channel (neglecting variation in water surface elevation) [9]. In the case of $Q = 10$ m^3/s, we have $2L/\sqrt{gh} \approx 3022s$. Figures 1.4 and 1.5 show, respectively, time series of the water surface elevation at the 20th horizontal node for $Q = 10m^3/s$ for all three bed friction types and graphs of superimposed power spectra of the horizontal velocities at a number of randomly selected points. Note the increasing range for water surface elevation as flow speed

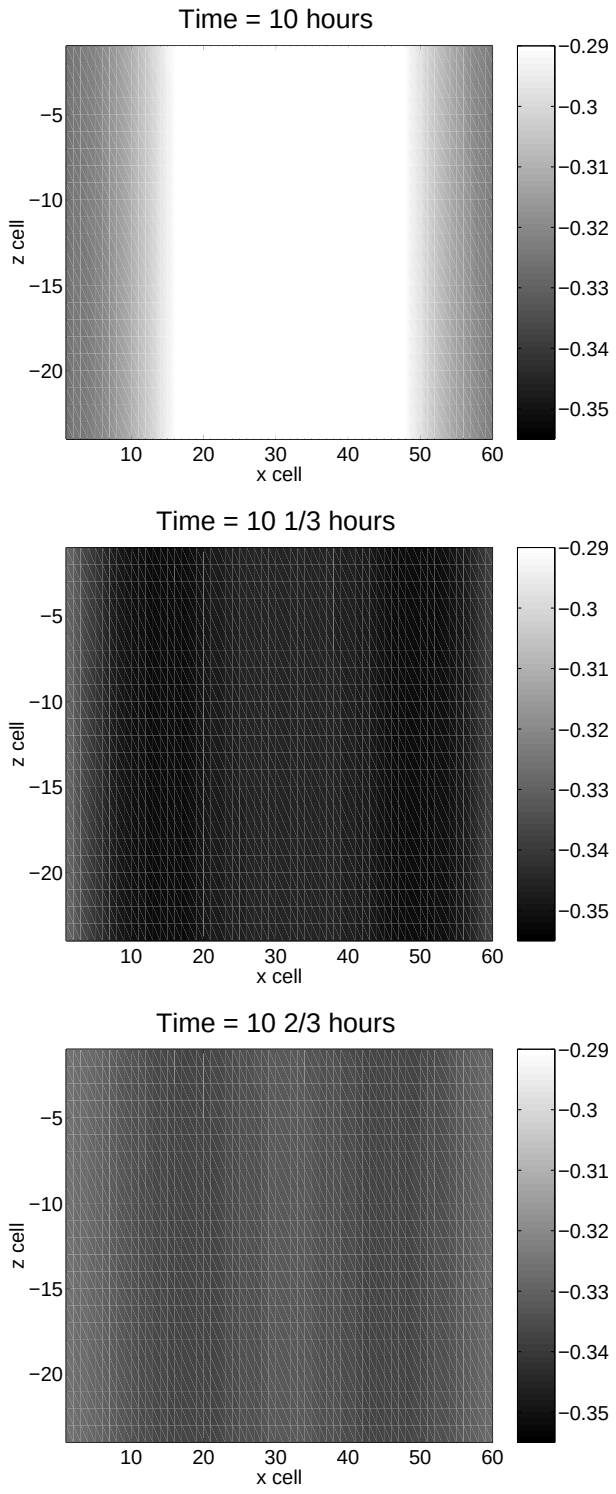

Figure 1.1: Velocity in the x-z plane for $Q = 10$ m^3/s and $C_d = 0$, shown at 20 minute intervals. Oscillations are clearly visible.

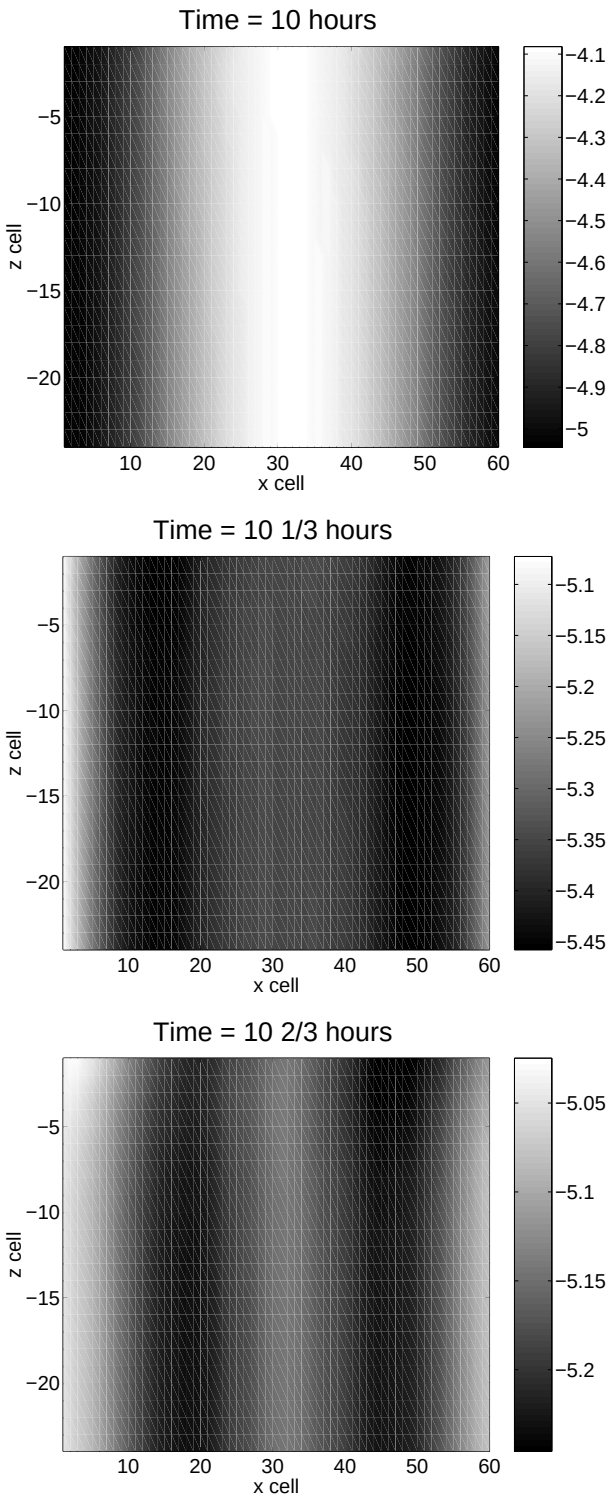

Figure 1.2: Velocity in the x-z plane for $Q = 155$ m^3/s and $C_d = 0$, shown at 20 minute intervals. Oscillations are clearly visible.

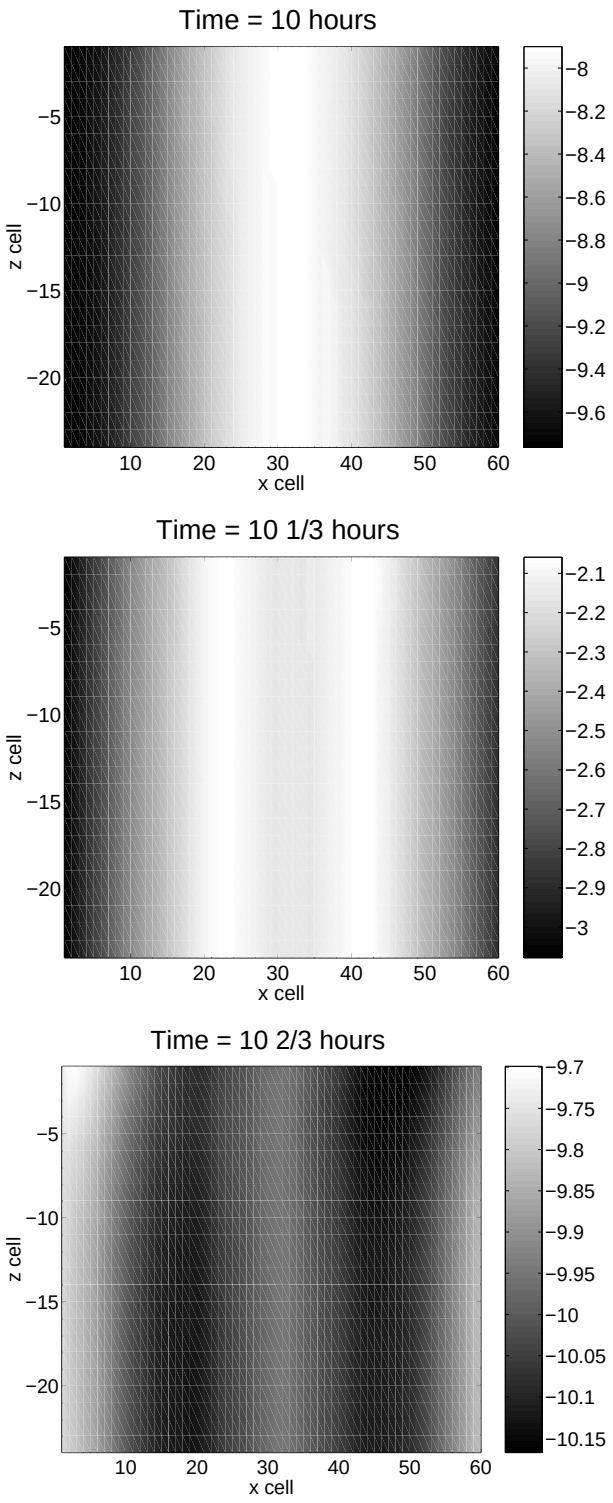

Figure 1.3: Velocity in the x-z plane for $Q = 300$ m^3/s and $C_d = 0$, shown at 20 minute intervals. Oscillations are clearly visible.

increases. As period and frequency are inverse relations, we expect the first mode of the seiche to have frequency $1/3022 \approx 0.00033$, and we see from the power spectral density (PSD) graphs that a large spike appears at approximately that position. (The PSD describes how the power, or variance, of a time series is distributed with frequency and is defined as the Fourier Transform of the autocorrelation sequence of the time series.) Further evidence of the first mode may be seen by looking at the water surface elevation wave, which appears to have a period of approximately $0.85 * 3600 = 3060$. Taking aliasing into account, we can identify the other peaks in energy as 2nd, 3rd, and 4th modes of the seiche.

Figures 1.6, 1.7, and 1.8 show plots of velocity for the case of a moderate bottom drag ($C_d = 0.002$). Clearly, the drag affects velocity in the entire water column and has its greatest effect away from the open boundaries and as flow becomes stronger. Irregularities are apparent at the boundaries, which is to be expected, as the velocities are being held constant there. Oscillations, especially in the upper half of the water column, are still apparent and again, as can be seen in Figures 1.9 and 1.10, are consistent with the first mode, and to a certain extent, higher order modes, of a seiche.

Figures 1.11, 1.12, and 1.13 show plots of velocity for the case of a larger bottom drag ($C_d = 0.01$). Here the large drag again has its greatest effect away from the boundaries and as flow becomes stronger. By the time 10 hours have elapsed, the drag has largely damped out the oscillations seen before, although Figure 1.15 shows power spectra that look very similar to those in the lower drag cases, and Figure 1.14 shows water surface elevations that at least initially show clear oscillations. As the flow rate increases, the oscillations are more rapidly damped out and we see thicker horizontal bands of slower water close to the channel bottom.

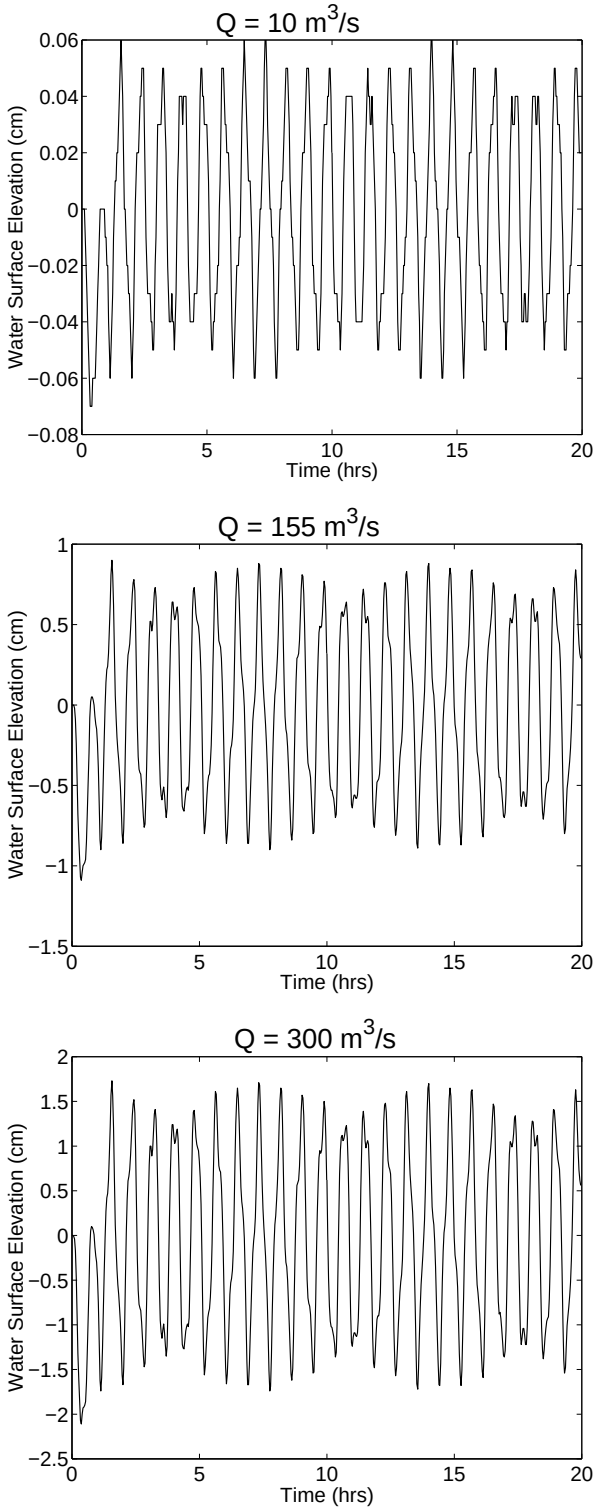

Figure 1.4: Water surface elevations over time (hrs) for increasing flow rates for the case of no bottom drag ($C_d = 0$)

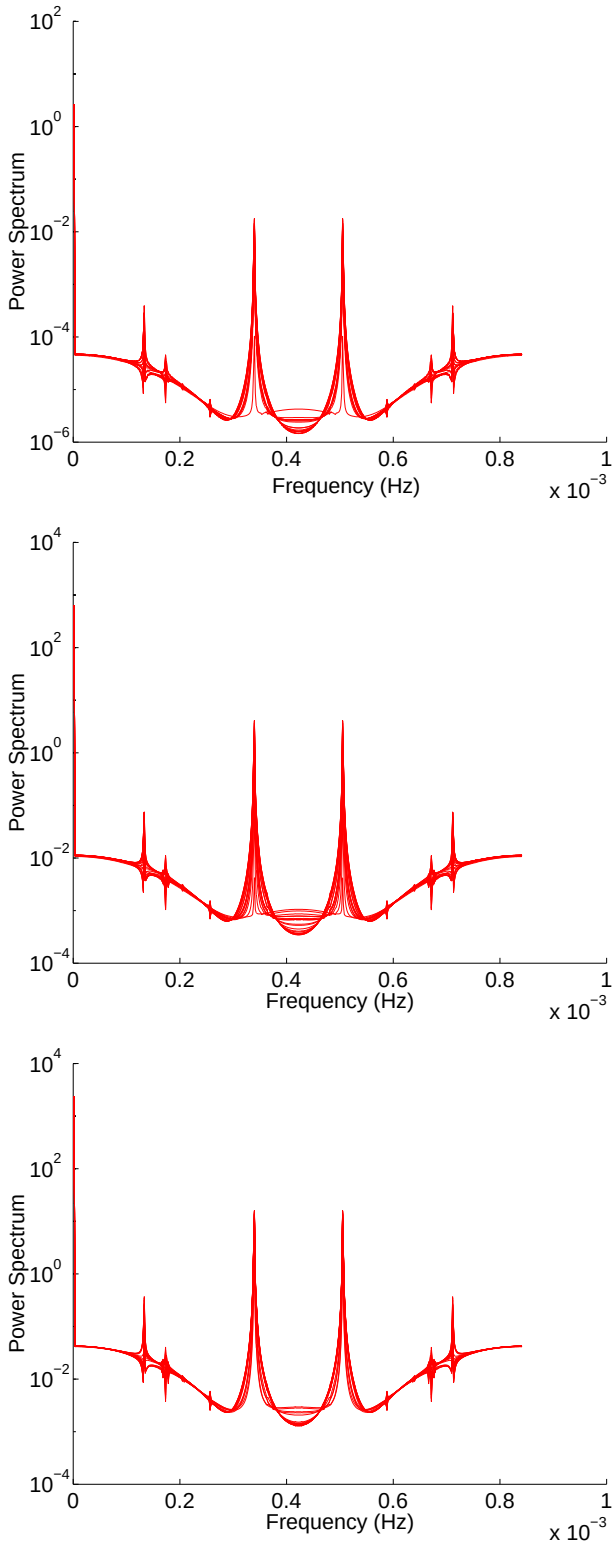

Figure 1.5: Spectra for increasing flow rates for the case of no bottom drag ($C_d = 0$)

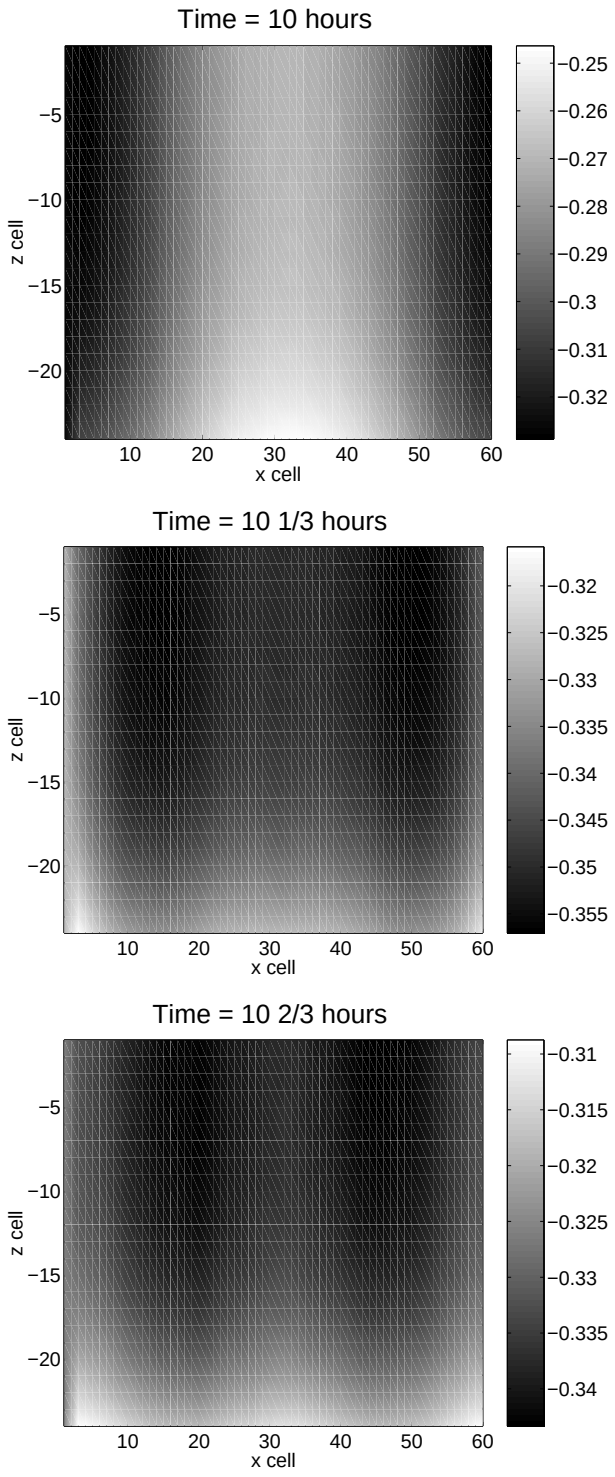

Figure 1.6: Velocity in the x-z plane for $Q = 10$ m^3/s and $C_d = 0.002$, shown at 20 minute intervals.

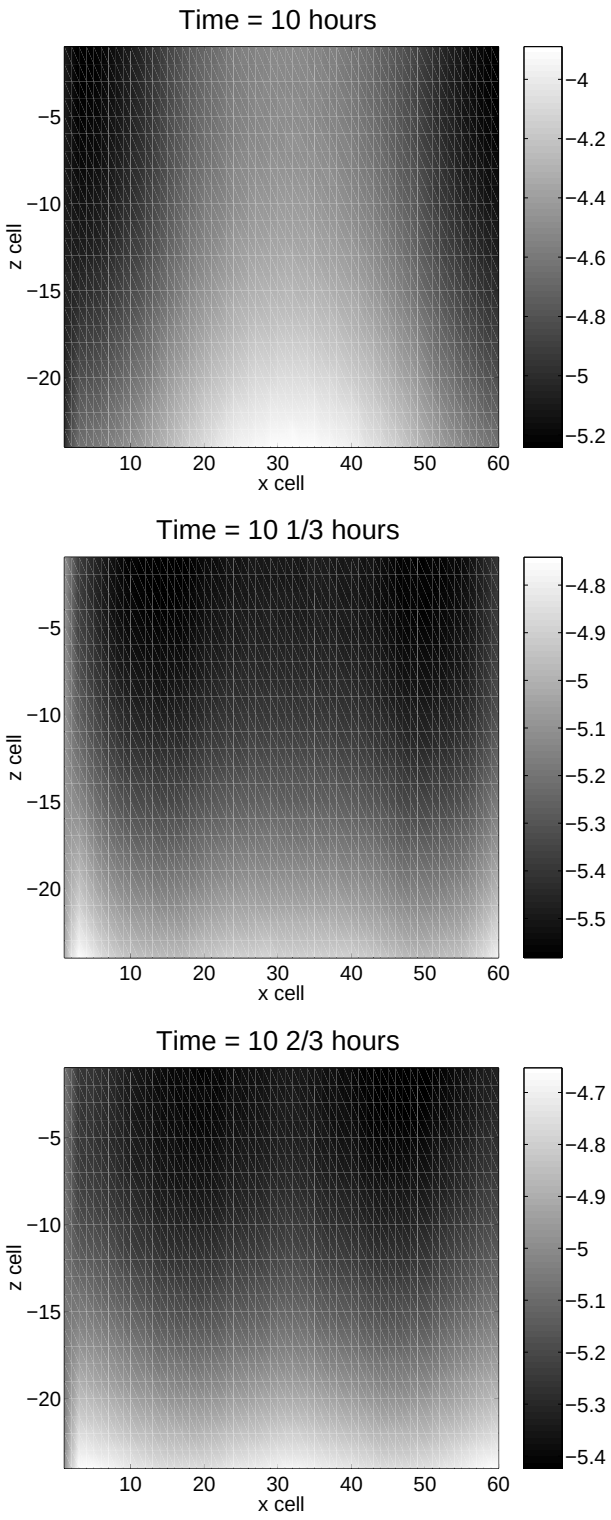

Figure 1.7: Velocity in the x-z plane for $Q = 155$ m^3/s and $C_d = 0.002$, shown at 20 minute intervals.

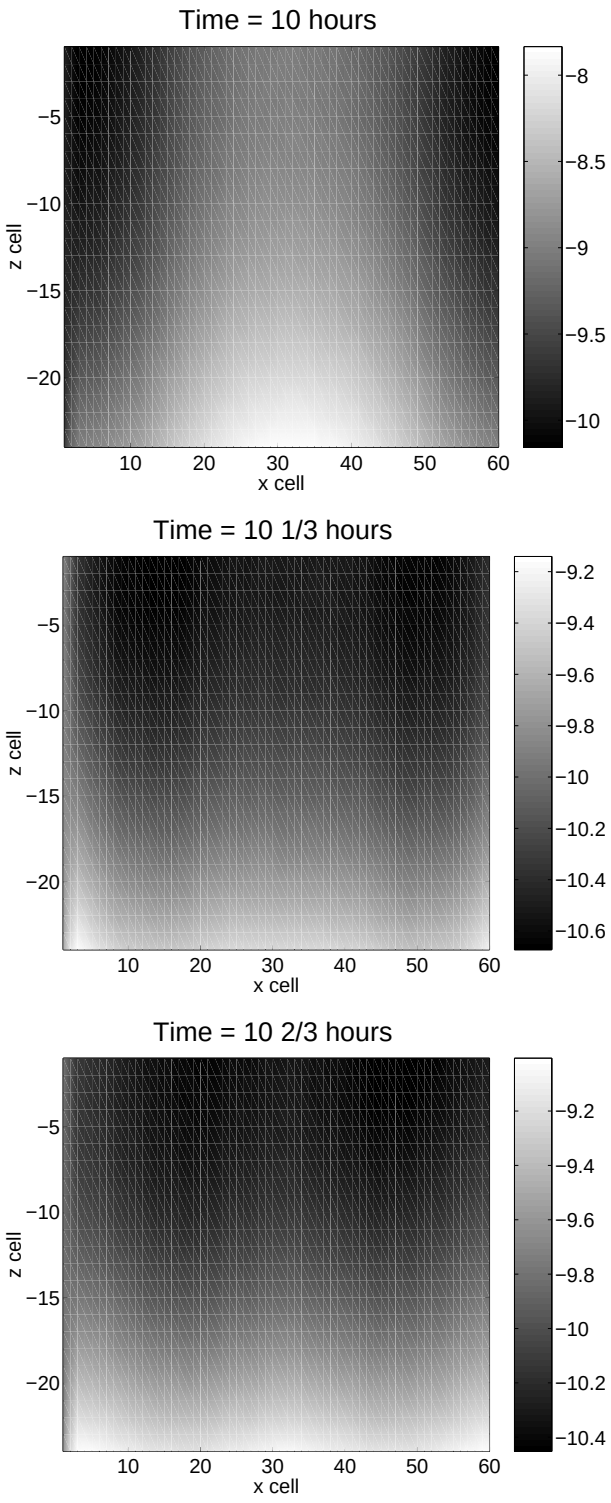

Figure 1.8: Velocity in the x-z plane for $Q = 300$ m^3/s and $C_d = 0.002$, shown at 20 minute intervals.

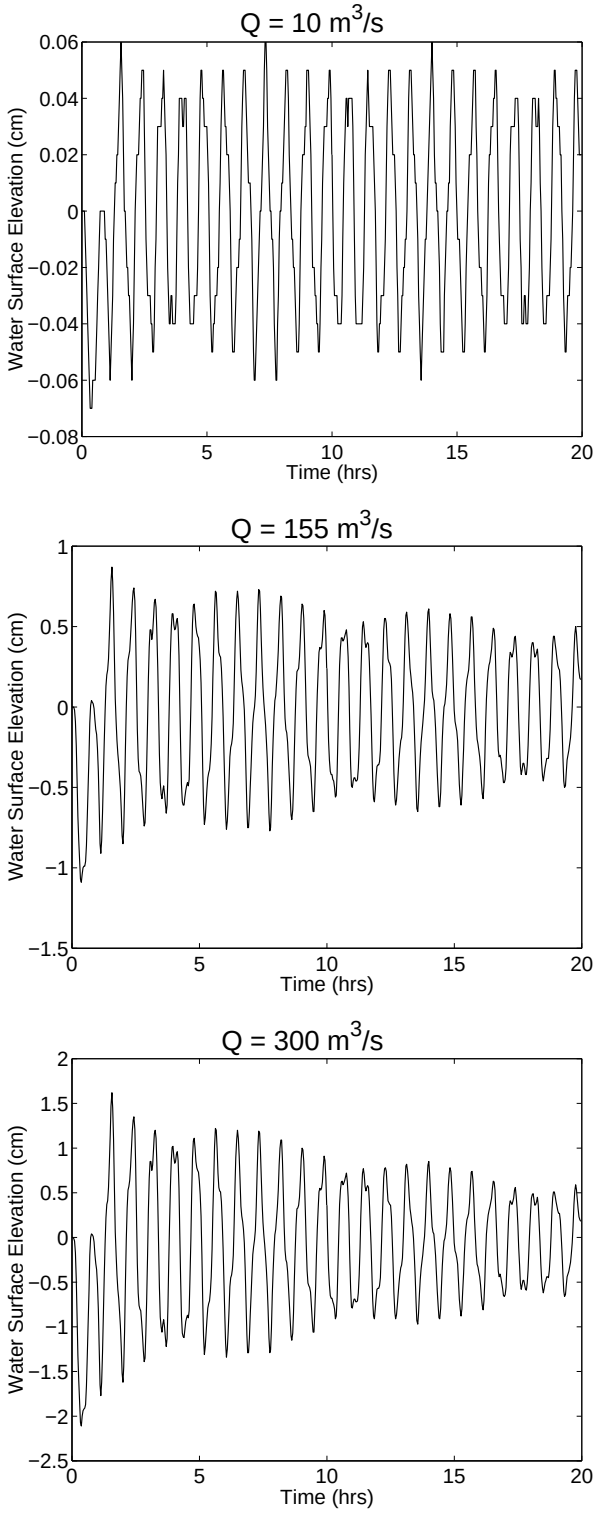

Figure 1.9: Water surface elevations over time (hrs) for increasing flow rates for the case of moderate bottom drag ($C_d = 0.002$)

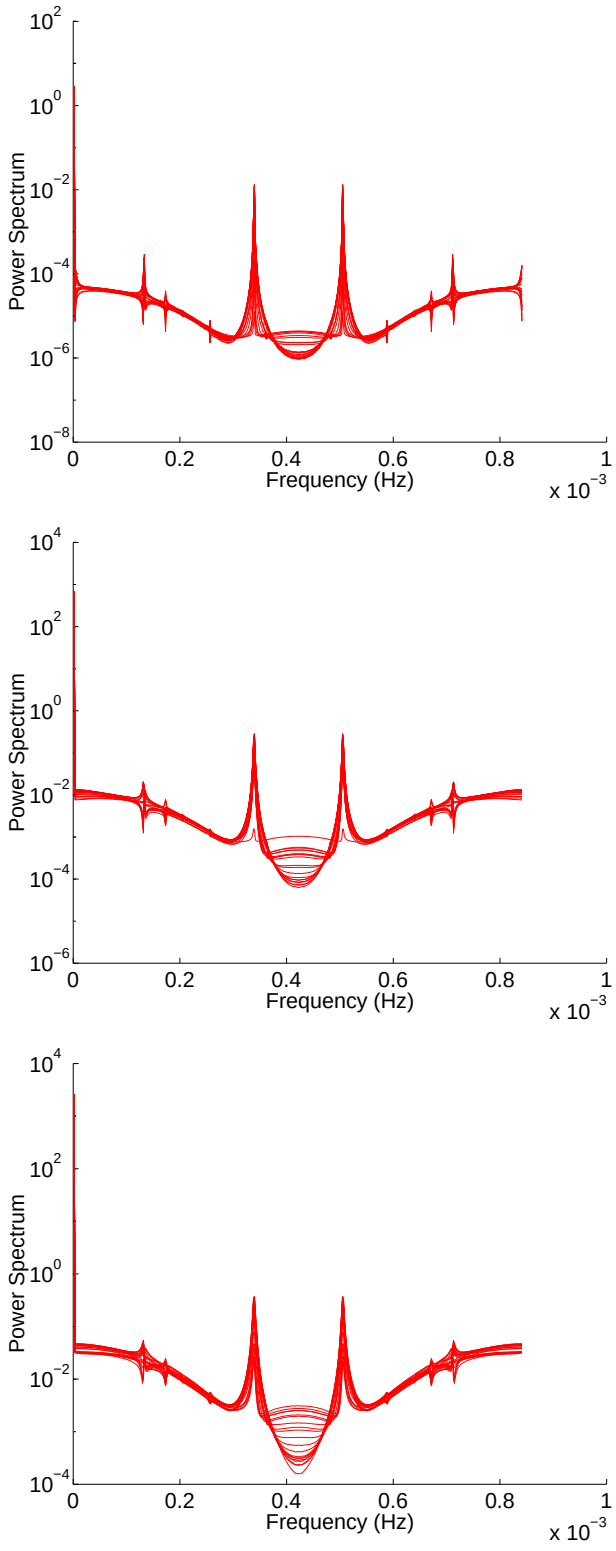

Figure 1.10: Spectra for increasing flow rates for the case of moderate bottom drag ($C_d = 0.002$)

We have already noted the increasing range for water surface elevation as flow speed increases. Comparing with Figures 1.4 and 1.9, we observe that for any particular flow rate, the range for water surface elevation decreases with increasing bottom drag, so that flow rate and drag appear to have contrary effects on water surface elevation.

To make sure that the implementation of advection is working as expected, we would like to check that the flow is steady. However, we know that oscillations exist, so that the flow at any one point cannot be constant. As an approximate check that mass is conserved, we can compute the mass balance, which requires that the rate of accumulation of mass within the control volume be equal to the difference between the flow rates into and out of the control volume. Thus, if V is the volume between vertical planes A and B of width Δy cross-cutting the channel at two points, (where water flows through B before A) , then we must have (approximately)

$$\frac{\partial V(t)}{\partial t} = \left(\int_B u dz - \int_A u dz \right) \Delta y \tag{1.17}$$

We calculate changes in V at each time step and flux through V at each time step and use the Index of Agreement (d) to give us some idea of whether mass is being conserved by SI3D. As we have two numerical approximations, rather than a solution and a numerical approximation to it, we believe that error measure d is the appropriate measure in this case. We take the lefthand side of equation 1.17 as the 'analytical solution,' with n as the time step, so that A_n is the change in volume at time n, while N_n is the flux at time n computed using the righthand

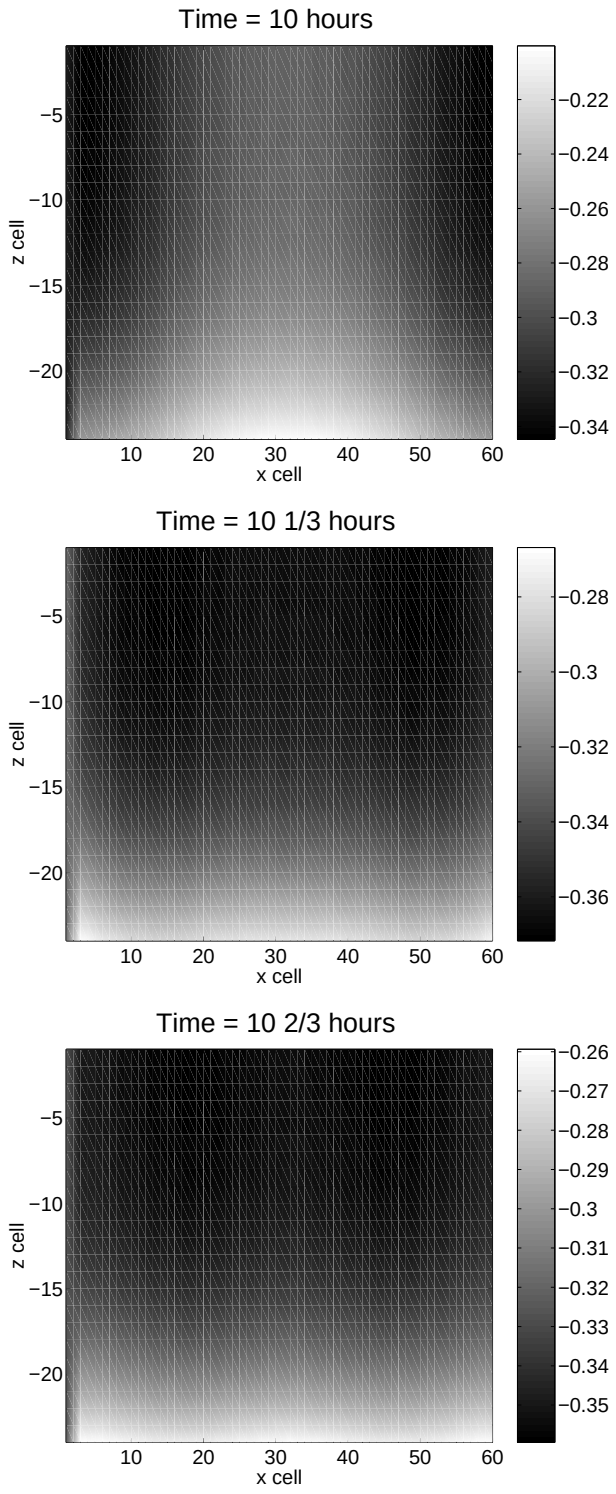

Figure 1.11: Velocity in the x-z plane with for $Q = 10$ m^3/s and $C_d = 0.01$, shown at 20 minute intervals.

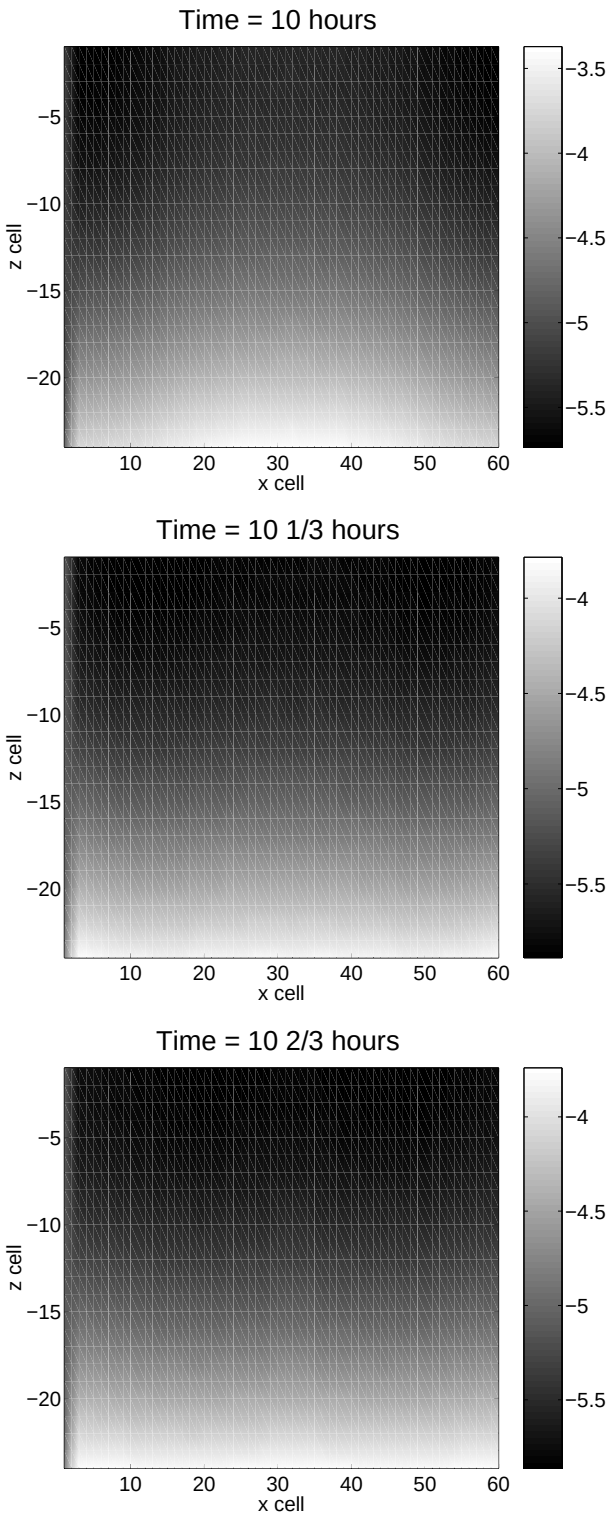

Figure 1.12: Velocity in the x-z plane for $Q = 155$ m^3/s and $C_d = 0.01$, shown at 20 minute intervals.

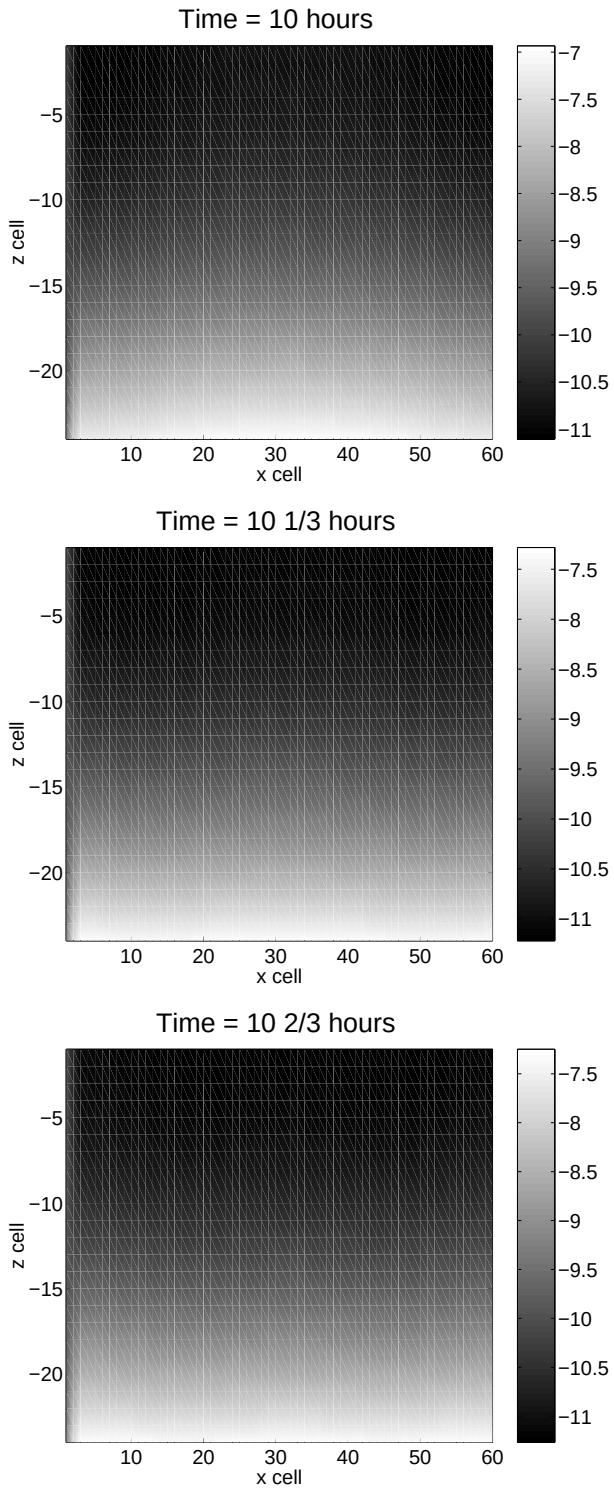

Figure 1.13: Velocity in the x-z plane for $Q = 300$ m^3/s and $C_d = 0.01$, shown at 20 minute intervals.

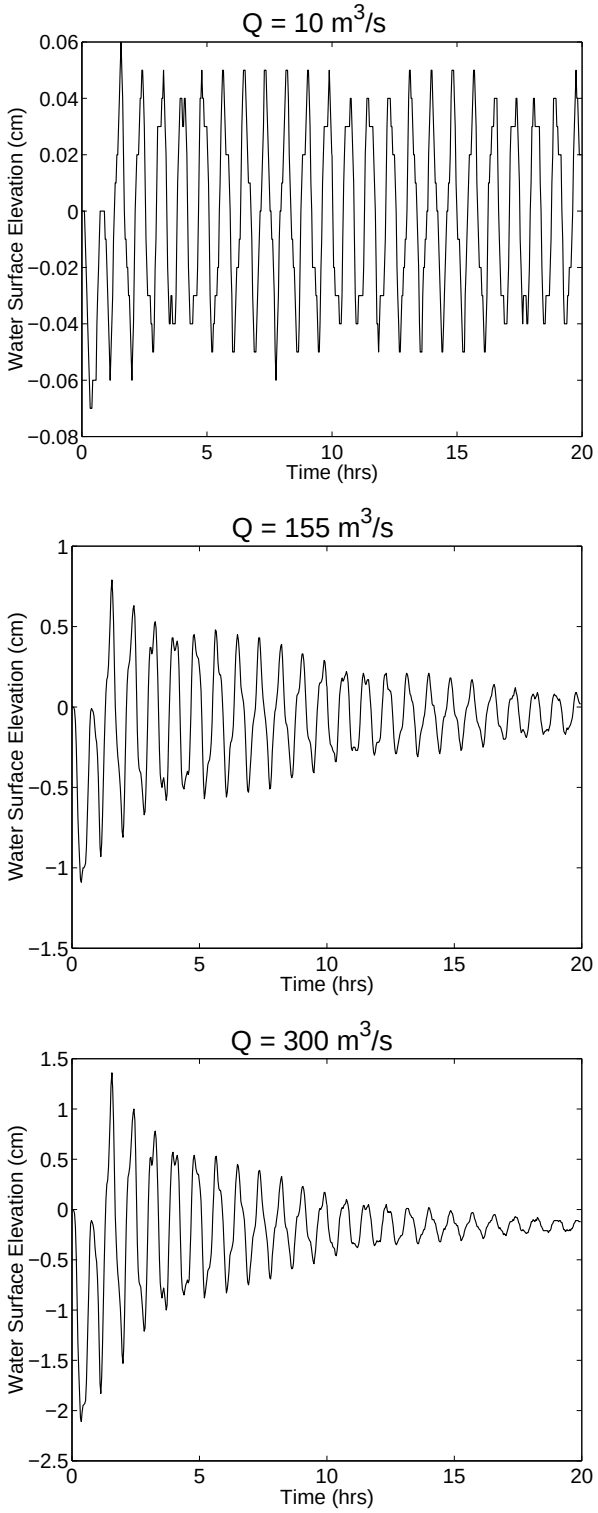

Figure 1.14: Water surface elevations over time (hrs) for increasing flow rates for the case of high bottom drag ($C_d = 0.01$)

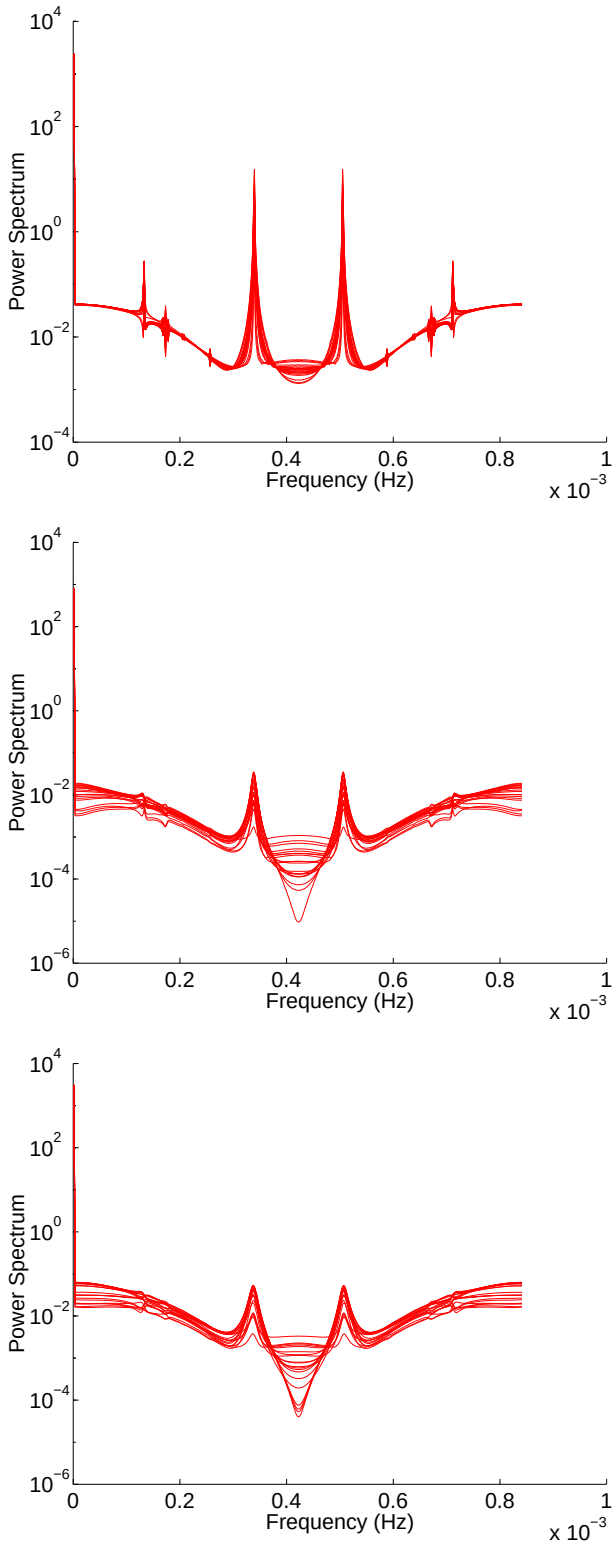

Figure 1.15: Spectra for increasing flow rates for the case of high bottom drag ($C_d = 0.01$)

side of equation 1.17. N'_n and A'_n are then the deviations of the flux and change in volume at time n, respectively, from the mean change in volume. In Table 1.3 are values of d for each combination of flow rate (Q) and drag coefficient. The small values of d support the conclusion of conservation of mass in the system.

Table 1.3: Values of d, the Index of Agreement, between left and right sides of equation 1.17 for all combinations of flow rate and bottom drag.

d	0	0.002	0.01
10 m^3/s	-0.0145	-0.0129	0.0049
155 m^3/s	0.0175	0.0001	-0.0009
300 m^3/s	0.0205	-0.0007	-0.0026

1.6 Test Case 2: Lock-Exchange Problem Under No-Flow Conditions

1.6.1 Description and Objectives

The lock-exchange, or dam-break, problem involves fluids of different densities (in this case due to temperature differences) that are separated by a vertical barrier, or lock gate. When the vertical barrier is removed, the extra weight of the denser fluid induces a larger pressure in this fluid than in the lighter fluid, which causes the denser fluid to flow along the bottom of the channel, underneath the lighter fluid, which flows in the opposite direction along the top of the channel. When the densities are very similar, the flows appear to be approximately symmetric, with the denser and lighter gravity currents of similar depth and progressing at virtually the same speed but in opposite directions. (If the upper boundary is

a rigid lid, then the flows are actually symmetric.) These currents travel at essentially constant speed after an initial transient [15], evidence that the pressure force is balanced by a hydrodynamic drag, due in some part to bottom friction but more importantly to momentum between the two fluids. In general, the interface between the two currents is poorly-defined, irregular, and unsteady. The front of the current consists of a raised 'head,' directly behind which is a shallower, turbulent area, and somewhere beyond that the interface becomes approximately horizontal. Von Karman deduced that the interface between the denser current and the channel bottom is at an angle of 60° with the bottom [38]. (See Shin et al [33] for a current introduction to gravity currents produced by full and partial lock releases.)

Benjamin [2] developed an approximate hydraulic theory for the steady propagation of a gravity current in a two dimensional rectangular channel. He assumed hydrostatic flow far from the fronts and no relative flow within the currents. Additionally assuming conservation of energy, Benjamin found that the depth of the current in a finite-depth channel should be one half the depth of the channel. Furthermore, he predicted a Froude number of $F = \frac{1}{2}$, where the Froude number $F = U/\sqrt{g'H}$, represents the ratio of flow speed to the speed of gravity waves. Here U is the front speed, H is the channel depth and g' is reduced gravity, where $g' = g(\rho_2 - \rho_1)/\rho_2$ for $\rho_2 < \rho_1$. Although dissipation from turbulence and mixing can significantly affect gravity currents, early experiments involving Boussinesq miscible gravity currents (those involving small density differences) found current speeds similar to Benjamin's prediction [19], [1]. Keulegan [19] and Barr [1] both found that the Froude number increases with Reynolds number. Furthermore, Shin et al [33] investigated high Reynolds number scenarios and found that although

mixing occurs in this case, the energy dissipation and amount of reduction in current speed are small. In addition, Keulegan discovered that the aspect ratio of the channel had no effect on current speed.

Although Benjamin's theory seems to provide a reasonable approximation to current speed in the lock release scenario, several of the assumptions he made do not seem very realistic in many cases. For example, Lowe et al [24] found velocities within the current to generally be about ten percent of the current speed. Moreover, waves can propagate along the interface between currents, changing the balance of energy and momentum, so that Benjamin's energy-conserving model analysis may not be entirely appropriate. Much work has been done since Benjamin on the basic dynamics of gravity currents resulting from lock exchange phenomena (for examples see [15], [14], [6]). Progress in this area is hindered by the inability of direct numerical simulation (DNS) to be used on larger Reynolds number flows, as the numerical resolution required is determined by the range of scales involved, which in turn is directly related to inertial and viscous scales [15].

The lock-exchange or dam-break problem tests the discretization and implementation of the substantial derivative of temperature in the scalar transport equation. The substantial derivative is denoted $\frac{D}{Dt}$ and is equivalent to $\frac{\partial}{\partial t} + u\frac{\partial}{\partial x} + v\frac{\partial}{\partial y} + w\frac{\partial}{\partial z}$, representing both the unsteady and advective terms. In these simulations, three types of open boundary conditions were tested: 1) the water surface elevation above a reference value was set to 0 at both open boundaries, 2) flow rates at both open boundaries were set to 0, or 3) the water surface elevation above a reference value was set to 0 at the western boundary and the flow rate at the eastern boundary was set to 0. Using any of these boundary conditions, movement of the water should be based solely on momentum due to the transport of

temperature. Thus, the implementation of the baroclinic terms in the momentum equations is also tested. For all types of boundary conditions, simulations were performed using no bottom drag, as well as a drag of 0.002.

Scalar transport using monotonized central-difference (MC) limiters in all three directions is utilized for temperature transport, as this method outperformed the remaining six transport methods implemented in SI3D using simple test scenarios. MC limiter methods approximate a conservation law using a high-order accurate scheme for areas in which a smooth solution exists and a low-order monotone scheme for areas in which the solution is discontinuous or poorly resolved [10], which avoids spurious ripples near gradients with poor resolution.

1.6.2 Assumptions

- Channel initially divided vertically into two regions of constant temperature
- ρ is not constant
- Flow driven entirely by baroclinic force

1.6.3 Governing Equations

Continuity

$$u_x + v_y + w_z = 0$$

$$\zeta_t + u_x H + v_x H = 0$$

Momentum

$$\frac{\partial u}{\partial t} + u\frac{\partial u}{\partial x} + v\frac{\partial u}{\partial y} + w\frac{\partial u}{\partial z} = -\frac{1}{\rho_0}\frac{\partial p}{\partial x} + \frac{\partial}{\partial x}\left(K_H\frac{\partial u}{\partial x}\right) + \frac{\partial}{\partial y}\left(K_H\frac{\partial u}{\partial y}\right) + \frac{\partial}{\partial z}\left(K_V\frac{\partial u}{\partial z}\right) \tag{1.18}$$

$$\frac{\partial v}{\partial t} + u\frac{\partial v}{\partial x} + v\frac{\partial v}{\partial y} + w\frac{\partial v}{\partial z} = -\frac{1}{\rho_0}\frac{\partial p}{\partial y} + \frac{\partial}{\partial x}\left(K_H\frac{\partial v}{\partial x}\right) + \frac{\partial}{\partial y}\left(K_H\frac{\partial v}{\partial y}\right) + \frac{\partial}{\partial z}\left(K_V\frac{\partial v}{\partial z}\right) \tag{1.19}$$

$$0 = -\frac{\rho}{\rho_0}g - \frac{1}{\rho_0}\frac{\partial p}{\partial z} \tag{1.20}$$

Scalar Transport

$$\frac{\partial s}{\partial t} + u\frac{\partial s}{\partial x} + v\frac{\partial s}{\partial y} + w\frac{\partial s}{\partial z} = \frac{\partial}{\partial x}\left(D_H\frac{\partial s}{\partial x}\right) + \frac{\partial}{\partial y}\left(D_H\frac{\partial s}{\partial y}\right) + \frac{\partial}{\partial z}\left(D_V\frac{\partial s}{\partial z}\right) + \Delta_s$$

1.6.4 Boundary Conditions

$$\left.\frac{\partial u}{\partial y}\right|_{y=0} = \left.\frac{\partial u}{\partial y}\right|_{y=B} = u|_{x=0} = u|_{x=L} = 0$$

$$\left.\frac{\partial v}{\partial x}\right|_{x=0} = \left.\frac{\partial v}{\partial x}\right|_{x=L} = v|_{y=0} = v|_{y=B} = 0$$

$$\left.\frac{\partial u}{\partial z}\right|_{z=-H} = \left.\frac{\partial v}{\partial z}\right|_{z=-H} = \left.\frac{\partial u}{\partial z}\right|_{z=\zeta} = \left.\frac{\partial v}{\partial z}\right|_{z=\zeta} = 0$$

Note that the conditions $u|_{x=0} = u|_{x=L} = 0$ are true for flow boundary conditions but not for water surface elevation boundary conditions.

1.6.5 Initial Conditions

$$
\begin{aligned}
u, v, w|_{t=0} &= 0 \\
T &= 13^{\circ}C \quad for\ 0 \leq x \leq L/2 \\
T &= 18^{\circ}C \quad for\ L/2 < x \leq L
\end{aligned}
$$

1.6.6 Results

Figures 1.16, 1.17, and 1.18 show temperature field results from a longer channel (71,424 m) at 12 hour intervals in the no-drag case for flow, water surface elevation, and mixed boundary conditions, respectively. The channel was lengthened in order to be able to more easily compare the initial as well as longer term results against results from laboratory experiments [33]. However, it should be remembered that the results here simply show temperature fields, rather than tracking the two fluids directly, as in [33]. As described above in 'Initial Conditions', the temperature difference is set up initially in the middle of the channel to attempt to avoid the effects of a finite-length lock, and a full-depth lock release is effected.

Generally correct lock-exchange behavior is observed initially under all types of boundary conditions, with the warmer water in the eastern part of the channel moving westward over the colder water at the bottom. A dense gravity current travels to the right along the lower boundary and a buoyant current travels to the left along the upper boundary. With all flow and with mixed boundary conditions, the currents appear symmetric and occupy approximately half of the depth of the channel and although the interface is poorly defined, it is very regular. On the other hand, with all water surface elevation boundary conditions, the interface is

more irregular, and the denser current appears to move much faster and take up more of the water column than the lighter current; in addition, the colder water is clearly pushing the warmer water out the upstream boundary. None of these three simulations show a raised head at the front of the current.

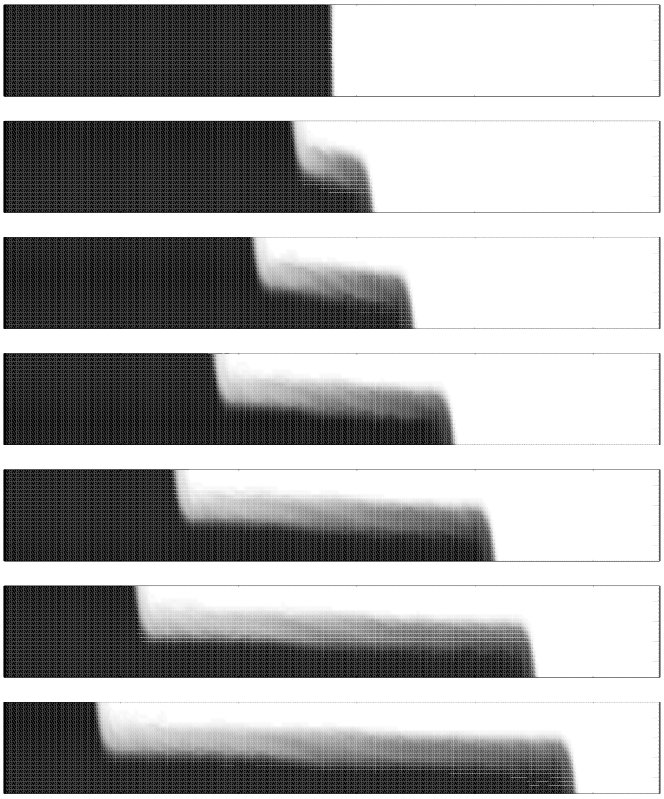

Figure 1.16: Temperature field in the x-z plane for the lock-exchange problem with flow boundary conditions at each boundary and no drag, shown at 12 hour intervals. The heavier fluid starts in the western part of the channel.

Figures 1.19, 1.20, and 1.21 show temperature field results for simulations using the three types of boundary conditions with drag. Results again are shown every 12 hours. While lock-exchange experiments and analysis have generally assumed a negligible amount of bottom drag, we are interested in a moderate amount appropriate for a muddy and/or sandy channel bottom. Adding drag creates a sloped,

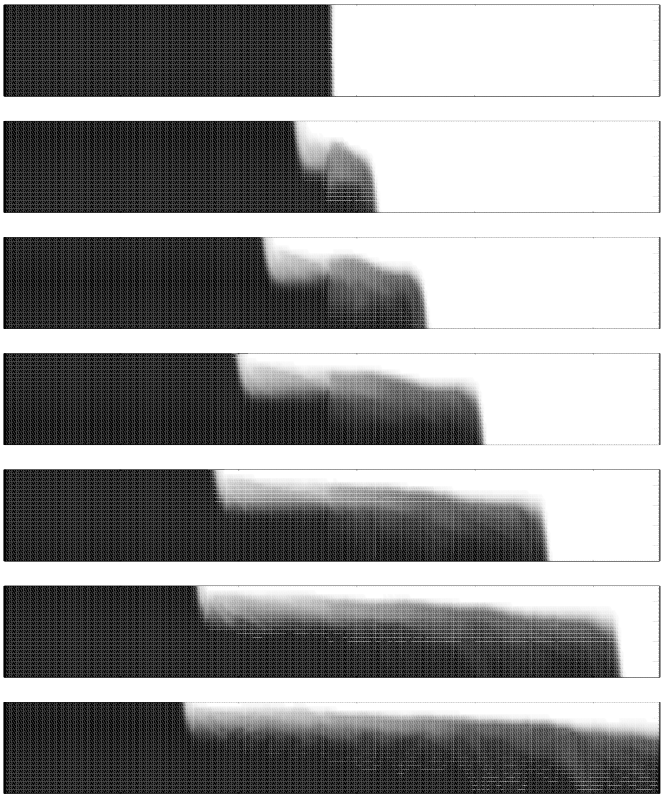

Figure 1.17: Temperature field in the x-z plane for the lock-exchange problem with water surface elevation boundary conditions at each boundary and no drag, shown at 12 hour intervals. The heavier fluid starts in the western part of the channel.

rather than horizontal, interface between the two currents, with the tail of the current taking up increasingly more of the water depth. In general, the interface is better defined than in the no drag case. Furthermore, in the flow and mixed boundary condition cases, as might be expected, a slight retarding of movement of the colder water at the bottom is seen, and the front head and the channel bottom meet at an angle of approximately 60°. The simulation using flow conditions at both boundary conditions shows the most evidence of a raised head at the front of the current with mixing immediately behind. On the other hand, adding drag in the water surface elevation boundary case has a somewhat larger effect on the

scalar movement; the denser current actually appears to be moving faster than the lighter current; additionally, the head is exceptionally poorly defined and the interface slope is much greater than for the other two cases, with the interface almost reaching the surface by day 3.

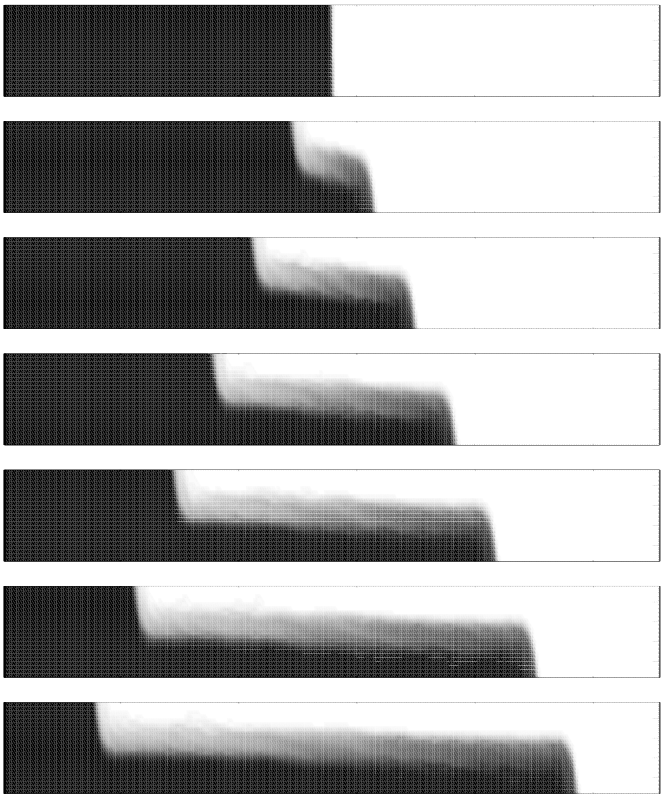

Figure 1.18: Temperature field in the x-z plane for the lock-exchange problem with eastern flow and western water surface elevation boundary conditions and no drag, shown at 12 hour intervals. The heavier fluid starts in the western part of the channel.

Using Benjamin's Froude number of 1/2 [2] for the nondimensional velocity, we can determine an approximate velocity for the currents in the current simulations of $U = \frac{\sqrt{g'H}}{2} \approx 0.1519$m/s. Figure 1.22 shows velocity profiles at hour 18 of the simulation for all types of boundary conditions tested, and allows a more

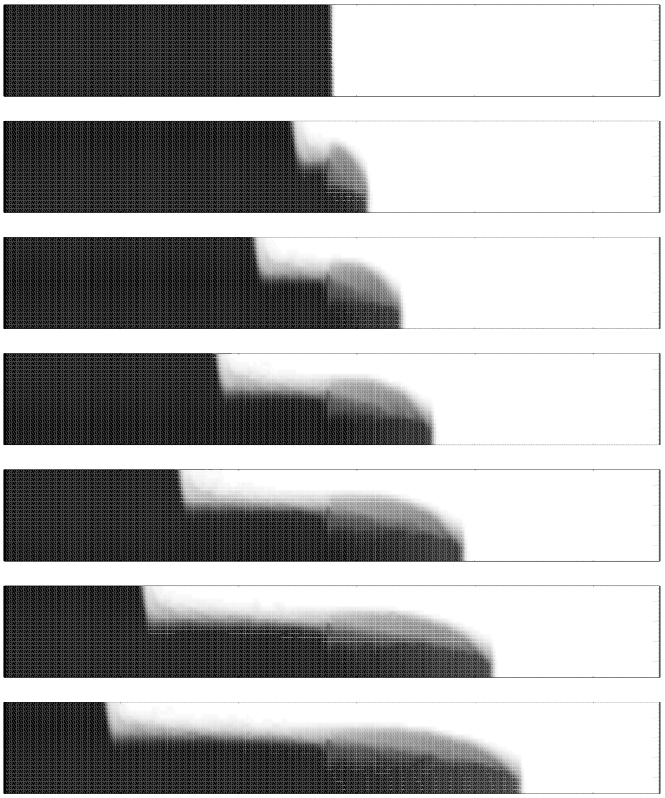

Figure 1.19: Temperature field in the x-z plane for the lock-exchange problem with flow boundary conditions at each boundary and drag, shown at 12 hour intervals. The heavier fluid starts in the western part of the channel.

direct comparison of the effect of bottom drag on front speeds. As suggested from the previous temperature profiles, the different open boundary scenarios not only produce velocity fronts differing greatly in shape and clarity but also differing greatly in range of velocities. In general, in the case without drag, all boundary types overestimate the front speed of the denser current with respect to Benjamin's approximation. The denser current in the water surface elevation boundary case moves at almost twice the predicted speed, while the lighter current moves at a speed considerably slower than the analytically predicted speed. Fortunately, both the flow and mixed boundary condition cases produce only a slight overestimation

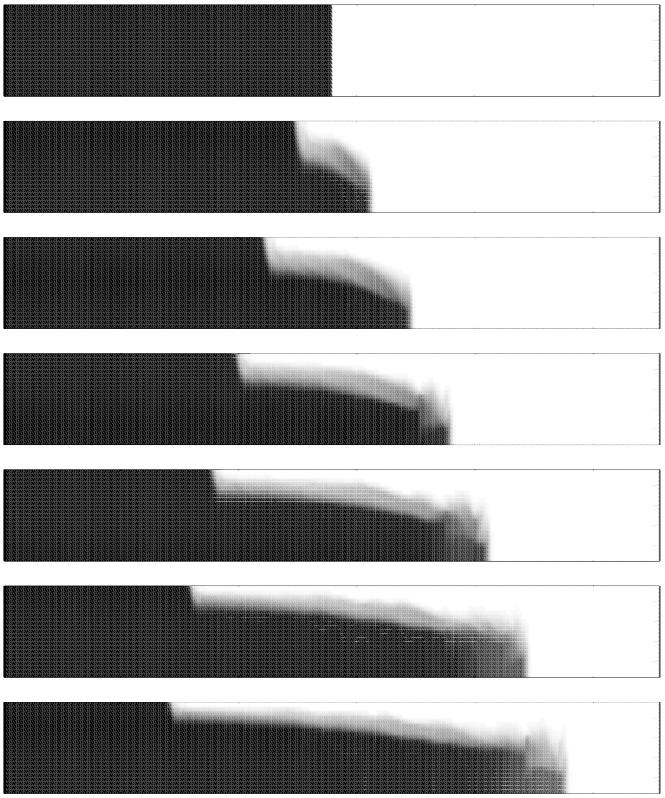

Figure 1.20: Temperature field in the x-z plane for the lock-exchange problem with water surface elevation boundary conditions at each boundary and drag, shown at 12 hour intervals. The heavier fluid starts in the western part of the channel.

of the lighter current speed, resulting in fairly symmetric velocity profiles for the opposing currents, as expected. For all three types of boundary conditions, adding drag reduces the speed of the denser current, and in the case of water surface elevation boundary conditions, including drag almost cuts the colder current speed in half, relative to the no drag case. The result is a fairly sharply defined dense current front in all three cases, with the interface in the water surface elevation case occuring significantly above the halfway point.

In order to investigate the lock-exchange current velocities more closely, Table 1.4 gives, for all six boundary condition/drag combinations, the analytical front

speed for the top six cells in the middle of the channel at hour 18, after the current has had time to establish itself. An attempt was made to determine the front of the current using temperature, but as temperature is only a proxy for the actual current fluid and the current speed is approximately constant after an initial transient, we decided that velocities at a vertical cross-section of the channel should give a good indication of current speed. The top six cells were chosen in order to avoid the irregular, unsteady area near the interface between the two currents.

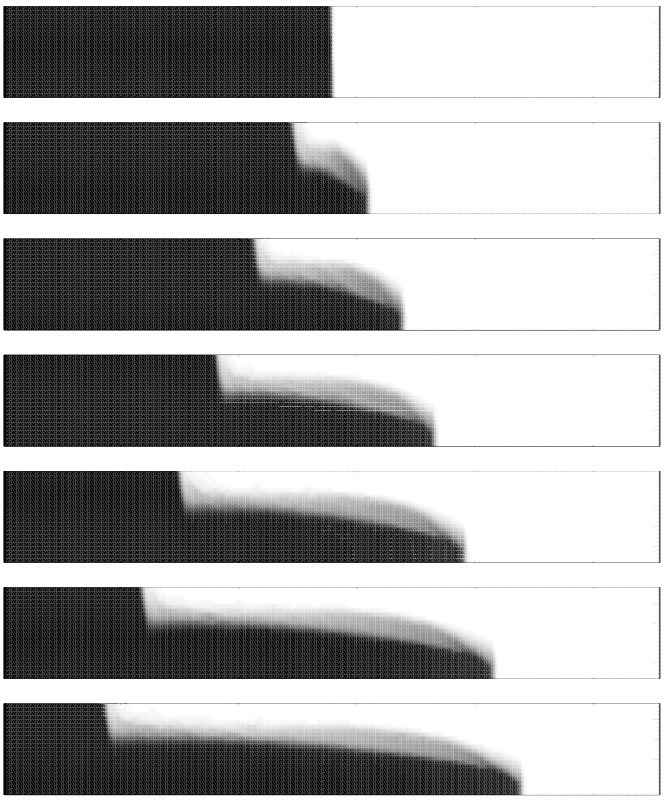

Figure 1.21: Temperature field in the x-z plane for the lock-exchange problem with eastern flow and western water surface elevation boundary conditions and drag, shown at 12 hour intervals. The heavier fluid starts in the western part of the channel.

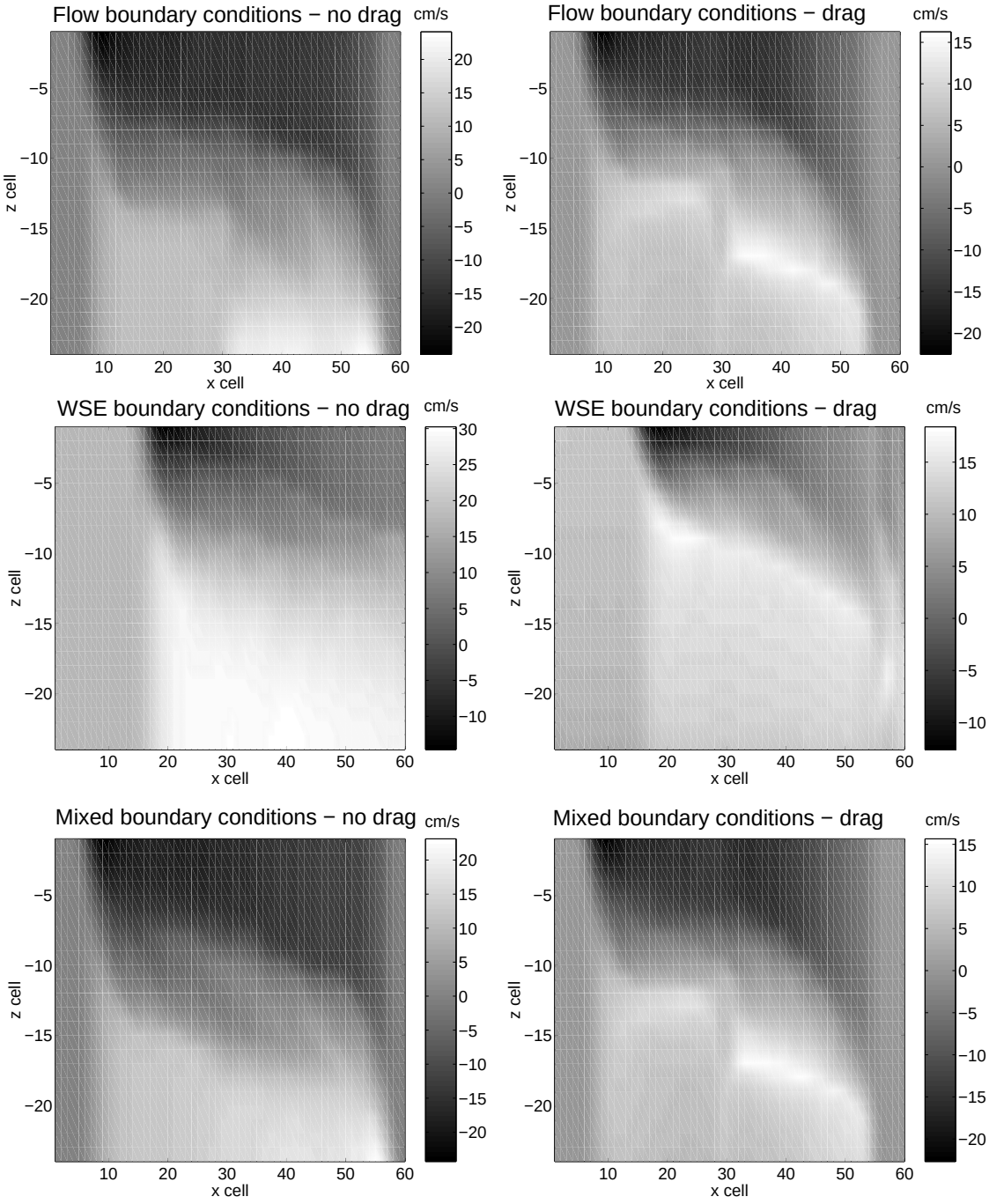

Figure 1.22: Velocity fields in the x-z plane for all boundary condition/drag combinations, shown at 18 hours. WSE = water surface elevation. The temperature change is initialized at x cell 32. The heavier fluid starts in the western part of the channel.

Clearly, flow and mixed boundary conditions produce current speeds reasonably close to the predicted value of 0.1519, while velocities using water surface elevation boundary conditions lead to the most extreme errors, regardless of whether drag is included. In the flow and mixed boundary conditions cases, moderate bed friction causes the denser front to slow down near the bottom of the channel and at the same time produces higher than predicted lighter current speeds close to the water surface (although adding drag under mixed boundary conditions does decrease the magnitude of the velocity relative to simulations without drag). On the other hand, while drag does appear to retard the progress of the heavier current when using water surface elevation boundary conditions, current speeds near the surface are also retarded so that they are much lower than expected. In addition, the raised interface can be seen in the switch from negative to positive velocities by 1.5m from the surface in the case of water surface elevation boundary conditions. (For flow and mixed boundary conditions, by 2.5 m from the surface, the interface is clearly being felt and the current is slowing down.) Moreover, water surface elevation boundary conditions lead to the most relative variation in current velocities (3-17% versus $> 200\%$).

In an attempt to quantify the departure of the current speeds in the present simulation from the predicted speed, using Benjamin's approximation, for the first eight hours of simulation, we compared the speed for the top six cells at the temperature front to the speed predicted analytically, and we quantified the results using a variety of error measures (Table 1.5). In general, the water surface elevation boundary conditions, whether with or without drag, produce results that are farther from the analytical solution than do either the flow boundary conditions or the mixed boundary conditions. While the water surface elevation results with

Table 1.4: Numerical results at hour 18 for the speed of the temperature front for cells 1-6, representing 0-2.5m from the surface.

	0 m	0.5 m	1 m	1.5 m	2 m	2.5 m
Flow (no drag)	-.1537	-.1533	-.1530	-0.1526	-.1522	-.1491
Flow (drag)	-.1556	-.1552	-.1548	-.1533	-.1493	-.1252
WSE (no drag)	-.0397	-.0394	-.0354	0.0040	0.0266	.0514
WSE (drag)	-.0413	0.0408	-.0270	0.0215	0.0393	0.0608
Mixed (no drag)	-.1631	-.1626	-.1622	-.1614	-.1611	-.1580
Mixed (drag)	-.1613	-.1609	-.1596	-.1577	-.1550	-.1335

Table 1.5: Discrepancy between numerical propagation of temperature front and analytical solution for propagation, quantified via five error measures, for the four boundary condition/drag combinations used in Test 2.

Error Measures	d	l_1	l_2	l_∞	RMSE
Flow - No Drag	-0.0852	0.0089	0.0102	0.0180	0.0097
Flow - Drag	-0.0752	0.0445	0.0736	0.1753	0.0695
WSE - No Drag	-64.8688	0.7844	0.7904	0.9737	1.2965
WSE - Drag	-82.4546	0.7467	0.7512	0.8587	1.1329
Mixed - No Drag	-33.4503	0.0629	0.0639	0.0739	0.0588
Mixed - Drag	-0.0830	0.0588	0.0666	0.1212	0.0616

drag tend to have less error than results without drag, the errors in both cases are so great as to preclude their use for this scenario. The error measures for flow and mixed boundary conditions, on the other hand, tend to be about an order of magnitude lower in general. For the more realistic cases including a modest amount of bottom drag, these values seem quite reasonable, given the rapidly decreasing flow values toward the center of the channel and the approximate nature of Benjamin's calculation for wavespeed.

1.7 Test Case 3: Lock-Exchange Problem Under Steady-State Flow

1.7.1 Description and Objectives

This test case involves the more realistic condition of lock-exchange under flow conditions, in this case steady-state flow (with $C_d = 0.002$). The lock-exchange problem checks the discretization and implementation of the substantial derivative of temperature in the scalar transport equation. In addition, the steady-state flow condition checks the discretization and implementation of the advection terms in the momentum equation, as well as the mass conservation. The flow at the boundaries is set in motion by using a flow boundary condition at the upstream boundary, with a water surface elevation boundary condition at the downstream open boundary, so that movement of the water is based on advection as well as momentum due to the transport of temperature, and the implementation of the barotropic as well as the baroclinic terms in the momentum equations are tested.

1.7.2 Assumptions

- Channel initially divided vertically into two regions of constant temperature
- ρ is not constant
- Flow driven by both baroclinic and barotropic forces

1.7.3 Governing Equations

Continuity

$$u_x + v_y + w_z = 0$$

$$\zeta_t + u_x H + v_x H = 0$$

Momentum

$$\frac{\partial u}{\partial t} + u\frac{\partial u}{\partial x} + v\frac{\partial u}{\partial y} + w\frac{\partial u}{\partial z} - fv = -\frac{1}{\rho_0}\frac{\partial p}{\partial x} + \frac{\partial}{\partial x}\left(K_H\frac{\partial u}{\partial x}\right) + \frac{\partial}{\partial y}\left(K_H\frac{\partial u}{\partial y}\right) + \frac{\partial}{\partial z}\left(K_V\frac{\partial u}{\partial z}\right) \tag{1.21}$$

$$\frac{\partial v}{\partial t} + u\frac{\partial v}{\partial x} + v\frac{\partial v}{\partial y} + w\frac{\partial v}{\partial z} + fu = -\frac{1}{\rho_0}\frac{\partial p}{\partial y} + \frac{\partial}{\partial x}\left(K_H\frac{\partial v}{\partial x}\right) + \frac{\partial}{\partial y}\left(K_H\frac{\partial v}{\partial y}\right) + \frac{\partial}{\partial z}\left(K_V\frac{\partial v}{\partial z}\right) \tag{1.22}$$

$$0 = -\frac{\rho}{\rho_0}g - \frac{1}{\rho_0}\frac{\partial p}{\partial z} \tag{1.23}$$

Scalar Transport

$$\frac{\partial s}{\partial t} + u\frac{\partial s}{\partial x} + v\frac{\partial s}{\partial y} + w\frac{\partial s}{\partial z} = \frac{\partial}{\partial x}\left(D_H\frac{\partial s}{\partial x}\right) + \frac{\partial}{\partial y}\left(D_H\frac{\partial s}{\partial y}\right) + \frac{\partial}{\partial z}\left(D_V\frac{\partial s}{\partial z}\right) + \Delta_s$$

1.7.4 Boundary Conditions

$$\left.\frac{\partial u}{\partial y}\right|_{y=0} = \left.\frac{\partial u}{\partial y}\right|_{y=B} = 0$$

$$\left.\frac{\partial v}{\partial x}\right|_{x=0} = \left.\frac{\partial v}{\partial x}\right|_{x=L} = v|_{y=0} = v|_{y=B} = 0$$

$$\left.\frac{\partial u}{\partial z}\right|_{z=-H} = \left.\frac{\partial v}{\partial z}\right|_{z=-H} = \left.\frac{\partial u}{\partial z}\right|_{z=\zeta} = \left.\frac{\partial v}{\partial z}\right|_{z=\zeta} = 0$$

1.7.5 Initial Conditions

$$\begin{aligned} u, v, w|_{t=0} &= 0 \\ T &= 13^{\circ}C \quad for\ 0 \leq x \leq 32 \\ T &= 18^{\circ}C \quad for\ 32 < x \leq 64 \end{aligned}$$

1.7.6 Results

Based on Test 2, using water surface elevation boundary conditions can lead to large errors in the velocities of both the cold and warm gravity currents, with the effect worsening as time increases. However, with flow-flow boundary conditions, the solution depends strongly on the initial condition as there are, in theory, an infinite number of solutions for the water surface profile in a channel corresponding to a given flow rate and bottom frictional resistance. Thus, non-zero flow-flow BC's should be avoided. Instead, we set up the problem with mixed boundary conditions - water surface elevation as the downstream boundary condition and flow as the upstream boundary condition, with the flow value determining the virtually steady-state flow in the channel. Temperature again was set to be $13^{\circ}C$ in the western part of the channel and $18^{\circ}C$ in the eastern part. We performed two different tests,

based on the relationship of the background flow in the channel, $\bar{V}$, to the velocity of the temperature front, V_f. When $\bar{V} \ll V_f$, the background advection is small relative to the baroclinic flow and, as in Test 2, the flow should continually move upstream at the bottom of the channel. When $V_f \ll \bar{V}$, advection dominates the flow, and outflow occurs, with eventual homogeneity of temperature in the channel at the warmer value.

Figure 1.24 shows the results at three times separated by 6 hours for the case in which $\bar{V} \ll V_f$. The background flow speed is set by using an eastern flow boundary condition to be approximately 0.03 cm/s. As expected, the upstream flow of colder water at the bottom of the channel is evident. When the background velocity is small or nonexistent, we are essentially looking again at the scenario from the second test case, in which the lock-exchange controls the dynamics in the channel. Thus, we also see a symmetric warmer water current moving downstream at the top of the channel. (In contrast, if both boundary conditions are water surface boundary conditions, we see an asymmetric lock exchange taking place, with warmer water gradually being pushed upstream and replaced with colder water (figure 1.24).)

Figure 1.25 shows temperature plots over time for the case $\bar{V} \gg V_f$. In this case the downstream flow (with speed approximately 21 cm/s) gradually overwhelms the baroclinic force and allows the warmer water to be advected down the channel, displacing the colder water, as expected. Demonstrating the dominance of the eastern flow boundary condition, after 30 hours, the cold water has been almost completely displaced.

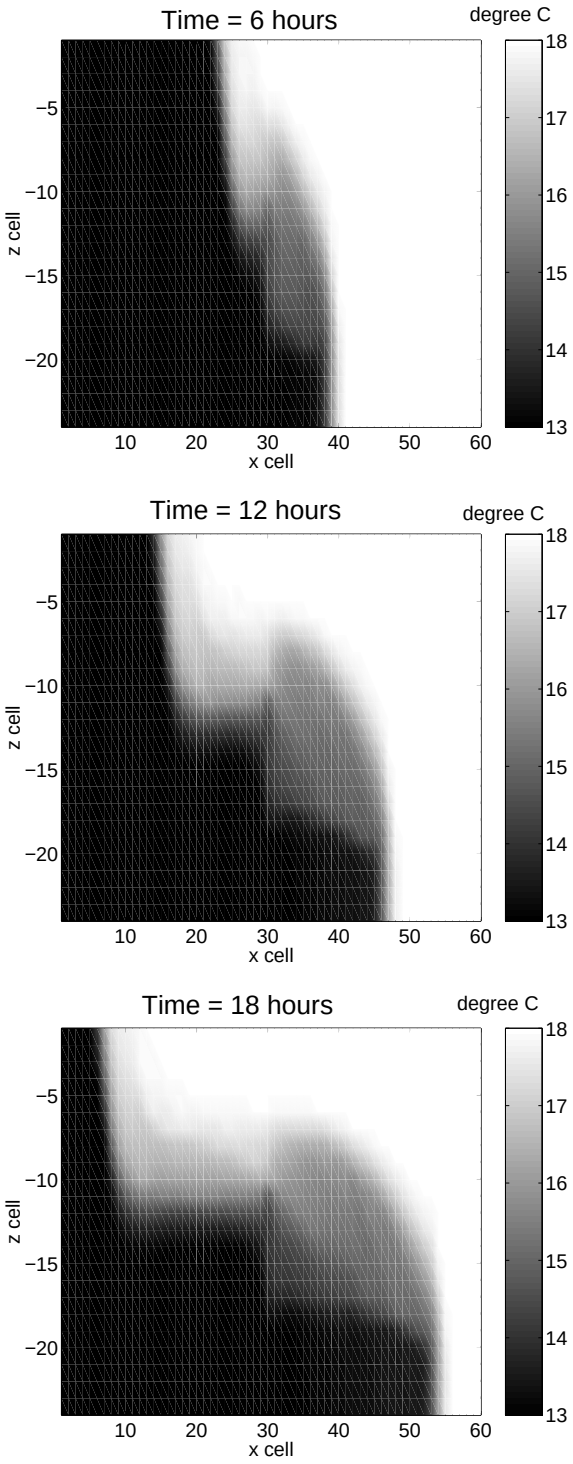

Figure 1.23: Time series of the temperature field in the x-z plane for the lock-exchange problem with eastern flow and western water surface elevation boundary conditions for the case $\bar{V} \ll V_f$.

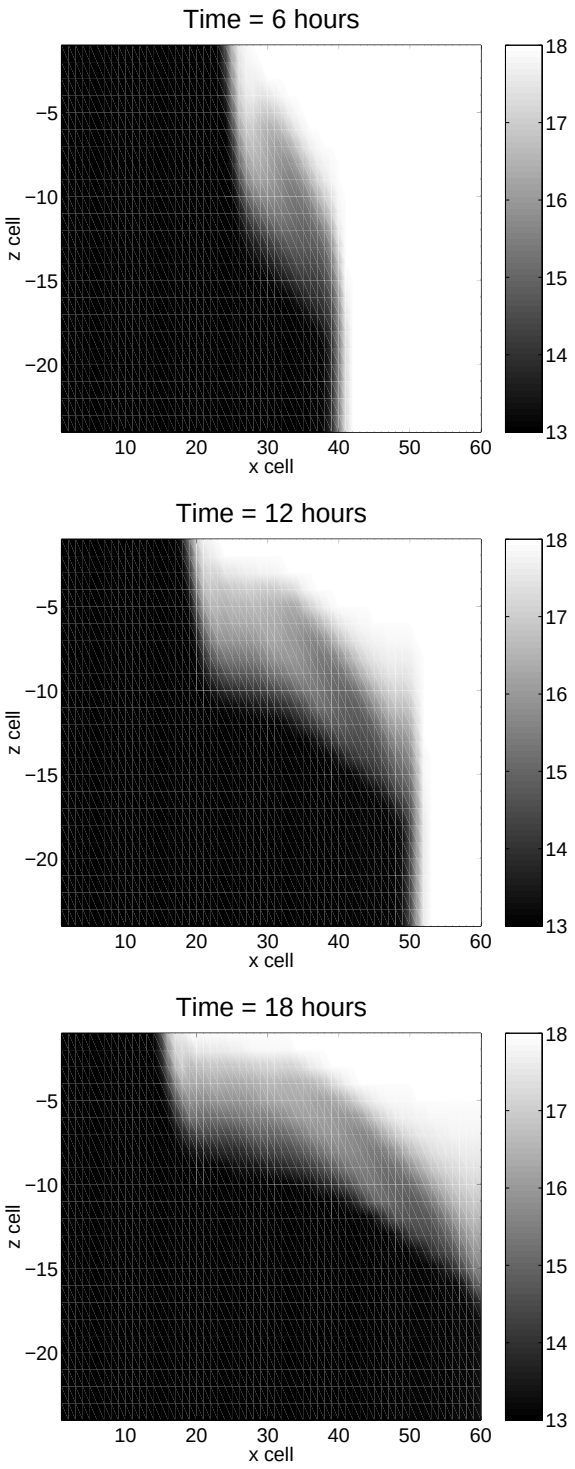

Figure 1.24: Time series of the temperature field in the x-z plane for the lock-exchange problem with water surface elevation boundary conditions for the case $\bar{V} \ll V_f$.

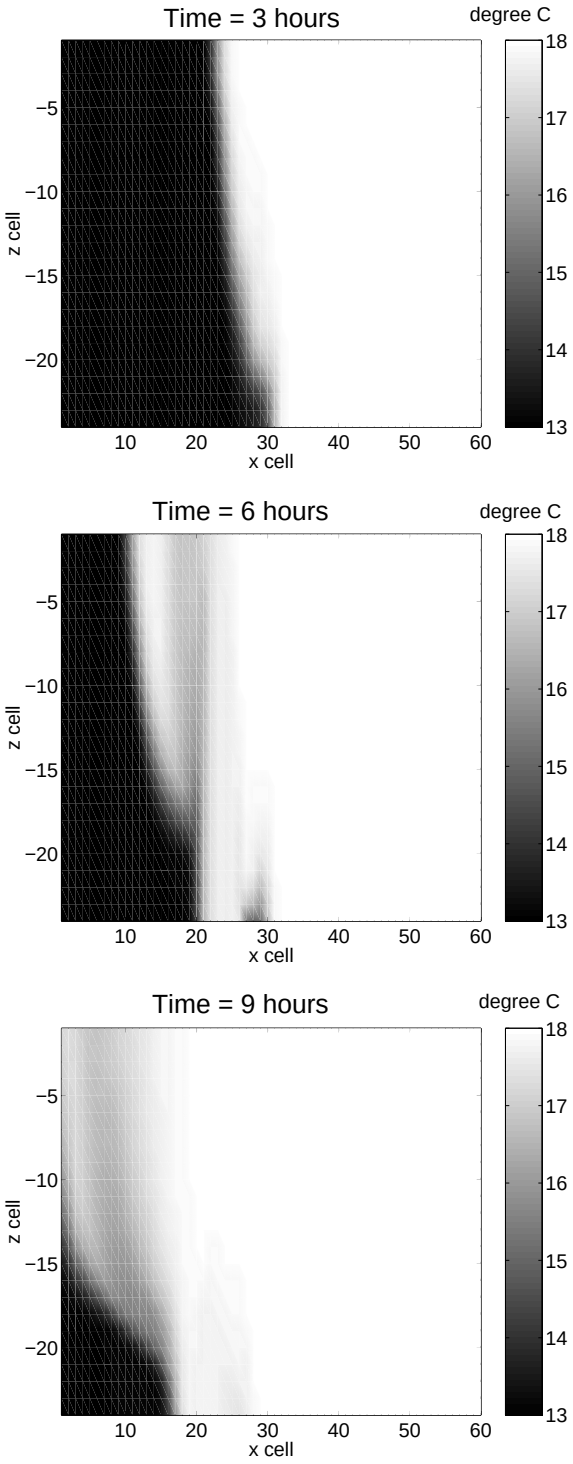

Figure 1.25: Time series of the temperature field in the x-z plane for the lock-exchange problem with eastern flow and western water surface elevation boundary conditions for the case $\bar{V} \gg V_f$.

1.8 Summary

Overall, the test suite demonstrated that SI3D is working basically as expected. Test case 1 showed that flow-flow boundary conditions created steady flow of the magnitude expected, with mass approximately conserved (shown by computing a mass balance). However, oscillations were visible in the velocity field and in the water surface elevation. Although these waves may simply be a function of water reaching the boundaries of a finite-length channel, PSD plots suggest that the oscillations are also consistent with a first mode, as well as higher order, seiche. Drag tends to damp out these oscillations as its value increases and as the flow rate increases, while flow rate and drag appear to have opposite effects on water surface elevation.

Scalar transport, although not as easy to test directly, also gave evidence of reasonable results. Typical lock-exchange behavior was observed initially using all types of boundary conditions, although water surface elevation boundary conditions at each end of the channel prevented the warmer current from moving as quickly as expected and pushed the colder water along the bottom more quickly than expected. Using very crude measurements of expected front speed, water surface elevation boundary conditions performed poorly, regardless of whether drag was included or not. Flow and mixed boundary conditions both led to an overestimation of the temperature bore speed, with mixed boundary conditions leading to slightly higher velocities (with the exception of the cells closest to the water column center where the speed decreased). Adding drag led to somewhat larger errors in the case of flow-flow boundary conditions but did not make much difference in the case of mixed boundary conditions. As flow boundary conditions can in general lead to unpredictable results, we decided to use mixed boundary

conditions for test case 3 and for future simulations when temperature transport and advection are both important.

Test 3 involved testing both the barotropic and baroclinic terms in the governing equations by changing the relationship of the background flow in the channel to the velocity of the temperature front. As expected, if the mean background flow speed was much smaller than the speed of the temperature bore, the colder water at the bottom continually moved upstream. Similarly, if the background advection is large relative to the baroclinic flow, then advection dominates and forces warm water into the channel, eventually displacing all of the colder water. These relationships held whether the boundary conditions are both water surface elevation conditions or mixed conditions.

1.9 Conclusions

In the scenarios tested, SI3D appears to adequately handle advection and temperature transport separately as well as when both occur simultaneously. 'In the scenarios tested' is an important qualifier, however. Using flow-flow boundary conditions, water is advected down the channel as expected and steady flow eventually achieved. However, the ubiquitous oscillations in water velocity and water surface elevation seen in testing, especially in low drag/high flow rate scenarios, are to be expected. In addition, as flow-flow boundary conditions are commonly avoided in practice (see discussion above), this test is of limited importance. Fortunately, tests of SI3D's transporting of water due to temperature differences showed a mixture of flow and water surface elevation boundary conditions or flow-flow boundary conditions superior to water surface elevation boundary conditions under moderate drag, which is the scenario later used for particle tracking. Even with these

boundary conditions, though, the velocity profile near the bed varied more than expected when approaching the channel center based on analytical considerations. Importantly, when utilizing mixed boundary conditions to induce advection and also including a lock-exchange situation in order to initiate scalar transport, results of simulations in which the relationship of the background advection to the speed of the temperature bore is gradually varied appear reasonable. However, no analytical method was devised for testing the results of these simulations; greater resolution test scenarios would give more confidence in the overall results and would allow the determination of the degree to which the simulation results match the relationship of advection and bore speeds and how these results are affected by changes in values of eddy coefficients.

Given the reasonable amount of testing undertaken it thus seems safe to employ SI3D to model water flow down a channel under the conditions shown to produce reliable results in the foregoing tests. Namely, we can fairly confidently undergo testing using a regular, rectangular channel, mixed boundary conditions, and moderate drag under the range of flow rates tested.

Boundaries often present problems when performing numerical simulations and, as seen here, may contribute to oscillations in velocity in general and abrupt changes in velocity at the boundaries, depending on the scenario modelled. Accordingly, in future simulations we plan to use a channel long enough that under the highest flow rate simulated, water flowing in the channel will not be able to reach either channel end over the time of the simulation. Thus, irregularities at the boundaries should not affect simulation results.

APPENDIX

Turbulence is a dissipative, irregular flow regime characterized by rapid variation of pressure and velocity in three-dimensional space and time that causes rapid mixing and increases the rates of momentum, heat, and mass transfer. Turbulence in estuaries and embayments is very complex and can be caused by irregularities near the bed, internal waves and density-gradient effects (Kelvin-Helmolz instabilities) in the water column, and wind-generated waves and drift at the surface. Occurring at a range of scales, the largest turbulent eddies are on the order of the dimensions of the basin and the smallest are determined by the fluid viscosity, with length, time and velocity scales around 0.1 cm, 1 s and 0.1 cm/s, respectively. However, while turbulence has been studied for over 100 years, it is still an unsolved problem. Computational studies by Ruddick et al [31] and Goosse et al [13] comparing results from different mixing parameterizations have shown that if the production, dissipation, and diffusion of turbulence are ignored, qualitatively reasonable results cannot be expected for coastal seas and the world ocean, respectively. Thus, to make any progress, modelers must attempt to represent turbulence in models before completely understanding it, with the knowledge that model results help refine the simplifications necessary in producing a realistic turbulence model.

While computational methods exist for resolving the entire turbulence spectrum (Direction Numerical Simulation) and resolving large eddies while paramterizing turbulence at smaller scales (Large Eddy Simulation), they are only practical for relatively small-scale problems. As important turbulent processes occur on spatial and temporal scales which are not practical to represent computationally, Reynold's averaged Navier-Stokes equations (RANS), in which all turbulent motion

is paramterized, are most suitable for more complex flows. This method involves averaging the quantities in the Navier-Stokes equations in such a way that the stochastic part of the flow due to turbulence is separated from the deterministic mean flow using a procedure called "ensemble averaging." The velocity, pressure, density, and tracer (temperature only, in this case) terms are decomposed into mean and fluctuating parts, with the mean value of a property defined as the average of a theoretically infinite number of realizations of that property.

The result of averaging the basic Navier-Stokes equations is the Reynolds equations, which are the same as the Navier-Stokes equations except for the extra terms $\langle \tilde{u}_i \tilde{u}_j \rangle$ and $\langle \tilde{u}_i \tilde{s} \rangle$, the Reynolds (momentum) stresses and turbulent heat fluxes, respectively. Here the tilde denotes the fluctuating part of the velocity or temperature. These terms are second moments (correlations between two flow properties in the same place) and represent fluxes of momentum and heat due to turbulent fluctuations. (The momentum fluxes act as stresses on the fluid similar to viscous stresses in gases caused by the momentum flux due to molecular fluctuations.) With these turbulent stress and heat terms, the number of unknowns (10) is greater than the number of equations, leading to the so-called turbulent closure problem and a potentially infinite system of equations known as the Friedmann-Keller system [18].

To solve the turbulence closure problem, additional algebraic or differential equations need to be introduced. Among the algebraic models, those using Boussinesq's well-known eddy viscosity concept [4] are the most common; in these models, the turbulent stress or tracer transport is set equal to the product of the eddy coefficient and a fluid deformation tensor or the gradient of the tracer concentration. Bulk, or mixed-layer, models [22] take advantage of the fact that within boundary

layers, water properties are almost uniform; the well-mixed region is parameterized and the development of the mixed-layer in response to surface and interior shear stresses is represented by ordinary differential equations.

In contrast, statistical (diffusion) models are ODE models that are based on approximations to the exact transport equations for the turbulent stresses in which turbulent mixing is parameterized as a diffusion process. Although these diffusion models may mix inefficiently and might not be able to adequately account for important physical processes such as surface and internal waves and Langmuir circulation (leading to an underpredicted mixed layer depth [25]), they are the most promising and popular type of closure model and, according to Burchard [7], the most appropriate; advantages include the calculation of many higher statistical moments such as the turbulent kinetic energy, dissipation rate, and temperature variance, which leads to a better understanding of complex small-scale phenomena. Statistical turbulence closure models are most useful when they are fairly general, theoretically sound and computationally practical.

To develop the statistical turbulent closure models, transport equations for the momentum and heat fluxes can be derived from the shallow water Navier-Stokes equations and Reynold's averaged equations. Exact transport terms for turbulence kinetic energy and dissipation rate can be developed similarly. In these equations, third order correlations among unknown fluctuating velocities, pressure, and temperature fields appear, for which transport equations could be derived [16]; this process could in principle continue forever. Instead, the typical solution takes advantage of the fact that in general, the importance of a term decreases as its order increases and makes assumptions about the unknown terms based on empirical data.

The goal of second-moment closures, the most popular type of statistical model, is to develop a closed system of equations from the second-moment equations for $\langle \tilde{u}_i \tilde{u}_j \rangle$ and $\langle \tilde{u}_i \tilde{s} \rangle$. Third-order moments can be neglected [7] or parameterized by approximations using the down-gradient or other approaches [7], [17], [8]. The down-gradient approach, the most simple and widely-used approach, involves relating third moments to the gradients of second moments by using an eddy diffusivity [7]. Other simplifications that are commonly made include parameterization of pressure-strain correlation terms, involving products of velocity fluctuations and gradients of pressure fluctuations, parameterization of dissipation terms, a boundary layer approximation, and simplification of the transport of second moments. With these simplifications, a closed system of equations, which combines accuracy and computational efficiency, can be obtained for the 10 unknown second moments. This information on the second moments is embodied in the so-called stability functions, which are found algebraically from the transport equations for the Reynolds stresses, describe the effects of shear and stratification, and are used to compute eddy viscosities and diffusivities.

At this point, the turbulence kinetic energy, k, and dissipation rate, ϵ, are still unknowns. For complete closure, the second-moment closure schemes are often combined with two-equation turbulence models that include one conservation equation for k and a second equation for a length-scale related turbulent quantity that might be turbulent dissipation rate, ϵ, macro length scale, L, or turbulence frequency, ω. Using a standard equation for the macro length scale which relates L to ϵ and ω, a second transport equation for any of these quantities could, in principle, allow the calculation of the dissipation rate. Possible two-equation models are the $k-\epsilon$, $k-kL$, and $k-\omega$ models, with $k-\epsilon$ and $k-kL$ the most common.

Once the turbulence kinetic energy and the dissipation rate have been determined, the eddy viscosity, K, and eddy diffusivity, D, can be represented using the relation of Kolmogorov [20] and Prandtl [29] by

$$K = c_\mu \frac{k^2}{\epsilon}, \qquad D = c'_\mu \frac{k^2}{\epsilon}$$

where c_μ and c'_μ represent the stability functions.

The eddy viscosity and eddy diffusivity (referred to as 'eddy coefficients') vary throughout the flow field as a function of the length and velocity scales of the turbulent eddies. In a continuum fluid, the dynamic viscosity relates the frictional forces in the fluid to the gradients of flow velocity. While the analogy is far from perfect, the eddy viscosity can be thought of as relating the turbulent transport of momentum to gradients of the mean velocity, and similarly, the eddy diffusivity is introduced to relate the turbulent transport of a tracer (temperature) to its gradient. (The molecular viscosity and diffusivity are often at least several orders of magnitude smaller than the smallest possible eddy coefficients, so the molecular term can be neglected.) In estuaries, the turbulent Schmidt or turbulent Prandtl number, the ratio of kinematic viscosity to eddy viscosity or diffusivity, respectively, can generally be considered to be close to 1 [35], and thus the ratio of the eddy viscosity to the diffusivity should also be close to 1.

Because the horizontal and vertical length scales of estuaries and embayments often differ by orders of magnitude, the intensity and size of the eddies in those directions can differ greatly as well, and often separate horizontal and vertical eddy coefficients are defined. Turbulent mixing in the vertical direction is significantly more complicated than mixing in the horizontal directions [37]; the variation in mean flow properties in the horizontal directions is typically much more gradual

than the vertical variations, and especially for flows with constant or slowly-varying geometries, a constant value for the horizontal eddy coefficients is often reasonable. In the case of more complex bathymetry, a method such as that of Smagorinsky [34], which determines the magnitude of the horizontal eddy coefficients based on the largest turbulent eddies and on a local deformation field or to the vorticity, is often used (and is implemented in SI3D).

SI3D provides a variety of turbulence models that determine the eddy coefficients to use in the Reynold's averaged version of the Navier-Stokes equations. At the simplest extreme, the user may define constant eddy coefficients and at the most complex extreme are second-moment turbulence closure schemes augmented with two-equation models.

In estuaries, vertical eddy coefficients generally should not be assumed to be constant. For steady, unstratified open channel flow, theory and experiments have shown that eddy viscosities and diffusivities have a parabolic distribution in the water column, with values of zero at the surface and bottom and a maximum value at mid-depth [28]. Another available method of computing eddy coefficients takes advantage of this known distribution by determining eddy coefficients that vary with time and are distributed parabolically in the vertical based on the friction velocity. In stratified flows, the distribution becomes bimodal, with a zero value at the density gradient and parabolic distributions both above and below the density gradient [5] [37]. Several turbulence models in SI3D determine the eddy coefficients with a mixing length model and adjust for stratification using one of a number of damping function types.

While simpler methods, such as constant eddy coefficients and algebraic methods, require careful choice of appropriate eddy coefficients for the particular simu-

lation scenario, two-equation models rely on instantaneous flow properties and are therefore more versatile for multiple scenarios and/or situations in which the flow is not fully understood. Mellor and Yamada [26] developed a transport equation for kL based on data for decaying homoegeneous grid turbulence, closed-channel, and boundary layer flows. The Mellor-Yamada model in general refers to a hierarchy of models ranging from a more computationally intensive full set of second-moment equations (the level 4 model) to a simpler model neglecting all material derivative and diffusion terms which assumes a production-dissipation balance (the level 2 model). The level 2.5 model does not assume this production-dissipation balance, and the level 3 model includes the material derivative and diffusion terms as well but still allows a complete algebraisation of the equations due to neglect of tracer-related transport terms. Since 1982, turbulence closure models using the kL equation have been widely utilized in simulations of geophysical fluid flows. Versions of the 2, 2.5, and 3 level kL model are included in SI3D.

The $k - \epsilon$ equation, which was developed at the Imperial College in London [23] also has its proponents, but as Rodi argues, "The arguments for the relative merits of the ϵ and the kL equations are rather academic because both equations are fairly empirical and, with the constants suitabl[y] adjusted, perform in a similar manner." [30] One disadvantage of the kL method is that it requires a wall function to make sure that diffusion is positive. No version of the $k - \epsilon$ model is included in SI3D.

Although the 2.5 level of the MY hierarchy of models has been widely used in geophysical applications and was the preferred general scheme for the vertical mixing parameterization in SI3D [32], it does have some drawbacks. Solutions using MY2.5 do not produce eddy coefficients that follow the log law and did

not match experimental data in the case of steady pressure-driven open channel flow [39]. In addition, this model results in lower bottom stresses and less overall mixing [39]. Possible reasons for these problems include inconsistent length scale limitations, as well as an inadequate parabolic wall proximity function [39].

The stability functions of Galperin et al [12] assumed quasi-equilibrum and were able to improve the performance of the stability functions proposed by Mellor and Yamada [26], which had been found to be unstable numerically. In addition, MY2.5 resulted in a surface mixed layer that was too shallow, while Galperin's model was able to correct this problem. While an improvement over MY2.5, this model underestimates mixing, which can lead to the water column surface being systematically too warm. SI3D includes both 2 and 3 level versions of the Galperin formulation.

The most advanced second-moment, two-equation turbulent closure scheme implemented in SI3D was developed by Kantha and Clayson [17] who modified the quasi-equilibrium Galperin et al model in two important ways. First, they incorporated recent findings from LES modeling at NCAR [40], [27] into modeling the pressure-covariance terms in the second-moment closure. Second, an empirical Richardson number-based mixing model, needed in case of stably-stratified but strongly sheared flow just below the mixed layer, remedies the most serious problem of MY2.5, inadequate mixing. This second modification should make this model much more robust for a variety of geophysical mixed layer and circulation scenarios and indeed has performed well when compared against observational data in a variety of mixed-layer simulations from the world ocean varying in latitude and time scale [7]. In contrast to the warm sea surface temperature biases from the earlier models, the model of Kantha and Clayson exhibits a cool water bias if

anything, which can be dealt with by a slight adjustment to the model. Blumberg et al's [3] suggestion for a wall proximity function for open channel flow greatly improves the reliability of the Kantha and Clayson model for this particular flow regime [39].

Bibliography

[1] D. I. H. Barr. Densimetric exchange flows in rectangular channels. *La Houille Blanche*, 22:619–631, 1967.

[2] T. B. Benjamin. Gravity currents and related phenomena. *Journal of Fluid Mechanics*, 31(2):209–248, 1968.

[3] A. F. Blumberg, B. Galperin, and D. J. O'Connor. Modeling vertical structure of open-channel flows. *Journal of Hydraulic Engineering*, 118:1119–1134, 1992.

[4] J. Boussinesq. Essai sur la theorie des eaux courantes. *Memoires presentes par divers savants a l'Academie des Sciences*, 23(1):1–680, 1877.

[5] K. F. Bowden. *Studies - Geophysics - Estuaries, Geophysics, and the Environment*, chapter Chapter 5: Turbulent processes in estuaries, pages 46–56. National Academy of Sciences, Washington, D.C., 1977.

[6] R. E. Britter and J. E. Simpson. Experiments on the dynamics of a gravity current head. *Journal of Fluid Mechanics*, 88(2):223–240, 1978.

[7] H. Burchard. *Applied Turbulence Modelling in Marine Waters*. Number 100 in Lecture Notes in Earth Sciences. Springer, Berlin, 2002.

[8] V. M. Canuto, A. Howard, Y. Cheng, and M. S. Dubovikov. Ocean turbulence I: one-point cloure model. momentum and heat vertical diffusivities. *Journal of Physical Oceanography*, 31:1413–1426, 2001.

[9] R. G. Dean and R. A. Dalrymple. *Water Wave Mechanics for Engineers and Scientists, Vol. 2*. World Scientific Press, Portland, 1991.

[10] D. R. Durran. *Numerical Methods for Wave Equations in Geophysical Fluid Dynamics*. Springer, New York, 1999.

[11] H. B. Fischer, E. J. List, R. Koh, J. Imberger, and N. Brooks. *Mixing in inland and coastal waters*. Academic Press, New York, 1979.

[12] B. Galperin, L. H. Kantha, S. Hassid, and A. Rosati. A quasi-equilibrium turbulent energy model for geophysical flows. *Journal of Atmospheric Sciences*, 45:55–62, 1988.

[13] H. Goosse, E. Deleersnijder, T. Fichefet, and M. H. England. Sensitivity of a global coupled ocean-sea ice model to the parameterisation of vertical mixing. *Journal of Geophysical Research*, 104:13,681–13,695, 1999.

[14] J. Hacker, P. F. Linden, and S. B. Dalziel. Mixing in lock-release gravity currents. *Dynamics of Atmospheres and Oceans*, 24:183–195, 1996.

[15] C. Hartel, E. Meiburg, and F. Necker. Analysis and direct numerical simulation of the flow at a gravity-current head. part 1. flow topology and front speed for slip and no-slip boundaries. *Journal of Fluid Mechanics*, 418:189–212, 2000.

[16] J. O. Hinze. *Turbulence*. McGraw-Hill, 2nd edition, 1975.

[17] L. H. Kantha and C. A. Clayson. An improved mixed layer model for geophysical applications. *Journal of Geophysical Research*, 99:25,235–25,266, 1994.

[18] L. Keller and A. Friedmann. Differentialgleichungen fur die turbulente Bewegung einer kompressiblen Fussigkeit. In *Proceedings of the First International Congress on Applied Mechanics*, pages 395–405, Delft, 1924.

[19] G. H. Keulegan. The motion of saline fronts in still water. Technical Report 5813, 1958.

[20] A. N. Kolmogorov. The equations of turbulent motion on an incompressible fluid. *Izv. Akad. Nauk SSSR, Seria fizicheska*, VI(1-2):56–58, 1942. English translation: Imperioal College, Mech. Eng. Dept. Rept. ON/6, 1968.

[21] P. J. Kundu. *Fluid Mechanics*. Academic Press, San Diego, 1990.

[22] W. G. Large, J. C. McWilliams, and S. C. Doney. Oceanic vertical mixing: a review and a model with nonlocal boundary layer parameterisation. *Reviews of Geophysics*, 32:363–403, 1994.

[23] B. E. Launder and D. B. Spaulding. *Mathematical Models of Turbulence*. Academic Press, New York, 1972.

[24] R. J. Lowe, P. F. Linden, and J. W. Rottman. A laboratory study of the velocity structure in an intrusive gravity current. *Journal of Fluid Mechanics*, 456:33–48, 2002.

[25] P. J. Martin. Simulation of the mixed layer at OWS November and Papa with several models. *Journal of Geophysical Research*, 90:903–916, 1985.

[26] G. L. Mellor and T. Yamada. Development of a turbulence closure model for geophysical fluid problems. *Rev. Geophys. Space Phys.*, 20:851–875, 1982.

[27] C.-H. Moeng and P. P. Sullivan. Comparison of shear- and buoyancy-driven planetary boundary layer flows. *Journal of Atmospheric Sciences*, 51:999–1022, 1994.

[28] I. Nezu and W. Rodi. Open-channel flow measurements with a laser doppler anemometer. *Journal of Hydraulic Engineering*, 112(5):335–354, 1986.

[29] L. Prandtl. Uber ein neues Formelsystem fur die ausgebildete Turbulenz. *Nachr. Akad. Wiss. Gottingen, Math.-Phys. Klasse*, page 6, 1945.

[30] W. Rodi. Examples of calculation methods for flow and mixing in stratified flows. *Journal of Geophysical Research*, 92:5305–5328, 1987.

[31] K. G. Ruddick, E. Deleesnijder, P. J. Luyten, and J. Ozer. Haline stratification in the Rhine-Meuse freshwater plume: a three-dimensional model sensitivity analysis. *Continental Shelf Research*, 15:1597–1630, 1995.

[32] F. J. Rueda. *A three-dimensional hydrodynamic and transport model for lake environments*. PhD thesis, University of California, Davis, 2001.

[33] J. O. Shin, S. B. Dalziel, and P. F. Linden. Gravity currents produced by lock exchange. *Journal of Fluid Mechanics*, 521:1034, 2004.

[34] J. Smagorinsky, S. Manabe, and J. L. Holloway. Numerical results from a nine-point general circulation model of the atmosphere. *Monthly Weather Review*, 93:727–768, 1965.

[35] P. E. Smith. *A three-dimensional, finite-difference model for estuarine circulation*. PhD thesis, University of California, Davis, 1997.

[36] P. E. Smith. Analytical Test Cases. In *ASCE Monograph*. 2005.

[37] J. W. Stijnen, A. W. Heemink, and H. X. Lin. An efficient 3d particle transport model for use in stratified flow. *International Journal of Numerical Methods in Fluids*, 51:331–350, 2006.

[38] T. von Karman. The engineer grapples with nonlinear problems. *Bulletin of the American Mathematical Society*, 46:615–616, 2001.

[39] J. C. Warner, C. R. Sherwood, H. G. Arango, and R. P. Signell. Performance of four turbulence closure models implemented using a generic length scale method. *Ocean Modelling*, 8:81–113, 2005.

[40] J. C. Wyngaard and C.-H. Moeng. *Large Eddy Simulation of Complex Engineering and Geophysical Flows*, chapter Large eddy simulation in geophysical turbulence parameterization. Cambridge University Press, New York, 1993.

Chapter 2

Are Physical or Behavioral Forces More Important in Determining the Fate of Zooplankton? Using an Individual-Based Model to Study Biological Residence Time

2.1 Abstract

While zooplankton have often been thought to be passive tracers, completely at the mercy of physical processes, the prevalence of zooplankton patches, as well as field studies showing evidence of microorganism movement against the primary flow, suggest the importance of other factors. Although physical processes may determine large scale zooplankton patterns, individual zooplankton behavior such as predation or vertical/horizontal migration may dominate at smaller scales. The fact that many small aquatic/marine organisms manage to persist in their native environment in the presence of constant advection is known as the 'drift paradox.' Using a hydrodynamic model to create various flows in an idealized channel, we model zooplankton behavior with an individual-based model and explore the extent to which biological processes can counteract physical drivers. In particular, we investigate how different zooplankton migration behaviors affect biological retention time under a variety of flow regimes and whether a combination of physical/biological regimes exists that can solve the drift paradox problem - i.e., allow

the zooplankton to stay in the study system (avoid washout) for time periods much greater than the hydrologic retention time.

2.2 Introduction

Although physical processes were once believed to be solely responsible for non-random zooplankton spatial patterns, we now know that biological processes also contribute to zooplankton patchiness. For example, large-scale horizontal patches of cholorophyll can sometimes be explained better by their correlation with primary productivity than with passive tracers [31]. Over large scales, physics may dominate, or behavior may combine with physical processes to induce spatial heterogeneity. Over smaller scales, where behavioral processes such as diel vertical migration (DVM) and predation may control zooplankton production, individual behavior may be crucial. In particular, many zooplankton in lakes or oceans show clear vertical migratory movement, covering significant distances daily. Migrating plankton usually move from deeper water to surface strata at dusk and then descend again at dawn.

While DVM has been studied extensively, the motivations, mechanisms and extent of migration are still not well-understood, with possible motivations as disparate as light or predator avoidance and increased genetic exchange. As a result, field or laboratory studies have either attempted to uncover a general principle of migration behavior or simply observed the migration behavior of particular organisms. As an example of the latter, George [12] accumulated precise data on distance (3-5 m in 24 hours) and speed (0.05-0.18 mm/s) of migration for the rotifers *Polyarthra vulgaris, Filinia terminalis and Eratella quadrata*, although he did not discover the mechanism of the migration. In addition, Valiela [34] displays

seasonal data on day and night abundances of *E. elongata* and *S. elegans*, as well as *Pseudocalanus*. Hays [16] studied 41 copepod taxa in the northeast Atlantic and found that larger taxa demonstrated significantly stronger DVM than did smaller taxa. In addition, in larger taxa the propensity to migrate was correlated to a lesser extent with body morphology, with more elongate copepods not migrating, while in smaller taxa, heavy pigmentation is more highly correlated with DVM than is body morphology. Studies of *Metridia lucens* and *Calanus finmarchicus* [16] suggested that more elongate species have a faster avoidance speed from predators, which leads to a lower susceptibility to predation, thus explaining the tendency of more elongate species to forego DVM. Bollens [2] determined that the extent of DVM in certain marine copepods may correlate with abundance of planktivorous fish. Some work has been done on horizontal, as well as vertical, migration [24].

While plankton typically migrate upwards at dusk and downwards at dawn, reverse migration may reduce the risk of being eaten by non-visual predators, who feed in the upper strata at night [34]. Chae [4] studied the vertical distributions and diel vertical migrations of sapphirinid copepods in tropical and subtropical waters of the eastern Indian Ocean, South China Sea and western Pacific. Three groups of species were recognized with regard to their patterns of vertical distribution, with clear reverse DVM observed in many of the upper epipelagic species and to some extent in lower epipelagic species. The iridescent color of the males and distribution of light in the ocean suggests that daytime distribution of sapphirinids are determined by underwater light conditions. In addition, the well-developed eye and iridescence of the males, as well as daytime shoaling, may be related to a mate-finding mechanism.

Model studies have also been performed. Harris et al [14] gives a good, re-

cent overview of both Lagrangian and Eulerian approaches to the modeling of spatial dyamics of plankton, while Kamykowski [21] focuses specifically on models of trajectories of marine dinoflagellates (generally applicable to all flagellated autotrophs) based on dinoflagellate propulsion system, swimming speed and swimming direction, including vertical migration. Han and Straskraba [13] investigated the modeling of vertical migration as a reaction to a minimum change in sensed predation pressure. Iwasa [20] used a habitat-selection game between predator and prey to investigate the hypothesis that zooplankton migrate to avoid predators that hunt by sight at the cost of reduced grazing on phytoplankton. Numerous studies varying in the extent to which they use observed data attempt to model particular organisms in specific locations.

Behavior is far from the only factor exerting influence on plankton and other aquatic organisms. Even if plankton were to exhibit no active behavior other than vertical migration, we would still need to take into account the hydrodynamics and properties of the water bodies in which plankton are found when trying to understand the causes and results of plankton movement. As well as influencing plankton behavior, different physical environments clearly affect plankton directly. In particular, channels linking rivers or embayments with some larger, external water body are often assumed to be areas of high throughput in which plankton would not be expected to be retained for any length of time (i.e., would have a low organismal 'residence time'). An understanding of an organism's residence time in a body of water requires an understanding of water flow and mixing as well as of the behavior of the organisms. Water motions in (channel-like) embayments are governed primarily by wind stress and a combination of density gradients and gravitational forces (as opposed to rotation of the Earth). The temperature dis-

tribution mainly determines the density field; the temperature is a result of many factors, including air-water exchange of heat, advective transport, and vertical turbulent mixing. In embayments with low water residence times, the lake that the embayment empties into can have a major effect on the physical behavior of the embayment. The temperature stratification in the lake, its vertical thermal structure, largely determines the quality of the water in the embayment, as it produces water stability, damping turbulent mixing, restricting the vertical flow of oxygen and in other ways affecting the biomass productivity.

Migration behaviors need to be considered to gain a better understanding of overall ecosystem function, including the importance of endogenous versus exogenous influences on zooplankton movement. Plankton is at the base of the food chain and therefore zooplankton in large lakes largely determine the health of the ecosystem in the lakes, including a channel's potential for algal blooms as well as the behavior of its fish. Motivated by large amounts of zooplankton found in moderate-to-fast-flowing channel-like embayments (freshwater estuaries) [7, 15], we ask whether zooplankton in this type of environment can somehow avoid being flushed out of the system (as opposed to simply reproducing quickly enough to sustain a steady population in the embayment). The embayment environment, compared to the lake into which it empties, is likely warmer and more nutrient-rich, potentially leading to a higher growth rate, among other benefits. Thus, if zooplankton behave in ways so as to take advantage of the physical environment of the embayment, they might increase their retention time and have a distinct advantage over unadapted zooplankton. 'Drift paradox' refers to the seemingly contradictory fact that some weakly swimming organisms can avoid being carried along by largely unidirectional flow. In this paper, we focus on understanding the

extent to which biological processes can counteract physical drivers to solve the drift paradox; specifically, how zooplankton vertical migration behaviors affect biological retention time under a number of different freshwater channel flow regimes and whether a combination of flow type and biological behavior can allow organisms to stay in the channel 'indefinitely'. We take a first step toward answering these questions by combining a three-dimensional hydrodynamic model of shallow water flow, SI3D [27, 29], with an individual-based post-processing particle tracking module, ptrack [27], in order to investigate zooplankton residence time in a channel under a variety of flow regimes.

2.3 Methods

2.3.1 Hydrodynamic Model

Hydrodynamic flows were modeled using SI3D [27, 29], a semi-implicit three-dimensional hydrodynamic and transport model for lake environments. (See Chapter 1 for a more thorough description of SI3D.) While a number of codes are available to perform similar modeling, SI3D is easy to obtain, relatively simple to use, and the semi-implicit nature of SI3D allows the maximization of computational efficiency and the minimization of numerical dissipation. The embayment size and shape for this study is based on the bathymetry of Floodwood pond, a distinct and enclosed lake-level embayment on the eastern shore of Lake Ontario. For the sake of simplicity and numerical accuracy, we retained the general length, width, and depth of the main channel of water flow through Floodwood pond, but used an exactly rectangular geometry (1400m long, 10m wide, and 3m deep). The embayment of interest is embedded in a much longer simulation channel (ultimately a channel

length of 124,000m was decided upon); this length was chosen to avoid issues with channel flow encountering either the western or eastern boundary, possibly generating unphysical oscillations that could artificially affect simulation results. Thus, this extended channel is simply a device for avoiding possible boundary effects. Figure 2.1 shows a schematic of the simulated channel and the embayment's position within the channel. Note that distance down the channel is measured from west to east; the part of the channel representing the embayment of interest starts approximately 83,000 m from the westward end of the simulation basin and 40,000 m from the eastern end of the simulation basin.

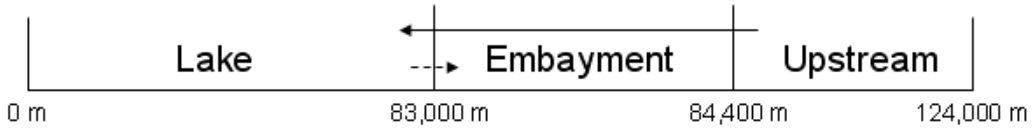

Figure 2.1: Sideview of the computational channel, showing the relative position of the study embayment. The solid arrow denotes westward background flow, while the dashed line represents potential lock-exchange flow.

Field data from Lake Ontario embayments suggest that water from Lake Ontario can flow into embayments and, correspondingly, water from its embayments can enter the lake. A possible mechanism for this type of water movement, so-called exchange flow, which may serve as a means of retaining zooplankton in an embayment, is a temperature difference between the embayment and the lake, with the lake, a larger, deeper body of water, having the colder temperature in mid-to-late summer (see Chapter 1). This type of hydrodynamic regime was implemented at the beginning of each SI3D simulation through the initiation of a dam break at the mouth of the embayment; a dam-break, or lock-exchange, involves fluids of different densities (in this case due to temperature differences) that are sepa-

rated by a vertical barrier, or lock gate. When the vertical barrier is removed, the extra weight of the denser fluid induces a larger pressure in this fluid than in the lighter fluid ahead, causing the denser fluid to flow along the bottom of the channel, underneath the lighter fluid, which flows in the opposite direction along the top of the channel. Thus, exchange flow develops, and at lower speeds it can persist, with colder water flowing upstream along the bottom of the channel at the same time that warmer water is flowing out the top. In the case of no background flow, Benjamin's classic gravity current result [1] gives an approximate velocity for both upstream and downstream currents of $U = \frac{\sqrt{g'H}}{2} \approx 0.0759$m/s, where H is the channel depth and $g' = g(\rho_2 - \rho_1)/\rho_2$ for $\rho_2 < \rho_1$ is reduced gravity [1]. Flow speeds in this study range from almost no flow, 0.0006m/s, at which the lock-exchange flow would be expected to dominate the background flow, to relatively fast flow of 0.0822m/s, at which the background flow should be dominant. The simulation is run for approximately five days before particle tracking is begun to allow baroclinic adjustment of the density field and to allow the interplay between the background flow and the flow induced by the dam break to stabilize.

Figure 2.2 shows the walls of water of different temperatures on each side of the 'dam,' along with qualitatively typical velocity and temperature profiles for high and low background flow speeds after virtual steady state has been reached. Gray scale indicates temperature, while direction and size of arrows indicate direction and magnitude, respectively, of flow. In the low flow case, exchange flow occurs in an essentially stratified channel, while for the high flow case, the warmer water has pushed the colder water out the end of the channel and all of the water is flowing in one direction.

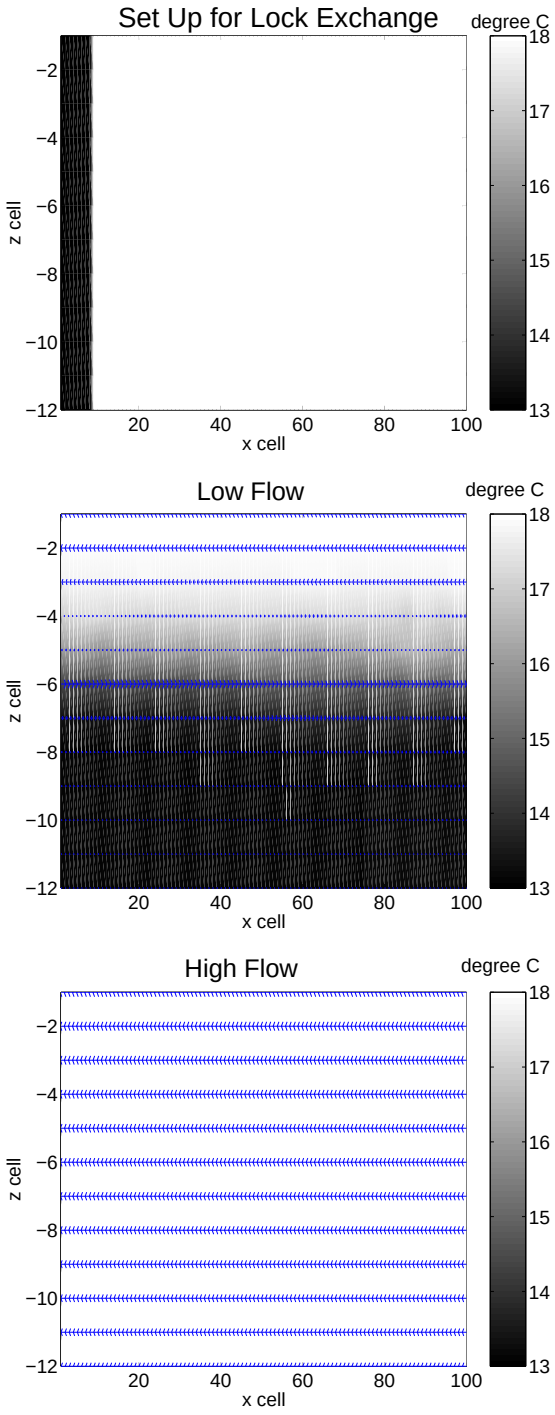

Figure 2.2: Figures showing, for part of the simulation region, the region before the 'dam break,' along with the steady flow regime after dam break, for a low flow (0.06 cm/s) and a high flow (8.22 cm/s) case. Shades of gray indicate temperature, while arrows indicate direction and relative magnitude of velocity.

Turbulence can greatly affect mixing and circulation in estuaries. In a natural flow situation with nonsmooth boundaries and moderate flow speed, accounting for turbulence can be assumed important in order to achieve qualitatively accurate results. (At typical embayment temperatures and lowest flow speeds considered, the Reynolds number is about 1800, transitional between laminar and turbulent flow.) In SI3D, we used the Smagorinsky model [28] to determine horizontal eddy coefficients and the Kantha and Clayson formulation of the original Mellor and Yamada 2.5 second moment closure two-equation model to determine vertical eddy viscosities and diffusivities. The Kantha and Clayson model, like MY2.5, generates an essentially parabolic eddy coefficient profile, but is more numerically stable than MY2.5, includes recent findings from LES models to improve the modeling of terms in the second-moment closure, and resolves MY2.5's problem of inadequate mixing [35, 3]. This grid-scale turbulence model was complemented by subgrid-scale turbulence in ptrack by means of a random step term added to the particle position in each coordinate direction at each time step. This random step was calculated based on the vertical eddy coefficients output from SI3D and constant horizontal coefficients computed in ptrack [9]. See Chapter 1 for a more detailed discussion of computation of turbulent eddy diffusivities.

2.3.2 Zooplankton Modelling

Zooplankton populations can be modeled either as populations in an advection-diffusion model or as individual particles in an i.b.m. (individual based model). While using the advection-diffusion approach would have been computationally efficient, it is not clear how amenable this essentially Eulerian scheme would be to the inclusion of individual zooplankton behaviors. Using an individual based

model in which individual particles are followed (Langrangian approach) is naturally suited for modeling organisms that may exhibit a wide range of behaviors and that may interact with each other, and allows for the inclusion of aggregating or disaggregating behaviors of the zooplankton based on social factors [38, 10, 11]. An add-on to the SI3D model, ptrack, uses velocities computed in SI3D to simulate the motion of passive particles. We modified ptrack to allow migration behavior.

Using ptrack and a source of organisms in the form of a plankton cloud, we modelled three basic types of migration behavior: 1) no migration, 2) 'normal' vertical migration, and 3) 'reverse' vertical migration. Case 1) is equivalent to passive particle tracking, while cases 2) and 3) involve movement from a specified location in the upper stratum to a specified location in the lower stratum and vice versa depending on the time of day; 'normal' migration means that organisms descend in the water column during the day and ascend at night and 'reverse' migrators follow a complementary schedule. In addition to the different types of migration, we also investigated the impact of various starting sizes of zooplankton clouds.

Ptrack simulations involved four parameters: background flow rate, start time, migration type, and standard deviation of the initial zooplankton cloud size. Eighteen flow rates were used, ranging in magnitude from 0.018 to 2.466 m^3/s, corresponding to a range in velocity of 0.06 cm/s to 8.22 cm/s. Start times were midnight, 8 am, and 4 pm, while migration types were either normal, reverse, or no migration. Initial zooplankton clouds were spherical, with approximate diameters of 1/4, 1/2, or 2/3 of the water column height; these values were chosen to constitute the range of plankton cloud sizes observed in the field [23], [26], [5], [36], [17], [18]. A cloud of 250 zooplankton was centered in the middle of the channel laterally

and at such a depth or height, depending on the combination of the migration and start time parameters, as to just allow the cloud to remain completely in the water column, while in the longitudinal direction, the mean of the zooplankton cloud was set to be at the upstream beginning of the embayment. For each combination of flow rate and start time, SI3D generated a binary file containing the velocities at each computational grid point at each output time. This file was then utilitized by ptrack to perform particle tracking for all combinations of migration type and zooplankton cloud size standard deviation.

For each simulation, zooplankton trajectories were monitored and quantified in several ways, including average biological residence time and number of zooplankton remaining in the channel over time. For each flow scenario, the behaviors of organisms under the various migration strategies were compared to determine if they had substantially different retention times when using the different strategies and whether the effect of migration type changed with flow speed. A multiple regression analysis, quantifying the effect of each parameter, allowed them to be ranked according to their contribution to the variance of zooplankton residence times, with the ultimate goal of determining which combination of parameters led to the greatest biological residence time in the channel.

2.3.3 Model for Individual-Based Zooplankton Behavior and Transport

Passive Particle Tracking

The Lagrangian, or particle tracking, method represents particle position by the sum of successive particle displacements over time and is a highly accurate way

of numerically solving the advection-diffusion (transport) equation [8]. Following Dunsberger and Stelling [8], each displacement can be described by a stochastic differential consisting of a deterministic part (the first term below) and a stochastic part (the second term below):

$$dx_i = a_i(\mathbf{x}, t)dt + \sum_{j=1}^{3} b_{ij} dW_j(t), \tag{2.1}$$

where $\mathbf{x} = (x, y, z)$ is the particle position and $W_j(t)$ represents the Wiener process, or Brownian motion. $W_j(t)$ is simulated using a Gaussian number generator, with a mean of 0 and variance determined by the time step. In addition, a_i and b_{ij} must satisfy the following equations for consistency with the advection-diffusion equation describing the transport of mass [6], [8], [33], [19], [22]:

$$a_i = u_i + \sum_{j=1}^{3} \frac{\partial D_{ij}}{\partial x_j} \tag{2.2}$$

$$1/2 \sum_{k=1}^{3} b_{ik} b_{jk} = D_{ij}, \tag{2.3}$$

where u_i is velocity, a_i is drift, b_{ij} is stochastic influence, or noise [8],[30], and D_{ij} is diffusion, which is assumed to be horizontally isotropic. Thus, the deterministic component of the displacement is influenced by the local velocity and the gradient of the turbulent diffusivity, and the stochastic component requires the diffusivity. These quantities, namely the velocity field and the (vertical) eddy diffusivity, are available from SI3D output and allow the use of ptrack as a post-processing tool. The horizontal eddy diffusivity is treated as a constant for the purposes of particle tracking and computed based on Fischer et al [9].

Ptrack tracks particles in each of the three coordinate (x, y, z) directions separately. Thus, adding zooplankton behavior in the vertical direction was a relatively

simple task. Drawbacks of this method include the strong dependency of the solution accuracy on the number of particles simulated [19] and the need to simulate a time much longer than the Lagrangian time scale to avoid an overestimation of diffusion [25]. The particles in ptrack are assumed to be neutrally buoyant. The code includes a reflection algorithm that relocates particles in the water body when they run into physical boundaries, so that no mass is lost during particle tracking. After advecting each particle, ptrack also includes a drift subroutine, which adds the effect of the variation of diffusion coefficients in the vertical particle displacement, as well as a random step, representing particle displacement due to turbulence.

2.3.4 Modifications for Modelling Zooplankton Behavior

Ptrack modifications enable model particles to exhibit 'behavior' at appropriate times in the z (vertical) direction, instead of being passive tracers. Specifically, zooplankton behavior consists of vertical migration, with zooplankton either not migrating vertically at all (the 'no migration' case), migrating down in the water column at dawn and up at dusk (the 'normal migration' case), or migrating up in the water column at dawn and down at dusk (the 'reverse migration' case). Vertical migration takes place between 5:30 am and 6:00 am and between 8:30 pm and 9:00 pm, with plankton moving with a constant step size so that the movement is divided evenly over the half hour, until each plankter's preferred height, or depth (see below), as appropriate, is reached. The algorithm for tracking passive particles can be modified to account for this vertical migration behavior as follows.

The deterministic displacement of a particle requires the local flow velocity, as well as the space-varying diffusivity. As the particle positions do not often coincide

exactly with the nodes used in the hydrodynamic model, a method for finding a continuous velocity field, along with continuously defined diffusion coefficients, is needed. A first order finite difference scheme can be used to find the desired diffusion coefficients, but because it does not ensure that the continuity equation is satisfied at each point in space, such a method cannot be used to find a continuous flow field. Instead, again following Dunsbergen and Stelling [8], we write the continuous extension of the flow field as

$$u_i^{ext}(\mathbf{x},t) = \left(\frac{\partial u_i}{\partial x_i}\right)_{num} x_i + (u_i|_{x_i=0})_{num} \equiv A_i x_i + B_i,$$

where A_i refers to the numerical implementation of $\partial u_i/\partial x_i$. The divergence of the continuous extension of the discrete velocity field = 0, showing that a mass conserving hydrodynamic model implies a mass conserving advective particle tracking step. The streamline through a particular point $\mathbf{x} = \mathbf{x}_p$ can now be found by solving the following ordinary differential equation:

$$\frac{\partial x_i(t)}{\partial t} = u_i^{ext}(\mathbf{x},t) \tag{2.4}$$

$$x_i(t_0) = (\mathbf{x}_p)_i, \tag{2.5}$$

or, in one dimension:

$$\frac{\partial x}{\partial t}(t) = Ax + B \tag{2.6}$$

$$x(0) = x_p, \tag{2.7}$$

Distinguishing between the case $A \approx 0$ and $A \neq 0$ in order to avoid problems with machine dependent rounding off error, and defining $C = B/A$, we can easily solve for $A \neq 0$:

$$x(t) = (x_p + C)exp(At) - C$$

and for $A = 0$:

$$x(t) = Bt + x_p \tag{2.8}$$

Dunsbergen and Stelling [8] demonstrate that the numerical particle displacements found this way can be no more accurate than the accuracy of the physical quantities computed from the hydrodynamic model. This streamline can then be used to determine the time to exit one computational cell and enter another as well as the exit point [8].

To implement plankton vertical migration, A may be set to 0 and B may be set to be the velocity at which the plankton need to move vertically in order to complete their migration in the time allotted. By equation 2.8, $x(t)$ will equal the distance to move vertically added to the original location in the z-direction. This modification is only applicable to vertical movement.

To prevent zooplankton from penetrating the channel bottom or water surface, at the beginning of the prack simulation each zooplankter is assigned a 'preferred' height and depth and upon reaching this height and depth, a flag is set and further migration is prevented for that organism (although passive advection of the zooplankter is allowed to take place; otherwise, the implication would be that the zooplankton were actively resisting the water movement). These preferred heights and depths were chosen, independently from each other for each zooplankter, from a normal distribution whose standard deviation was the same as for the initial zooplankton cloud. In addition, the possible time for migration was extended slightly

past half an hour in case advection took the zooplankton closer than expected to either surface or bottom so that after a half hour of migration the preferred locations had not been reached. At the end of each vertical advective step, the new z-position of the zooplankter is checked and if it is above the water surface or below the bottom of the channel, it is set back to the preferred height or depth, as appropriate. Similarly, after each migration step in the z coordinate direction, the new value for z is tested against the preferred height or depth as appropriate and if it is too small or large, respectively, it is reset to the preferred value.

2.3.5 Testing

The SI3D simulations used a cell size of 0.25 m in the vertical direction and 10 m in the lateral direction. With this cell size, the channel required one cell in the lateral direction and 24 cells in the vertical direction, which should allow a reasonable resolution of the vertical distribution of the flow and plankton density. This lateral resolution is appropriate as the dynamics of interest in the study system are primarily two-dimensional. Zooplankton migration, which acts primarily in the vertical direction, and advection by the water, which acts primarily in the longitudinal direction, are the chief forces acting on the zooplankton, and the speed of the zooplankton longitudinally down the channel is our primary concern.

To determine an appropriate size for computational cells in the x-direction, simulations were performed using cell lengths of 50 meters and 25 meters at both the slowest simulation flow speed and the fastest simulation flow speed, and the results were compared in terms of scalar transport. The channel length used in these simulations was the original length of 59,950 meters, which guaranteed that under the highest flow speeds no zooplankton would reach the downstream boundary and

thus boundary effects should not be a problem.

The results for these two speeds appear in Figures 2.3 and 2.4. The plots show approximately 5000m of the simulation channel, including the output to the lake, in the left side of the graph, where the initial lock exchange occurs. Due to Courant-Friedrichs-Lewy (CFL) constraints, which require the time step in any time-marching computer simulation to be less than the time taken for fluid to travel across a computational cell, the time step was halved to achieve stability for the fastest flow/25 m case. By inspection of graphs such as these, 50 m cells were judged to be adequate for our purposes.

In addition, the size of the cells in the y-direction was investigated to assure that a channel width of one cell was appropriate, allowing us to look at the problem two-dimensionally instead of in three dimensions. Simulations were performed using cell widths of 5 meters and 10 meters, again at both the slowest and fastest simulation flow speeds (Figures 2.5 and 2.6). At the faster speed, the difference between simulations using two versus one cell in the lateral direction is quite noticeable close to the mouth of the channel, but as very little of this area is part of the embayment of interest and the additional computational expense incurred in increasing the lateral granularity would be considerable, we decided to retain the lateral cell size of 10 m.

Although the simulation results using the approximately 60,000 m long channel appeared reasonable, after making some changes in the SI3D simulations, most notably with respect to vertical turbulent diffusivity calculations, we were concerned that the steady movement of the colder water up the channel bottom and out the upstream boundary - an effect which was not seen in earlier simulations - would interact with the flow boundary condition at the upstream end of the channel,

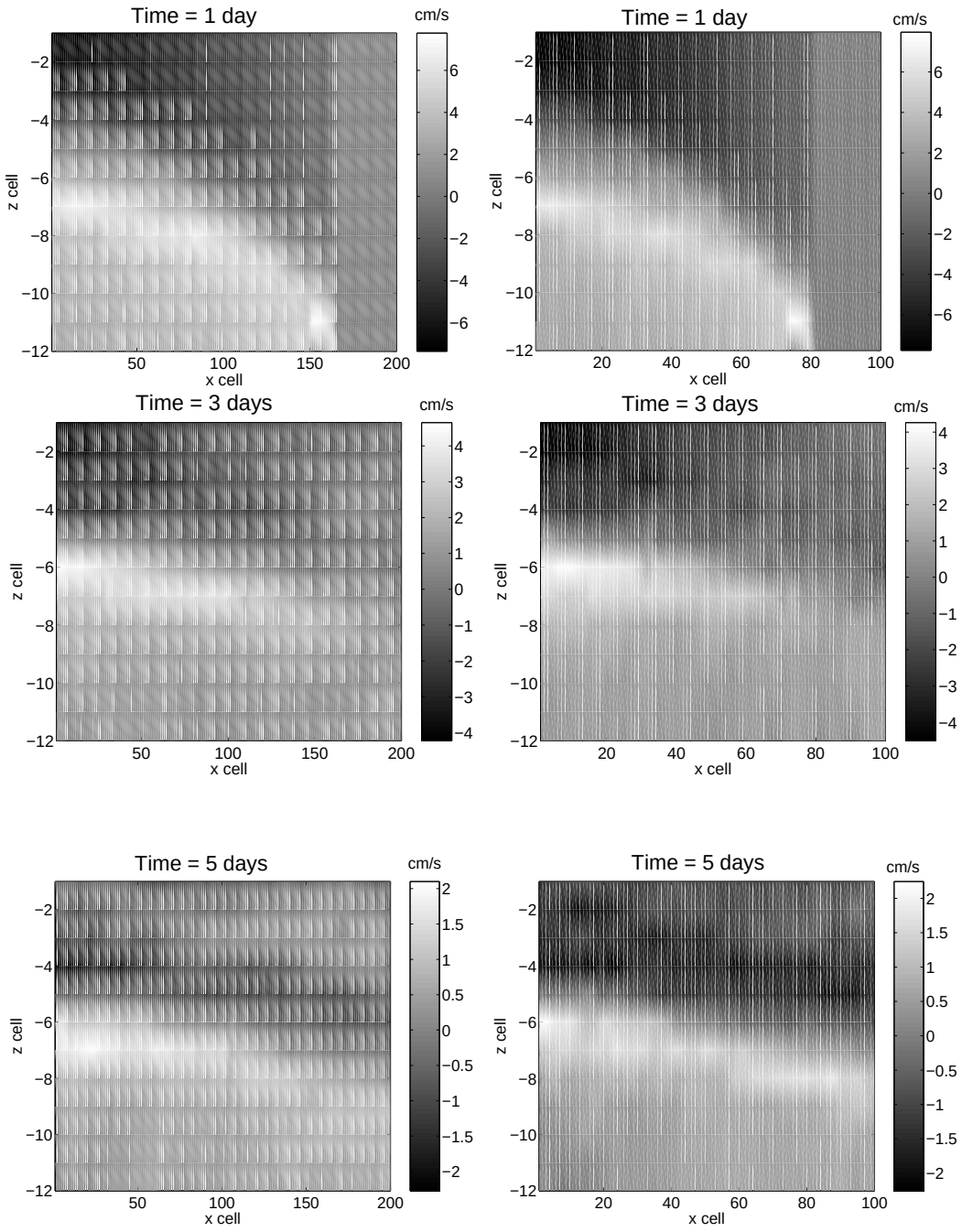

Figure 2.3: Velocity fields in the x-z plane for the slowest flow speed at 2 day intervals, for cell lengths of 25m (left column) and 50m (right column), respectively.

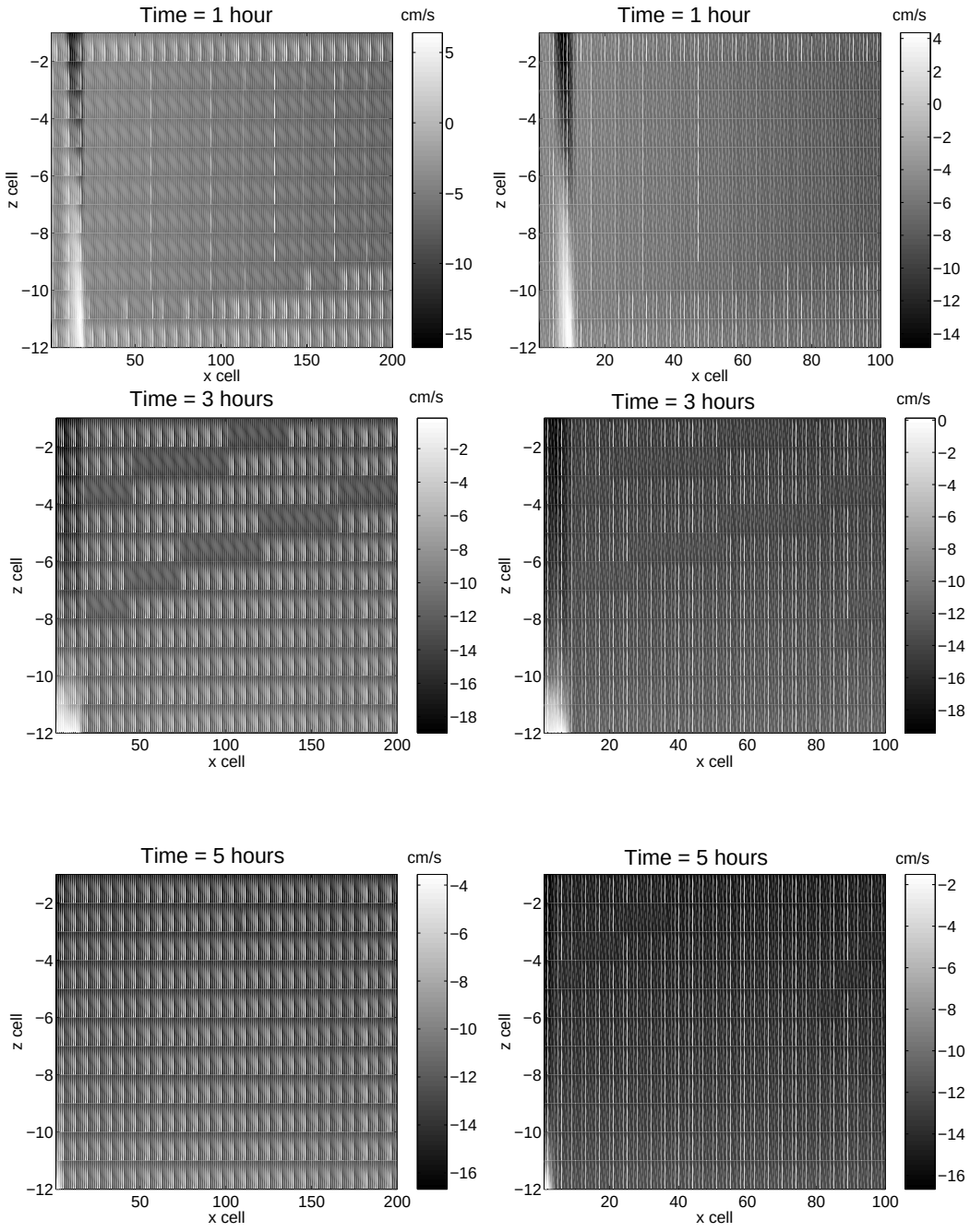

Figure 2.4: Velocity fields in the x-z plane for the fastest flow speed at 2 hour intervals, for cell lengths of 25m versus 50m, respectively.

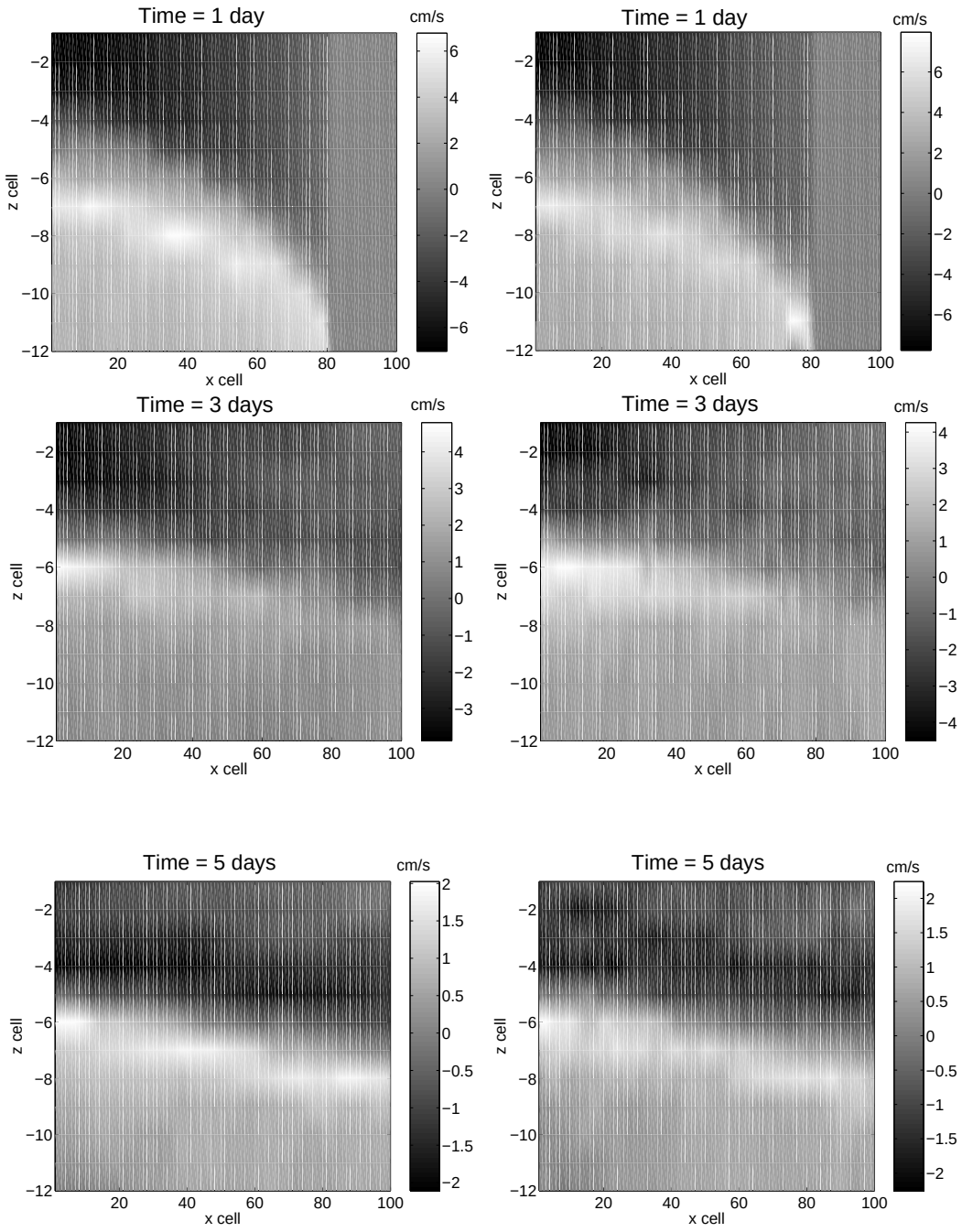

Figure 2.5: Velocity fields in the x-z plane for the slowest flow speed at 2 day intervals, for cell widths of 5m versus 10m, respectively.

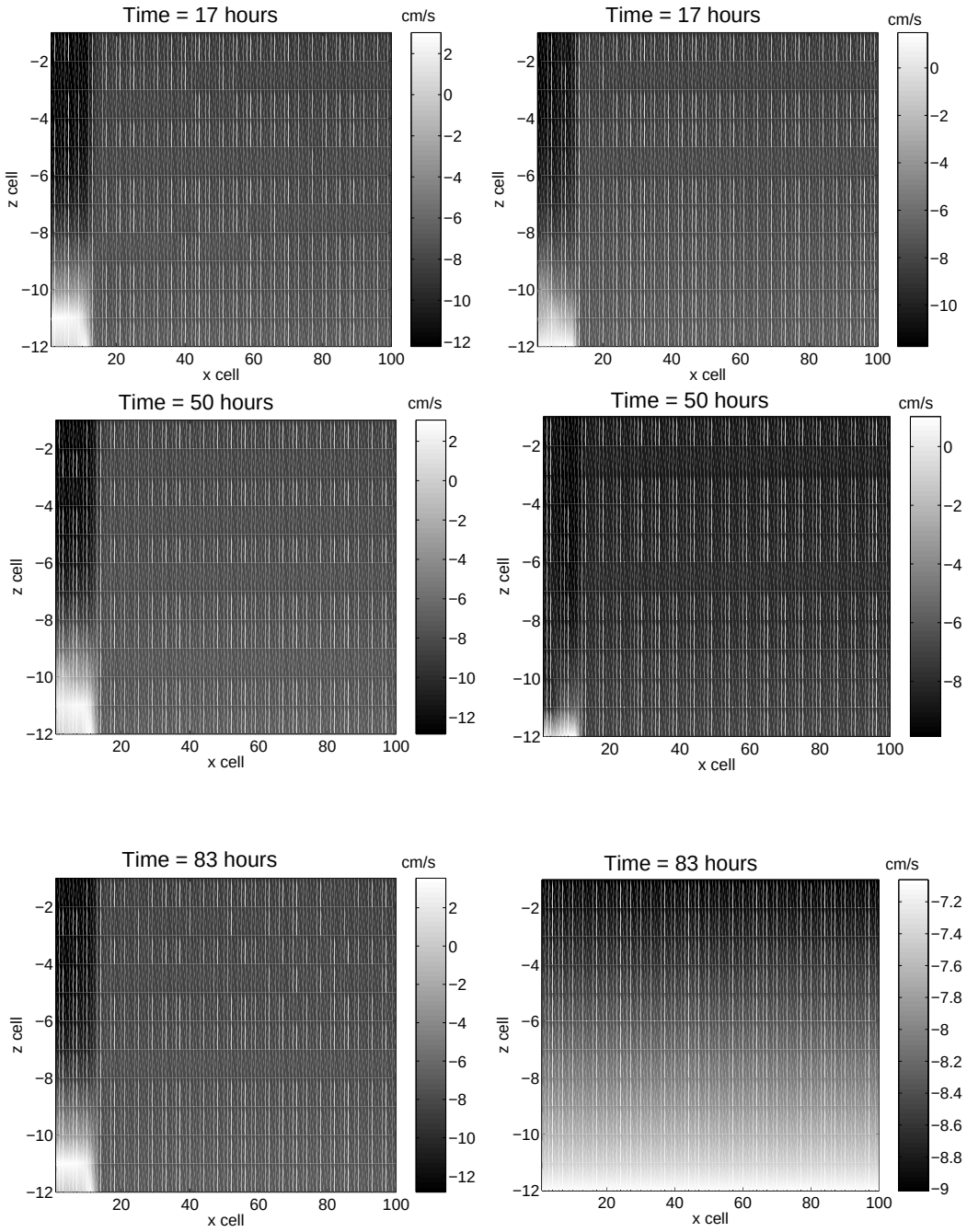

Figure 2.6: Velocity fields in the x-z plane for the fastest flow speed at 33 hour intervals, for cell widths of 5m versus 10m, respectively.

causing cold water to hit the boundary and 'bounce back' into the channel. To prevent this occurrence, we increased the overall length of the simulation channel to 124,000 m and relocated the 1400 m embayment of interest so that no water from this region would be able to reach either the western or eastern boundaries and reenter the embayment during the time of the simulation. Simulations again using the slowest and fastest flow speeds and the same simulation times as before were run using this extended channel, with the results shown in Figures 2.7 and 2.8. While the results for the slower flow speed look qualitatively similar, the flow speeds are larger and reach a relative steady state more quickly in the case of the extended channel. At the faster flow speed, the cold water is not pushed out of the channel as quickly as it is in the case of the shorter channel, but the flow eventually becomes uni-directional.

2.4 Results

Figure 2.9 shows a plot of the steady state east-west velocity profile in cm/s for three different background flows: a 'slow' speed, 0.06 cm/s, an 'intermediate' speed, 4.38 cm/s, and a 'fast' speed, 8.22 cm/s. The axes are labeled using cell number instead of length in meters, but the area in each figure is the same as in the zooplankton trajectory figures (Figures 2.11, 2.12, 2.13, 2.15). The flow induced by lock-exchange under the slow and intermediate background speeds is clear here and persists throughout the area shown, with water flowing to the west in the top half of the channel and to the east in the bottom half. As the background flow speed increases, a greater proportion of the water column carries water westward and at higher speeds, while the colder water at the bottom decreases in speed. At the highest background velocity, the background flow eventually nullifies any effect

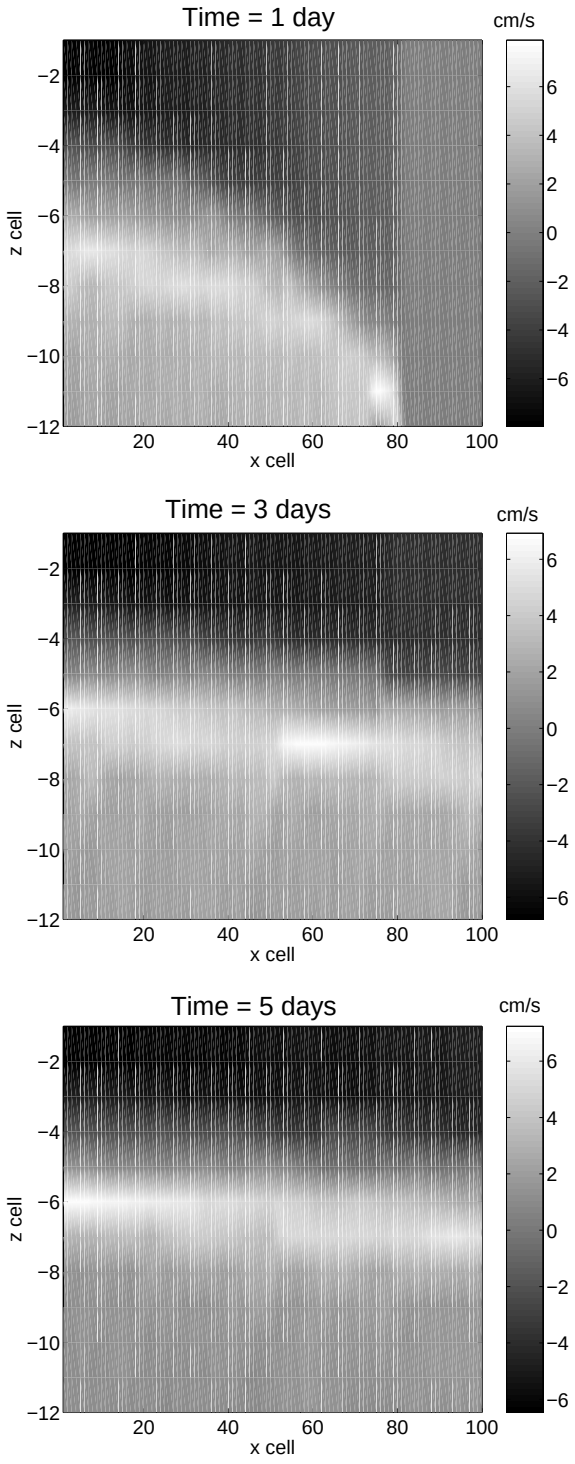

Figure 2.7: Velocity in the x-z plane for the slowest flow speed at 1, 3, and 5 days, respectively, for a cell length of 50m, using the extended channel.

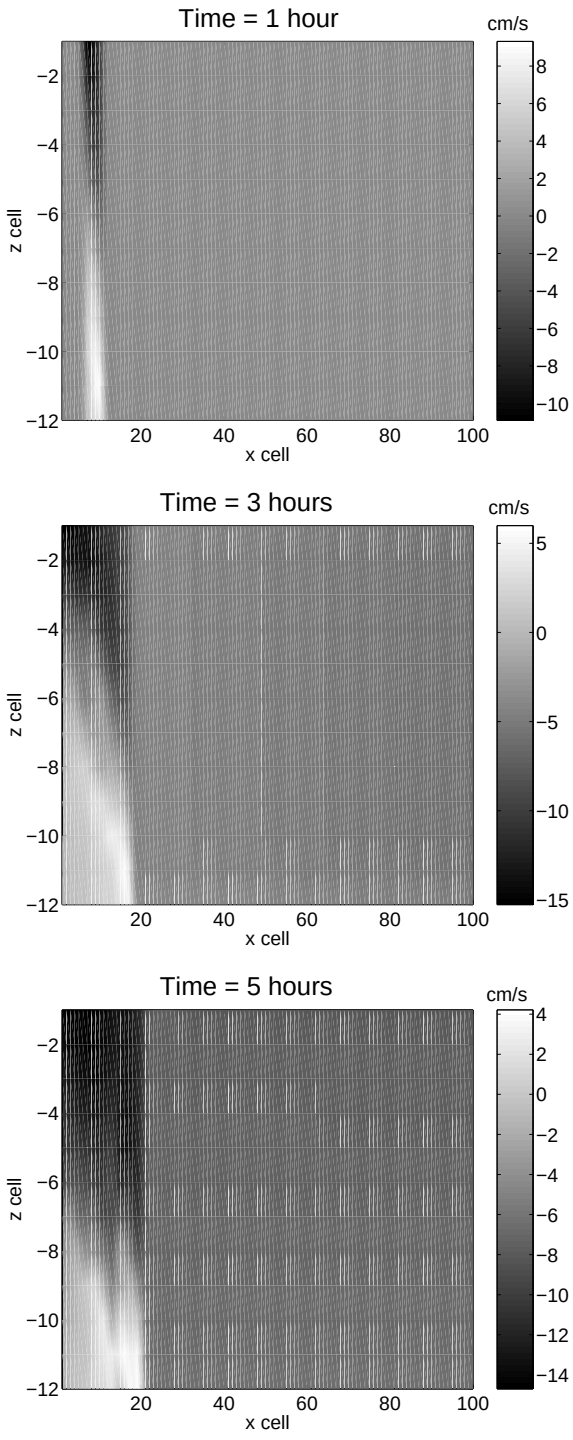

Figure 2.8: Velocity in the x-z plane for the fastest flow speed at 1, 3, and 5 hours, respectively, for a cell length of 50m, using the extended channel.

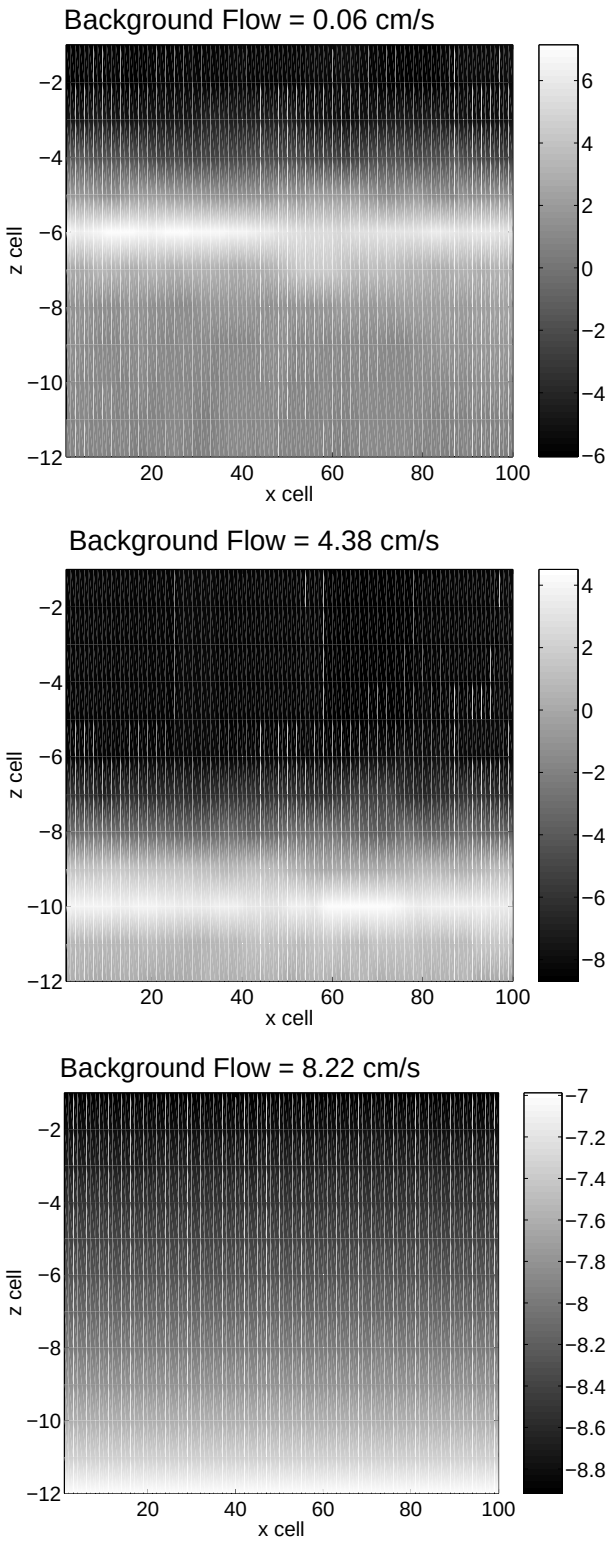

Figure 2.9: Steady flow field for background flow of 0.06 cm/s, 4.38cm/s and 8.22 cm/s. Colors in the colorbar are in cm/s and display east-west flow.

of the lock-exchange, pushing water from east to west throughout the water column after an initial transient (not shown here) at approximately the background flow speed, although flow is retarded at the bottom due to drag. Note that this mean flow under the high background flow rate is greater than the expected plume speed of 7.59 cm/s generated by a lock-exchange. A difference in biological residence time under the two lower flow rates versus the high flow rate can logically be imputed to the difference between uni-directional versus exchange flow. Figure 2.10 shows the steady state for a speed between the intermediate and high flow speeds, at which a small exchange flow occupies the western part, and unidirectional flow the eastern part, of the channel.

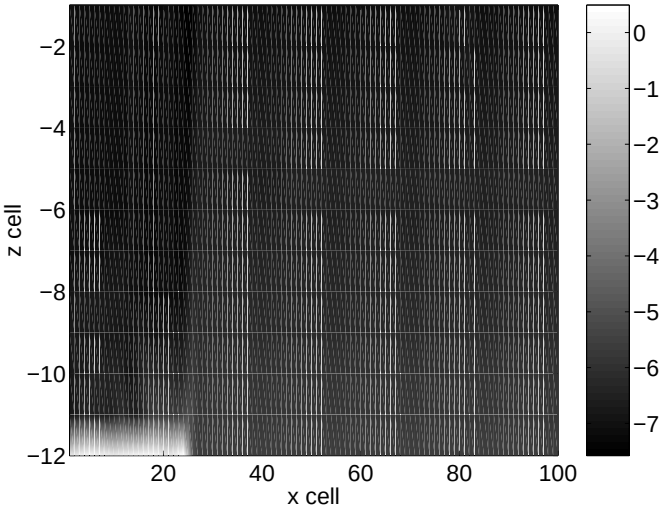

Figure 2.10: Steady flow field for background flow of 6.3 cm/s. Colors in the colorbar are in cm/s and display east-west flow.

Figures 2.11, 2.12, 2.13 show typical plots of the beginning paths of the zooplankton clouds under the three different migration schemes: no migration, normal migration, and reverse migration. Each figure shows paths for each of the three flow speeds represented in the previous velocity field graphs. Zooplankton clouds

all start with their means in the x-direction set at 84,400 m and the channel empties into the lake at 83,000 m. As flow speed and migration type are assumed to be the most important factors affecting biological residence time, the starting time and initial zooplankton cloud standard deviation values are kept constant at midnight and the middle value for standard deviation (see Section 2.3.2) in these figures. Darker shades represent earlier time periods, with color getting lighter with passing time. Cloud position is plotted every 2.5 hours, beginning with midnight. At midnight, zooplankton that are non-migrators or normal migrators are located at the top of the water column, while zooplankton that are reverse migrators are located at the bottom of the water column.

When the zooplankton do not vertically migrate (Figure 2.11), the cloud basically moves straight down the channel, and in at most 15 hours, under any background flow speed, at least some of the zooplankton are gone or leaving the embayment. The background flow at 0.06 cm/s is clearly dominated by the lock-exchange induced flow; flow is faster toward the top of the water column, although not as fast (7.59 cm/s) as under a pure lock-exchange flow (see Section 2.3.1) and slower toward the middle, which produces some shear in the zooplankton cloud. Although lock-exchange flow still exists in the intermediate flow speed case, the zooplankton cloud is unsheared and moving at an average speed of about 7.6 cm/s, the speed expected due to the lock-exchange. In contrast, at the high flow rate, the background flow quickly pushes the lock-exchange flow out of the channel and flow is always in the downstream direction; the embayment water is moving at approximately the same velocity throughout the channel in the vertical and the entire cloud moves as a cohesive unit (as is demonstrated conclusively after 2.5 hours when the turbulent diffusivity stretches the plankton cloud throughout the

water column). However, while the background flow appears to dominate the lock-exchange flow, the downstream velocity of the zooplankton cloud again appears to be approximately 7.6 cm/s, less than the background flow speed of 8.22 cm/s, demonstrating the complex interplay between background and lock-exchange flow. Only for much higher background flow speeds do we find a steady flow speed approximating the background flow speed.

When zooplankton migrate normally (Figure 2.12), the zooplankton cloud starts at the top of the water column. With a low background flow rate, the zooplankton cloud drifts downstream at first due to the exchange flow and then moves to the bottom of the water column at daybreak. At this point the zooplankton are carried upstream, but the previous migration upstream was sufficient so that the (mean) cloud at the end of the cycle is somewhat upstream from where it started; it is also much more spread out in the horizontal than it was initially due primarily to the shear experienced near the water surface. As shearing will continue to take place, some zooplankton will not be able to remain in the embayment indefinitely; however, this combination of parameters seems a promising strategy for the retention of a large number of the zooplankton. Under the higher background flow regimes, the zooplankton cloud still initially moves downstream but faster and with no shearing. The interaction of the faster background flow with the lock-exchange flow clearly results in a lessened shearing effect. While for the 4.38 cm/s background speed the zooplankton have time to migrate to the bottom of the water column and advance upstream to a certain degree before being advected out of the channel permanently, for the highest background speed, the zooplankton are simply advected out of the channel before they have a chance to undergo vertical migration (which wouldn't help retain them in the channel).

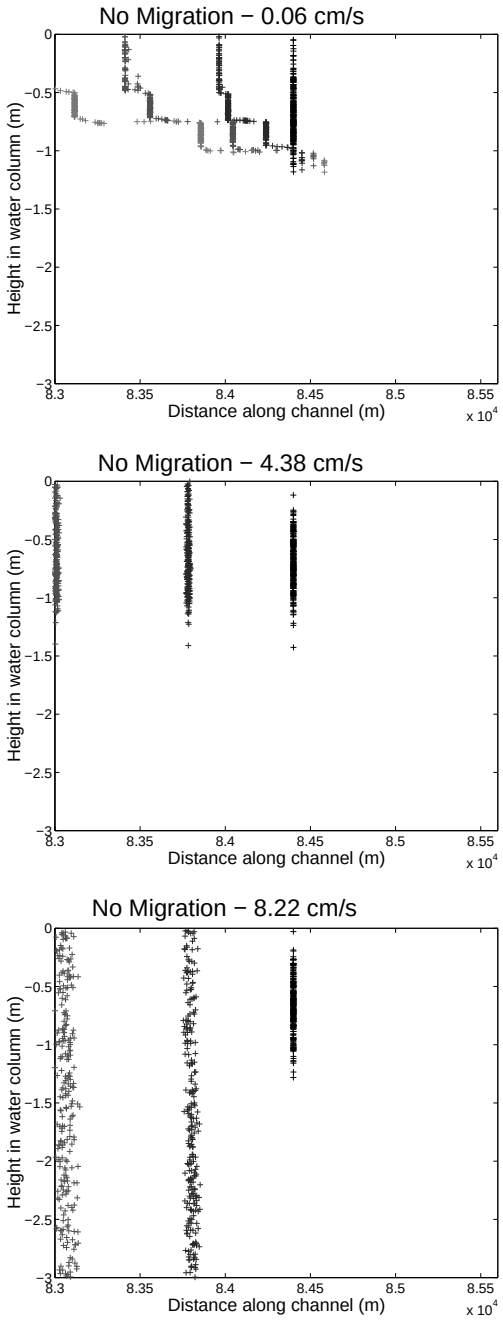

Figure 2.11: Zooplankton cloud movements with no migration, respectively, for background flow speeds of 0.06 cm/s, 4.38 cm/s, and 8.22 cm/s, respectively, starting at midnight, with moderate plankton cloud standard deviation. Lighter shades of gray indicate increasing time, with sequential zooplankton clouds representing increments of 2.5 hours. Background flow east to west.

When the zooplankton undergo reverse migration (Figure 2.13), for the low flow exchange-flow regime the zooplankton cloud starts out at the bottom of the water column and moves upstream a short distance before migrating up in the water column. By the time five more hours have passed, at least half of the zooplankton are too far downstream to be able to maintain the type of semi-stationary cycle that occurred under normal migration; each time midnight comes around, the zooplankton do not have enough time to recover their former upstream position before they have migrated upwards and are moving downstream again. Shear carries some plankton out of the channel early, but eventually all will be advected out of the embayment before the end of seven days. This result, compared with the previous result for zooplankton that migrate normally, is perhaps not surprising considering the fact that reverse migrating zooplankton are at the water surface during daylight hours, and the simulation assumes more daylight than dark hours per day. In the case of a 4.38 cm/s background speed, some of the zooplankton are carried slightly upstream from their starting location, while others are dispersed downstream, before all of the plankton migrate up in the water column and are advected out of the embayment. Under the highest background speed, as in the normal migration case, the zooplankton are simply advected out of the channel before they have a chance to undergo vertical migration. Under these higher speeds, the zooplankton cloud position in the x-direction at any particular time ends up about the same regardless of the migration type, and all zooplankton clouds leave the embayment at about the same time; clearly, migration has very little effect on biological residence time at this speed as the flow is uni-directional and differs little in the vertical.

The mean residence time for zooplankton under every combination of flow rate,

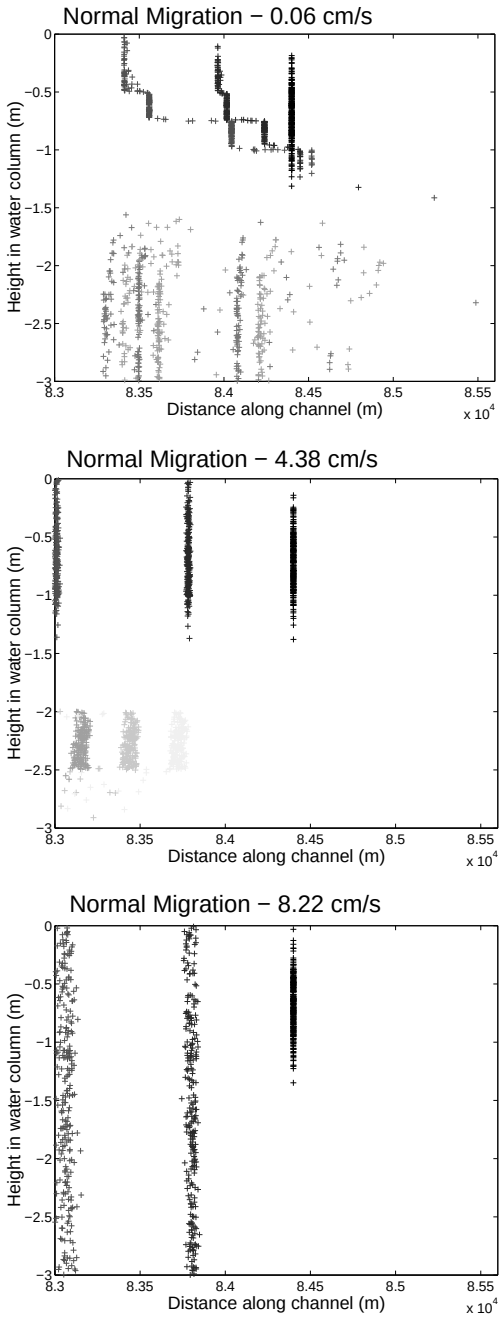

Figure 2.12: Zooplankton cloud movements under normal migration, respectively, for background flow speeds of 0.06 cm/s, 4.38 cm/s, and 8.22 cm/s, respectively, starting at midnight, with moderate zooplankton cloud standard deviation. Lighter shades of gray indicate increasing time, with sequential plankton clouds representing increments of 2.5 hours. Background flow east to west.

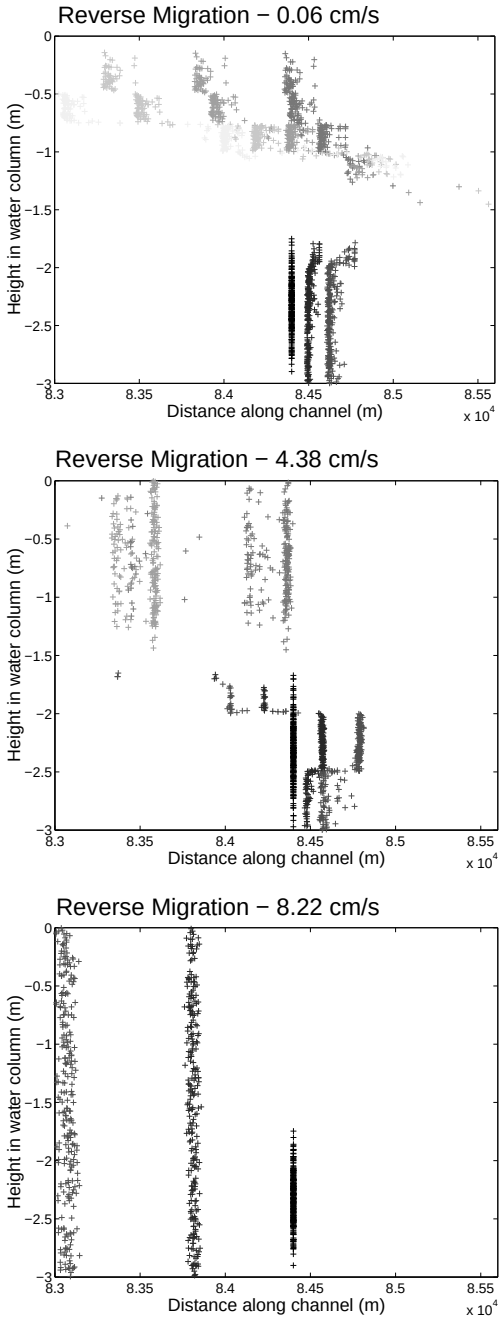

Figure 2.13: Zooplankton cloud movements under reverse migration, respectively, for background flow speeds of 0.06 cm/s, 4.38 cm/s, and 8.22 cm/s, respectively, starting at midnight, with moderate plankton cloud standard deviation. Lighter shades of gray indicate increasing time, with sequential zooplankton clouds representing increments of 2.5 hours. Background flow east to west.

start time, migration type, and zooplankton cloud size was computed in order to determine if these trends between migration type and biological residence time hold over the range of flow speeds investigated, as well as whether simulation start times and zooplankton cloud standard deviations have a significant effect on biological residence time results. Assuming conservatively that lake conditions are inhospitable and/or that the zooplankter might not be able to return to the embayment once in the lake, the first time that the zooplankton drifted through the mouth of the embayment and into the lake was taken as the residence time for the zooplankter. These times for all 250 zooplankton were then averaged to get a (mean) residence time in days. Figure 2.14 gives plots for each combination of zooplankton cloud standard deviation and start time demonstrating how each of the three migration types influences the average biological residence time across the range of flow speeds studied. As the simulation time was seven days, a mean residence time of seven days indicates that the zooplankton have avoided washout, at least on a small timescale.

Flow speed, migration type, and zooplankton cloud standard deviation all have a noticeable influence on biological residence time, although none of the conditions tested allowed all 250 zooplankton to remain in the embayment for the entire seven days. The effect of simulation start time, on the other hand, appears to be quite small. Not migrating in general leads to the lowest residence times, although the effect is negligible at moderate-to-high flow speeds. Reverse migrating always does somewhat better at retaining plankton in the embayment under low flow speeds than does not migrating, with the greatest effect occuring when the simulation starts at midnight or 4 pm. Furthermore, in most cases, undergoing normal migration at very low flows does the best job of keeping the zooplankton

in the embayment, with residence times that are as much as two days longer than under reverse migration, but at moderate flow speeds, a dropoff in residence time occurs and normal migration loses its advantage. Normal migration appears to have the biggest advantage for a start time of 8 am, due to the fact that simulations that start at 8 am allow the zooplankton to move upstream for 12 hours at the beginning of the simulation.

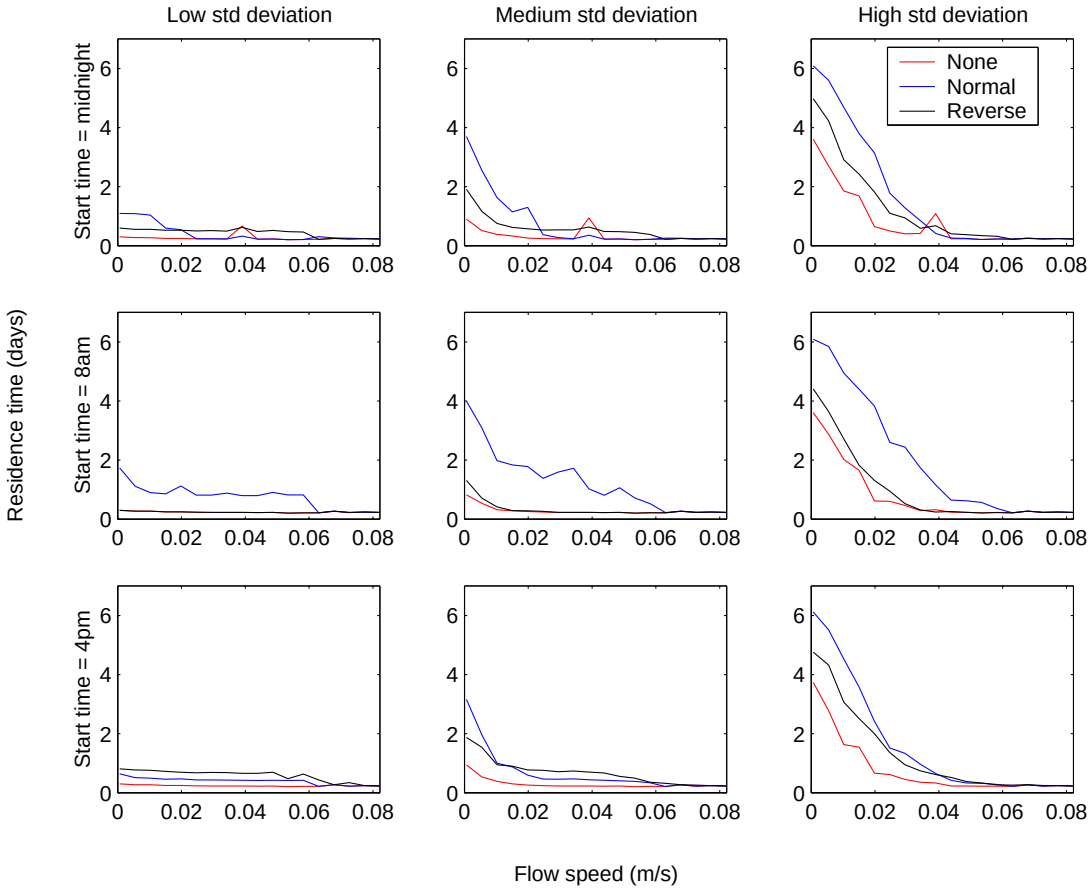

Figure 2.14: Background flow speed versus mean biological residence time by migration type for the nine zooplankton cloud standard deviation/start time combinations.

As flow speed increases, mean biological residence time tends to decrease, with the most difference in residence time found at the lower flow speeds. This decrease

is not strictly monotonic, due largely to the stochastic nature of the simulations. For all three standard deviation values, a spike in the biological residence time is seen at a flow speed of 3.9 cm/s. This speed is low enough to still allow exchange flow but high enough to produce a turbulent diffusivity that, together with the exchange flow, allows some particles to get caught in the upstream motion in the bottom of the channel and thus increases the mean biological residence time.

Zooplankton cloud standard deviation also plays an important role in determining biological residence time, especially at low flow speeds. Regardless of start time, all three migration types tend to increase their residence times at low flow speeds as standard deviation increases. Increasing standard deviation increases the amount of water column taken up by the cloud and potentially places some zooplankton in water flowing in the opposite direction from the rest of the group, and thus diversifies the movement of the plankton cloud as a whole. Figure 2.15 shows typical zooplankton movements for a start time of 8 am under normal migration at a flow speed of 0.06 cm/s. Note that for the sake of clarity, particle trajectories are only shown every 5, instead of 2.5, hours. As the standard deviation increases the zooplankton become more scattered, and in particular, the shearing effect in the upper half of the water column increases, spreading the zooplankton out in the x-direction along the channel and even carrying some east beyond the portion of the channel pictured. This shearing effect, combined with the exchange flow possible at these lower speeds, has the greatest effect for simulations with a start time of 8 am, due to the advantage of moving upstream along the bottom of the channel at the start of the simulations.

Migration times were set in ptrack to be appropriate for mid-summer in the Great Lakes region, resulting in a longer day than night. As other day lengths

occur in other locations and times, we decided to rerun the simulations using equi-length days and nights, with migration times of 7:30-8:30 am and 7:30-8:30 pm. The results are shown in Figure 2.16. Although flow speed and standard deviation have similar effects on biological residence as in the original simulations, now reverse migration vies with normal migration to give the higher biological residence times. Not surprisingly, reverse migration simulations produce higher residence times for simulations with start times allowing more night hours in the first 12 hours, namely simulations with start times of midnight and 4 pm.

While the mean residence time is informative, it only indicates the fate of the zooplankton cloud on average. Information about individual zooplankton trajectories is necessary to clearly determine the factors leading to zooplankton cloud residence time as a whole. To account for individual organisms, the number of zooplankton left in the embayment over time was plotted for background flow speeds of 0.06 cm/s, 4.38 cm/s, and 8.22 cm/s, along with all migration types, start times, and zooplankton cloud standard deviations. From the previous plots of biological residence time, migration might be expected to promote retention in the embayment at lower flow speeds but not higher speeds.

In the low flow speed/midnight start time case shown in Figure 2.17, non-migrators do the worst job of staying in the embayment at all standard deviations. The most zooplankton remain in the embayment for normal migration and a large zooplankton cloud. Reverse migrators do better than non-migrators but not nearly as well as normal migrators. Initial cloud standard deviation has a big effect on the number of zooplankton that remain in the embayment for all seven days; as standard deviation increases, more zooplankton survive until the end of the simulation. Low standard deviation zooplankton clouds leave the channel

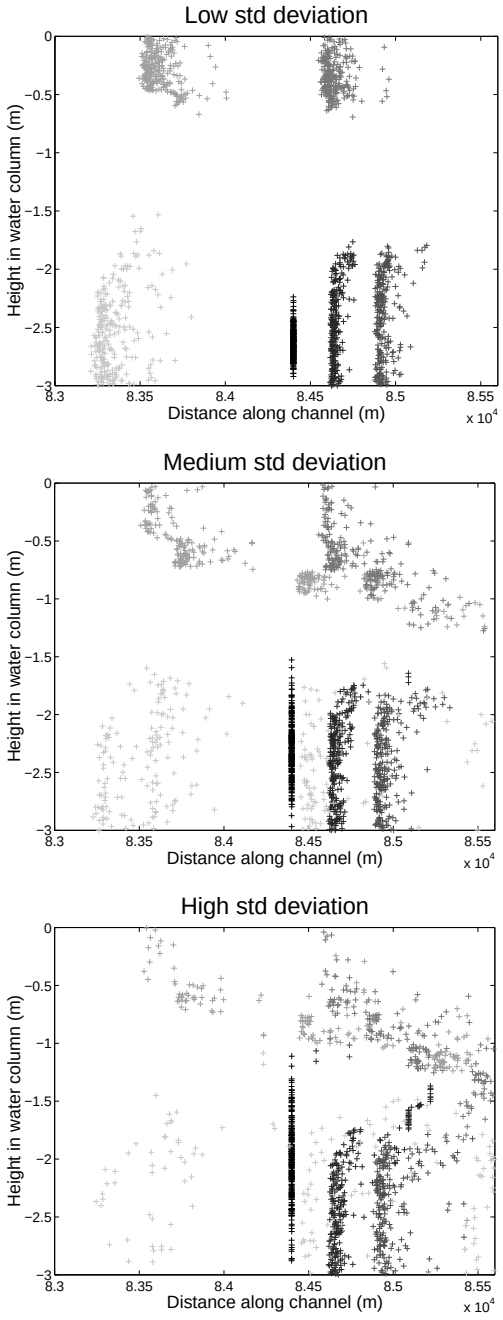

Figure 2.15: Particle trajectories for case of background flow of 0.06 cm/s under low, medium, and high standard deviation, respectively, normal migration and a start time of 8 am. Lighter shades of gray indicate increasing time, with sequential zooplankton clouds representing increments of 5 hours. Background flow east to west.

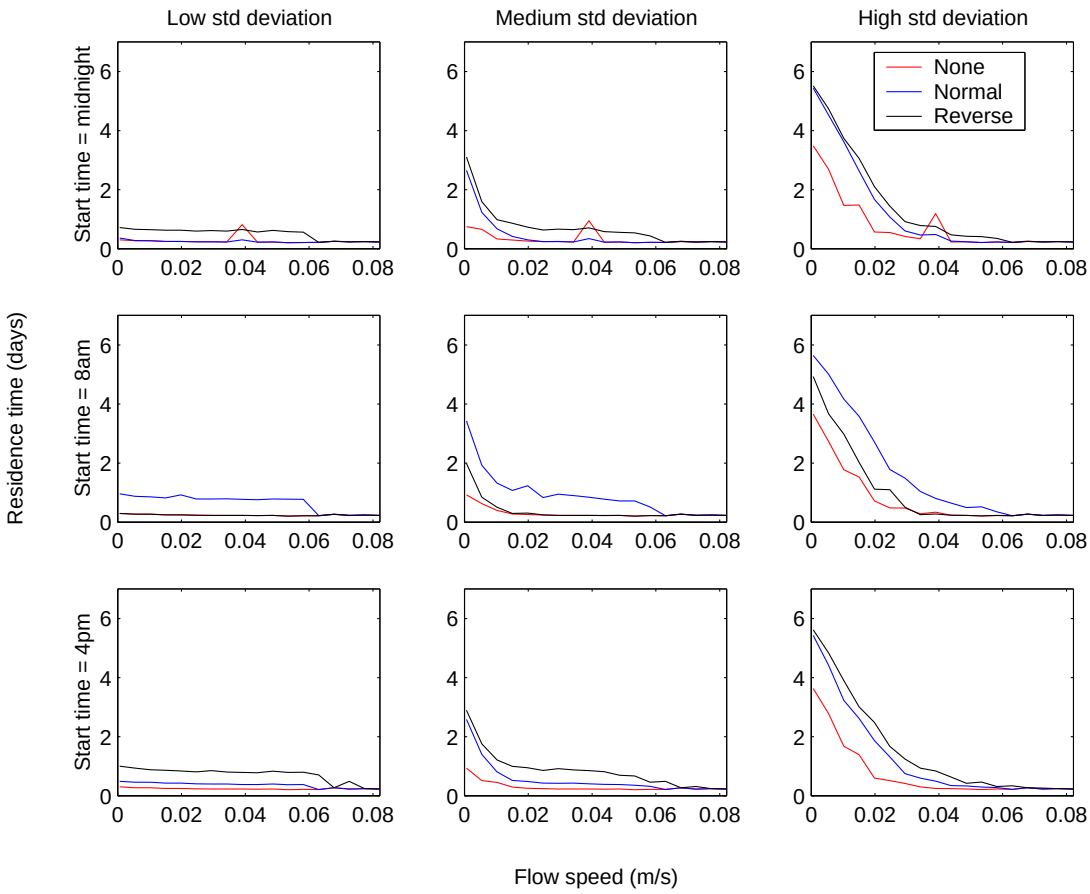

Figure 2.16: Background flow speed versus mean biological residence time by migration type for the nine zooplankton cloud standard deviation/start time combinations, assuming an equal length day and night.

essentially all at the same time, while higher standard deviation clouds leave in spurts. This effect is presumably again a result of shearing caused by the exchange flow, which effectively divides the original zooplankton cloud up spatially into subgroups.

Overall, at low background speed, start time and zooplankton cloud standard deviation do seem to exert an effect, although the consequences of changing the start time are not as great as changing the cloud standard deviation. For a start time of 8 am, normal migrators are retained for a longer period of time before

being flushed out of the embayment than for the other start times, presumably because they spend the first half day moving upstream at the bottom of the water column. Similarly, normal migrators start leaving the embayment faster than reverse migrators in simulations started at 4 pm. Additionally, at a start time of 8 am, reverse migrators start leaving the embayment at the same time as the nonmigrators, due to the fact that they're all moving down the channel at the top of the water column.

Zooplankton cloud standard deviation has a somewhat simpler interpretation. For all three migration types with the same start time, as standard deviation increases, the number of zooplankton left in the embayment after seven days increases. In general, the first group to leave the embayment contains fewer zooplankton as standard deviation increases, although for any set start time, the first zooplankton to leave start out at about the same time.

Figure 2.18 shows the number of zooplankton left in the embayment for an intermediate flow speed of 4.38 cm/s, with a start time of midnight. For all types of zooplankton clouds, nonmigrators and normal migrators essentially leave the embayment in a clump after about six hours have passed, while reverse migrators finish leaving the embayment after about half a day. Contrary to the situation at low flow speeds, for migrators that don't leave the embayment all at once, as the zooplankton cloud standard deviation increases, the zooplankton tend to start leaving the embayment sooner and in larger clumps. Similar to the zooplankton at low flow speeds, normal migrators at the 8am start time and lower zooplankton cloud standard deviation start leaving the embayment later than reverse and nonmigrators, while reverse migrators are the last to start leaving the embayment at the midnight and 4 pm start times (Figure 2.19). Additionally, 4pm is the only

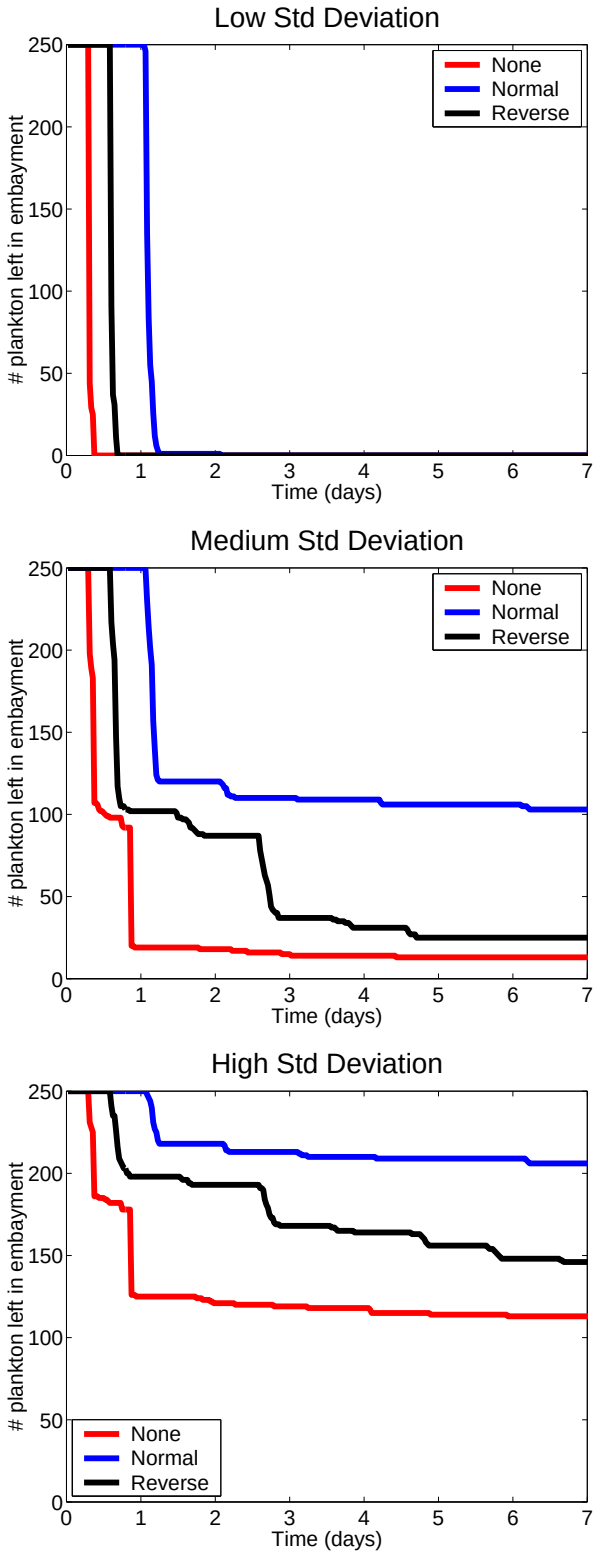

Figure 2.17: Number of plankton left in embayment under a range of zooplankton cloud sizes for background flow speed 0.06 cm/s, starting at midnight.

start time when nonmigrators do noticeably worse than the other migration types at remaining in the embayment.

Figures 2.20 shows a plot of zooplankton left versus time for a background flow speed of 8.22 cm/s for a midnight start time and moderate zooplankton cloud standard deviation. Only one plot is shown as neither standard deviation nor start time affected biological residence time at this higher flow speed. For all migration types, start times and standard deviations the zooplankton cloud leaves the embayment all at once after about six hours. In this case, the background flow is too high for the lock-exchange to create a lasting exchange flow; instead, the high background flow alone forces the cloud out of the embayment quickly.

2.5 Statistical Analysis of Results

To quantify the influence of the various model inputs on biological residence time, simulations were run and biological residence time computed for all combinations of the parameters flow rate, simulation start time, migration type, and standard deviation of the zooplankton cloud and a multiple regression analysis was performed using this data. For the purpose of this analysis, standard deviation ranged in value from 0.25 to 0.75, with consecutive values differing by 0.05, and 18 values of flow rate, ranging from 0.018 m^3/s to 2.466 m^3/s, were used, while migration type was one of 1, 2, or 3 representing no, normal, or reverse migration, and start time was 1, 2, or 3 representing midnight, 8:00am, and 4:00pm. Standard deviation and flow rate were considered continuous variables, while start time and migration type were treated as categorical variables. As a linear model did not provide an adequate fit to the data, a generalized additive model was used. Generalized additive models are similar to generalized linear models except that smoothing functions of

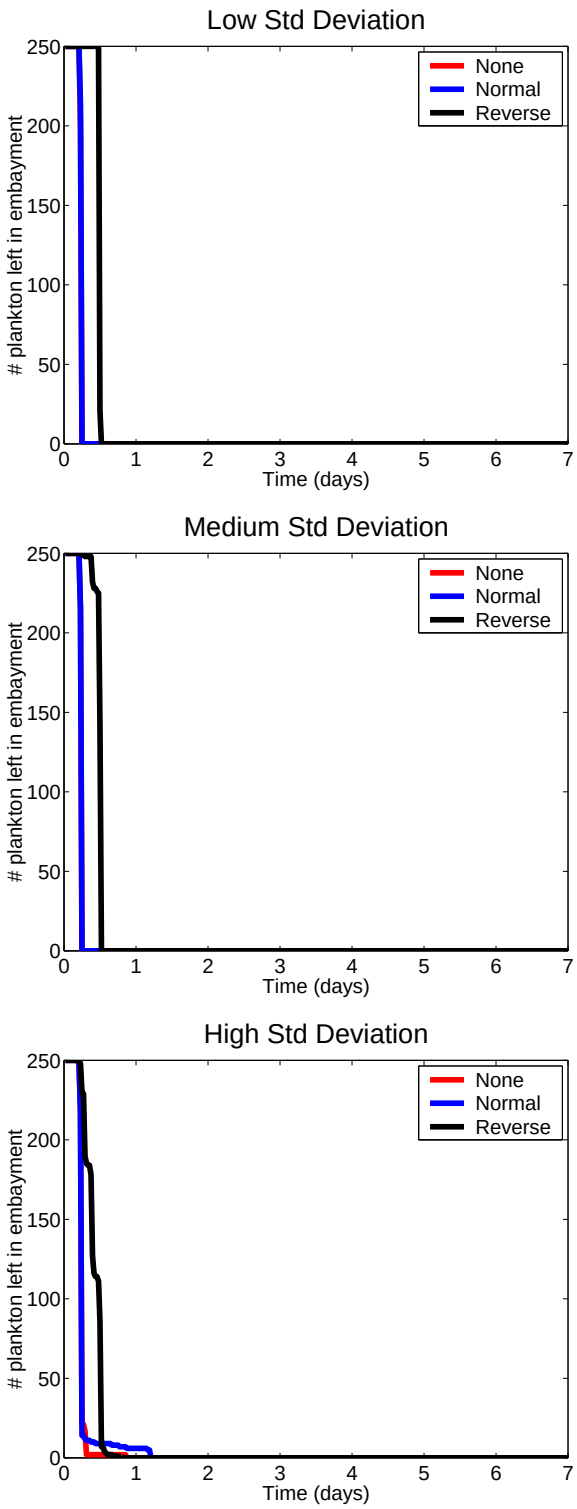

Figure 2.18: Number of plankton left in embayment under a range of plankton cloud sizes for background flow speed 4.38 cm/s, starting at midnight.

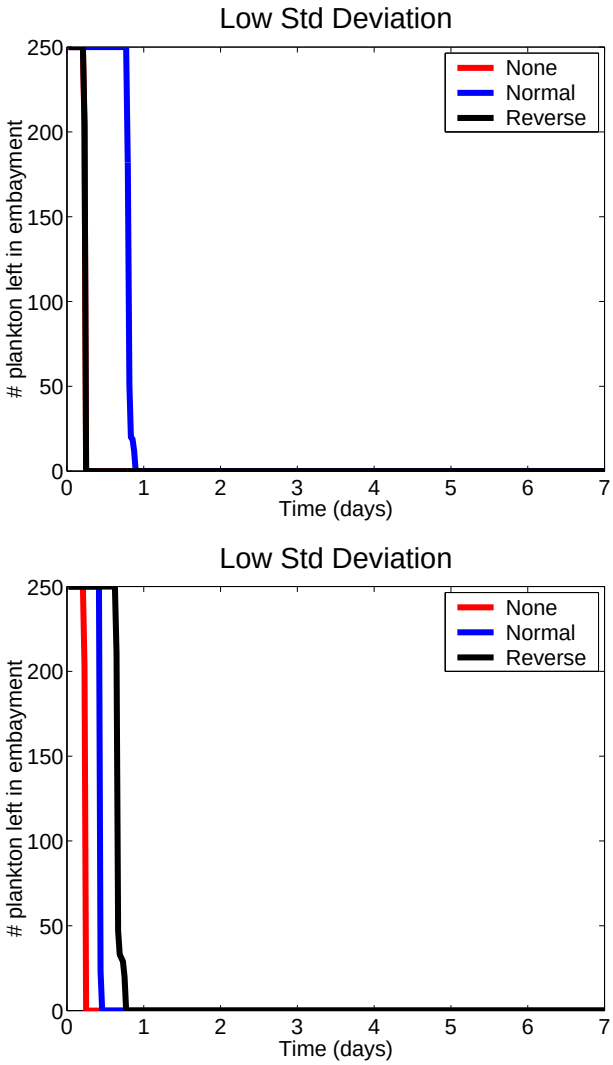

Figure 2.19: Number of plankton left in embayment under low zooplankton cloud standard deviation for background flow speed of 4.38 cm/s, starting at 8am and 4pm, respectively.

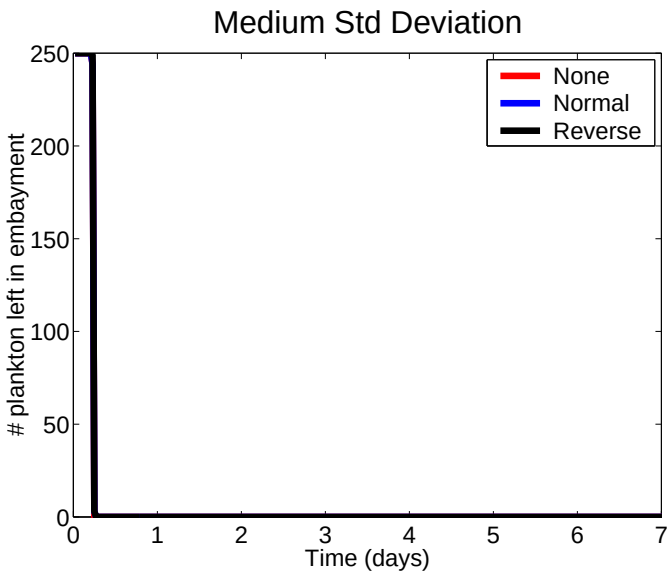

Figure 2.20: Number of zooplankton left in embayment under a medium zooplankton cloud size for a background flow speeds of 8.22cm/s, starting at midnight.

the covariates may be used, along with the usual linear model terms, and the mean of the dependent variable is assumed to depend on an additive predictor through a nonlinear link function. In this case, spline smooths and an identity link function were utilized. Different forms and combinations of explanatory variables were tried (using the gam function in the mgcv library [37] in R [32]) until a model was found that accounted for an adequate amount of the overall variance in biological residence time and that was stable regardless of additions or removals of terms accounting for small amounts of variance. The results are shown in Table 2.1.

From Table 2.1, flow rate by itself accounts for almost a third of the variance in biological residence time, while the initial size of the zooplankton cloud (which also affects zooplankton preferred heights and depths) has the the next largest effect. Start time accounts for virtually none of the variance, as expected. The independent contribution of migration type to biological residence time is relatively small; however, interactions of migration type with other parameters are significant,

Table 2.1: Percentages of variance in biological residence time explained by the four possibly key parameters determining biological residence time. 'Flow/Migration Type' denotes the two-way interaction between flow rate and migration type, while 'Flow/Migration Type/Cloud Standard Deviation' denotes the three-way interaction between flow rate, migration type, and the zooplankton cloud size standard deviation. The proportion of total variation in biological residence time explained by the independent variables, or R^2, is 0.94.

Parameter	Percentage of Variance Explained
Start Time	0.07%
Migration Type	6%
Standard Deviation	11%
Flow Rate	31%
Flow/Migration Type	20%
Flow/Migration Type/Standard Deviation	26%

with the three-way interaction of flow rate, standard deviation of zooplankton cloud, and migration type accounting for about a quarter of the variance and the interaction between flow rate and migration type alone accounting for about 20%.

2.6 Discussion

Simulation studies demonstrate that the temperature difference between a channel and lake can create flow that can significantly influence zooplankton residence time. Statistical analyses indicate that factors affecting zooplankton residence time, in decreasing order of importance, include flow speed, diameter of the zooplankton

cloud, migration strategy, and start time of the simulation; these analyses were corroborated by observations of zooplankton trajectories simulated using various combinations of parameters.

As background flow speed increases, exchange flow becomes less influential and zooplankton are not advected upstream as fast when they migrate to the channel bottom. At the higher speeds tested, biological residence time is less than if the lock-exchange induced-flow were the primary driving force, and washout seems inevitable. Significantly, however, low flow speed by itself is not at all effective at increasing residence time; instead, as the background flow speed decreases, the channel flow is increasingly controlled by the flow created by the dam break. Normal and reverse vertical migration under low flow conditions may both promote persistence but are more effective at different start times, which might be due to the schedule of migration and the fact that during the summer, the day (when reverse migrators are at the surface) is longer than the night (when the reverse migrators are at the bottom of the water column). Nonmigrating zooplankton do not fare as well and are swept out of the embayment at essentially the speed of the plume induced by the lock-exchange.

Zooplankton cloud standard deviation appears to have an effect on biological residence time, but it is unclear whether the effect is consistent across migration types and flow speeds. Increasing standard deviation often causes the plankton cloud to break into smaller groups, sometimes hastening the beginning of the plankton exodus and often lengthening the time needed for the entire cloud to exit the embayment. At lower flow speeds, increasing zooplankton cloud standard deviation appears to decrease the amount of zooplankton in the first clump to depart the channel, while at moderate flow speeds, the number of zooplankton in

the first departing group appears to increase.

Although the particular combination of bathymetry, flow fields, and zooplankton behavior used in this study do not allow the zooplankton to remain in the embayment for the full seven days, a number of steps can be taken to obtain more conclusive evidence about the ability of flow and vertical migration to increase retention of zooplankton in real channels. First, simulations can be run (including reproduction or not) for longer than seven days with a potentially longer simulation embayment, in order to determine whether the biophysical retentive effect persists with time. Furthermore, given adequate data collection, simulations can include more realistic bathymetry, flow regimes, and zooplankton behaviors appropriate for Floodwood or similar embayments. Extending the model to include temporal and/or spatial data on macrophyte growth, nutrients, light, and zooplankton type and spatial and temporal (seasonal and diurnal) abundance would move research efforts away from purely hypothetical scenarios and toward those with more promise of elucidating mechanisms behind the commonly observed drift paradox in nature.

Bibliography

[1] T. B. Benjamin. Gravity currents and related phenomena. *Journal of Fluid Mechanics*, 31(2):209–248, 1968.

[2] S. M. Bollens and B. W. Frost. Predator-induced diel vertical migration in a planktonic copepod. *Journal of Plankton Research*, 150:28–35, 1989.

[3] H. Burchard. *Applied Turbulence Modelling in Marine Waters*. Number 100 in Lecture Notes in Earth Sciences. Springer, Berlin, 2002.

[4] J. Chae and S. Nishida. Verticle-distribution and diel migration in the iridescent copepods of the family Sapphirinidae - a unique example of reverse migration. *Marine Ecology - Progress Series*, 119:111–124, 1995.

[5] P. Dawidowicz, J. Pijanowska, and K. Ciechomski. Vertical migration of chaoborus larvae is induced by the presence of fish. *Limnology and Oceanography*, 35(7):1631–1637, 1990.

[6] K. N. Dimou and E. E. Adams. A random-walk, particle tracking model for well-mixed estuaries and coastal waters. *Estuarine, Coastal and Shelf Science*, 37:99–110, 1993.

[7] R. Doyle-Morin. personal communication, 2006.

[8] D. W. Dunsbergen and G. S. Stelling. A 3-D particle model for transport problems in transformed coordinates. Technical Report 93-7, Delft University of Technology, Department of Civil Engineering, Hydraulic and Geotechnical Engineering Division, Hydromechanics Group, Delft, Netherlands, 1993.

[9] H. B. Fischer, E. J. List, R. Koh, J. Imberger, and N. Brooks. *Mixing in inland and coastal waters*. Academic Press, New York, 1979.

[10] G. Flierl, D. Grunbaum, S. Levin, and D. Olson. From individuals to aggregations: the interplay between behavior and physics. *J. Theor. Biol.*, 196:397–454, 1999.

[11] C. L. Folt and C. W. Burns. Biological drivers of zooplankton patchiness. *TREE*, 14(8):300–305, 1999.

[12] M. G. George. Diurnal migration in three species of rotifers in Sunfish Lake, Ontario. *Limnology and Oceanography*, 15(2):218–223, 1970.

[13] B. Han and M. Straskraba. Modeling patterns of zooplankton diel vertical migration. *J. Plankton Res.*, 20:1463–1487, 1998.

[14] R. Harris, P. Wiebe, J. Lenz, H. R. Skjoldal, and M. Huntley, editors. *ICES Zooplankton Methodology Manual*, pages 624–643. Academic Press, 2000.

[15] K. E. Havens. Zooplankton dynamics in a fresh-water estuary. *Archiv fur Hydrobiolgie*, 123:69–97, 1991.

[16] G. C. Hays, C. A. Proctor, W. G. John, and A. J. Warner. Interspecific differences in the diel vertical migration of marine copepods: The implications of size, color, and morphology. *Limnology and Oceanography*, 39(7):1621–1629, 1994.

[17] J. Horppila. Diurnal changes in the vertical distribution of cladocerans in a biomanipulated lake. *Hydrobiologia*, 334:215–220, 1997.

[18] J. Horppila, T. Malinen, L. Nurminen, P. Tallberg, and M. Vinni. A metalimnetic oxygen minimum indirectly contributing to the low biomass of cladocerans in lake hiidenversi - a diurnal study on the refuge effect. *Hydrobiologia*, 436:81–90, 2000.

[19] J. R. Hunter. *Numerical modelling: applications to marine systems*, chapter The application of Lagrangian particle-tracking techniques to modelling of dispersion in the sea. Elsevier Sciences Publishers B.V., North-Holland, 1987.

[20] Y. Iwasa. Vertical migration of zooplankton: A game between predator and prey. *American Naturalist*, 120(2):171–180, 1982.

[21] D. Kamykowski. Trajectories of autotrophic marine dinoflagellates. *J. Phycol.*, 31:200–208, 1995.

[22] P. K. Kitanidis. Particle-tracking equations for the solution of the advection-dispersion equation with variable coefficients. *Water Resources Research*, 30(11), 1994.

[23] W. Lampert, U. Sommer, and J. F. Haney. *Limnoecology: The Ecology of Lakes and Streams*. Oxford University Press, New York, 1997.

[24] C. Macquartmoulin and E. R. Maycas. Inshore and offshore diel migrations in european benthopelagic mysids, genera *Gastrosaccus, Anchialina* and *Haplostylus* (*Crustacea, Mysidacea*). *Journal of Plankton Research*, 17(3):531–555, 1995.

[25] E. Naslund, J. C. Rodean, and J. S. Nasstrom. A comparison between two stochastic diffusion models in a complex three-dimensional flow. *Boundary-Layer Meteorology*, 67:369–384, 1994.

[26] M. D. Ohman, B. W. Frost, and E. B. Cohen. Reverse diel vertical migration: An escape from invertebrate predators. *Science, New Series*, 220(4604):1404–1407, 1983.

[27] F. J. Rueda. *A three-dimensional hydrodynamic and transport model for lake environments*. PhD thesis, University of California, Davis, 2001.

[28] J. Smagorinsky, S. Manabe, and J. L. Holloway. Numerical results from a nine-point general circulation model of the atmosphere. *Monthly Weather Review*, 93:727–768, 1965.

[29] P. E. Smith. *A three-dimensional, finite-difference model for estuarine circulation*. PhD thesis, University of California, Davis, 1997.

[30] J. W. Stijnen, A. W. Heemink, and H. X. Lin. An efficient 3D particle transport model for use in stratified flow. *International Journal of Numerical Methods in Fluids*, 51:331–350, 2006.

[31] P. G. Strutton. Phytoplankton patchiness: quantifying the biological contribution using fast repetition rate fluorometry. *J. Plankton Res.*, 19:1265–1274, 1997.

[32] R Development Core Team. R: A language and environment for statistical computing. Technical report, R Foundation for Statistical Computing, Vienna, Austria, 2006.

[33] A. F. B. Tompson and L. W. Gelhar. Numerical simulation of solute transport in three-dimensional, randomly heterogeneous porous media. *Water Resources Research*, 26(10), 1990.

[34] I. Valiela. *Marine Ecological Processes*. Springer, New York, 1995.

[35] J. C. Warner, C. R. Sherwood, H. G. Arango, and R. P. Signell. Performance of four turbulence closure models implemented using a generic length scale method. *Ocean Modelling*, 8:81–113, 2005.

[36] L. J. Weider and H. B. Stich. Spatial and temporal heterogeneity of Daphnia in Lake Constance; Intra- and interspecific comparisons. *Limnology and Oceanography*, 37(6):1327–1334, 1992.

[37] S. N. Wood. *Generalized Additive Models: An Introduction with R*. Chapman and Hall/CRC, 1979.

[38] H. Yamazaki, D. L. Mackas, and K. L. Denman. *The Sea*, volume 12, chapter Coupling small-scale physical processes with biology, pages 51–112. John Wiley and Sons, Inc., New York, 2002.

Chapter 3

The Effect of Macrophytes on the Drift Paradox Problem

3.1 Abstract

The fact that many small aquatic and marine organisms manage to persist in their native environment in the presence of constant advection is known as the 'drift paradox.' Previous studies have examined the extent to which zooplankton behavioral traits can mitigate the effects of primarily unidirectional water flow. Most of these studies have assumed flow relatively unimpeded by vegetation, but macrophytes are present in many freshwater embayments for at least part of the year and can have a significant influence on water flow. Creating various flows in an idealized channel using a three-dimensional hydrodynamic model, and modelling zooplankton behavior with an individual-based model, we explore the extent to which biological processes can counteract physical drivers. In particular, we examine how different zooplankton migration behaviors affect biological retention time under a variety of flow regimes, and whether a combination of physical/biological regimes exists that will solve the drift paradox - i.e., allow the zooplankton to stay in the study system (avoid washout) for time periods much greater than the hydrologic retention time. The hydrodynamic flows involve the influence of macrophytes as well as possible exchange of water between embayment and lake caused by temperature differences. Zooplankton behavior includes no, normal, and reverse vertical migration, as well as two types of normal migratory behavior modified by the presence of macrophytes. For each flow scenario, the behaviors of organisms

under the various migration strategies were compared to determine if they had substantially different retention times when using the different strategies and whether the effect of migration type changed with flow speed. Regression analysis, quantifying the effect of each parameter, allowed them to be ranked according to their contribution to the variance of zooplankton biological residence times, with the ultimate goal of determining which combination of parameters led to the greatest biological residence time in the channel and how the presence of macrophytes changes the biological residence time in general. A combination of low flow rate, normal migration, and a fully vegetated channel allowed the zooplankton to remain in the embayment for the full length of the simulation. Flow rate was the only individual parameter with a significant effect on biological residence time, although zooplankton cloud size had a significant influence on biological residence time when combined with flow rate.

3.2 Introduction

The fact that many small aquatic and marine organisms manage to persist in their native environment in the presence of constant advection is known as the 'drift paradox.' Motivated by large numbers of zooplankton found in moderate-to-fast-flowing channel-like embayments [15], in Chapter 2, we attempted to find an explanation for the drift paradox in an unvegetated channel but were unsucessful. Now, we add rooted macrophytes to the channel and focus on understanding the extent to which biological processes can counteract physical drivers in this type of environment; specifically, how zooplankton vertical migration behaviors affect biological retention time under a number of different freshwater channel flow regimes in the presence of macrophytes and whether a combination of flow type

and biological behavior can allow organisms to stay in the channel 'indefinitely'.

Traditionally, vegetation in areas such as tidal marshes, wetlands, streams, and rivers has been seen as an obstruction by hydraulic engineers and has typically been harvested in waterways of practical importance to improve water movement. While turbulent flow in these environments has been studied, the purpose has in general been to understand the processes determining momentum, heat, and mass exchange between the atmosphere and the plant canopy, processes which regulate the plant microclimate, allow photosynthesis to occur, and remove byproducts of transpiration. Now it is generally understood that this vegetation plays the important role of stabilizing banks and channels, as well as providing habitat and food for animals and recreational areas for humans. These realizations have in recent years led to a shift away from empirical and/or observational research on plant canopies toward a desire to understand the related transport processes in natural environments.

Characterization of mean flow in the presence of macrophytes, as well as of turbulent structure and its related transport processes, received much attention in the 1990's. Largely motivated by a desire to understand transport of pollutants, heat, sediment, carbon dioxide, etc., in the natural environment, experimental studies of atmospheric flows over plant canopies [74, 57], wind tunnel investigations using simulated plants [55], and studies of vegetated open channel flows [50, 16, 64], produced a large body of knowledge concerning the turbulence structure of fully rough flows (with plants providing the roughness). In particular, studies using terrestrial canopies have yielded much information about flow through unconfined canopies [56]. A defining feature of these canopies is the presence of a strong shear layer, where free shear layer flow is observed at the top of the canopy. Inside

the canopy, the flow is chiefly determined by turbulent stresses, i.e., the vertical turbulent transport of momentum from the overlying flow; pressure gradients play little or no role [55]. This model can also be used to represent flow through deeply submerged aquatic canopies, in which the water depth is large relative to the canopy height. In many channels, however, at least during some part of the summer, this depth ratio is not large, which can affect both the mean and turbulent flow.

In addition and more pertinent to hydraulic engineers, a number of experimental or numerical studies have been performed looking at flow through submerged aquatic canopies using both flexible and rigid plant-like structures (for example, [49, 41, 43]). In addition, a few studies have investigated emergent vegetation [5, 50]. Nepf and Vivoni [52], using model vegetation in a high Re number flow laboratory setting, explored the transition from emergent to submergent canopies with respect to momentum sources, turbulence, and exchange dynamics. Three transitions were expected and observed: 1) flow becomes driven by turbulent stress rather than by pressure gradient, 2) the main source of shear production becomes the shear layer at the canopy top rather than stem wakes, and 3) vertical turbulent exchange rather than longitudinal advection becomes the chief mechanism for exchange with the surrounding water column. Moreover, both experimental and observational studies have investigated the consequences of monami, the coherent waving of aquatic vegetation. Grizzle et al [25] made underwater observations of eelgrass undulations and determined that the waving was the cause of large variability in horizontal water current speeds as well as of enhancing turbulent mixing above the canopy, mixing which may help steer larvae into such seagrass beds. Ghisalberti and Nepf [24] experimentally determined that the downstream

advection of large, coherent vortices in the mixing layer within and just above an unconfined canopy create the monami, along with enhanced turbulent vertical transport of momentum.

Most of the early theoretical work on fluxes in plant canopies relied on the local diffusion equation. Although this approach has yielded useful insight (e.g., into computer crop models), the assumptions needed to use this approach are generally acknowledged to be questionable. As a result, turbulence closure schemes were utilized. Wilson and Shaw recognized the limitations of first level closure schemes and in 1977 [74] developed a higher order closure model for atmospheric flows above plant canopies. In 1983, Burke and Stolzenbach [5] investigated a two equation, turbulence closure scheme of the k-ϵ type [58] for free surface flows through obstructions, with the presence of vegetation indicated by drag-related terms introduced into the turbulent kinetic energy (tke) and the dissipation equations. Lopez and Garcia [42] analyzed the ability of turbulence models based on k-ϵ and k-ω [73] closure schemes to compute mean flow and turbulence structure in open channels with rigid, nonemergent vegetation. The study focused on the estimation of resistance laws, mean velocity distributions, and the determination of approximate rules for the partition of the total action of gravity between friction drag, due to bed roughness, and form drag, due to plants. Both models accurately predicted experimental observations on mean flow and turbulence quantities up to second-order statistics and provided a good representation of the production, inertial diffusion and dissipation terms in the tke budget. Furthermore, Christensen [8] made a simpler attempt to close the turbulence problem, using a mixing length approach to compute eddy viscosities and to develop an explicit formula for the velocity profile over a flexible roughness layer in heavily vegetated rivers and

channels.

Roig and King [59] attempted to model flows in tidal marshes by modifying the classical equations of 2D vertically averaged equations for incompressible open channel flow, producing a continuum model with a bulk fluid velocity (instead of modeling the actual path of each fluid parcel). This approach avoids the problem of having to describe the effects of turbulence between stems of the macrophytes. Instead, resistance to flow is related to the characteristic diameter and spacing of vegetation stems by utilizing a statistical sample of stem diameter distribution, stem height distribution, and stem spacing. Roig and King's model attempted to describe the tidal marsh as a function of water surface elevation and the variable flow resistance mechanisms operating at distinct elevations, while at the same time parameterizing the mean hydraulic properties of an inhomogeneous porous medium; i.e., a Manning or Chezy relationship [68] was used to describe the combined effects of bottom shear and drag caused by vegetation. Roig and King's proposed modifications for bottom friction and shallow intermittent flows can be implemented with finite element or finite difference methods.

For biological organisms, physics tends to dominate over large scales, while individual behavior has more of an impact at smaller scales. Physical environments differing in temperature, light, oxygen, food, and predators can influence zooplankton behavior, such as diel vertical migration, as well as affect zooplankton directly. In particular, channels linking rivers or embayments with some larger, external water body are often assumed to be areas of high throughput in which plankton cannot be retained for any length of time. An understanding of an organism's residence time in a body of water requires an understanding of water flow and mixing as well as of the behavior of the organism. Water motions in

(channel-like) embayments are governed primarily by wind stress and a combination of density gradients and gravitational forces (as opposed to rotation of the Earth). The temperature distribution mainly determines the density field; the temperature is a result of many factors, including air-water exchange of heat, advective transport, and vertical turbulent mixing. In embayments with low water residence times, the lake that the embayment empties into can have a major effect on the physical behavior of the embayment. The temperature stratification in the lake, its vertical thermal structure, largely determines the quality of the water in the embayment, as it produces water stability, damping turbulent mixing, restricting the vertical flow of oxygen and in other ways affecting the biomass productivity. Seasonally, many channels linked to bays and embayments have significant macrophyte growth, typically causing model flow results to deviate wildly from reality; in the extreme case, groundwater flow is represented as open channel flow. Experiments in which rhodamine (dye) was released directly upstream of one particular embayment (freshwater estuary) of Lake Ontario, Sterling Pond (with areas of both low Reynolds number and high Reynolds number flow), have shown a variation of water residence times from several hours to a week or more [33]. Understanding the true flow regimes in such channels is an essential step in answering fundamental questions about ecosystem function, determining the relative importance of exogenous versus endogenous influences in the bays/embayments, understanding the fates and movements of nutrients and (toxic) chemicals, and investigating the effects of varying external water levels.

Hardy and Gunther [26] first proposed the idea of 'plankton navigation,' by which organisms take advantage of horizontal currents of various speeds and directions during their upward and downward movements. In mid-to late summer,

the embayment environment is typically warmer and more nutrient-rich than the lake into which it empties, which can increase the zooplankton growth rate. Zooplankton that exhibit behavior that takes advantage of the horizontal currents can potentially avoid washout into the lake. We build onto our understanding of biophysical processes and their effects on zooplankton movement from Chapter 2 by modifying SI3D [60, 66], a three-dimensional hydrodynamic model of shallow water flow, to handle a channel covered with submerged vegetation. Ptrack [60] is a post-processing computer code designed to be used with the program SI3D which takes the velocities computed in SI3D and uses them to simulate the motion of passive particles. Combining this individual based model with the output from SI3D allows us to investigate plankton residence time in a channel under a variety of flow regimes. In addition, the difference in biological residence time for zooplankton in a vegetated environment versus an environment with typical bottom drag (see Chapter 2) is considered.

3.3 Methods

3.3.1 Hydrodynamic Model

The computer code SI3D, a semi-implicit three-dimensional hydrodynamic and transport model for lake environments, was modified to be applicable to macrophyte-inhabited channels and used for our simulations. Quite a few computer codes exist that can simulate water flow in a relatively shallow basin using the shallow water form of the Navier-Stokes equations. SI3D was readily available, and its semi-implicit nature allowed the maximization of computational efficiency and minimization of numerical difficulties. (Chapter 1 describes SI3D's characteristics

in some detail.) The embayment size and shape for this study are based on the bathymetry of Floodwood pond, a distinct and enclosed lake-level embayment on the eastern shore of Lake Ontario. We used a simplified, rectangular geometry (1400m long, 10m wide, and 3m deep) for computational purposes. The embayment of interest is embedded in a much longer simulation channel of 124,000m total length in order to avoid the possibility of embayment water eventually coming into contact with an open boundary and causing spurious oscillations or other unnatural effects (see Chapter 2). Figure 3.1 shows the study basin from the side, along with the relative position of the embayment of interest.

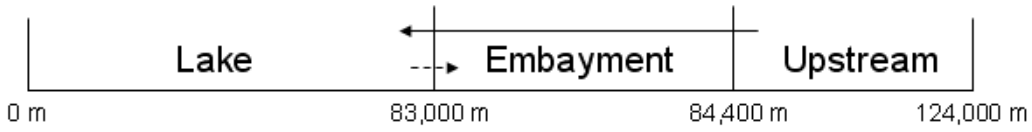

Figure 3.1: Sideview of the computational channel, showing the relative position of the study embayment. The solid arrow denotes westward background flow, while the dashed line represents potential lock-exchange flow.

Water in lakes and embayments is commonly exchanged via above-ground conduits between the two bodies of water. This so-called exchange-flow, which can help increase zooplankton residence time in embayments, may result due to temperature differences between lake and embayment; the lake water, typically denser than the water in the embayment, is forced to flow underneath the lighter embayment water along the bottom of the embayment basin. Exchange-flow was initiated at the beginning of each SI3D simulation by implementing a virtual vertical barrier, or 'lock,' at the output from embayment to lake; the temperature on the lake side was set to 13°C, while the embayment water was set to 18°C (typical temperatures for summer in moderate latitudes). At the start of the simulation, then,

with nothing to stop the moving and mixing of the two water bodies, exchange flow develops. Over time, at lower background flow speeds, exchange-flow can persist, while at higher speeds the colder water ends up being pushed out of the embayment by the faster flow from upstream in the embayment. Intermediate cases may involve a steady flow with a downstream region of exchange-flow and an upstream region of unidirectional flow. If the basin is initially at rest, an approximate velocity for both upstream and downstream currents is $U = \frac{\sqrt{g'H}}{2} \approx 0.0759$m/s, where H is the channel depth and $g' = g(\rho_2 - \rho_1)/\rho_2$ for $\rho_2 < \rho_1$ is reduced gravity [1]. Eighteen equally spaced flow speeds were used in this study, ranging from 0.06cm/s to 8.22cm/s. The model was run for five days before particle tracking was started so that the exchange-flow and background flow could interact and reach a quasi-steady state. Figure 3.2 shows the initial setup of the basin (shown from the side) with the virtual lock toward the lefthand end. The other plots show qualitatively typical velocity and temperature profiles for high and low background flow speeds (without macrophytes) after a virtual steady state was reached. Note that exchange flow in the low flow scenario leads to an almost stratified channel, while for the high flow case, the warmer water pushed the colder water out the end of the channel and the water flow is unidirectional.

The current study used a cell size of 0.25 m in the vertical direction and 10 m in the lateral direction. Thus, the study basin required one lateral cell and 24 vertical cells. As the dynamics of interest in the study system are occurring primarily in the downstream and vertical directions, this crude resolution was deemed adequate. In addition, a cell size of 50 m in the longitudinal direction, which was shown in Chapter 2 to be adequate for our purposes, was again used in the present study, leading to 2480 cells in the x direction. In general, a time step of 120 seconds was

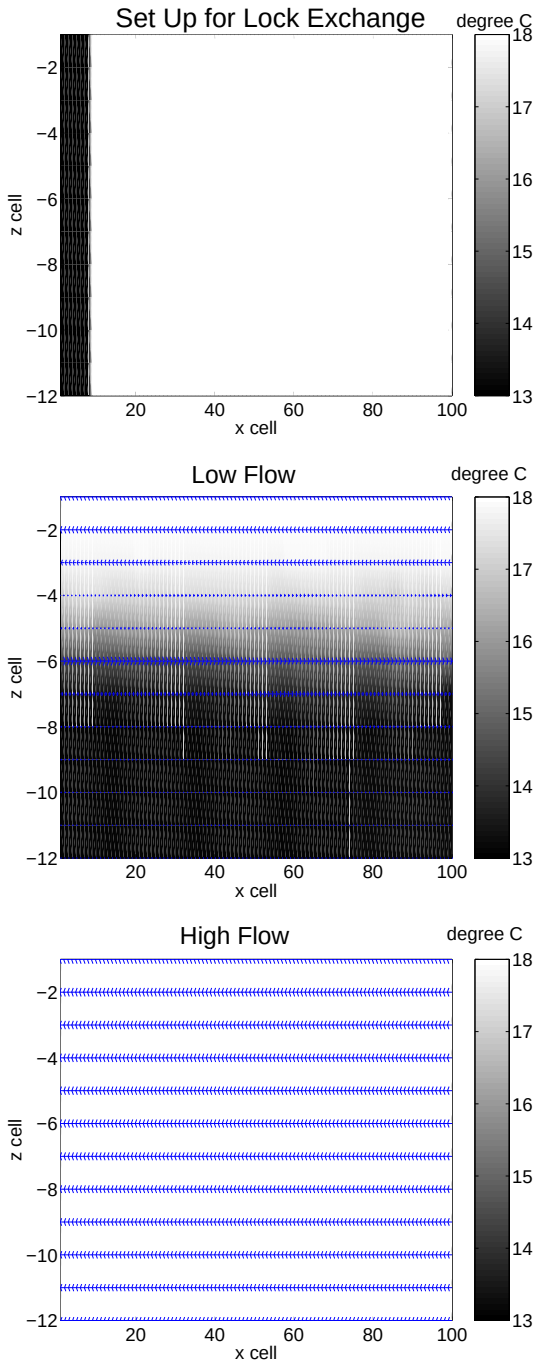

Figure 3.2: Figures showing, for part of the simulation region, the region before the 'dam break,' along with the steady flow regime after dam break, for a low flow (0.06 cm/s) and a high flow (8.22 cm/s) case. Shades of gray indicate temperature, while arrows indicate direction and magnitude of velocity.

used, but Courant-Friedrichs-Lewy (CFL) constraints required frequent reductions in time step, resulting in time steps as small as 1 second for several of the runs using the two highest flow speeds (7.74 cm/s and 8.22 cm/s). (The CFL condition requires the time step to be less than the time taken for fluid to travel across a computational cell.)

3.3.2 Modelling Macrophyte-Influenced Water Flow

Sand-Jensen [62] studied hydrodynamic forces on submerged macrophytes with various numbers of shoots and found an essentially linear relationship between the log of the free stream water velocity, U, and the drag coefficient, $C_{d(S-J)}$:

$$\log C_{d(S-J)} = \log 3 - 1.35 \log U$$

Sand-Jensen implies that this coefficient can be described as a ratio of drag force to hydrodynamic force:

$$C_{d(S-J)} = \frac{F_D}{\frac{1}{2}\rho U^2 A}$$

In this case, $A = A_w$, where A_w is the total wetted surface area. Thus, the drag force, F_D, represents the force on the entire macrophyte stand.

SI3D assumes a similar relationship between velocity and drag, with $A = A_{bed}$, the area of the base of a cell, as shear stress is assumed to act only at the base of a cell (a perfect-slip condition is applied at the walls). In this case, the drag coefficient, C_d, is determined at the level of a single cell. However, the drag force provides a convenient way of translating between $C_{d(S-J)}$ and C_d.

We first calculate an approximate value for A_w for a specific configuration of macrophytes in the channel. For any particular free stream velocity, we can use the

empirical relationship with drag coefficient, as well as A_w, to determine the drag force. A dried stem of the common invasive milfoil, *Myriophyllum spicatum*, was weighed and the surface area measured and found to be $0.091 m^2/g$ [31]. (Note: The surface area of one face was measured and then doubled.) Assuming milfoil biomass to be $200 g/m^2$ [31] yields 18 m^2 of plant surface area per m^2 of channel bottom. Thus, if macrophytes cover the entire channel, then the wetted surface area for a 10m by 1400m channel is 252,000 m^2. Taking $\rho = 1 g/cm^3$ and assuming a free stream velocity U, then we can solve for F_D as

$$F_D = \frac{1}{2}\rho U^2 A_w C_{d(S-J)} \tag{3.1}$$

$$= \frac{1}{2}\rho U^2 A_w 10^{\log 3 - 1.35 \log U} \tag{3.2}$$

SI3D takes a drag coefficient as an input parameter and uses it to create the appropriate amount of bed stress, assuming that the drag is caused by some roughness on the bottom of the bed. In order to propagate drag up in the water column to account for the effect of macrophytes, we assumed that macrophytes could be considered to create the same type of drag, to a larger extent and in more than one computational horizontal layer. Assuming that macrophytes inhabit half of the water column of 3 m, and that the height of each cell is 0.25 m, we propagated the bed stress through the bottom 6 layers. To convert the drag coefficient from the form of Sand-Jensen to that of SI3D, we kept F_D as a total force and converted A_{bed} to a total bed area (or, equivalently, converted F_D to a force per cell) by multiplying the total bottom area covered by macrophytes by the number of horizontal layers inhabited by macrophytes to find $A_{bed-tot}$. The drag coefficient applicable to an individual SI3D cell can then be calculated as

$$C_d = \frac{F_D}{\frac{1}{2}\rho U^2 A_{bed-tot}} \tag{3.3}$$

$$= \left(\frac{A_w}{A_{bed-tot}}\right) 10^{\log 3 - 1.35 \log U} \tag{3.4}$$

given a free stream velocity U.

Figure 3.3 shows flow profiles in the presence of macrophytes for both a low (0.06 cm/s) and high (8.22 cm/s) background downstream flow. Even though the exchange flow at the western end of the embayment interacts with the background flow and macrophytes, the resulting horizontal flow profile is not dissimilar to profiles in the literature obtained experimentally ([52], Figure 4). In the case of the low flow regime, the flow profile is nearly vertical in the macrophyte bed, with a sharp increase in magnitude of velocity starting at the water/macrophyte interface persisting almost to the water surface. The profile in the high flow case still possesses the prominent increase in velocity magnitude beginning at the top of the macrophytes, but without as pronounced of a vertical profile within the macrophytes. The macrophytes used here are only crude representations of real vegetation, and the macrophyte type and height as well as the type of flow forcing used here differ from any study we have found in the literature, but the similarity in velocity profile is promising.

In a natural water body with nonsmooth boundaries, especially under at least a moderate flow speed, accurate accounting of turbulence is important for obtaining the correct flow field; in particular, the presence of aquatic vegetation can control the turbulent flow structure [52] and thus have a significant impact on the transport of passive particles or partially active particles such as zooplankton. In SI3D the horiziontal turbulence that results from the large scale advective processes is

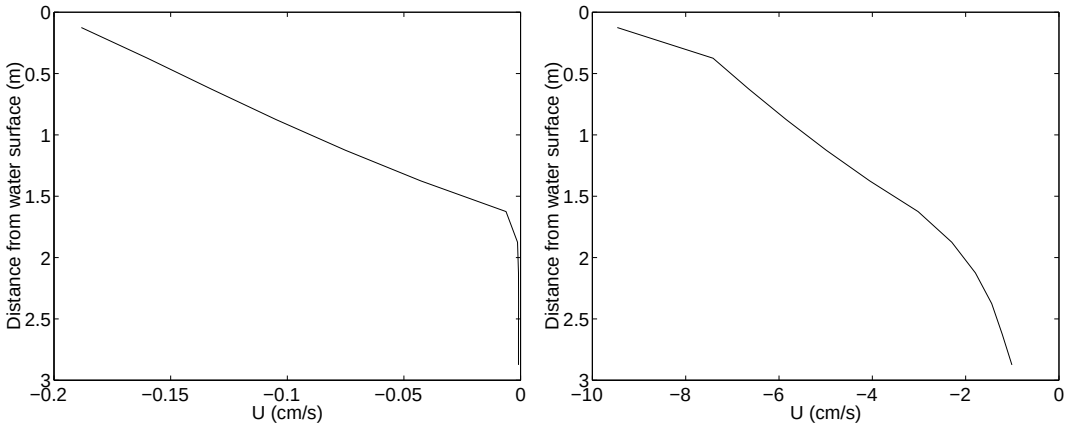

Figure 3.3: Velocity profiles for a low background flow (0.06 cm/s) and a high background flow (8.22 cm/s) regime in the presence of a macrophyte patch covering the entire embayment length and width.

considered to be isotropic and the Smagorinsky scheme [65] is used to determine horizontal eddy coefficients. Horizontal mixing is often modeled as the gradient of a mean property multiplied by an empirical constant. In particular, Smagorinsky et al [65] assumed that the horizontal eddy coefficients are related to the largest eddy size that is resolved in the model as well as to the local deformation field. SI3D uses the Kantha and Clayson version [32] of the Mellor and Yamada 2.5 second moment closure two-equation model [46] to find vertical eddy viscosities and diffusivities controlled mainly by small-scale motion. In the nonstratified case, the Kantha and Clayson model generates an approximately parabolic eddy coefficient profile, but is more numerically stable than MY2.5, includes improved modeling of terms in the second-moment closure, and adds improved mixing to MY2.5 [71, 4]. While these methods for horizontal and vertical turbulence take care of mixing at the grid scale, at the sub-grid scale, ptrack adds a random step to the particle position in each coordinate direction at each time step, and also calculates a drift term which

adds the effect of variation in the vertical diffusion coefficients. These terms are calculated based on the vertical eddy coefficients output from SI3D and constant horizontal coefficients computed in ptrack based on Fischer et al [20], [19].

Flow fields for slow (0.54 cm/s), intermediate (4.38 cm/s), and fast (8.22 cm/s) background velocities are shown in Figure 3.4. These flow fields, in general, are considerably more complicated than their plantless counterparts (Chapter 2). For the two slower flows, the macrophytes interact with the exchange flow, which is not pushed all the way out of the embayment, while in the high flow case, even in the presence of macrophytes, the flow eventually becomes unidirectional. At a background speed of 0.54 cm/s, and it seems as though the macrophytes have pushed the colder water into the upper half of the water column, causing exchange flow there. In constrast, in the case of a background flow of 4.38 cm/s, most of the flow is downstream, although the effect of the macrophytes is seen in the considerably smaller velocity where macrophytes fill the channel. Exchange flow is able to persist to a height of half the water column in this case. At the highest background flow speed, the baroclinic flow is washed out of the embayment and the flow is unidirectional. Compared to the version of these flow fields without macrophytes (from Chapter 2), the magnitudes of the downstream flow velocities are just as high, if not higher (for medium and high background flows), while the upstream flows are slower.

3.3.3 Zooplankton Modelling

Zooplankton populations were modelled as individual particles in an individual based model (ibm), ptrack, to allow the zooplankton to exhibit a wide range of behaviors. In addition, while the zooplankton act only on an individual basis in

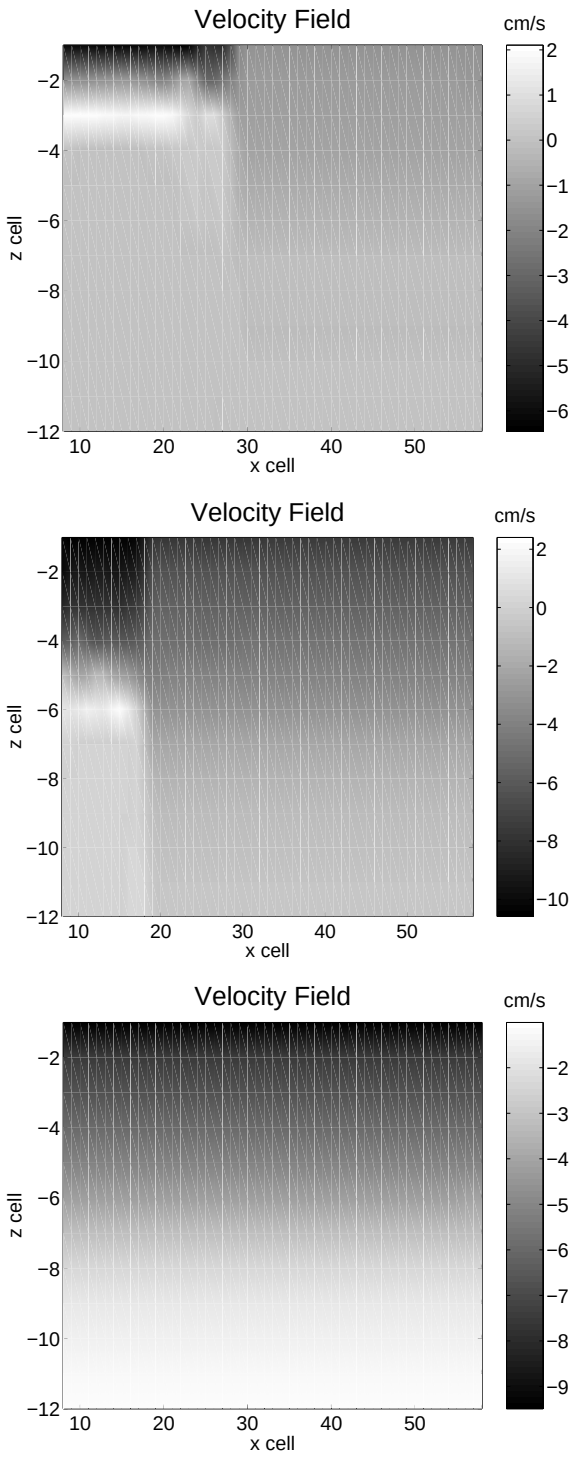

Figure 3.4: Steady state flow fields for background velocity of 0.54 cm/s, 4.38 cm/s, and 8,22 cm/s for a macrophyte-covered embayment.

this study, using an ibm allows group behaviors, such as aggregation and disaggregation, to be easily added later on [77, 21, 22]. The original formulation of ptrack and modifications made to allow migration behavior are described briefly below and in greater detail in Chapter 2.

Zooplankton simulations involved five parameters: flow rate, type of migration, zooplankton cloud standard deviation, lateral drag type, and longitudinal drag type. Eighteen evenly spaced flow rates were used, ranging in magnitude from 0.018 m^3/s to 2.466 m^3/s, or a range in velocity of 0.06 cm/s to 8.22 cm/s. Initial spherical zooplankton clouds composed of 250 zooplankton were centered in the middle of the channel in the lateral direction and 1400 meters upstream from the embayment mouth in the longitudinal direction. In addition, the zooplankton clouds were placed at the top or the bottom of the water column as appropriate for the combination of migration type and start time and at such a position in the vertical as to just remain completely in the water column. Starting positions were chosen for each zooplankter from a normal distribution with standard deviations of 1/4 or 1/2 of the water column height; these cloud sizes were chosen to cover a reasonable range of zooplankton cloud sizes observed in nature [37], [53], [10], [72], [28], [29] while ensuring that the entire zooplankton cloud was initially either completely inside or completely outside of the macrophytes. While start time was a parameter used in the previous study, results from that study showed that start time was by far the least relevant factor for biological residence time and thus all simulations in the current study began at the same time (midnight).

Migration Types for Zooplankton

In general, vertical migrations are believed to be a consequence of a foraging rate - predation risk trade off [75]. Although the potential for vertical migration in shallow lakes is limited due to the absence of stratification [38], macrophytes covering the bottom may offer zooplankton daytime refuge from pelagic planktivorous fishes [7] as well as diverse surfaces on which organisms can settle and feed. In addition, environmental complexity can encourage the coexistence of competing species by providing refuges that help limit strong interactions. Although vertical migration in the presence of macrophytes still usually involves zooplankton movement upwards at dusk and downwards at dawn [35], macrophytes can influence the fate of zooplankton in several ways. As well as increasing drag and directly affecting zooplankton advection, macrophytes can also modify zooplankton migration patterns, which can indirectly affect biological residence time.

To find out how macrophytes might modify zooplankton migration, we performed a literature review using the Web of Science Citation Index Expanded (SCI-EXPANDED) and the key words plankt*, zooplankt*, larv*, macrophyte*, and migrat* in all possible combinations of three words at a time in October, 2005, and also performed a search of The Journal of Plankton Research around the same time using the journal's website and the keywords zooplankton, migration, and macrophytes. Based on the publications found in these searches, we can classify zooplankton migration in the presence of macrophytes into three basic categories. To more easily compare the effect of macrophytes on zooplankton retention, as well as give a conservative estimate of biological residence time, we will again assume that our theoretical zooplankton migrate only vertically and that the extent of their migration upwards into the water column is the same whether or not

macrophytes occur. Thus, the three categories will differ only with regard to how far zooplankton penetrate into macrophytes when migrating down in the water column.

In addition to the macrophyte-specific types of vertical migration (discussed below), we also include the 'base' case of no migration (type 1), as well as reverse migration (type 2), so that we can compare the results with those of Chapter 2, as well as for completeness. Kuczynska-Kippen [35] studied rotifers for whom vertical migration is likely not a good strategy due to the presence of predators in the open water; as a result, these rotifers remained most of the time in the water just above the macrophyte stand. In addition, in other rotifers, Lair et al [36] found reverse migration in the presence of macrophytes, which can help reduce exploitative competition.

Type 3 zooplankton can be thought of as 'normal' migrators, fleeing the open water during the daytime to migrate down into the macrophytes, with no preferred (by the group) terminal vertical position. During the daytime, large zooplankton in shallow lakes tend to leave the open water, aggregating in or near submerged plant beds [38] [40], with daytime zooplankton abundance in vegetation negatively correlated with mortality from daytime predation [7]. In general, vertical migration between open water and macrophytes confers an advantage on zooplankton without much swimming ability who largely cannot determine their position in the water column actively. Even for the better swimmers, once zooplankton are inside a stand of macrophytes, little is known about their exact positions; most sampling is crude sampling of zooplankton location in either macrophytes or open water [75]. This category may contain zooplankton that inhabit macrophytes in order to avoid daytime open water predation and are repelled from the macrophytes at night by

predators or chemical cues in the vegetation or lack of food sources there.

Type 4 zooplankton migrate down to a position in the water column just above the macrophyte stand but do not enter the vegetation. Several observations and experiments have shown that large zooplankton tend to avoid macrophytes [27] [54] [14], largely because of repellant chemical cues in the macrophytes. Several studies found that in daphnids, fish chemical cues overrode chemical cues from macrophytes [6] [39], even though the macrophyte chemicals were more harmful to the daphnids [6]. Thus, this category may contain zooplankton that are in the presence of open water predators but whose aversion to the chemicals or predators found in the nearby macrophytes is great enough to prevent them from actually entering the macrophytes.

Type 5 zooplankton migrate down to the base of the macrophytes. While in a macrophyte stand, greater densities of zooplankton may be found near the benthos for several reasons. First, due to the reduction of water velocity within their stems and especially their prop roots [63], macrophytes may act as filters, so that remaining in the prop roots and near the benthos may help poor swimmers avoid advection [18]. Furthermore, in densely populated macrophyte stands, predation risk is typically lowest at the benthos, but food availability and oxygen concentration are also low there [2][23] [3], especially at night, so remaining close to the sediment in the daytime could be advantageous for zooplankton due to a predation risk - food availability - oxygen tradeoff [45]. Zooplankton in this category may face an exceptional predation risk in their current environment and/or an exceptionally nutrient-poor and/or predator-rich environment were they to be advected out of their current habitat. For both types 4 and 5, zooplankton clouds upon downward migration are assumed to have a diameter of approximately nine inches

[31].

In the field, the extent to which zooplankton migrate and their exact paths will depend on the individual zooplankton species as well as on predator and macrophyte species present, light levels, bathymetry, and other factors. In addition, in the daytime zooplankton may avoid less dense macrophytes while being attracted to more dense macrophyte beds [38] [61] due to their disadvantages for zooplanktivorous fish [67] [44][9], [11] [48], [13] [7]. Thus, we will assume that the effect of predation and light levels is a basic 'normal' vertical migration strategy into intermediate-to-high macrophyte densities.

For each flow rate, SI3D output a binary file with the water speeds at each computational grid point at each output time. Ptrack was then run for all combinations of migration type and zooplankton cloud size standard deviation, using the velocities from SI3D.

3.3.4 Passive Particle-Tracking Model and Modifications

The particle tracking method used by ptrack solves the transport equation by representing particle position as the sum of particle displacements over time. Each displacement consists of a deterministic part (the first term below) and a stochastic part (the second term below) [17]:

$$dx_i = a_i(\mathbf{x}, t)dt + \sum_{j=1}^{3} b_{ij} dW_j(t), \tag{3.5}$$

where $\mathbf{x} = (x, y, z)$ is the particle position, $W_j(t)$ represents Brownian motion, simulated using a Gaussian number generator, with a mean of 0 and variance determined by the time step, and a_i and b_{ij} have to satisfy certain conditions, for

consistency with the transport equation [12], [17], [70], [30], [34]. The deterministic component requires the local velocity and the gradient of the turbulent diffusion, while the stochastic component requires the diffusivity. These quantities are either readily available from SI3D output (velocities and vertical turbulent diffusivities) or approximations are easily obtained (horizontal turbulent diffusivities). After the deterministic component advects each particle, the stochastic comonent of ptrack adds the effect of the variation of diffusion coefficients in the vertical particle displacement (drift), as well as a random step, representing particle displacement due to turbulence. Ptrack also includes a reflection algorithm that relocates particles in the water body when they run into physical boundaries so that no mass is lost during particle tracking.

Ptrack moves particles in each of the three coordinate (x, y, z) directions separately. Modifications to ptrack allowed model particles to 'behave' at set times in the z (vertical) direction, instead of only behaving passively. Zooplankton start vertical migration at 5:30 am and 8:30 pm, and for the most part they finish each migration period within a half hour. When migrating, the zooplankton move with a constant step size at each time step, until they reach their preferred height or depth (see below), as appropriate.

The algorithm for tracking passive particles can be modified to account for this vertical migration behavior as follows. After finding a continuous velocity field and continuously defined diffusion coefficients [17], the streamline through a particular point (in one dimension) $\mathbf{x} = \mathbf{x}_p$ can now be found by solving the following ordinary differential equation in one dimension:

$$\frac{\partial x}{\partial t}(t) = Ax + B \tag{3.6}$$

$$x(0) = x_p, \tag{3.7}$$

Distinguishing between the case $A \approx 0$ and $A \neq 0$ in order to avoid problems with machine dependent rounding off error, and defining $C = B/A$, we can easily solve for $A \neq 0$:

$$x(t) = (x_p + C)exp(At) - C$$

and for $A = 0$:

$$x(t) = Bt + x_p \tag{3.8}$$

To allow zooplankton to vertically migrate, A may be set to 0 and B may be set to the distance to be moved vertically, divided by the time allowed for migration. The value for B uses the maximum distance for migration, as, regardless of the type of migration employed by the zooplankton, the speed of migration remains constant in ptrack. At each time step, $x(t)$ will then equal the distance to move vertically added to the original location.

When particles participate in such a migration scheme, they are no longer prevented from crossing the bottom of the channel or the water surface, (or from descending into the macrophytes in the case of type 4) by physical principles. Thus, at the beginning of the prack simulation each zooplankter is assigned a 'preferred' height and depth. When this height and depth is reached, no further migration is allowed at that time for that particular zooplankter, although passive advection

of the zooplankter is allowed to occur. At the end of each vertical advective step, and after each migration step in the z direction, the current z-position of the zooplankter is checked and if it is above or below the preferred height or depth, respectively, it is set back to the preferred height or depth, as appropriate. These preferred heights and depths are chosen, independently from each other for each zooplankter, from a normal distribution whose standard deviation is the same as for the initial zooplankton cloud in the case of migration types 1, 2, and 3. In the case of types 4 and 5, the preferred depths are chosen from a normal distribution reflecting the smaller diameter of the zooplankton clouds upon migration down to the top of the macrophytes or down to the prop roots of the macrophytes.

In general, we would expect the zooplankton to be moving more slowly up and down in the macrophytes than they do in the open water above the macrophytes, due to the drag caused by the presence of the macrophytes, and, to a lesser extent, the potential desire of the zooplankton to associate themselves with the vegetation for purposes of food or protection. However, SI3D does not include a way of accounting for decreased vertical velocities due to vegetation, and diffusivity isn't linked to the presence of macrophytes in the vertical turbulence routine. As a result, the original simulations using the flow fields discussed above spread out and bounced the zooplankton around in the vertical over the entire water column, due to the increased diffusivity present at the interface between the macrophytes and the water above the vegetation. Figure 3.5 shows a vertical cross-section of diffusivity for unidirectional flow in both the presence and absence of macrophytes. The diffusivity curve is still approximately parabola-shaped, as expected, with an increased maximum turbulent diffusivity at the interface between plants and water. As the diffusivity has to come back close to zero at the surface and bottom of the

channel, a large diffusivity gradient develops, causing the drift and random step components of the particle tracking module to increase and helping to spread out the zooplankton in the vertical. This effect of diffusivity, combined with the lack of a way of dealing in SI3D with the vertical drag caused by the macrophytes, leads to unrealistic vertical motion for the zooplankton so that the effect of any parameter other than flow speed is washed out. As a reasonable way of dealing with this problem for the time being, we decreased the effect of drift and the random step in the vertical direction in ptrack to avoid zooplankton being unexpectedly pulled out of the macrophytes.

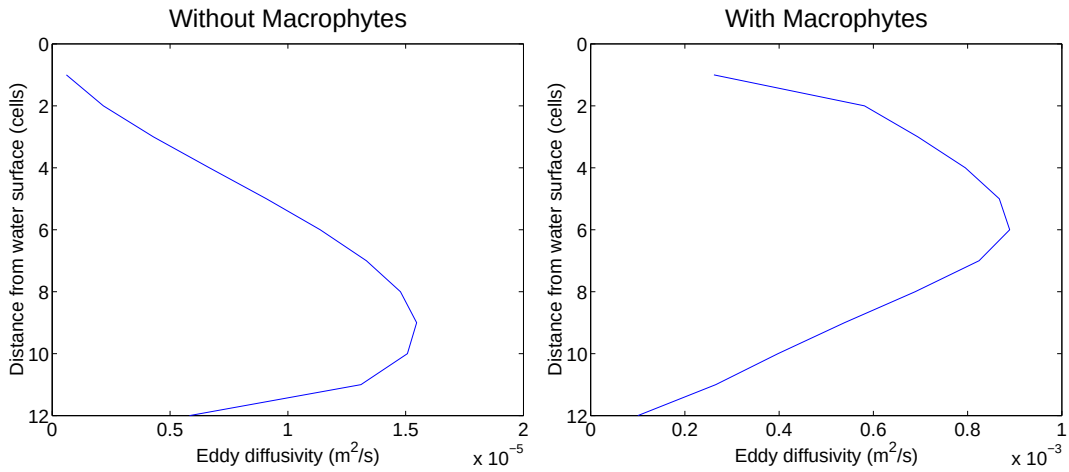

Figure 3.5: A typical vertical eddy diffusivity profile for a primarily unidirectional flow without and with macrophytes, respectively.

3.4 Results

We first consider the simplest flow regime, in which macrophytes fill the channel laterally as well as longitudinally, as the base case. Figures 3.6, 3.7, 3.8, 3.9, and 3.10 show typical plots of the beginning paths of zooplankton clouds under

the five different migration schemes for the larger of the two initial zooplankton cloud sizes. Each figure shows paths for each of the three flow speeds represented in the previous velocity field graphs. Distance down the channel is measured from west to east; the part of the channel representing the embayment of interest starts approximately 83,000 m from the westward end of the simulation basin and 40,000 m from the eastern end of the simulation basin in order to avoid issues with channel flow encountering either the western or eastern boundary, generating unphysical oscillations that could artificially affect simulation results (see Figure 3.1). Zooplankton clouds all start with their means in the x-direction set at 84,400 m and the channel empties into the lake at 83,000 m. Darker shades represent earlier time periods, with color getting lighter with passing time. Cloud position is plotted every two and a half hours, beginning with midnight. At midnight, zooplankton that are non-migrators or normal migrators are located at the top of the water column, while zooplankton that are reverse migrators are found at the bottom of the water column.

Figures 3.6 shows that when zooplankton are treated as passive particles, they move downstream above the macrophytes and out of the channel. In the part of the embayment in which the zooplankton cloud is initially seeded, the flow is downstream with a magnitude on the order of the background flow speed. Moving down in the water column toward the top of the macrophytes, flow speed decreases, which causes shear in the zooplankton cloud at all background flow speeds (in the absence of macrophytes, shear does not develop at higher background flow speeds). In the case of the two lower background flow speeds, the remnants of lock-exchange flow are encountered in the western part of the channel; their interaction with the background downstream flow produces intensified horizontal as well as

vertical flows at this intersection, resulting in vertically and horizontally stretched zooplankton clouds. Biological residence time in the case of the lowest flow is about a day, while at the intermediate flow speed, the zooplankton are retained in the embayment for an average of just over eight hours. In contrast, at the high flow rate, the background flow quickly pushes the lock-exchange flow out of the channel and flow is always in the downstream direction, resulting in the entire cloud moving as a cohesive unit out of the embayment within approximately six hours. Thus, the more complicated flow resulting from the complex interplay of exchange flow, macrophytes and background downstream flow result in biological residence times that are significantly different for all flow speeds, in spite of the sheared flow common to all.

When zooplankton undergo normal migration (Figure 3.7) with a start time of midnight, the cloud starts at the top of the water column. Under the lowest background flow speed, the zooplankton cloud moves downstream slightly at first but then moves to the bottom of the water column at sunrise, where it is more spread out in the horizontal than it was originally due to the shear experienced near the water surface and the randomness of preferred stopping depths. Due to the drag exerted by the macrophytes, essentially no horizontal motion exists inside the vegetation at this background flow speed, so that the zooplankton cloud basically sits there until sunset, when it migrates upward and to the west of its last location at the top of the water column. Thus, while retarding the downstream movement temporarily (residence time in this case is over five days), the macrophytes do not allow the migration upstream along the bottom of the embayment necessary for longterm retention. For the faster flow speed cases, the zooplankton cloud again initially moves downstream as it did in the case of no migration. In the inter-

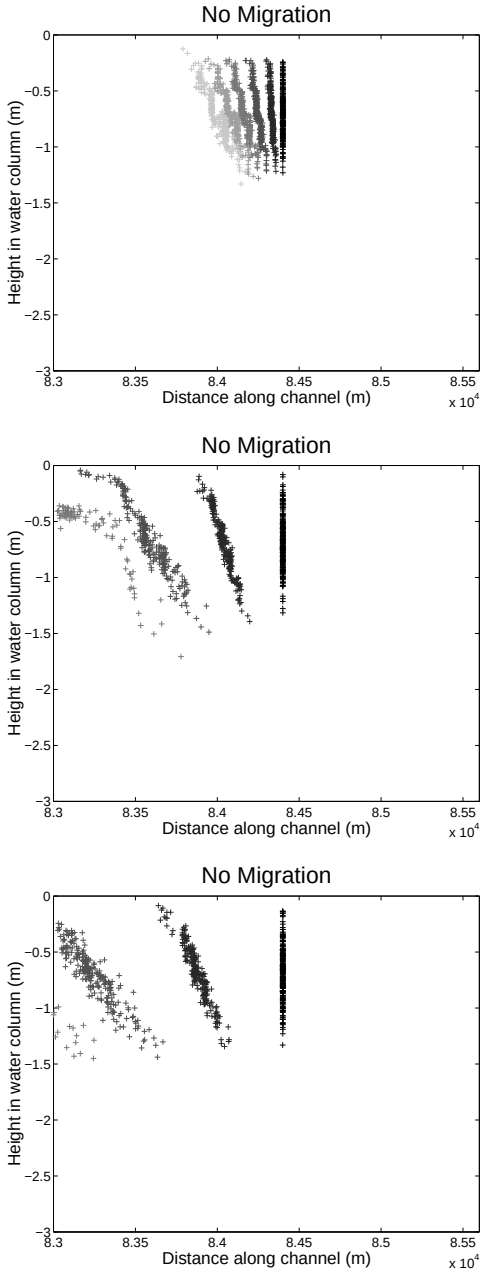

Figure 3.6: Zooplankton cloud movements in a macrophyte-filled channel under no migration for background flow speeds of 0.54 cm/s, 4.38 cm/s, and 8.22 cm/s, respectively, starting at midnight, with moderate plankton cloud standard deviation. Lighter shades of gray indicate increasing time, with sequential zooplankton clouds representing increments of 2.5 hours. Background flow east to west.

mediate flow speed case, the zooplankton have time to migrate to the bottom of the water column at a location affected by the exchange flow in such a way as to allow little horizontal movement (where some undergo vertical advection before being advected out of the channel), while under the highest background speed, some zooplankton are able to migrate down but most are simply advected out of the channel before they have a chance to undergo vertical migration (which would reduce the speed of their advection of the channel but would not in the end help retain them in the channel).

Under reverse migration (Figure 3.8), the zooplankton start out in the macrophytes. While the horizontal flow in the case of the lowest background flow speed is negligible, downstream flow speed increases in the macrophytes with increasing background flow speed, as well as with distance from the embayment floor, producing shear in the zooplankton cloud. In the case of the lowest flow speed, the zooplankton are not able to make any progress upstream before they migrate vertically upward and begin their advection downstream. They are retained long enough to migrate again but end up with an average residence time of under two days, about twice as long as the nonmigrating zooplankton. This result, compared with the previous result for zooplankton that migrate normally, is perhaps not surprising considering the fact that reverse migrating zooplankton are at the water surface during daylight hours, and the simulation assumes more daylight than dark hours per day. Under a background flow speed of 4.38 cm/s, the zooplankton are at the bottom of the water column in a horizontal location at which the flow is noticeably downstream; when migration up in the water column takes place, the zooplankton are simply advected out of the channel, giving a residence time of half of a day. In the case of the fastest background flow, the macrophytes prevent

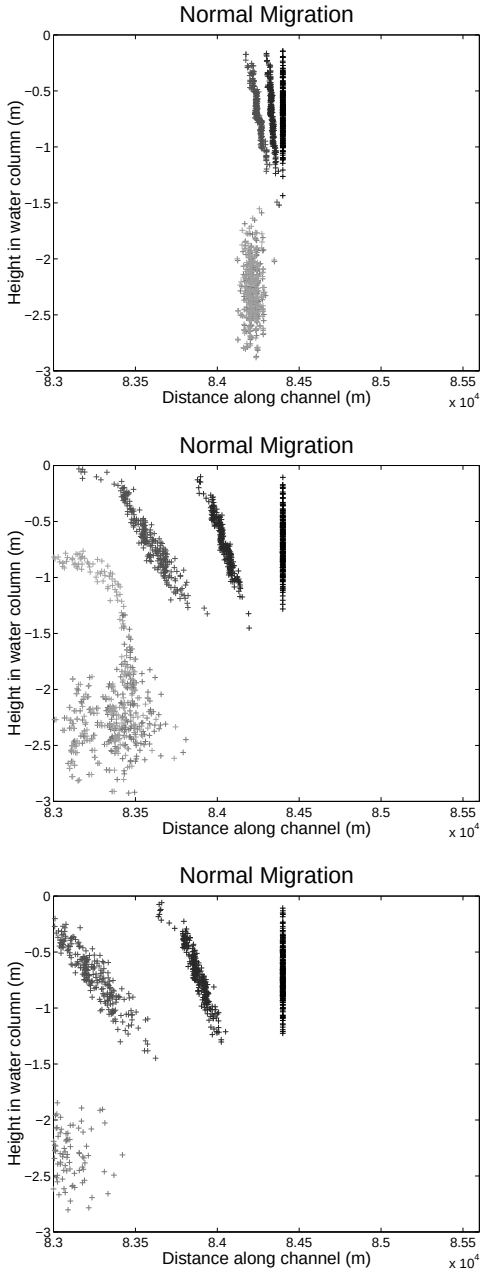

Figure 3.7: Zooplankton cloud movements in a macrophyte-filled channel under normal migration, respectively, for background flow speeds of 0.54 cm/s, 4.38 cm/s, and 8.22 cm/s, respectively, starting at midnight, with moderate plankton cloud standard deviation. Lighter shades of gray indicate increasing time, with sequential zooplankton clouds representing increments of 2.5 hours. Background flow east to west.

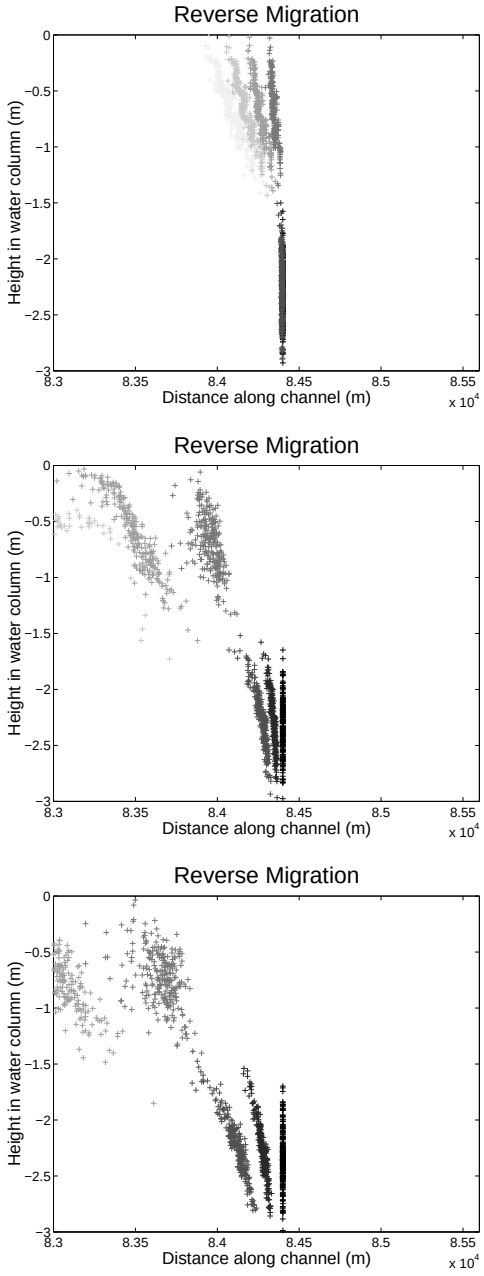

Figure 3.8: Zooplankton cloud movements in a macrophyte-filled channel under reverse migration, respectively, for background flow speeds of 0.54 cm/s, 4.38 cm/s, and 8.22 cm/s, respectively, starting at midnight, with moderate plankton cloud standard deviation. Lighter shades of gray indicate increasing time, with sequential zooplankton clouds representing increments of 2.5 hours. Background flow east to west.

upstream movement along the bottom of the embayment but at the same time, they prevent the zooplankton from being sharply sheared and/or simply advected out of the embayment, as happens in the absence of macrophytes (Chapter 2). Thus, reverse migration at these high background flow speeds leads to a residence time about twice as long as for nonmigrating zooplankton and about half again as long as for normally migrating zooplankton.

When the zooplankton undergo normal migration but only to the top of the macrophytes (Figure 3.9), the flow field in the bottom half of the embayment becomes virtually irrelevant. In the lowest flow speed case, the cloud is again spread out horizontally when it has migrated down in the water column, but instead of moving imperceptibly downstream, it is moving relatively quickly, with an average residence time of three days. At a background speed of 4.38 cm/s, the zooplankton again have time to migrate down to the top of the macrophytes and get caught in the complicated horizontal and vertical flow at the interface between downstream and exchange flow, which retains some of the zooplankton for longer than under no migration and leads to a residence time of over half a day. At the highest background flow speed, the movement of the zooplankton cloud appears very similar to that under the no migration scenario, with the zooplankton again leaving the embayment after approximately five hours.

When the zooplankton undergo normal migration with the modification that they cluster closer to the bottom in order to hide among the macrophyte roots (Figure 3.10), they tend to be retained in the embayment longer than if they clustered at the top of the macrophytes. For the lowest flow speed, when the zooplankton have migrated down to the bottm, they undergo almost no movement, either horizontal or vertical, until sunset, when they migrate up in the water column

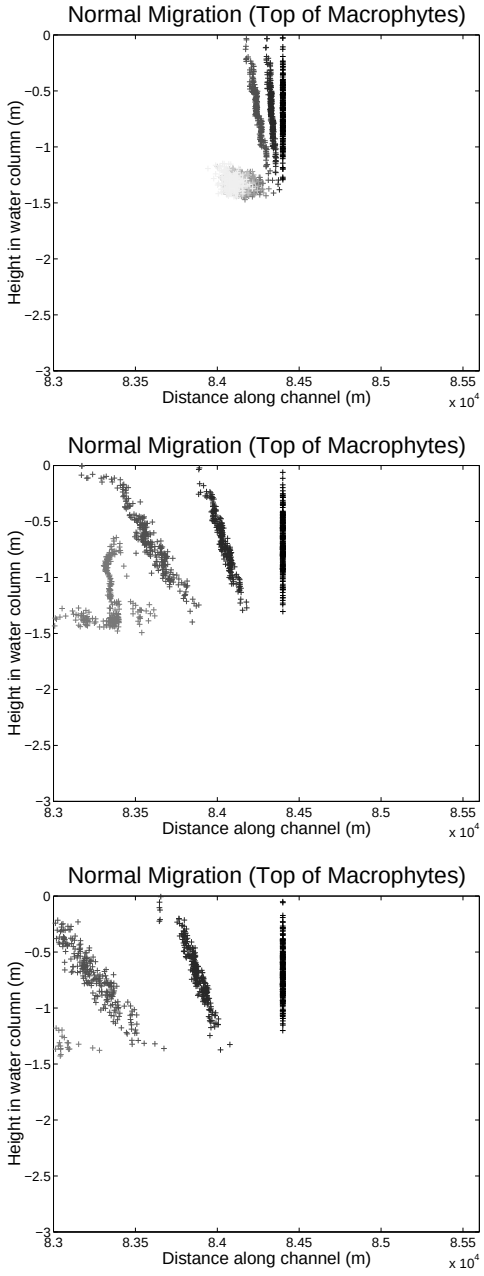

Figure 3.9: Zooplankton cloud movements in a macrophyte-filled channel under normal migration to the top of the macrophytes, respectively, for background flow speeds of 0.54 cm/s, 4.38 cm/s, and 8.22 cm/s, respectively, starting at midnight, with moderate plankton cloud standard deviation. Lighter shades of gray indicate increasing time, with sequential zooplankton clouds representing increments of 2.5 hours. Background flow east to west.

again; although they haven't managed to move upstream along the bottom, they haven't lost anything by migrating downwards. Biological residence time in this case is more than four days. In contrast, some slight upstream movement (in the remaining exchange flow region in the southwestern corner of the embayment) occurs under a background flow speed of 4.38 cm/s after migration down to the bottom of the channel, giving an increased biological residence time compared to migration type 4 of about 19 hours. At the highest flow speed, again migration occurs for some of the zooplankton before they are washed out of the embayment. However, the homogeneous downstream flow and, relative to the smaller background flows, lack of a sharp velocity difference in the macrophytes, means that regardless of where the zooplankton are vertically in the channel, they will endure the inexorable advection downstream and out of the embayment; in this case they do not remain any longer in the channel when they normally migrate than they did when not migrating at all.

Initial zooplankton cloud standard deviation can play an important role in determining biological residence time, especially at low flow speeds. All migration types tend to increase their residence times as standard deviation increases, sometimes twice as much or more, with the increase diminishing as flow speed increases. This result is reasonable as increasing standard deviation spreads the cloud out in the water column and thus potentially diversifies the movement of the plankton cloud as a whole, especially in the more complex flow fields. Figure 3.11 shows normal migration for a small and a larger zooplankton cloud under a low background flow. Due to differential horizontal velocities with depth, the larger zooplankton cloud remains larger and becomes more widely dispersed both horizontal and vertically, leading to an (eventually) larger biological residence time.

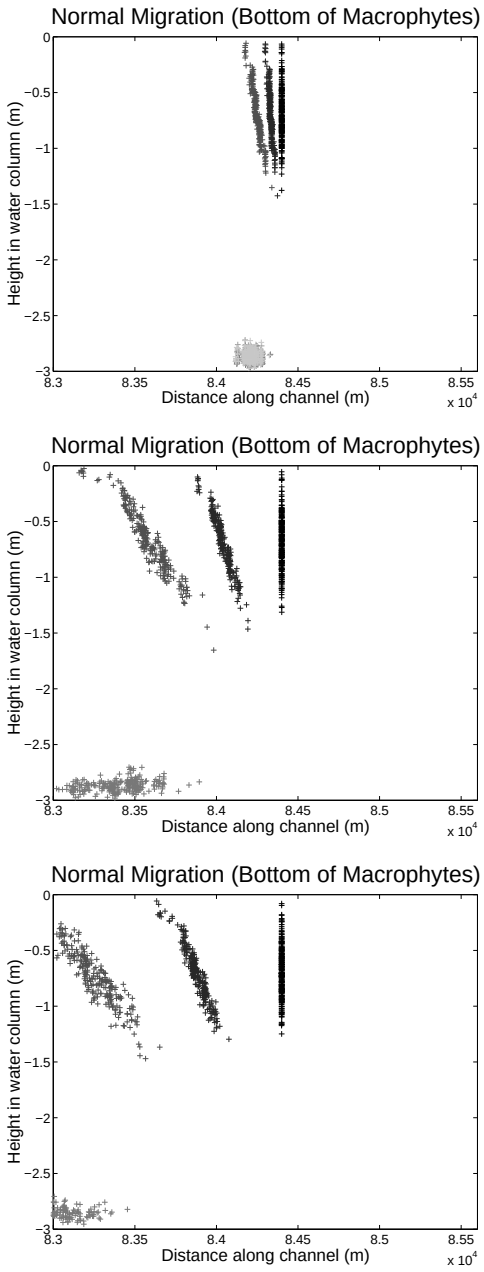

Figure 3.10: Zooplankton cloud movements in a macrophyte-filled channel under normal migration to the bottom of the macrophytes, respectively, for background flow speeds of 0.54 cm/s, 4.38 cm/s, and 8.22 cm/s, respectively, starting at midnight, with moderate plankton cloud standard deviation. Lighter shades of gray indicate increasing time, with sequential zooplankton clouds representing increments of 2.5 hours. Background flow east to west.

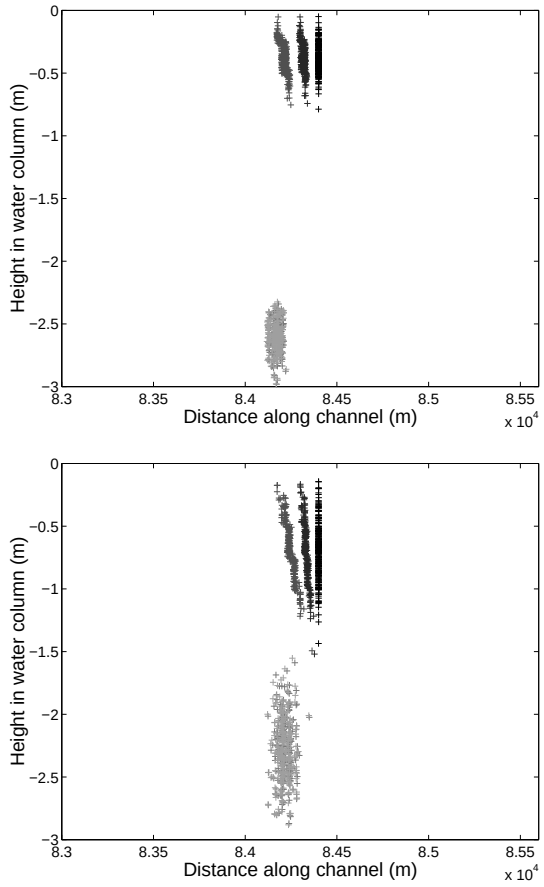

Figure 3.11: Zooplankton cloud movements under normal migration for a low background flow speed with low (top) and larger (bottom) zooplankton cloud standard deviation. Lighter shades of gray indicate increasing time, with sequential zooplankton clouds representing increments of 5 hours. Background flow east to west.

To determine if these trends between migration type and biological residence time hold over the range of flow speeds investigated, as well as whether zooplankton cloud sizes have a significant effect on biological residence time results, the mean residence time for zooplankton under every combination of flow rate, migration type, and zooplankton cloud size was computed. As lake conditions are potentially dangerous for the zooplankton and zooplankton may not be able to return to the embayment once in the lake, the first time that the zooplankton was advected into

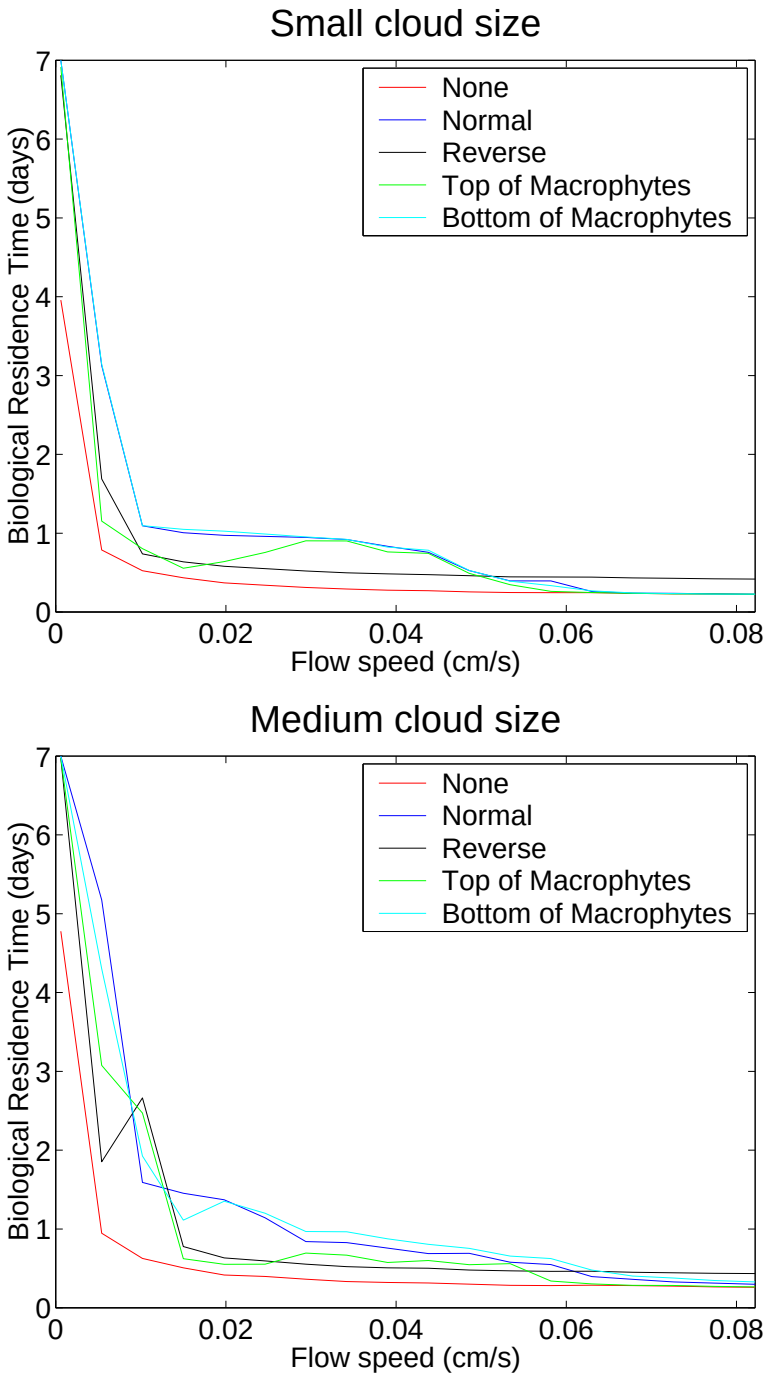

Figure 3.12: Background flow speed versus mean biological residence time by migration type for simulations starting at midnight for a zooplankton cloud with low (top) and medium (bottom) standard deviation.

the lake was taken as the residence time for the zooplankter. These times for all 250 plankton were then averaged to get a (mean) residence time in days. Figure 3.12 plots, for both zooplankton cloud sizes, how each of the five migration types influences the average biological residence time across the range of flow speeds studied. A mean residence time of seven days indicates that the zooplankton have avoided washout for the length of the simulation.

Some broad trends are clear from these two figures. Flow speed and migration type clearly exert a major influence on biological residence time, with all, or almost all, of the zooplankton able to remain in the embayment for the entire seven days for simulations using the lowest flow speed, any of the normal migration types, and an embayment-wide macrophyte patch. As flow speed increases, mean biological residence time tends to decrease; the greatest influence on residence time is found at lower flow speeds. Exceptions to this trend occur largely because of complexities in the flow field due to the combination of exchange flow, background flow, and drag from macrophytes interacting with each other. In general, not migrating produces the lowest average residence times, while some type of normal migration always does somewhat better at retaining plankton in the embayment under lower flow speeds, and reverse migrating zooplankton have average residence times somewhere in the middle. Normal migration and normal migration to the bottom of the macrophytes result in an increased residence time compared to normal migration to the top of the macrophytes, typically due to small downstream velocities at the top of the macrophytes. For the upper third of the flow speeds, migration type matters very little. The effect of zooplankton cloud size is clear from Figure 3.12. At lower background flow speeds, smaller zooplankton clouds have, in general, a noticeably smaller biological residence time.

Although the biological residence time versus flow speed plots are quite informative, they only give information about the fate of the zooplankton cloud as a whole. Knowledge of individual zooplankton trajectories is necessary to more clearly determine the factors impacting biological residence time in general. To account for individual organisms, we looked at the number of zooplankton left in the embayment over time (Figure 3.13). The figure shows zooplankton left for all five migration types and for the low, medium and high flow speeds considered earlier. Again, when determining the number of zooplankton left in the embayment, once a zooplankter is carried to the west of the outlet to the lake, it is considered to be no longer resident in the embayment.

The top two plots in Figure 3.13 give the number of zooplankton left in the embayment over time for the lowest background flow speed and for a zooplankton cloud with low and medium standard deviation, respectively. Non-migrators clearly do the worst job of staying in the embayment at the lower speeds, with all of the zooplankton washing out in a big clump before a day for the low standard deviation zooplankton cloud and at less than a day and a half for the medium standard deviation cloud. At the other end of the spectrum, normal migrators and normal migrators to the bottom of the macrophytes do the best job of staying in the embayment, no matter the standard deviation of the cloud; they are advected upstream when they migrate down in the water column and start leaving the embayment after the other types do and thus have more zooplankton left in the embayment at the end of the seven days. Moreover, they are clearly affected in similar ways (not surprisingly) by the flows they encounter, with zooplankton leaving the embayment under either migration scheme at similar times. In contrast, normal migrators to the top of the macrophytes encounter downstream flow when they

migrate downwards; they do considerably worse at the smallest zooplankton cloud size, leaving in one clump not long after the non-migrators. In the higher standard deviation case, they begin leaving the embayment soon after the non-migrators, but end up with about a third of the zooplankton remaining in the embayment at the end of the simulations, due to the spread of the zooplankton in the vertical and the complexity of the flow field close to the mouth of the embayment above the macrophytes. Reverse migrators do better than non-migrators but not nearly as well, in general, as the two normal migration types which migrate down to the bottom of the water column. Migration times were set in ptrack to be appropriate for mid-summer in the Great Lakes region, resulting in a longer day than night; as reverse migrators are in the upper half of the water column, in which flow is largely downstream, this result is perhaps not surprising. At this low flow speed, initial cloud standard deviation has a big effect on the number of zooplankton that remain in the embayment for all seven days; as standard deviation increases, more zooplankton survive until the end of the simulation. Interestingly, we cannot, in the case of these more complex flows, make the same generalization as in Chapter 2 that low standard deviation zooplankton clouds leave the channel essentially all at the same time, and higher standard deviation clouds leave in spurts. However, increasing the standard deviation of the cloud does 'spread out' the results, in the sense that the difference in worst and best migration schemes differ by less than 50 zooplankton left in the low standard deviation case and by about 150 in the medium standard deviation case.

The two middle plots in Figure 3.13 show the number of zooplankton left in the embayment for the medium background flow speed for both zooplankton cloud sizes. Regardless of the cloud standard deviation, the zooplankton start leaving

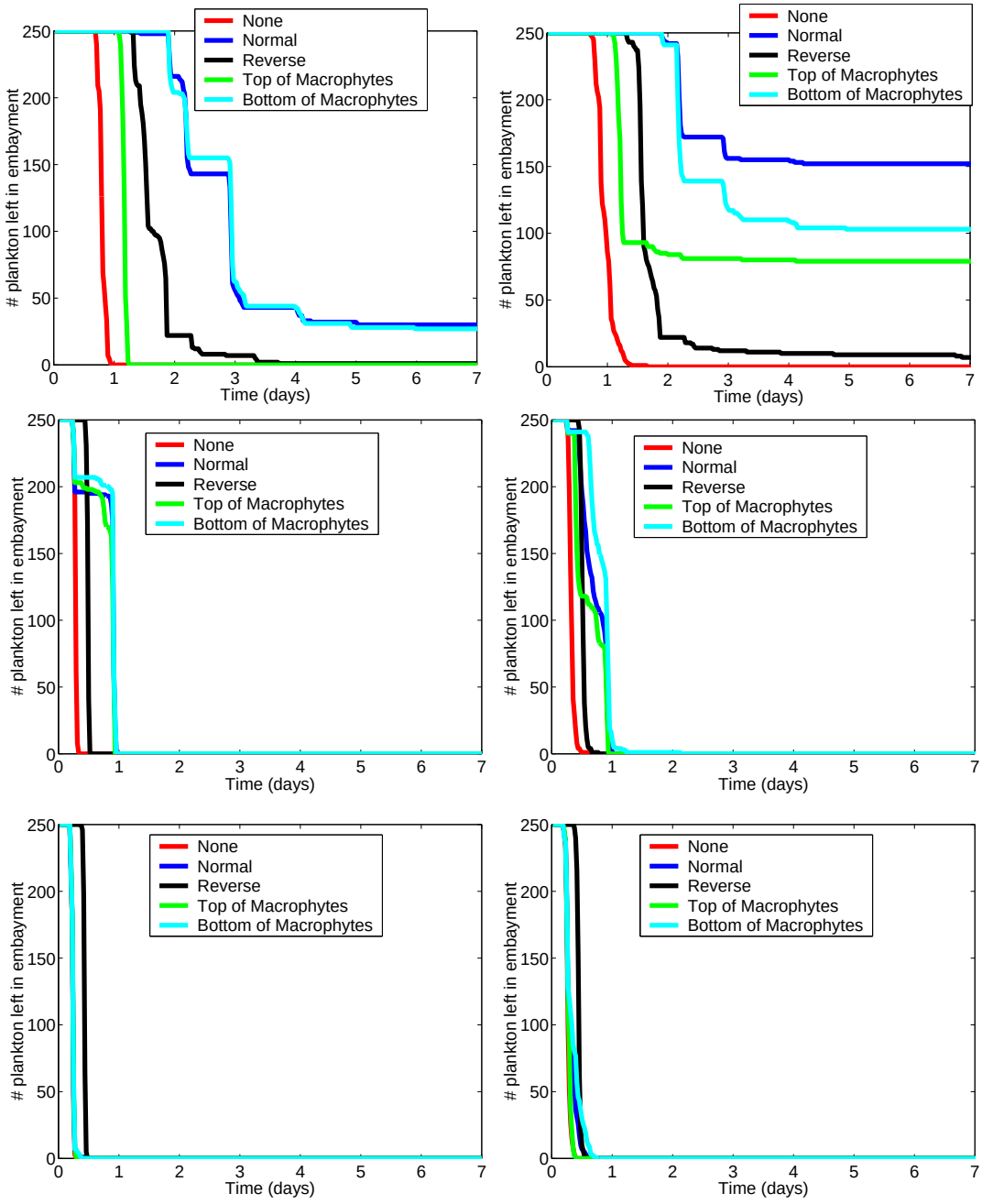

Figure 3.13: Number of zooplankton left in embayment versus time by migration type for simulations starting at midnight for a zooplankton cloud with low (left) and medium (right) standard deviation for low (top), intermediate (middle), and high (bottom) background flow speed.

the embayment after about half a day has passed. Although the reverse migrators are the last to start leaving the embayment, due to their retarded downstream movement while initially in the macrophytes, they are the next to completely leave the embayment, all in a single clump, after the non-migrators. While the normal migrators to the bottom of the macrophytes have the most zooplankton remaining in the embayment for the longest period of time, on about day one of the simulation, all normal migrators are washed out of the embayment.

The two bottom plots show zooplankton left versus time for a background flow speed of 8.22 cm/s for a midnight start time and low and moderate zooplankton cloud standard deviation. In this case, no exchange-flow exists and even the flow inside the macrophytes is still significant, so that the high background flow alone forces the cloud out of the embayment. Regardless of cloud size, the zooplankton start leaving the embayment at about the same time, after about eight hours, for all migration types except for reverse migrators. Reverse migrators can take advantage of the reduced downstream flow in which they find themselves at the start of the simulations in order to slow down their progress initially toward the embayment mouth. Eventually, however, after about half a day, they too are flushed out of the system. Increasing zooplankton cloud size does allow some normal migrators to slightly delay complete washout.

3.5 Statistical Analysis of Results

To more objectively determine the influence of the various model parameters on biological residence time, we simulated biological residence time for all combinations of the parameters: flow rate, migration type, and standard deviation of the zooplankton cloud. Using these data, a multiple regression analysis was performed.

Six evenly-spaced values for standard deviation were used, ranging from 0.25 to 0.5. Flow speed ranged from 0.06 m^2/s to 8.22 m^2/s, while migration type was one of 1, 2, 3, 4, or 5 representing no, normal, reverse, normal to the top of the macrophytes, and normal to the bottom of the macrophytes migration. Standard deviation and flow rate were considered continuous variables, while migration type was treated as a categorical variable. A linear model did not give an adequate fit to the data, so a generalized additive model with spline smooths was used. Different forms and combinations of explanatory variables were tried (using the gam function in the mgcv library [76] in R [69]) until a model accounting for an adequate amount of the overall variance in biological residence time and stable to additions or subtractions of terms accounting for small amounts of variance was found. The results are shown in Table 3.1.

Table 3.1: Percentages of variance in biological residence time explained by the three possibly key parameters determining biological residence time. 'Flow/Migration Type' denotes the two-way interaction between flow rate and migration type. The proportionate reduction of total variation in biological residence time associated with the use of the independent variables, or R^2, is 0.93.

Parameter	Percentage of Variance Explained
Cloud Standard Deviation	0.2%
Migration Type	1.1%
Flow Rate	35.4%
Flow/Migration Type	1.7%
Flow/Cloud Standard Deviation	54.4%

Flow rate by itself accounts for more than a third of the variance in biological residence time, while the other parameters don't have significant individual effects. The independent contribution of zooplankton cloud standard deviation to biological residence time is quite small, but, combined with its interaction with flow rate, overall it accounts for more than half of the variance in biological residence time. On the other hand, migration type has a small effect on residence time either in isolation or when combined with flow rate. In contrast with the earlier results from a plantless channel (Chapter 2), only about a third of the variance is accounted for by a single parameter, probably because the flow fields resulting from the presence of macrophytes are so complex that they do not have uniform effects on zooplankton for any particular migration type and zooplankton cloud standard deviation.

3.6 Discussion

Simulations using macrophytes represented by increased drag showed that the drift paradox problem can potentially be solved in the case of a low background flow when macrophytes fill half the height and all of the length and width of the channel and the zooplankton engage in some kind of normal migration strategy. We ended our simulations as of seven days as we did not want zooplankton reproduction to greatly complicate our conclusions about the impact of flow and zooplankton behavior on biological residence time [47]; high biological residence time values as of seven days do not distinguish between zooplankton that are about to be washed out of the channel, those that are oscillating back and forth in the channel, and those that are simply being advected upstream. Although longer simulations may be needed to determine whether the biophysical retentive effect persists with time

and clarify the effects of flow speed, migration type, and cloud size on zooplankton biological residence time, we can make some broad generalizations about the amount and type of influence of each of these factors. As was clarified by the statistical analysis, background flow speed is the most important factor controlling biological residence time, and in the presence of macrophytes flow speed is about three times as important as in their absence. Part of the reason is that when the channel is free of vegetation, exchange flow can persist even at faster flow speeds; however, the channel flow when macrophytes are present is much more tied to the background flow. (In contrast, in a vegetation-free channel, low background flow speed by itself is not at all effective at increasing residence time as exchange flow dominates). Thus, while the macrophytes might be thought of as barriers to zooplankton being advected downstream, they are also barriers to their drifting back upstream along the bottom of the channel. For high background flows, in which all steady flow is unidirectional, as in the case of clear water, biological residence time is low under any combination of the remaining parameters and zooplankton cannot avoid being flushed out of the system. Another effect of the macrophytes is that the downstream flow above the macrophytes has to be higher in general than the normal background flow. At lower flow speeds, the presence of macrophytes at the bottom of the channel pushes the remains of the exchange flow up above the macrophytes, which further increases the downstream flow at the top of the channel.

In a vegetationless embayment, the impact of various migration types is much clearer than in even the simplest type of channel including vegetation; in general, the non-migrating zooplankton have the shortest biological residence times, followed by the reverse migrators and then the zooplankton undergoing normal

migration. This result was not surprising given that migration times were set in ptrack to be appropriate for mid-summer in the Great Lakes region, resulting in a longer day than night, so that reverse migrators spent more time near the water surface than in the bottom of the embayment. In the simplest case involving vegetation of an embayment long and wide macrophyte patch, zooplankton that don't migrate in general start leaving the embayment first and have the lowest biological residence times for all flow speeds, while reverse migrators have a better biological residence time, although the number of zooplankton left at the end of the simulation may not differ much from the non-migrators. Normal migrators in general do the best, with 'regular' normal migrators and normal migrators to the bottom of the macrophytes tending to leave the embayment at similar times and have similar numbers of zooplankton left at the end of seven days under low flow speeds. Under low flow speeds, normal migrators to the top of the macrophytes spend all of their time in the high shear area above the macrophytes, leading to higher biological residence time and number of zooplankton left compared to the non-migrators; however, their relationship to the other migrating zooplankton in terms of biological residence time is indeterminate. In general, with more complexity in the flow, the relationship between migration type and biological residence time is not as clear; a complex flow insures that, regardless of migration type, the flow doesn't affect all of the zooplankton in a cloud in the same way, which has an averaging effect so that migration type doesn't matter as much. In spite of increased shear above the macrophytes at low-to-moderate background speeds, reverse migrators still have among the least amount of zooplankton left in the embayment at the end of the simulations for low flows and wash out before the normal migrators for intermediate background flows, perhaps due to the cloud not undergoing much

shear (in the macrophytes) early in the simulations. At higher speeds, the high downstream flow above the macrophytes doesn't allow the normal migrators time to migrate down in the channel and the slower moving reverse migrators in the macrophytes have an advantage.

The zooplankton cloud standard deviation has even less of an independent effect in this case (although it has quite an effect when combined with flow speed), perhaps because the range of zooplankton cloud sizes used in this study is less than in the previous (Chapter 2). In the presence of macrophytes, it is still true in general that the most zooplankton remain in the embayment for the duration of the simulation using a normal migration strategy and a larger zooplankton cloud. In addition, for all migration types, as cloud size increases, the number of zooplankton left in the embayment after seven days increases, and the first group to leave the embayment contains fewer zooplankton as standard deviation increases; the zooplankton don't necessarily start leaving the embayment any later but the increased cloud size allows the members of the cloud to be exposed to more of the diverse flow field, stretching out the amount of time that it takes for zooplankton to leave the channel. In contrast to Chapter 2, in the presence of vegetation the zooplankton do not appear to leave in more groups at higher standard deviation, probably due to the lack of influence of exchange flow.

As expected, the biological residence time was significantly better than without macrophytes at low flow speeds. These simulations show that even in slow-flowing embayments, macrophyte growth can dramatically affect water flow, potentially causing the original SI3D model flow results to deviate wildly from reality. The modifications to SI3D made to represent macrophytes, while helpful in determining the relative effects of background flow speed and increased drag, should be

refined [51] in order to more accurately represent real (and different) types of vegetation, and their effect on vertical as well as horizontal advection. With these refinements, model experiments may be done using a range of sizes and geometries of embayments, as well as a range of macrophyte abundances and configurations, in order to investigate the generality of these results. Understanding the true flow regimes in such bays/embayments is essential in answering fundamental questions about ecosystem function, determining the relative importance of exogenous versus endogenous influences in the bays/embayments, understanding the fates and movements of nutrients and (toxic) chemicals, and investigating the effects of varying external water levels. Eventually, using models such as these with suitable refinements, a seasonally much more realistic picture of the flow through such saltwater or freshwater channels should be possible, paving the way for incorporating the presence of macrophytes into management decisions relating to ecosystem restoration, chemical or sewage cleanup, and lake level, among other purposes.

Bibliography

[1] T. B. Benjamin. Gravity currents and related phenomena. *Journal of Fluid Mechanics*, 31(2):209–248, 1968.

[2] I. Blindow. The composition and density of epiphyton on several species of submerged macrophytes - the neutral substrate hypothesis tested. *Aquatic Botany*, 29:157–168, 1987.

[3] I. Blindow. Long- and short-term dynamics of submerged macrophytes in two shallow eutrophic lakes. *Freshwater Biology*, 28:15–27, 1992.

[4] H. Burchard. *Applied Turbulence Modelling in Marine Waters*. Number 100 in Lecture Notes in Earth Sciences. Springer, Berlin, 2002.

[5] R. W. Burke and K. D. Stolzenbach. Free surface flow through salt marsh grass. In *MIT-Sea Grant Report MITSG 83-16*. Massachusetts Institute of Technology, Cambridge, Mass., 1983.

[6] R. L. Burks, E. Jeppesen, and D. M. Lodge. Macrophyte and fish chemicals suppress Daphnia growth and alter life-history traits. *OIKOS*, 88:139–147, 2000.

[7] R. L. Burks, E. Jeppesen, and D. M. Lodge. Littoral zone structures as Daphnia refugia against fish predators. *Limnology and Oceanography*, 46(2):230–237, 2001.

[8] B. A. Christensen. Open channel and sheet flow over flexible roughness. In *Proc. Int. Assoc. for Hydr. Res. 21st Congress*, pages 463–467, Delft, The Netherlands, 1985. IAHR.

[9] L. B. Crowder and W. E. Cooper. Habitat structural complexity and the interaction between bluegills and their prey. *Ecology*, 63:1802–1813, 1982.

[10] P. Dawidowicz, J. Pijanowska, and K. Ciechomski. Vertical migration of chaoborus larvae is induced by the presence of fish. *Limnology and Oceanography*, 35(7):1631–1637, 1990.

[11] S. Diehl. Foraging efficiency of three freshwater fishes: effects of structural complexity and light. *OIKOS*, 53:207–214, 1988.

[12] K. N. Dimou and E. E. Adams. A random-walk, particle tracking model for well-mixed estuaries and coastal waters. *Estuarine, Coastal and Shelf Science*, 37:99–110, 1993.

[13] M. Dionne and C. L. Folt. An experimental analysis of macrophyte growth forms as fish foraging habitat. *Canadian Journal of Fisheries and Aquatic Sciences*, 48:123–131, 1991.

[14] J. Dorgelo and M. Heykoop. Avoidance of macrophytes by Daphnia longispina. *Verh. Int. Ver. Limnol.*, 22:3369–3372, 1985.

[15] R. Doyle-Morin. personal communication, 2006.

[16] C. Dunn, F. Lopez, and M. Garcia. Mean flow and turbulence structure induced by vegetation: Experiments. In *Hydraulic Engineering Series No. 51, UILU-ENG 96-2009*, Dept. of Civ. Engrg., University of Illinois at Urbana-Champaign, Urbana, Ill.

[17] D. W. Dunsbergen and G. S. Stelling. A 3-d particle model for transport problems in transformed coordinates. Technical Report 93-7, Delft University of Technology, Department of Civil Engineering, Hydraulic and Geotechnical Engineering Division, Hydromechanics Group, Delft, Netherlands, 1993.

[18] F. D. Ferrari, J. A. Fornshell, L. Ong, and J. W. Ambler. Diel distribution of copepods across a channel of an overwash mangrove island. *Hydrobiologia*, 499:147–159, 2003.

[19] H. B. Fischer. Mixing processes on the atlantic continental shelf, cape cod to cape hatteras. *Limnology and Oceanography*, 25(1):114–125, 1980.

[20] H. B. Fischer, E. J. List, R. C. Koh, J. Imberger, and N. H. Brooks. *Mixing in inland and coastal waters*. Academic, 1979.

[21] G. Flierl, D. Grunbaum, S. Levin, and D. Olson. From individuals to aggregations: the interplay between behavior and physics. *J. Theor. Biol.*, 196:397–454, 1999.

[22] C. L. Folt and C. W. Burns. Biological drivers of zooplankton patchiness. *Trends in Ecology and Evolution*, 14(8):300–305, 1999.

[23] J. D. Frodge, G. L. Thomas, and G. B. Pauley. Effects of canopy formation by floating and submerged aquatic macrophytes on the water quality of two shallow pacific northwest lakes. *Aquatic Botany*, 38:231–248, 1990.

[24] M. Ghisalberti and H. M. Nepf. Mixing layers and coherent structures in vegetated aquatic flows. *Journal of Geophysical Research*, 107(C2):3:1 – 3:11, 2002.

[25] R. E. Grizzle, F. T. Short, C. R. Newell, H. Hoven, and L. Kindblom. Hydrodynamically induced synchronous waving of seagrasses: 'monami' and its possible effects on larval mussel settlement. *Journal of Experimental Marine Biology and Ecology*, 206:165–177, 1996.

[26] A. C. Hardy and E. R. Gunther. The plankton of the south georgia whaling grounds and adjacent waters, 1926-1927. *Discovery reports*, 11:1–146, 1935.

[27] A. D. Hasler and E. Jones. Demonstration of the antagonistic action of large aquatic plants on algae and rotifers. *Ecology*, 30:359–364, 1949.

[28] J. Horppila. Diurnal changes in the vertical distribution of cladocerans in a biomanipulated lake. *Hydrobiologia*, 334:215–220, 1997.

[29] J. Horppila, T. Malinen, L. Nurminen, P. Tallberg, and M. Vinni. A metalimnetic oxygen minimum indirectly contributing to the low biomass of cladocerans in lake hiidenversi - a diurnal study on the refuge effect. *Hydrobiologia*, 436:81–90, 2000.

[30] J. R. Hunter. *Numerical modelling: applications to marine systems*, chapter The application of Lagrangian particle-tracking techniques to modelling of dispersion in the sea. Elsevier Sciences Publishers B.V., North-Holland, 1987.

[31] R. Johnson. personal communication, 2006.

[32] L. H. Kantha and C. A. Clayson. An improved mixed layer model for geophysical applications. *Journal of Geophysical Research*, 99:25,235–25,266, 1994.

[33] A. King. Field measurements of bulk flow and transport through a small coastal embayment having variable distributions of aquatic vegetation. Master's thesis, Cornell University, 2006.

[34] P. K. Kitanidis. Particle-tracking equations for the solution of the advection-dispersion equation with variable coefficients. *Water Resources Research*, 30(11), 1994.

[35] N. Kuczynska-Kippen. Diurnal vertical distribution of rotifers (rotifera) in the chara zone of budzynskie lake, poland. *Hydrobiologia*, 446/447:195–201, 2001.

[36] N. Lair, H. Taleb, and P. Reyes-Marchant. Horizontal distribution of the rotifer plankton of Lake Aydat (france). *Aquatic Sciences*, 58(3):253–268, 1996.

[37] W. Lampert, U. Sommer, and J. F. Haney. *Limnoecology: The Ecology of Lakes and Streams*. Oxford University Press, New York, 1997.

[38] T. L. Lauridsen and I. Buenk. Diel changes in the horizontal distribution of zooplankton in the littoral zone of two shallow eutrophic lakes. *Archiv. Hydrobiol.*, 137:161–176, 1996.

[39] T. L. Lauridsen and D. M. Lodge. Avoidance by Daphnia magna of fish and macrophytes: chemical cues and predator-mediated use of macrophyte habitat. *Limnology and Oceanography*, 41(4):794–798, 1996.

[40] T. L. Lauridsen, L. J. Pedersen, E. Jeppensen, and M. Sondegaard. Horizontal migration of zooplankton in the littoral zone in some shallow Danish lakes. *Lake Reservoir Manage.*, 9(2), 1994.

[41] F. Lopez and M. Garcia. Open-channel flow through simulated vegetation: suspended sediment transport modeling. *Water Resour. Res.*, 34(9):2341–2352, 1998.

[42] F. Lopez and M. H. Garcia. Mean flow and turbulence structure of open-channel flow through non-emergent vegetation. *Journal of Hydraulic Engineering*, pages 392–402, 2001.

[43] N. Louwen and T. Unny. Flexible roughness in open channels. *J. Hydraul. Div., Am. Soc. Civ. Eng.*, 99(HY 5):713–727, 1973.

[44] J. Manatunge, T. Asaeda, and T. Priyadarshana. The influence of structural complexity on fish-zooplankton interactions: a study using artificial submerged macrophytes. *Environmental Biology of Fishes*, 58:425–438, 2000.

[45] O. Marklund, I. Blindow, and A. Hargeby. Distribution and diel migration of macroinvertebrates within dense submerged vegetation. *Freshwater Biology*, 46:913–924, 2001.

[46] G. L. Mellor and T. Yamada. Development of a turbulence closure model for geophysical fluid problems. *Rev. Geophys. Space Phys.*, 20:851–875, 1982.

[47] J. E. Morris and C. C. Mischke. Plankton management for fish culture ponds. Technical Report 114, Iowa State University Agricultural Experiment Station, 1999. In cooperation with USDA's Cooperative State Research, Education and Extension Service.

[48] B. Moss, R. Kornijow, and G. J. Measey. The effects of nymphaeid (nuphar lutea) density and predation by perch (perca fluviatilis) on the zooplankton communities in a shallow lake. *Freshwater Biology*, 39:689–697, 1998.

[49] A. Murato, T. Fukuhara, and M. Sato. Turbulence structure in vegetated open channel flows. *J. Hydrol. Hydraul. Eng*, 2(1):47–61, 1984.

[50] H. M. Nepf. Drag, turbulence and diffusion in flow through emergent vegetation. *Water Resour. Res.*, 35(2):335–355, 1999.

[51] H. M. Nepf, J. A. Sullivan, and R. A. Zavistoski. A model for diffusion within emergent vegetation. *Limnology and Oceanography*, 42(8):1735–1745, 1997.

[52] H. M. Nepf and E. R. Vivoni. Flow structure in depth-limited, vegetated flow. *Journal of Geophysical Research*, 105(C12):28,547–28,557, 2000.

[53] M. D. Ohman, B. W. Frost, and E. B. Cohen. Reverse diel vertical migration: An escape from invertebrate predators. *Science, New Series*, 220(4604):1404–1407, 1983.

[54] R. W. Pennak. Some evidence for aquatic macrophytes as repellents for a limnetic species of Daphnia. *Int. Rev. Gesamten. Hydrobiol.*, 58:569–576, 1973.

[55] M. Raupach, R. Antonia, and S. Rajagopalan. Rough-wall tubulent boundary layers. *Appl. Mech. Rev.*, 44(1):1–25, 1991.

[56] M. Raupach, J. Finnigan, and Y. Brunet. Coherent eddies and turbulence in vegetation canopies: the mixing-layer analogy. *Boundary Layer Meteorology*, 60:375–395, 1996.

[57] M. R. Raupach and A. S. Thom. Turbulence in and above plant canopies. *Annual Reviews of Fluid Mechanics*, 13:97–129, 1981.

[58] W. Rodi. *Turbulence models and their applications in hydraulics: A state-of-the-art review*. International Association for Hydraulic Research, Delft, The Netherlands, 1984.

[59] L. C. Roig and I. P. King. Continuum model for flows in emergent marsh vegetation. In *Estuarine and Coastal Modeling*, pages 268–279, Tampa, Florida, November 1991. Waterway, Port, Coastal and Ocean Division of ASCE.

[60] F. J. Rueda. *A three-dimensional hydrodynamic and transport model for lake environments*. PhD thesis, University of California, Davis, 2001.

[61] S. D. Rundle and S. J. Ormerod. The influence of chemistry and habitat features on the microcrustacea of some upland welsh streams. *Freshwater Biology*, 26(3):439–451, 1991.

[62] K. Sand-Jensen. Drag and reconfiguration of freshwater macrophytes. *Freshwater Biology*, 48:271–283, 2003.

[63] K. Sand-Jensen and J. R. Mebus. Fine-scale patterns of water velocity within macrophyte patches in streams. *OIKOS*, 76:169–180, 1996.

[64] Z. Shi, J. S. Petchick, F. Burd, and B. Murphy. Velocity profiles in a salt marsh canopy. *Geo-Marine Letters*, 16:319–323, 1996.

[65] J. Smagorinsky, S. Manabe, and J. L. Holloway. Numerical results from a nine-level general circulation model of the atmosphere. *Monthly Weather Review*, 93:727–768, 1965.

[66] P. E. Smith. *A three-dimensional, finite-difference model for estuarine circulation*. PhD thesis, University of California, Davis, 1997.

[67] J. H. Stansfield, M. R. Perrow, L. D. Tench, A. J. D. Jowitt, and A. A. L. Taylor. Submerged macrophytes as refuges for grazing cladocera against fish predation: observations on seasonal changes in relation to macrophyte cover and predation pressure. *Hydrobiologia*, 342/343:229–240, 1997.

[68] V. L. Street, E. B. Wylie, and K. W. Bedford. *Fluid Mechanics, Third Edition.* WCB/McGraw-Hill, Boston, 1998.

[69] R Development Core Team. R: A language and environment for statistical computing. Technical report, R Foundation for Statistical Computing, Vienna, Austria, 2006.

[70] A. F. B. Tompson and L. W. Gelhar. Numerical simulation of solute transport in three-dimensional, randomly heterogeneous porous media. *Water Resources Research*, 26(10), 1990.

[71] J. C. Warner, C. R. Sherwood, H. G. Arango, and R. P. Signell. Performance of four turbulence closure models implemented using a generic length scale method. *Ocean Modelling*, 8:81–113, 2005.

[72] L. J. Weider and H. B. Stich. Spatial and temporal heterogeneity of Daphnia in lake constance; intra- and interspecific comparisons. *Limnology and Oceanography*, 37(6):1327–1334, 1992.

[73] D. C. Wilcox. Multiscale model for turbulent flows. *AIAA J.*, 26(11):1311–1320, 1988.

[74] N. R. Wilson and R. H. Shaw. A higher order closure model for canopy flow. *Journal of Applied Meteorology*, November:1197–1205, 1977.

[75] A. Wojtal, P. Frankiewicz, K. Izydorczyk, and M. Zalewski. Horizontal migration of zooplankton in a littoral zone of the lowland sulejow reservoir (central poland). *Hydrobiologia*, 506-509:339–346, 2003.

[76] S. N. Wood. *Generalized Additive Models: An Introduction with R.* Chapman and Hall/CRC, 2006.

[77] H. Yamazaki, D. L. Mackas, and K. L. Denman. *The Sea*, volume 12, chapter Coupling small-scale physical processes with biology, pages 51–112. John Wiley and Sons, Inc., New York, 2002.

Chapter 4

Implications of Zooplankton Vertical Migration for the 'Drift Paradox' in a Freshwater Embayment: A Modeling Approach

4.1 Abstract

The fact that many small aquatic and marine organisms manage to persist in their native environment in the presence of constant advection is known as the 'drift paradox.' The rate of advection in an embayment is chiefly affected by two factors: the rate at which water enters the embayment upstream (and moves downstream) and the temperature disparity at the mouth (causing different velocities of flow upstream). In addition, although advection may determine large scale biological patterns, individual behavior such as predation or vertical/horizontal migration can dominate at smaller scales. Possible mechanisms leading to the retainment of particular organisms in specific physical regimes have been studied in the field as well as using complicated hydrodynamic computer codes. We attempt to replicate, using a relatively simple partial differential equation containing both advective and behavioral components, basic residence time results from several numerical studies (Chapter2, Chapter3) of zooplankton in a channel-like freshwater embayment that might contain macrophytes (Chapter 3). The only behavior exhibited by the zooplankton is diel vertical migration. Water velocities used in our study are assumed

to be known and are taken from the previous studies. We compare biological residence times using this analytical model to an even simpler approximate residence time found by dividing channel length by mean longitudinal zooplankton velocity. For a channel without vegetation, both of the analytical methods give biological residence times that vary by at most a day from the computational results. When macrophytes are included, the analytical methods can greatly overestimate residence times for channels with low background flow rates, and the computational model should be used.

4.2 Introduction

Many organisms in linear habitats such as streams, rivers, and estuaries are continually subjected to predominantly unidirectional flow down a channel. Other examples of such a directional bias can exist in air (plants with windborn seeds) or saltwater (larvae influenced by ocean currents) as well. Some organisms can use obvious mechanisms such as strong swimming ability to swim back upstream or adaptations that lessen the likelihood of becoming entrained in the flow so as to remain in the channel. Some, such as most zooplankton, need to avoid being swept downstream completely out of this habitat and into another that might be much less hospitable. The fact that many organisms manage to persist in the presence of constant advection is known as the 'drift paradox.' As plankton populations indicate the health of an embayment ecosystem [12, 9], we need to understand under what conditions they will be washed out into inhospitable territory or advected back upstream into possibly equally inhospitable territory.

One possible solution to the drift paradox is the existence of an appropriate colonization cycle. Müller [10], [11] explained the unexpectedly high upstream

density of larval aquatic insects by suggesting that when competition becomes too high upstream, some larvae drift downstream, with the life cycle being completed when adults fly back upstream before oviposition. Tropical freshwater shrimps apparently undergo a similar colonization cycle (March et al. [8]). However, organisms that are continuously subject to drift or are not mobile or strong enough to overcome downstream drift cannot take advantage of such a cycle, and certainly upstream movement is unlikely to match downstream movement exactly. Alternatively, Waters [21] hypothesized that organisms that drift represent excess production above and beyond the carrying capacity; however, this 'production hypothesis' doesn't explain how the organisms that remain are able to do so. Anholt [1] argued that the production hypothesis implies that areas that suffer greater drift must experience a higher rate of population growth, or that population regulation is density dependent; he investigated the hypothesis using computer simulations and concluded that density dependence is necessary for persistence. In addition, organisms could take advantage of refugia (such as vegetation or areas behind rocks) in streams (Lancaster and Hildrew [5], [6]; Winterbottom et al [22], [23]; Rempel et al [15]; Lancaster [4]) or crawl on the benthos (Anholt [1]; Speirs and Gurney [20]; Humphries and Ruxton [3]) as a way of avoiding washout.

The environments in which the drift paradox occurs are "predominantly unidirectional," but this description does not preclude turbulence or other variability in stream flow direction. Some recent studies have looked at the possibilities for persistence resulting from the fact that most natural channel-like water bodies do not exhibit uniform flow. Regions of very low flow can serve as refuges for lotic organisms (Reynolds et al [16], Lancaster and Hildrew [5], [6]; Robertson et al [17], Reckendorfer et al. [14]). Importantly, such refugia can serve as sources for

repopulation after downstream drift depletes populations. Another type of hydrodynamic complexity arises due to the presence of tidal currents in estuaries, which, combined with organism movement (swimming) in the water column, could positively (or negatively) affect persistence; upward swimming could exploit the landward flood tide, while downward swimming could take advantage of the fact that bottom drag reduces seaward drift.

Beyond speculation, researchers have attempted to model possible resolutions of the drift paradox. Anholt [1] demonstrated that any dispersal with some sort of upstream component, not solely flight, could result in population persistence, although density dependence which favored persistence was built into his model. In addition, Ruxton and Humphries [3] showed that Anholt's model could lead to extinction over long periods of time. Speirs and Gurney [20] recognized that random motion due to both water movement (i.e., turbulence) and organism behavior (random movements by individuals) might be an important factor in persistence in streams and rivers that had not received much attention. Using advection-diffusion equations in which the deterministic aspects of downstream drift are approximated by the advective terms and random movements are captured by the diffusive terms, they investigated an increasingly complex series of models. Their base model was $\frac{\partial n}{\partial t} = f(n)n - v\frac{\partial n}{\partial x} + D\frac{\partial^2 n}{\partial x^2}$, in which $n(x,t)$ represents the density of the population per unit area, $f(n)$ is the per capita growth rate of the population, v is the rate of advection, and D is the diffusion coefficient.

First, they looked at a one-dimensional, linear, well-mixed stream with constant advection, in which no organisms can enter from the upstream end or move beyond the top of the stream and organisms may not reenter the stream once they cross the bottom boundary. They determined the balance between advection, critical

domain size, and population growth rate necessary for population persistence of the above model. Next, they move on to a model in two spatial dimensions by investigating a weakly-mixed river, in which the rate of advection is dependent on the organism's position in the water column, with water near the bottom almost stationary and water near the surface moving more rapidly: $V_x = V_R\left(1 - \left(\frac{z}{D}\right)^2\right)$, D is the depth of the uniform channel, V_R is the velocity of the surface water, and V_x is the horizontal flow velocity at depth z below the surface. As the drag near the bottom again causes the layers nearer the benthos to be moving more slowly, a type of flow refuge exists and allows the possibility of benthic persistence. In Speirs' and Gurney's [20] second two-dimensional model, they include a tidal oscillation that is superimposed on the previous model to represent an estuary and investigate the effects of near-bottom landward flow. Using a discrete space-and-time simulation strategy (as the models are not tractable analytically), they determined that the hydrodynamic variants did not have significant effects on the outcome and they produced a set of 'approximate inequalities' giving conditions for persistence.

Pachepsky et al [13] extended the model of Speirs and Gurney to look at persistence in benthic organisms. Motivated by aquatic insects whose larvae mainly live on the benthos but occasionally jump into the flow, they divide the population into two interacting compartments, one for individuals in the benthos and one for individuals drifting in the flow. The switching rates between benthos and the flow can be determined by insect behavior and/or stream hydrodynamics, although in their model, Pachepsky et al assumed a constant rate of entry into the drift. Their results showed that the compartmentalization significantly affected population persistence. In addition, they calculated the critical domain size needed

for population persistence and compared their results with those of Speirs and Gurney to determine how much the compartment approach improves persistence. They also computed spread speed and determined that persistence criteria and propagation speed are closely related. Lutscher et al [1] noted the limitations of PDE models in depicting complex asymmetrical flows and took advantage of integrodifferential equations to model the persistence of stream insects, with their probabilities of jumping into the flow as the dispersal kernel and including long-distance dispersal. Using thin-tailed kernels, a weighted sum of thin-tailed kernels, and fat-tailed kernels, they developed theoretical results on critical domain size and invasion speeds and concluded that long-term persistence is always possible under high flow as long as long-distance dispersal events happen often enough and are of a sufficient magnitude.

Chen et al [2] recognized the importance of estuaries as nursery grounds for the zooplanktonic larvae of many marine organisms, with larvae needing to remain in or return to the estuary despite downstream flow. While the interaction between tidal motions and the vertical migration of larvae is probably important in keeping larvae in the estuary, Chen et al attempted to isolate the effects of the tides by numerically following passive particles in a model of idealized flow, patterned after a small coastal-plain estuary with simple bathymetry, whose flow field was forced by oscillating tidal currents at the downstream end of the estuarine channel. Net upstream drift resulted from the combined effects of shear in the vertical and tidally-caused vertical motion and could partially offset net downstream transport by water flow. In addition, as the effect of the tides was greatest closest to the estuary mouth, the velocity of upstream drift increased with distance downstream, which tended to stabilize the positions of larvae in the channel. Thus, by itself,

the hydrodynamics of tides could provide an important means by which larvae can be maintained in estuaries.

Chen et al [2] determined that including tidal motions in a model of an estuary could by itself promote persistence of zooplankton; this conclusion is perhaps not entirely surprising in the presence of symmetrically oscillating flow at the mouth of the estuary. We investigate a similar but non-symmetric situation in which, instead of oscillating flow in the x-direction being the main driver of the hydrodynamics, an essentially oscillating flow in the z-direction is set up by mobile zooplankton periodically experiencing a primarily (constant?) upstream flow along the bottom of the channel, in contrast to the underlying downstream drift closer to the surface. Such a situation might be found in a freshwater channel-like embayment emptying into a lake, in which, while some tidal oscillation might be present, the main driver of the dynamics mitigating the downstream drift is the temperature difference between embayment and lake which causes flow back up the channel bottom, while zooplankton in the channel are vertically migrating on a daily basis. The water flowing downstream in embayments is typically warmer than the water in the lake into which the embayment empties. Colder water has higher density than warmer water, so its hydrostatic pressure increases with depth at a higher rate than that of warmer water. If, at a certain depth, the baroclinic pressure gradient (pointing upstream) becomes strong enough to overcome the inertia of the flow downstream, it will cause upstream flow, usually at a lower depth.

Chapter 2 computationally investigated, using a three-dimensional hydrodynamic model, SI3D [19, 18], and a modified post-processing particle tracking module, ptrack [18], the retention time of a cloud of migrating zooplankton in a narrow rectangular embayment emptying into a lake. While vertical migration is not the

only movement zooplankton can undertake (and the version of vertical migration in this study is simplified), it is a good place to start as it is a common behavior, and, under a nonuniform vertical velocity profile, might be expected to have a significant impact on organism persistence. Depending on the speed of the background downstream flow, the temperature differential between embayment and lake generated flow upstream along the bottom of the embayment. Zooplankton movement was modelled using ptrack, which was developed for the tracking of passive particles but has been modified to allow various types of vertical migration. Organism residence time was studied as a function of background flow speed, vertical migration type, simulation start time, and initial zooplankton cloud size. Chapter 3 modified the three-dimensional hydrodynamic model to simulate, in a relatively crude way, the presence of macrophytes in the channel and investigated zooplankton residence time as a function of vegetation, flow speed, migration type, and initial zooplankton cloud size. Rooted macrophytes can provide a refuge from downstream drift and thus might be expected to increase biological residence time in general. However, along with preventing downstream flow, the vegetation also prevented much of the upstream part of the exchange flow existing in the plantless embayments, preventing macrophytes from having a large retentive effect in these simulations.

We investigate, using a relatively simple partial differential equation, whether vertical migration in an embayment and the flow induced by the interface between the embayment and its destination lake can interact with each other in such a way as to 'solve' the drift paradox (i.e., allow the zooplankton to remain in the embayment). To determine the success of the analytical model, we compare our results with the numerical model results of Chapter 2 and Chapter 3, noting the

magnitude of biological residence times and the relative importance of various parameters such as background flow speed, vertical migration type, and size of zooplankton cloud.

4.3 Methods

We utilized a continuous in space and time partial differential equation to describe the interaction between water flow and organism behavior in an embayment-type system. Lutscher et al [7] imply that integrodifferential equations are more useful than PDE's for depicting complex asymmetrical flow, but they primarily take advantage of the dispersal kernel to depict sudden jumping by aquatic insects, a movement that is intrinsically different from the relatively steady motion involved in vertical migration.

We started with the simplest case of a two-dimensional linear stream with constant (but not uniform) advection and an absorbing boundary at the lower end representing the transition to habitat unsuitable for population growth or persistence. The upper boundary is considered infinite for the purposes of this modeling as downstream movement into the lake is presumably more likely and more consequential than movement upstream in the embayment. The two dimensions in this case are the x- and z-dimensions; in order for migrating zooplankton to experience different flows as they move up and down in the water column, the embayment must have at least two vertical layers experiencing different flow speeds. For a continuously varying vertical velocity profile, an approach similar to that of Speirs and Gurney [20] above can be used. In that same paper, Speirs and Gurney represented the tidal forcing at the seaward end of the estuary by a time-dependent function for surface velocity. As we are attempting to reproduce results from a

previous study, in which flow speed and temperature variability between embayment and lake is not easily represented by a simple function, we used flow field results from Chapters 2 and 3 as inputs to the model.

Once a base model was developed, various aspects of the persistence of zooplankton were explored under several types of migration regimes and initial zooplankton cloud sizes. The zooplankton in Chapter 2 undergo relatively simple migratory behavior falling into one of three categories; (1) the zooplankton are essentially passive particles (the no migration case), (2) the zooplankton are moving at a constant speed up in the water column at sunset and down in the water column at sunrise (the normal migration case), or (3) the zooplankton are moving at a constant speed down in the water column at sunset and up in the water column at sunrise (the reverse migration case). Chapter 3 adds two additional types of migration: (4) normal migration for which the ending point of downward migration is just above the macrophytes, and (5) normal migration for which the ending point of downward migration is just above the embayment bottom. Chapter 2 uses three zooplankton cloud sizes ranging from approximately 1/4 to 2/3 of the water column. The macrophytes in Chapter 3 are assumed to take up the bottom half of the water column, and the largest cloud size was not used in these simulations.

'Persistence' implies here that the zooplankton density in the channel remains the same, not necessarily that the zooplankton stays in the same lateral position over time. Thus, in the absence of population growth, persistence will require that no zooplankton leave the channel. Otherwise, the zooplankton can partially persist, which we measure in terms of 'biological residence time,' i.e., the mean amount of time that a zooplankter remains in the embayment before exiting for the first time.

4.4 The Model

We start with the classical advection-diffusion equation:

$$\frac{\partial n}{\partial t} + \frac{\partial (un)}{\partial x} = \frac{\partial}{\partial x}\left(\alpha \frac{\partial n}{\partial x}\right),$$

where n is the zooplankton population density, u is the velocity of the zooplankton in the x-direction and accounts for both the water flow and zooplankton swimming (how this is done is explained below), α is a diffusion coefficient, and x increases from left to right. Negative values of u indicate downstream flow. In this formulation, the diffusion coefficient is possibly a function of time and/or space. Other assumptions include:

1) population density $n(x, z, t)$ varies with time, distance along the x-axis, and height along the z-axis
2) zooplankton only actively swim in the z-direction
3) water velocity is constant in the x-direction but not the z-direction

In addition, we write u in the equation above as $u(z)$, where z is itself a function of t. This change allows varying flow, even flow in opposite directions, at different heights in the channel, while at the same time incorporating the effect of zooplankton vertical migration. This step obviates the need to have a separate term for zooplankton swimming speed.

If we assume that the effect of the diffusion term is negligible, then equation 1 simplifies to

$$\frac{\partial n}{\partial t} + \frac{\partial (un)}{\partial x} = 0,$$

where the second term is equivalent to

$$u\frac{\partial n}{\partial x} + n\frac{\partial u}{\partial x}.$$

As u does not vary in the x-direction but only in the z-direction, this second term above disappears and equation 1 becomes

$$\frac{\partial n}{\partial t} + u\frac{\partial n}{\partial x} = 0.$$

If u is constant in time, zooplankton behave as passive particles so that u once again simply represents exchange flow, which changes with height in the column but not with time or distance along the channel, then we have a first order, linear PDE and the solution can be obtained simply by using the method of characteristics. With initial condition $n(0) = f(x_0)$, the solution of the above equation is $u(t) = f(x_0) = f(x - ut)$, which is a traveling wave, with u as the speed of propagation.

If we suppose that the zooplankton actively migrate, then u is a function of t through its dependence on z, and wave speed depends on the temporal coordinate. We have a variable coefficient advection equation of the form

$$n_t + u(t)n_x = 0.$$

The characteristic equation is $x'(t) = u(t)$ with initial condition taken to be $n(x, 0) = n_0(x)$. The solution here again is a traveling wave, this time with $u(t)$ as the speed of propagation:

$$n(x,t) \quad = \quad n_0\left(x - \int_0^t u(s)ds\right) \tag{4.1}$$

We can think of this solution in terms of subtracting off the mean flow speed.

Depending on the situation (how fast the background flow is, etc.), the diffusion term may be the relatively more important term and therefore its presence necessary. First, we assume that the diffusion coefficient, α, is constant. We start with the partial differential equation

$$\frac{\partial n}{\partial t} + u(t)\frac{\partial n}{\partial x} = \alpha \frac{\partial^2 n}{\partial x^2} \tag{4.2}$$

with initial condition

$$n(0, x) = A(x)$$

where $n = n(t, x, z)$, $t > 0$, $-\infty < x < +\infty$. As when using SI3D in Chapters 2 and 3, we consider in essence an infinitely long channel and make the reasonable assumptions

$$\begin{aligned} \lim_{|x|\to+\infty} \frac{\partial n}{\partial x}(t, x) &= 0 \\ \lim_{|x|\to+\infty} n(t, x) &= 0 \end{aligned} \tag{4.3}$$

Equation 4.2 with the given boundary conditions physically represents advection at a rate $u(t)$ superimposed on a heat kernel spreading over time. Hence, its solution is given by

$$n(t, x) \;=\; \int_{-\infty}^{+\infty} A(y) \frac{1}{2\sqrt{\alpha\pi t}} e^{-\frac{1}{4\alpha t}\left(\int_0^t u(\tau)d\tau - (x-y)\right)^2} dy$$

which represents a diffusing cloud of zooplankton that also moves along the x-axis based on the specific characteristics of $u(z(t))$. Assuming an initial condition of

$A(x) = \delta(x - x_0)$, so that a 'pulse' of zooplankton (zooplankton cloud) is located at x_0, the solution becomes

$$n(t,x) = \frac{1}{2\sqrt{\alpha\pi t}} e^{-\frac{1}{4\alpha t}\left((x-x_0)-\int_0^t u(\tau)d\tau\right)^2} \tag{4.4}$$

We can plot this function for different values of $z(t)$ and $u(z)$, i.e., different migration schemes and flows, to get an idea of what the cloud is doing, as well as look at $n(t,x)$ for specific values of t and x. In addition, we can determine how many zooplankton have not been carried out of the channel as of time t by integrating $n(t,x)$ over positive x:

$$\begin{aligned}\int_0^\infty n(t,x)dx &= \int_0^\infty \int_{-\infty}^\infty A(y)\frac{1}{2\sqrt{\alpha\pi t}} e^{-\frac{1}{4\alpha t}\left((x-x_0)-\int_0^t u(\tau)d\tau\right)^2} dydx \\ &= \int_{-\infty}^\infty A(y)\frac{1}{2\sqrt{\alpha\pi t}} \int_0^\infty e^{-\frac{1}{4\alpha t}\left((x-x_0)-\int_0^t u(\tau)d\tau\right)^2} dxdy\end{aligned}$$

Now let

$$\begin{aligned} v &= \frac{1}{2\sqrt{\alpha t}}\left(\int_0^t u(\tau)d\tau - (x - x_0)\right) \\ dv &= -\frac{1}{2\sqrt{\alpha t}}dx.\end{aligned}$$

Then the number of zooplankton in the channel becomes

$$\begin{aligned}\int_0^\infty n(t,x)dx &= \int_{-\infty}^\infty A(y)\frac{-1}{\sqrt{\pi}} \int_{\frac{1}{2\sqrt{\alpha t}}\left(\int_0^t u(\tau)d\tau + x_0\right)}^{-\infty} e^{-v^2} dvdy \\ &= \int_{-\infty}^\infty A(y)\frac{1}{\sqrt{\pi}}\left(\int_{-\infty}^0 e^{-v^2}dv \int_0^{\frac{1}{2\sqrt{\alpha t}}\left(\int_0^t u(\tau)d\tau + x_0\right)} e^{-v^2}dv\right) dy \\ &= \int_{-\infty}^\infty A(y)\left(\frac{1}{2} + \frac{1}{2}\text{erf}\left(\frac{1}{2\sqrt{\alpha t}}\left(\int_0^t u(\tau)d\tau + x_0\right)\right)\right) dy\end{aligned}$$

where $\text{erf}(x) = \frac{2}{\sqrt{\pi}} \int_0^x e^{-t^2} dt$ is the error function. The value along the x-axis used to represent positive infinity in the limits of integration can be determined for a particular flow regime based on maximum upstream velocities for that flow regime.

Numerical experiments were performed to evaluate the extent to which diffusion changes with time by considering a range of flows of a similar nature to what is considered in this model - i.e., primarily unidirectional flow in a channel with a lock-exchange at the downstream end and starting a zooplankton cloud at varying water column heights. We contrasted the amount of horizontal diffusion over time with height, which changes for zooplankton in a predictable way with time due to their diel vertical migration, and in this way, determined whether the degree to which diffusion changes with time is significant. These experiments showed virtually no diffusion with time in the faster flow regimes, while in the slower flow regimes some stretching out of the zooplankton cloud was observed with time, especially for clouds starting in the center of the channel. This effect was presumably due to the larger effect of the lock-exchange flow than the background flow on the flow field, which produced a shearing effect. Thus, even in the case of very low background flows, the change in diffusion with time was demonstrated to be insignificant compared to the resulting flow in the channel.

4.5 Simulations

Simulations were run for up to seven days to investigate biological residence time for different flow speeds, migration types, initial zooplankton cloud standard deviations, and macrophyte configurations. For the initial simulations, one zooplankter was simulated whose starting positions in the longitudinal (x) and vertical (z) directions were the center of the zooplankton cloud in those directions. Thus, while

the starting position in x was constant throughout the simulations, the vertical positions were determined by the initial cloud standard deviation. While 250 zooplankton were used in the original study, the number of zooplankton left in the embayment in the current simulations was determined by multiplying the total proportion remaining in the embayment by 250.

The flow regimes from Chapter 2 were usually quite homogeneous in the horizontal, with low background flow speeds producing dominant exchange-flow and high flow speeds producing dominant uni-directional flow. Thus, the steady flow fields of most of the 18 background flow rates studied essentially take one of these two forms. In Figure 4.1, the first plot shows a typical velocity profile for slower background flow speeds: relatively large negative (downstream) velocity at the surface, somewhat smaller positive velocity below mid-depth, and zero velocity somewhere around mid-depth. In contrast, the second plot shows that at higher flow speeds, advection is always downstream, with flow speed decreasing with water depth. However, at several intermediate flow speeds, exchange-flow and uni-directional downstream flow vie for dominance and thus flow is heterogeneous in the horizontal. In Chapter 3, the combination of varying widths and lengths of macrophyte patches, along with the temperature difference between embayment and lake, produce heterogeneous velocities in the x-direction.

The success of the analytical model is based largely on the appropriateness of the zooplankton migration behavior and on the water flow. As we have available flow regimes from the past numerical simulations (Chapter 2 and Chapter 3), we used these to provide us with appropriate u values for the model. For each of the 18 values for background flow speed, taking the longitudinal values for velocity over the 1400 m long channel, we averaged the velocities at each vertical grid cell

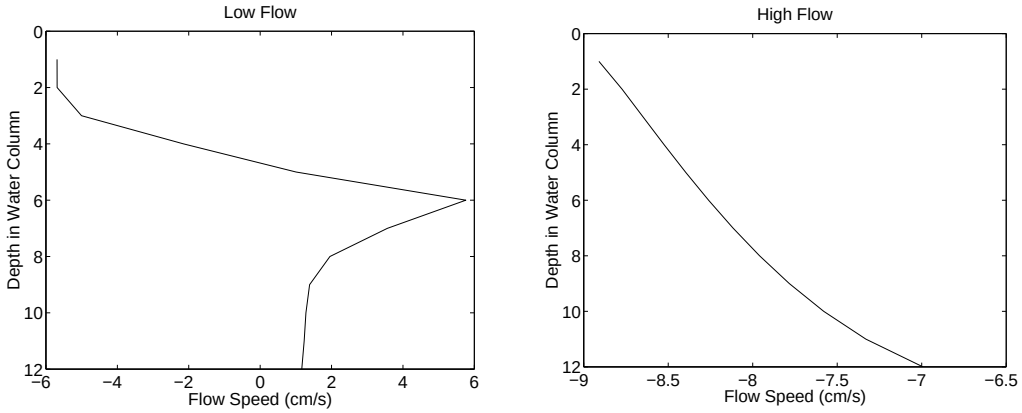

Figure 4.1: Flow fields for a low flow (-0.06 cm/s) and a high flow (-8.22 cm/s). From Chapter 2. Negative u represents downstream flow.

depth over all of the simulation time from Chapters 2 and 3. The hope is that this step averages out the effect of any oscillations, differing flow speeds and directions of flow and gives a more realistic overall result than would taking a cross-section at one particular location when the flow field is not homogeneous in the x-direction. Given zooplankton position in the vertical, linear interpolation was then used to find the appropriate value of u.

The vertical position of migrating zooplankton can be represented analytically by using a fairly simple function representing zooplankton position in the vertical with time, such as

$$z(t) = 1 - \frac{\tanh[\alpha \cos(\frac{2\pi t}{24})] + 1}{2},$$

where the cos function drives the periodicity, the tanh function generates a constant almost 12 hour day and night and the α applied to the tanh function drives the transition time from passive state to swimming state. The value of α controls how much intermediary time exists between the passive and active states. As α

gets larger and larger, the transition from the bottom of the water column to the top and vice versa becomes essentially instantaneous. In the previous studies, the zooplankton migrate for approximately half an hour. Thus, for our model, with a half hour time step, we decided to use a large α of 1000 so that the change from top to bottom of the water column would take about the same amount of time.

Chapter 2 investigated the effect of varying zooplankton cloud sizes, with the standard deviations of the clouds ranging from 1/4 to 2/3 of the height of the water column of 3 meters, with an intermediate value of 11/24 of the water column. Chapter 3, investigating a channel containing macrophytes whose height is half the height of the water column, only used the two smaller cloud sizes. In addition to our choice of α, we modified the generic function $z(t)$ to force the position function to have a maximum and minimum that are a distance equal to the radius of the zooplankton cloud from both the bottom and top, respectively, of the water column. This change was deemed desirable to keep the code relatively simple, yet take into account the fact that members of larger zooplankton clouds (having larger standard deviations) can find themselves in quite different flow fields than members of smaller clouds. Along with these changes, we shifted the function appropriately in order to provide the correct amount of nighttime hours, assuming a start time of midnight, before migration starts.

With these changes, the position functions for normal migration, with a start time of midnight, are as in Figure 4.2. Normal becomes reverse migration when a negative is applied to the tanh function. The position function for no migration is simply a horizontal line that is a distance of the zooplankton cloud mean from the surface. The term involving $z(t)$ can be disregarded and u treated as a function of z instead of t if the zooplankton do not migrate.

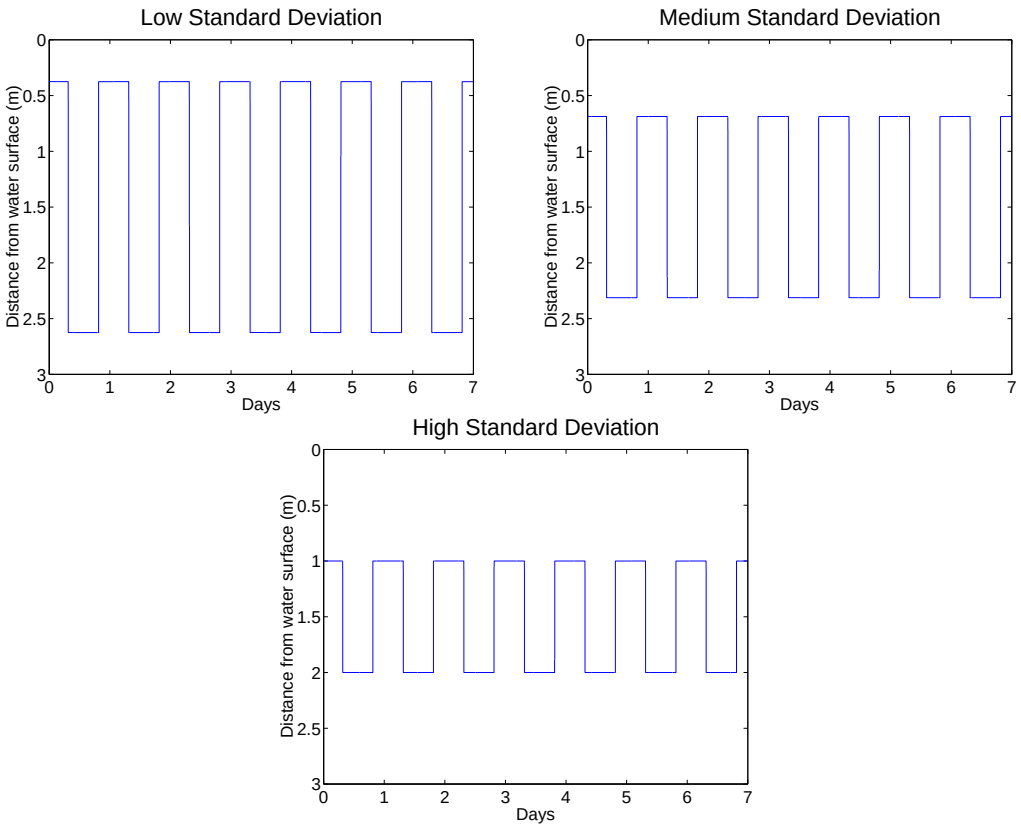

Figure 4.2: Generalized position of zooplankton in the water column by time, for the zooplankton cloud sizes used in Chapter 2. Vertically migrating zooplankton make a complete circuit every 24 hours, with simulations lasting for seven days and starting at midnight.

In Chapter 3, migration type 4 does not allow the zooplankton to enter the macrophyte bed and both migration types 4 and 5 assume, upon the completion of downward migration, that the zooplankton are contained in a cloud whose diameter is no larger than the height of the macrophyte roots, regardless of their initial zooplankton cloud standard deviation. Thus, the ending height in the position functions in figure 4.2 were modified appropriately for these migration types. Regardless of whether a zooplankter is a normal or reverse migrator, using this form of position function, the time spent at the top of the water column is equal to

the time spent at the bottom, or equivalently, night and day are of approximately equal lengths. We compare our results here with equal day/night simulations from Chapter 2 and new equal day/night simulations computed for various flow scenarios from Chapter 3.

While the zooplankton's starting longitudinal position never changes and is taken into account by the x_0 in the $n(t, x)$ equation, up to this point, we have been considering the zooplankton cloud as a point source whose position function follows the path of a zooplankter at the mean of the cloud. Thus, the different starting positions in the vertical direction of different zooplankton in the cloud are not taken into account. Especially as flow speed decreases and the spread of the initial zooplankton cloud increases, differing vertical placements could have a significant impact on the resulting biological residence time and should be considered (see Figure 4.3). Ideally, we would like to integrate biological residence time over vertical starting position. Given that the initial zooplankton cloud is normally distributed, we could think of the number of zooplankton left after seven days (168 hours), or any time t, as $250 * Pr(T > t)$, which, using the law of total probability can be rewritten as

$$P[T > t] = \int P[T > t | z_0 = z] \Phi(z) dz$$

where Φ denotes the probability of z being chosen from a normal distribution with given mean and standard deviation. However, true integration would be prohibitively expensive computationally. Alternatively, we could use the approximate integration method of Gaussian quadrature to estimate biological residence times, which should require computation of biological residence time at a relatively small number of starting vertical positions and gives greater accuracy than other ap-

proximate integration methods for the same number of computations. For these computations, the z position function stayed the same as before, except that for each Gaussian quadrature node its position in the water column shifted up or down the distance of the node value multiplied by the standard deviation of the zooplankton cloud. (Note that stopping locations for individual migrating zooplankton in ptrack were based on these same standard deviations, with position at the top and bottom of the migration path chosen separately.)

The original simulations (Chapters 2 and 3) used an individual based model, which allowed different scenarios for each zooplankter (a different initial position and preferred height and depth, based on the size of the zooplankton cloud). Significantly, the individual based model also allowed us to distinguish between zooplankton when they crossed over between embayment and lake so that we could take the first time such a crossing occurred when computing biological residence time. In contrast, for the pde model, we cannot distinguish between individual zooplankton and instead simply have a distribution that is moving up and down the channel. In our simulations, when a fraction of the distribution first crosses the embayment-lake boundary, we multiply that fraction by 250 (the number of zooplankton in a zooplankton cloud in the original studies) and determine that that number of zooplankton have exited the channel, which defines their biological residence time. If the distribution then moves back into the embayment, and then out again so that the same fraction is beyond the line separating the embayment from the lake, we assume that the same zooplankton have returned to the embayment and then departed again and do not compute any more biological residence times at this point. Only when a larger fraction of the distribution crosses into the lake do we assign the current time as the biological residence time for the

additional fraction. Unfortunately, while this method should avoid some "double counting" of zooplankton exits, the zooplankton should be assumed to be moving relative to each other because of turbulence, as well as experiencing different horizontal velocities due to having their own individual migration paths. Thus, when the same fraction of the distribution again crosses the embayment-lake boundary, if a new zooplankter is now in the lake, rather than the original that exited, its biological residence time will be overestimated.

To determine whether this overestimation is significant, we compared the results using the pde to another, simpler approximation. The mean horizontal zooplankton velocity over a day remains constant throughout the simulations, due to the assumption that u is homogeneous in x. Thus, we estimated the mean first time to exit for the zooplankton cloud as embayment length divided by the mean zooplankton horizontal velocity, found by averaging the u over a 24 hour period. (As in the analytical simulations discussed previously, values for horizontal water velocity were averaged over time and horizontally.) In the example above, this approximation might be expected to give a biological residence time that averages the first and second times that the "new" zooplankter crosses the lake-embayment boundary and thus might give results close to the true biological residence time.

4.6 Results

4.6.1 Simulations without Macrophytes

Simulations were first run in Matlab, for a single zooplankter whose migration path in the vertical extended between the mean of the zooplankton cloud at the top and at the bottom of the water column, for seven days for all combinations

of flow speed, migration type, and initial zooplankton cloud standard deviation. Results, shown in Figure 4.3 by standard deviation, show the residence times for the 18 flow speeds studied by migration type (keyed by color) and type of model (solid lines denote the analytical model, while symbols denote ptrack results). For the smallest zooplankton cloud, the analytical and computational results are very close, except in the case of flow 9 with the smallest variance and no migration (in which a downward vertical velocity forces some zooplankton to the bottom of the embayment at which point they are carried upstream and retained for longer than the average biological residence time).

The second plot in Figure 4.3, showing results for a medium-sized zooplankton cloud, demonstrates somewhat of a downward trend in biological residence time with flow speed and an upward trend with zooplankton cloud size, which we would expect based on the earlier results. In addition, it shows that not migrating leads to lower residence times than either type of active migration and that reverse migration typically leads to higher biological residence times than normal migration, at least with a starting time of midnight. The degree to which the reverse migrating zooplankton remain longer in the embayment than the normal migrating zooplankton also appears to be similar in general.

For the computational model in the medium variance case at lower speeds, the more spread out zooplankton cloud now contains some members that are low enough in the water column to be experiencing a slower downstream velocity or even the upstream part of the exchange flow (see Figure 4.1). As an example, Figure 4.4 shows the zooplankton positions every 2.5 hours for a zooplankton cloud with medium standard deviation migrating normally under a background flow of 0.06 cm/s (flow 1) using ptrack. The lowest zooplankton in the initial cloud are

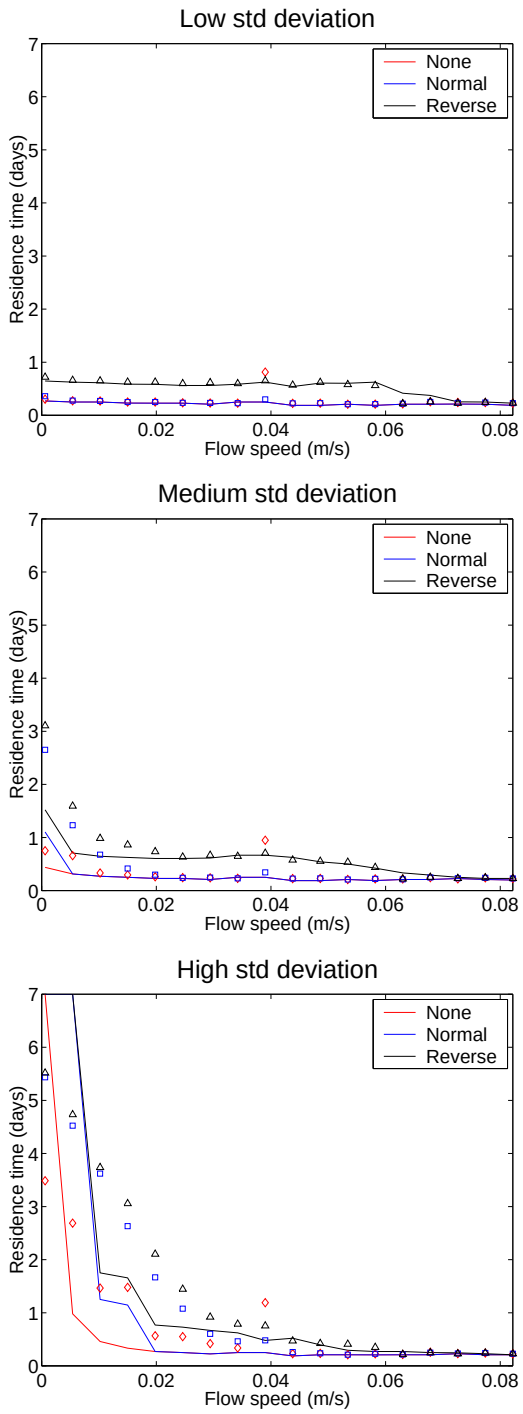

Figure 4.3: Flow speed versus residence time by zooplankton cloud standard deviation for Chapter 2 simulations (without macrophytes) compared with analytical results using one zooplankter. Solid lines represent analytical results from the current study, while symbols represent early computational results.

progressing slightly upstream instead of downstream and thus are in a position to be retained in the embayment and carried back upstream when migration starts. However, the analytical model follows a zooplankter, located at the mean in the vertical of the zooplankton cloud, which cannot benefit from the velocities further down in the water column. The disadvantage of this simplification in the analytical model is seen in the large differences for the first several flow speeds between the analytical and computational results, especially in the case of normal and reverse migration, when the differential vertical velocities lead to upstream flow for some zooplankton. At higher flow speeds, this problem does not occur, as the vertical velocity toward the upper part of the water column becomes more and more homogeneous, and, moreover, becomes fast enough at the highest speeds that the zooplankton are simply washed out of the embayment without an opportunity to migrate.

The results for the largest zooplankton clouds, shown in the third plot in Figure 4.3, demonstrate a more pronounced effect of flow speed on residence time. Due to the same shearing effect of velocity mentioned in the case of medium initial zooplankton cloud size, in this case even more pronounced because of the cloud protruding more deeply into the water column, very slow flows in the computational model allow the zooplankton to remain in the embayment for considerably longer than they did under the other two zooplankton cloud sizes. At moderately low flow speeds, the computational model results are again considerably larger than the analytical results, due to the retaining ability of this shearing effect. However, at the lowest flow speeds, the analytical results show that all of the zooplankton are retained for all seven days, while the computational zooplankton have a much lower biological residence time. Although this result might seem to contradict the

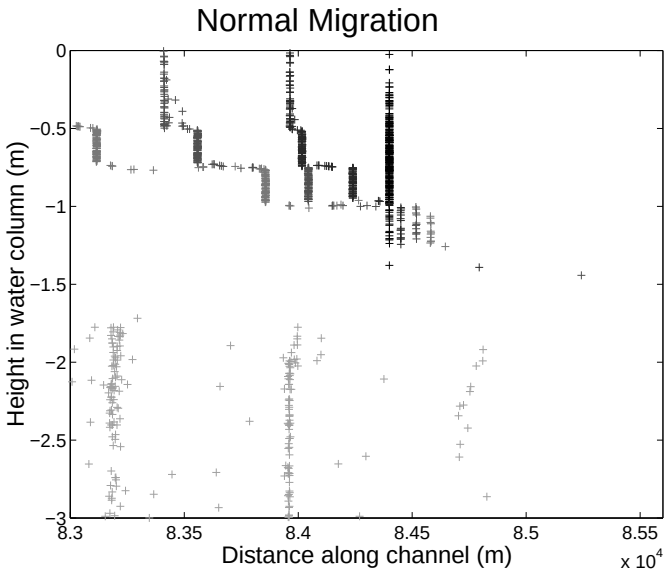

Figure 4.4: Output from ptrack showing zooplankton positions every 2.5 hours for an initial zooplankton cloud with a medium standard deviation, moving with a low background flow speed (0.06 cm/s) and undergoing normal migration. Plotting symbols become lighter as time progresses.

residence times for slightly larger flows, it is simply a consequence of the limited duration of the simulations. While the analytical clump of zooplankton has not yet exited the embayment and thus has a residence time of all seven days, zooplankton high in the water column farthest downstream in the computational model exit the embayment even though other zooplankton starting farther down in the water column lag behind. At such low flow speeds, the model would have to run for considerably longer for all of the computational zooplankton to wash out of the channel. If these longer residence times for individual zooplankton were averaged with the residence times of less than seven days, a much longer average residence time would be obtained.

Figure 4.5 gives another way of looking at both sets of biological residence time results, computational and analytical, by plotting them against each other on the

same set of axes. Most of the results that do not fall close to the 45° line are residence times from initially large zooplankton clouds. The results to the left of the line correspond to simulations in which all of the computational zooplankton wash out of the embayment, while the analytical model retains some zooplankton due to the shearing effect mentioned previously. The results to the right of the line represent scenarios in which the limited simulation time is to blame for the discrepancy.

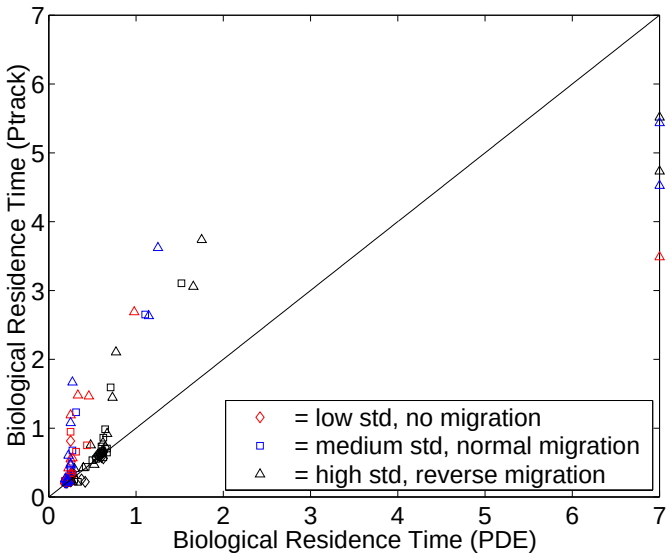

Figure 4.5: Plot of analytical biological residence time results using one zooplankter versus biological residence time results calculated using ptrack. Color denotes migration type while shape denotes size of initial zooplankton cloud standard deviation. Red = no migration, blue = normal migration, black = reverse migration. Diamond = low standard deviation, square = medium standard deviation, triangle = high standard deviation.

We performed Gaussian quadrature using seven nodes chosen assuming a normal distribution, with results shown in Figure 4.6 by standard deviation. While these analytical results sometimes overshoot and sometimes undershoot the true

results, they are much closer in general to the computational results than were the results when following only one zooplankter. The analytical results for non-migrating zooplankton are still not as close to the computational results for low flows as would be desirable, perhaps because these zooplankton stay at their initial starting heights (and therefore horizontal velocities) for the entire simulation and are therefore more sensitive to exactly which vertical locations are chosen as integration nodes. Because they do not migrate up and down in the water column, they are unable to take advantage of the averaging effects due to sampling a range of horizontal velocities in the water column. Figure 4.7 shows biological residence times computed using the analytical method versus using ptrack. Agreement between the two methods is clearly better here than for the simulations employing a z position function whose start and end locations are at the mean of the zooplankton cloud. As biological residence time increases, the points remain close to the line $y = x$, and the points in Figure 4.5 on the line $x = 7$ have moved much closer to their computational counterparts. Clearly, integrating over starting position in the z direction has largely done away with the problem of limited duration of the simulation, as well as shearing of zooplankton cloud by the flow field.

Figures 4.8, 4.9, and 4.10 show plots of the simple approximation to biological residence time, using distance travelled divided by mean horizontal zooplankton velocity, for all three zooplankton cloud sizes using Gaussian quadrature of degree 7, 14, and 30, respectively. Notice that as we are assuming equal day and night lengths, using this approximation gives equal values of biological residence time for normal and reverse migration. All three graphs show patterns similar to the analytical results, with reverse/normal migrators usually doing significantly better than the nonmigrators, and lower flow speeds allowing increased residence time

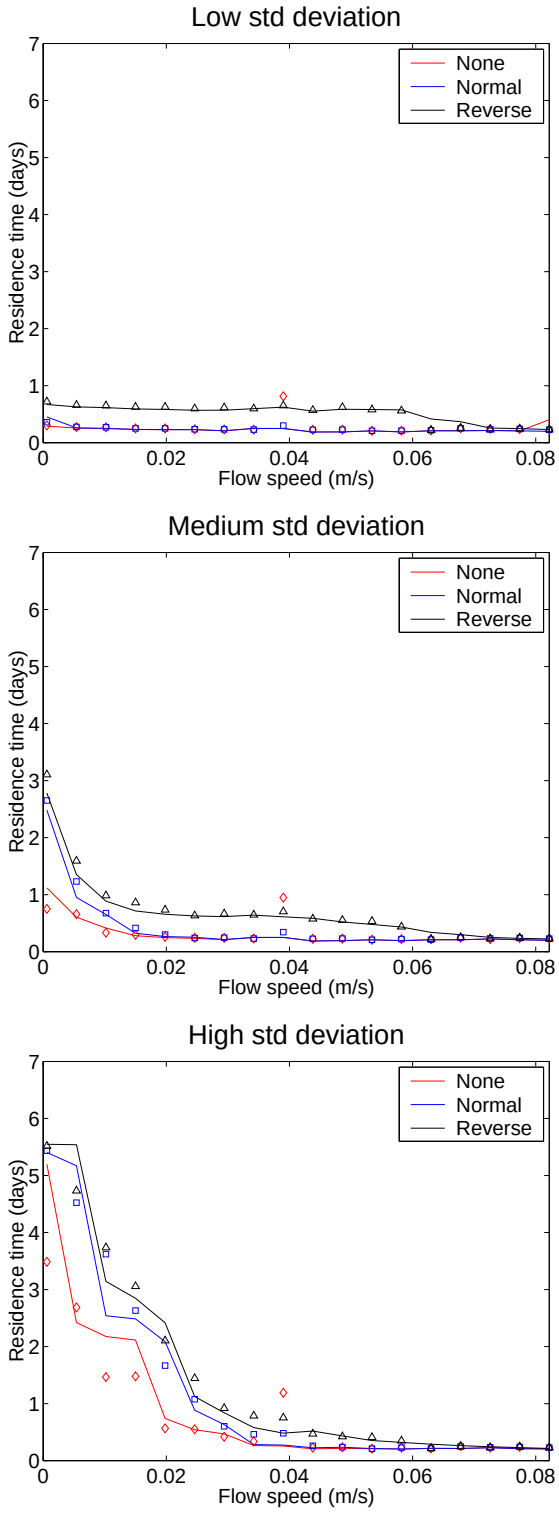

Figure 4.6: Flow speed versus residence time by zooplankton cloud standard deviation using Gaussian quadrature with seven nodes. Solid lines represent analytical results from the current study, while symbols represent computational results.

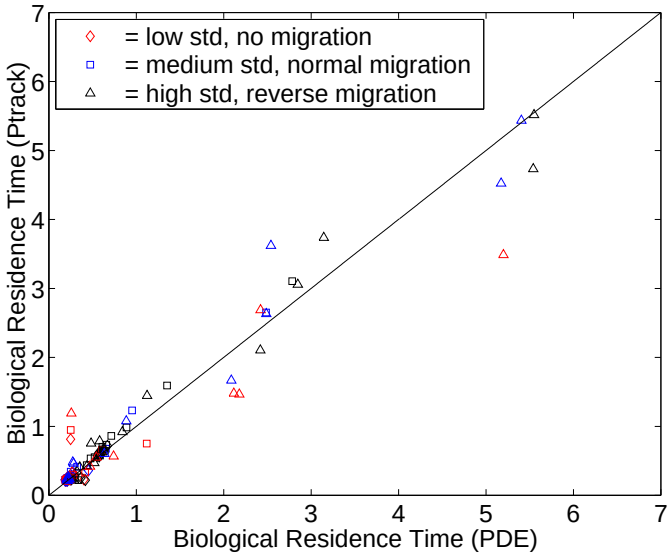

Figure 4.7: Plot of analytical biological residence time results using Gaussian quadrature of degree 7 assuming a normal distribution versus biological residence time results calculated using ptrack. Color denotes migration type while shape denotes size of initial zooplankton cloud standard deviation. Red = no migration, blue = normal migration, black = reverse migration. Diamond = low standard deviation, square = medium standard deviation, triangle = high standard deviation.

as the zooplankton cloud size increases. The approximate results again agree most closely with the computational results for the higher flow speeds and lower zooplankton cloud standard deviations. Figure 4.11 shows approximate versus computational results for all three Gaussian quadratures. Clearly, as the number of Gaussian nodes used increases, the results are closer to the computational results, although the improvement when using 30 versus 14 nodes is not significant. Additionally, Figure 4.12 plots the approximate versus analytical results when using seven Gaussian quadrature nodes, showing that the two methods give similar results, with the approximate method giving the same or a higher value for biological residence time, as expected.

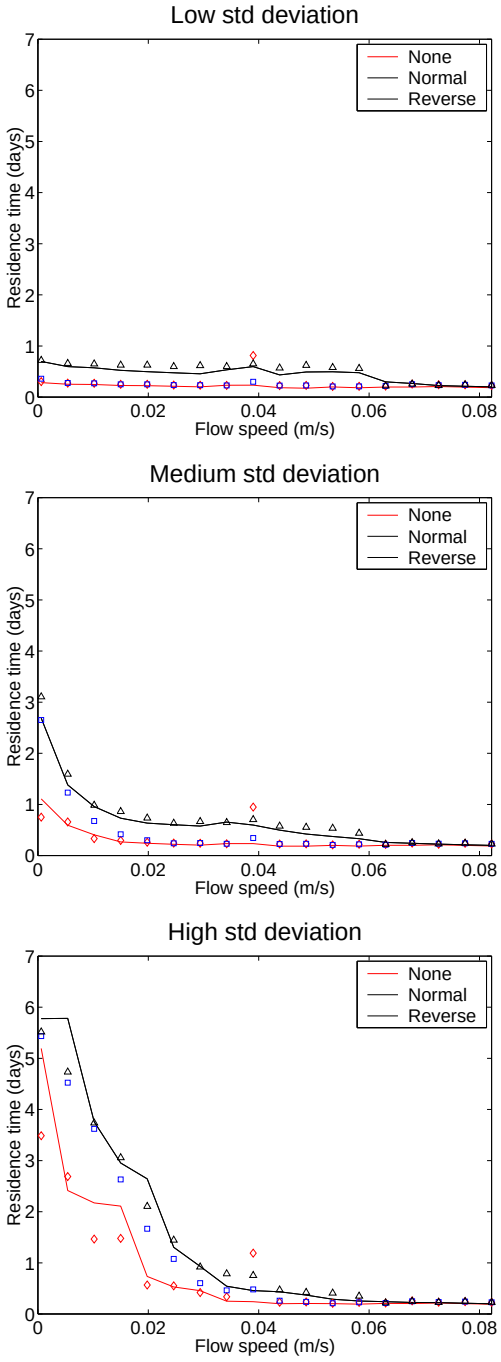

Figure 4.8: Flow speed versus residence time by zooplankton cloud standard deviation for Chapter 2 simulations (without macrophytes) compared with approximate results using Gaussian quadrature of degree 7. Solid lines represent approximate results from the current study, while symbols represent computational results.

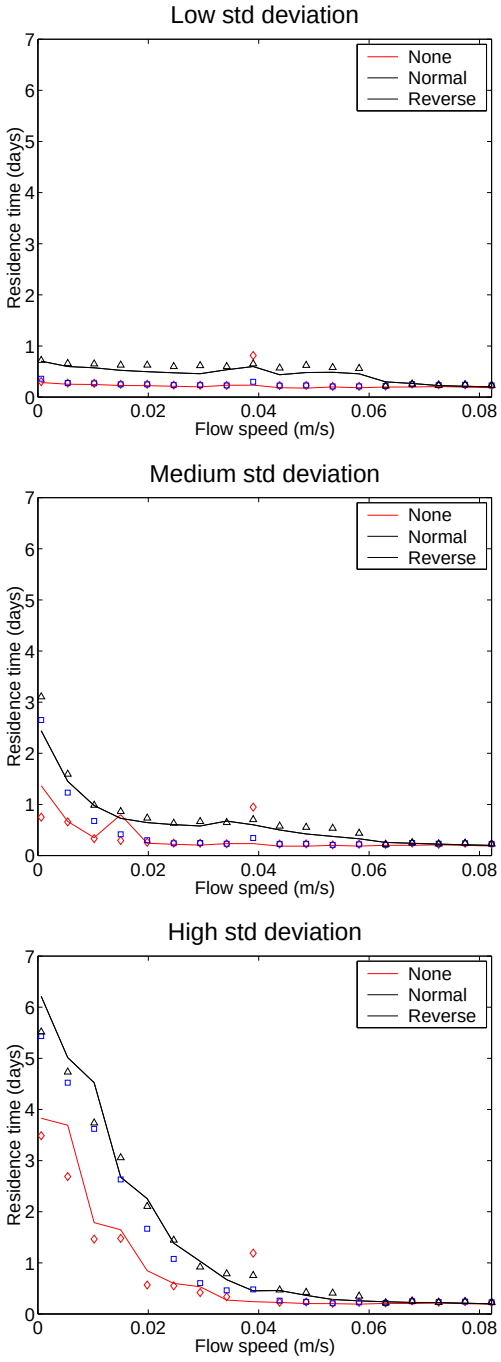

Figure 4.9: Flow speed versus residence time by zooplankton cloud standard deviation for Chapter 2 simulations (without macrophytes) compared with approximate results using Gaussian quadrature of degree 14. Solid lines represent approximate results from the current study, while symbols represent computational results.

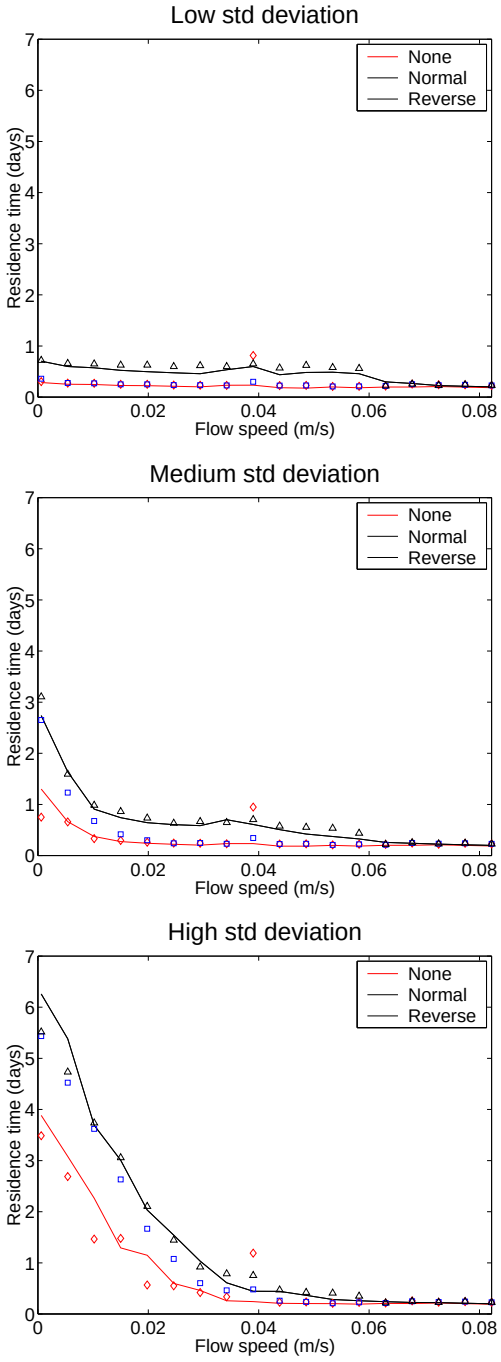

Figure 4.10: Flow speed versus residence time by zooplankton cloud standard deviation for Chapter 2 simulations (without macrophytes) compared with approximate results using Gaussian quadrature of degree 30. Solid lines represent approximate results from the current study, while symbols represent computational results.

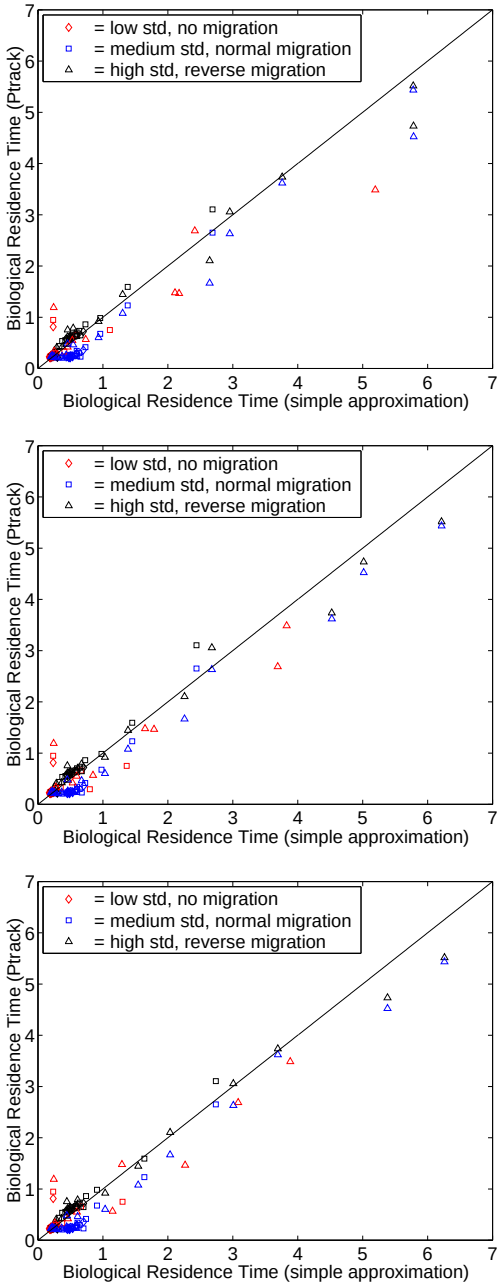

Figure 4.11: Plots of analytical biological residence time results using Gaussian quadrature of degree 7, 14, and 30, respectively, assuming a normal distribution versus biological residence time results calculated using ptrack. Color denotes migration type while shape denotes size of initial zooplankton cloud standard deviation. Red = no migration, blue = normal migration, black = reverse migration. Diamond = low standard deviation, square = medium standard deviation, triangle = high standard deviation.

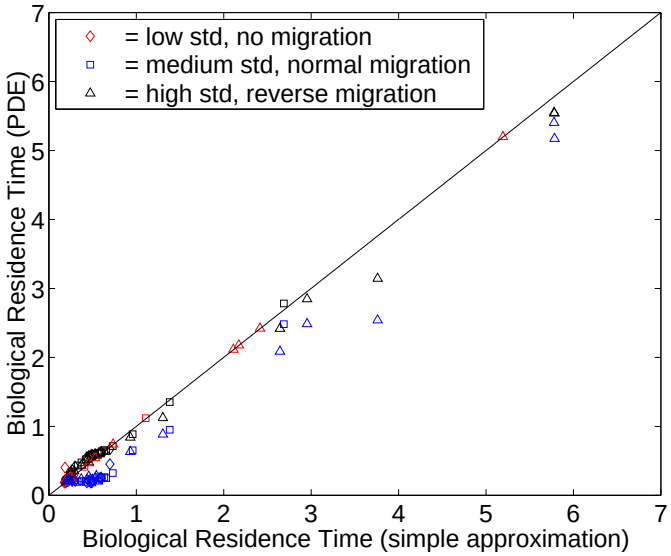

Figure 4.12: Plot of approximate biological residence time results versus analytical biological residence time results from the pde, both using Gaussian quadrature of degree 7 assuming a normal distribution. Color denotes migration type while shape denotes size of initial zooplankton cloud standard deviation. Red = no migration, blue = normal migration, black = reverse migration. Diamond = low standard deviation, square = medium standard deviation, triangle = high standard deviation.

The previous results using Gaussian quadrature have used z functions of the same height, and simply shifted them up or down in the water column, depending on the location of the Gaussian node. To insure that this practice did not bias our results, we performed one set of approximate simulations using 5 Gaussian quadrature nodes in which all combinations of nodes were utilized for the top and bottom positions of the z function. These computations were much more time-consuming than the previous analytical or approximate computations and did not result in improved estimates of biological residence time (see Figures 4.13, 4.14).

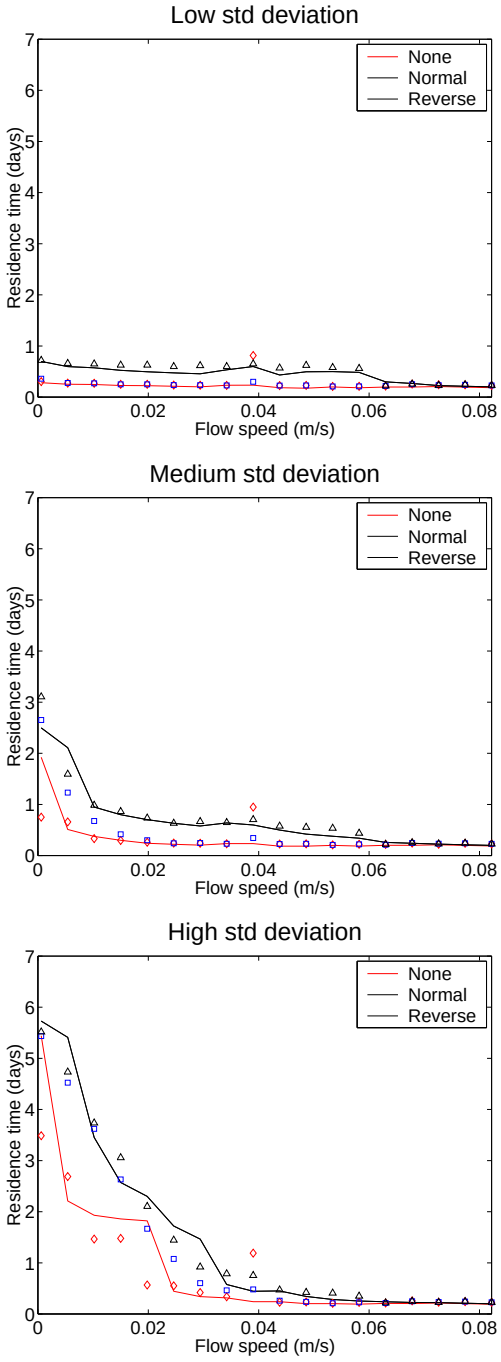

Figure 4.13: Flow speed versus residence time by zooplankton cloud standard deviation using the approximate method and extended Gaussian quadrature with 5 nodes. Solid lines represent approximate results from the current study, while symbols represent computational results.

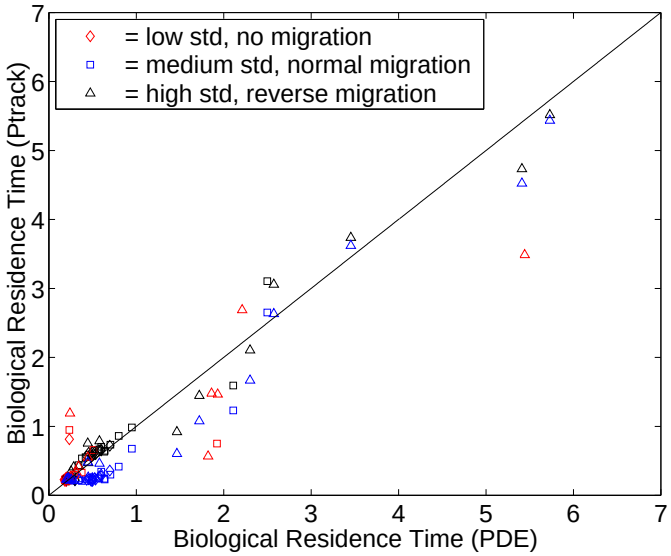

Figure 4.14: Plot of approximate biological residence time results using extended Gaussian quadrature of degree 5 assuming a normal distribution versus biological residence time results calculated using ptrack. Color denotes migration type while shape denotes size of initial zooplankton cloud standard deviation. Red = no migration, blue = normal migration, black = reverse migration. Diamond = low standard deviation, square = medium standard deviation, triangle = high standard deviation.

4.6.2 Simulations with Macrophytes

Chapter 3 used the same 18 background flows as in Chapter 2 and vegetation fills the entire embayment. Figure 4.15 plots, for one zooplankter, flow speed versus biological residence time for both the computational and analytical methods for the two different zooplankton cloud sizes. For the smaller zooplankton cloud size, again the computational and analytical biological residence times decrease as flow speed increases. In general, the computational and analytical results vary by a day or less, with the largest variation in either type of biological residence time found for

the low flow speeds. While normal migration sometimes yields the largest residence times, reverse migration keeps the zooplankton in the embayment the longest at the higher speeds. The no migration strategy still performs worst, especially for the first flow speed. In general, as flow speeds increase the flow becomes more uni-directional and thus homogeneous and the analytical model produces results that are closer to the computational results.

When zooplankton clouds are larger, we start to see some of the problems encountered before when macrophytes were absent; at low flow speeds, all of the migration types (even no migration) retain all of the zooplankton in the embayment for the entire seven days. Again, this effect is probably due to the fact that each point on the plot represents a single run using the zooplankton cloud means as vertical starting and stopping positions; we have not accounted for shear in the flow field, as well as possibly not running the simulations long enough for all of the original zooplankton in the computational study to have exited the embayment. While the analytical results always decrease with increasing flow speed, the computational results are not as monotonic, especially for the first four or five flow speeds, demonstrating the complexity of the flow field when macrophytes are present. At mid-to-higher flow speeds, the active migration types produce residence time results that are relatively (within a day) close to the computational results, with all results improving as flow speed increases and reverse migration again retaining the zooplankton for the longest. At intermediate flow speeds, no one migration scheme clearly outperforms the others. Clearly, for lower flow speeds, one analytical simulation does not give adequate results. Similar to the case without macrophytes, we used Gaussian quadrature assuming an underlying normal distribution in order to efficiently perform an integration of biological residence time results over position

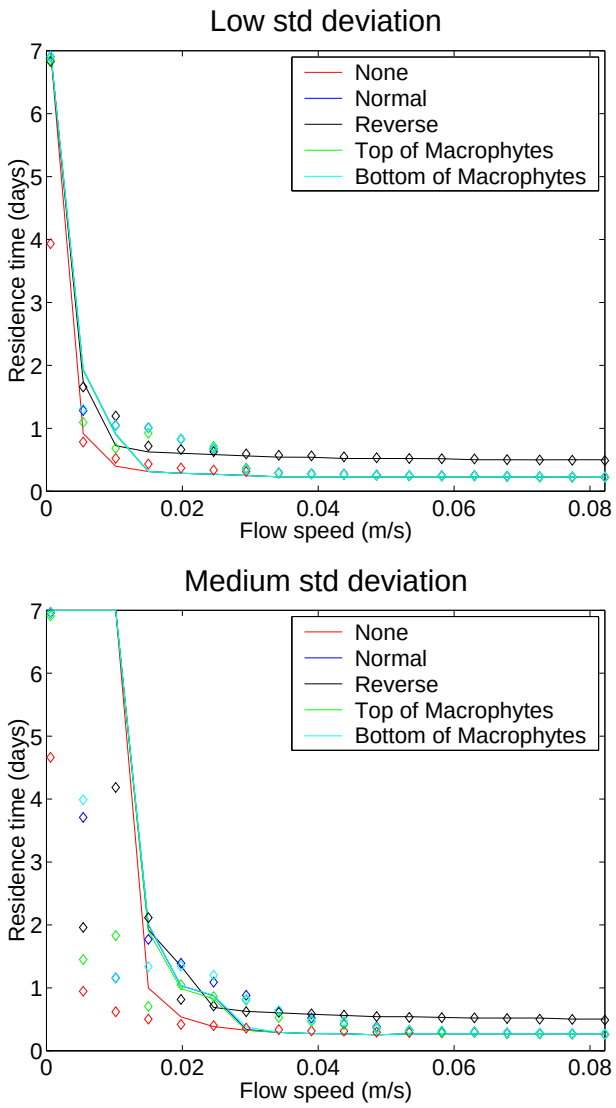

Figure 4.15: Flow speed versus residence time by zooplankton cloud standard deviation for an embayment filled with macrophytes. Solid lines represent analytical results from the current study, while symbols represent computational results.

with respect to z of the vertical position function. As we have no reason a priori to expect one set of quadrature points to give better results than another, we tried three different numbers of nodes (5, 7, and 9) that would all potentially provide a reasonably fast and simple way of approximating biological residence times. Results, shown in Figure 4.16 show that none of the Gaussian quadratures

provide an advantage over using just one point. While the averaging procedure has prevented the artificial analytical residence times of seven days seen earlier, the biological residence times for lower flow speeds are much too high almost without exception and migration type seems to make little difference. While the non-homogeneous horizontal velocity field (and perhaps an unlucky choice of nodes) is surely at least partly to blame, vertical velocities unaccounted for in the analytical model moving zooplankton to regions of faster downstream flow is probably a chief cause of the lower residence times seen when using the computational model (see Figure 4.17). This type of vertical velocity is often seen even in the case of a relatively simple macrophyte configuration when the downstream background flow meets exchange flow that has been forced up in the water column by the macrophytes below.

We also performed simulations using the simple distance/rate approximation to biological residence time and integrated the results using Gaussian quadrature with 5, 7, and 9 nodes (Figure 4.18). The results are quite similar to the analytical model results, with the exception of the 9 node case, in which none of the migration types perform as well for the lowest flow speeds in the case of the smaller zooplankton cloud; in the medium zooplankton cloud case, the results look remarkably similar to the results when using either 5 or 7 nodes. Still, as for the analytical model, the results when using the approximate model at lower flow speeds overestimate the biological residence time compared with the computational results to such a degree as to be useless.

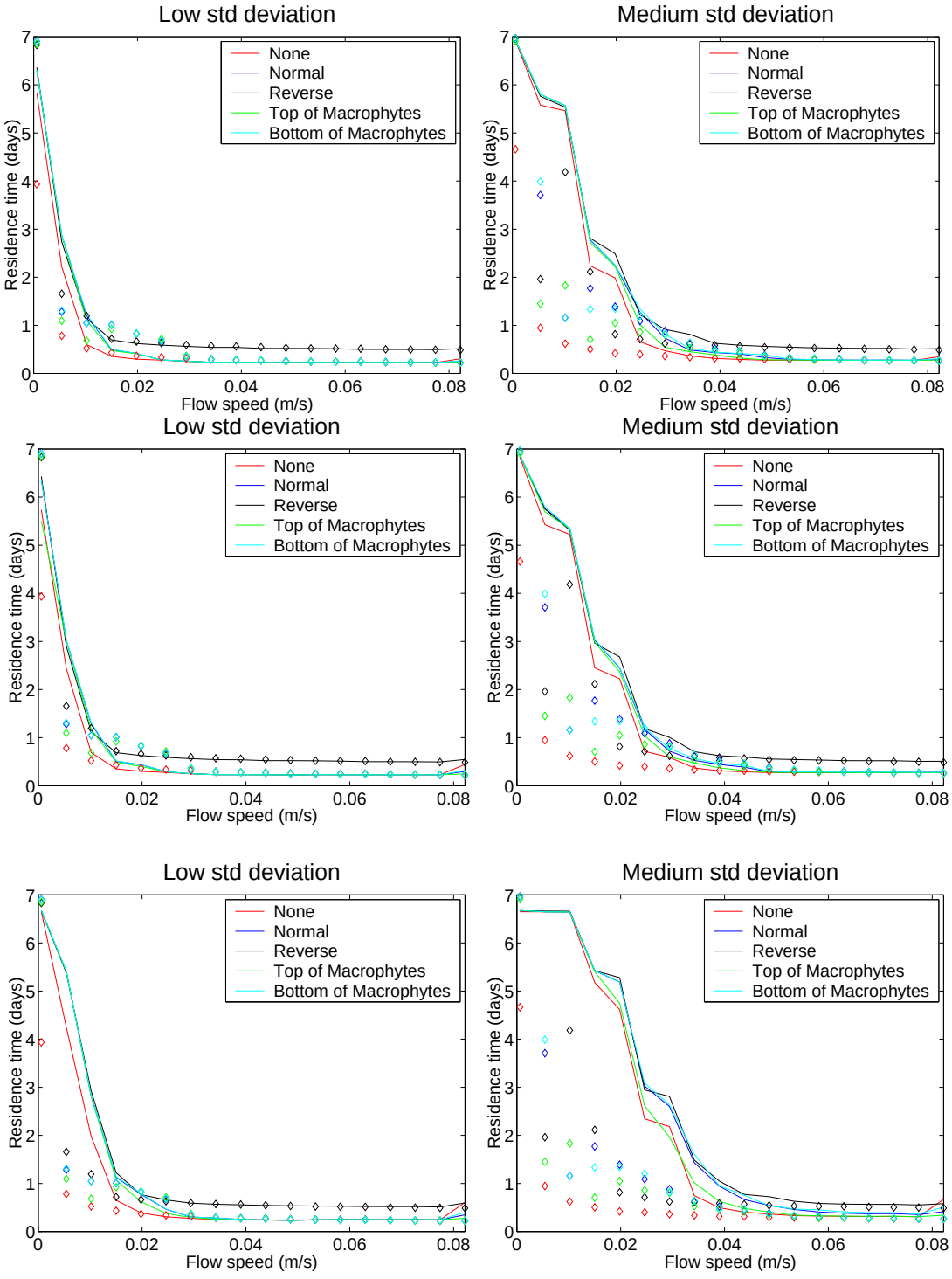

Figure 4.16: Flow speed versus residence time for low (left) and medium (right) zooplankton cloud standard deviations using 5 (top), 7 (middle), and 9 (bottom) Gaussian quadrature nodes. Solid lines represent analytical results from the current study, while symbols represent computational results.

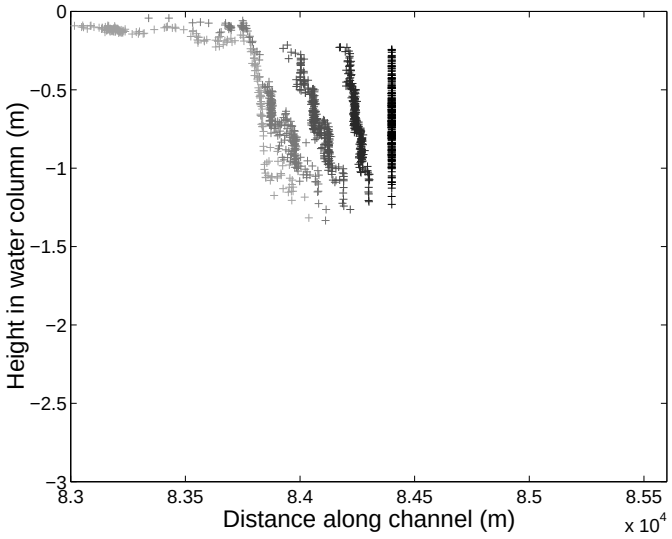

Figure 4.17: Output from ptrack showing zooplankton positions every 2.5 hours for an initial zooplankton cloud with a medium standard deviation, moving with a low background flow speed (0.54 cm/s) and not undergoing migration. Plotting symbols become lighter as time progresses.

4.7 Discussion

In the absence of vegetation, regardless of whether a simple (one node) analytical method, more complicated (Gaussian quadrature) analytical method, or very simple approximate method was used, some basic results from the earlier computational simulations still held. An inverse relationship between flow speed and biological residence time was seen, and reverse migrating zooplankton remained in the embayment longer than normally migrating zooplankton over the range of flow speeds studied, with non-migrating zooplankton always leaving the embayment first. When using a zooplankton cloud relatively small in diameter, the other parameters made very little difference, and the partial differential equation and simple approximation methods gave results very close to the computational

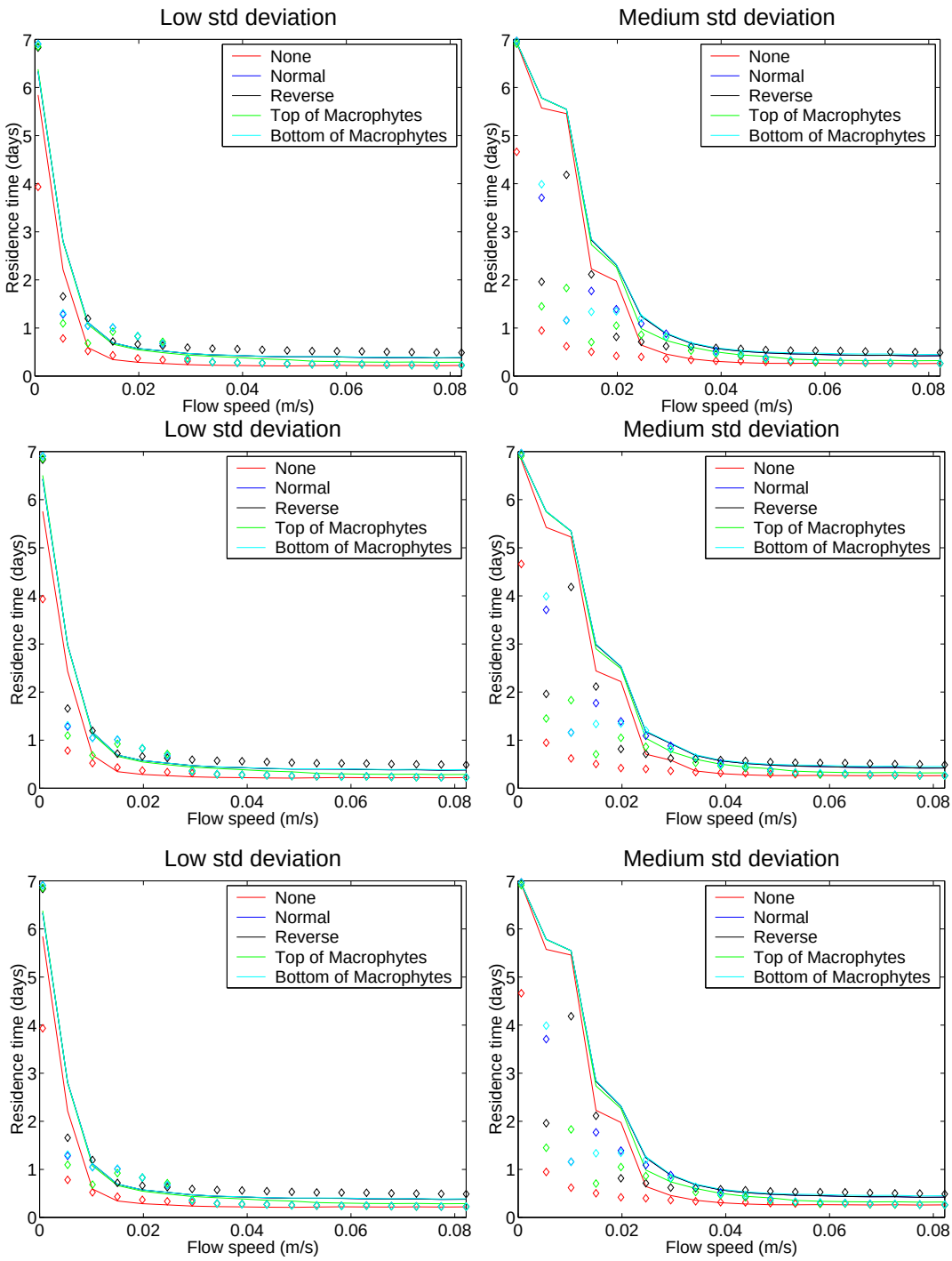

Figure 4.18: Flow speed versus residence time for low (left) and medium (right) zooplankton cloud standard deviations using 5 (top), 7 (middle), and 9 (bottom) Gaussian quadrature nodes. Solid lines represent approximate results from the current study, while symbols represent computational results.

results, even using just one simulation per parameter combination in the case of the pde. For zooplankton clouds larger in diameter, using Gaussian quadrature made an appreciable difference in biological residence time approximations for lower flow speeds. If exact results are not necessary, the analytical method provides a relatively quick, easy, and computationally inexpensive way to estimate biological residence times for any combination of zooplankton cloud size, flow speed, and migration type. As the number of zooplankton exiting the embayment at each time step does not need to be computed when using the simple approximation method, this method is considerably faster than using the pde and provides an essentially just as good, and arguably better, approximation to the true biological residence time.

However, the biological residence time results from the analytical or approximate model did not fare as well when macrophytes filled the channel. While the analytical and approximate results did not show a clear winner in terms of migration strategy, similar to the computational results, the actual magnitudes computed for biological residence time using the partial differential equation or simple approximation in the case of larger cloud standard deviation and lower flow speed were often different from the computational results by more than half the total simulation time. Using quadrature to attempt to negate the effect of differing horizontal velocities with depth and relatively short simulation length, while making the results closer to their computational counterparts, did not give residence times close enough to be an adequate substitute for actually performing the computational simulations using ptrack. Simplifications involved in producing a reasonably simple partial differential equation, and certainly involved in the simple approximation, include exclusions of particular relevance to simulations involving

macrophyte patches, such as not taking into account how the flow changes in the x direction or over time, as well as not taking into account vertical advection. While performing both the computational and analytical and/or approximate simulations for longer periods of time may help in producing closer biological residence time results, these simplifications do not suggest that significantly better results can be obtained by running longer simulations in general.

Thus, for flow regimes largely homogeneous in the horizontal with negligible vertical advection, a simple approximation and/or partial differential equation can be used to study questions of basic biological residence time, as well as related questions involving population growth, speed of spread, and critical domain size. A modified and/or more complicated equation incorporating temporally and spatially variable flow could be investigated to more adequately deal with zooplankton residence time in the presence of rooted vegetation. More generally, studying and applying the results of these kinds of simple models should make it easier to study these types of habitats and avoid unwittingly changing the dynamics of the zooplankton, which are basic to the health of the embayment/lake system, or zooplanktonic life stages of other organisms which require the embayment environment to survive past that stage.

Bibliography

[1] B. R. Anholt. Density dependence resolves the stream drift paradox. *Ecology*, 76:2235–2239, 1995.

[2] Y-H. Chen, P-T. Shaw, and T. G. Wolcott. Enhancing estuarine retention of planktonic larvae by tidal currents. *Estuarine, Coastal and Shelf Science*, 45:525–533, 1997.

[3] S. Humphries and G. D. Ruxton. Is there really a drift paradox? *J. Anim. Ecol.*, 71:151–154, 2002.

[4] J. Lancaster. Geometric scaling of microhabitat patches and their efficacy as refugia during disturbance. *J. Anim. Ecol.*, 63:442–457, 2000.

[5] J. Lancaster and A. G. Hildrew. Characterising instream flow refugia. *Can. J. Fish. Aquat. Sci.*, 50:1663–1675, 1993.

[6] J. Lancaster and A. G. Hildrew. Flow refugia and the microdistribution of lotic macroinvertebrates. *Journal of the North American Benthological Society*, 12:285–393, 1993.

[7] F. Lutscher, E. Pachepsky, and M. A. Lewis. The effect of dispersal patterns on stream populations. *SIAM J. Appl. Math.*, 65(4):1305–1327, 2005.

[8] J. G. March, J. P. Benstead, C. M. Pringle, and F. N. Scatena. Migratory drift of larval freshwater shrimps in two tropical streams, Puerto Rico. *Freshwater Biology*, 40:261–273, 1998.

[9] J. E. Morris and C. C. Mischke. Plankton management for fish culture ponds. Technical Report 114, Iowa State University Agricultural Experiment Station, 1999. In cooperation with USDA's Cooperative State Research, Education and Extension Service.

[10] K. Mueller. Investigations on the organic drift in north Swedish streams. Technical Report 34, Institute of Freshwater Research, Drottningholm, Sweden, 1954.

[11] K. Mueller. The colonization cycle of freshwater insects. *Oecologica*, 53:202–207, 1982.

[12] F. Luckey on behalf of the Lake Ontario Lakewide Management Plan. Ecosystem indicators for lake ontario. *Clearwaters*, 32(1), Spring 2002.

[13] E. Pachepsky, F. Lutscher, R. M. Nisbet, and M. A. Lewis. Persistence, spread and the drift paradox. *Theor. Pop. Biol.*, 67:61–73, 2005.

[14] W. Reckendorfer, H. Keckeis, G. Winkler, and F. Schiemer. Zooplankton abundance in the river Danube, Austria: the significance of inshore retention. *Freshwater Biol.*, 41:583–591, 1999.

[15] L. L. Rempel, J. S. Richardson, and M. C. Healey. Flow refugia for benthic macroinvertebrates during flooding of a large river. *Journal of the North American Benthological Society*, 18:24–48, 1999.

[16] C. S. Reynolds, P. A. Carling, and K. Beven. Flow in river channel: new insights into hydraulic retention. *Archiv fur Hydrobiologie*, 121:171–179, 1991.

[17] A. L. Robertson, J. Lancaster, and A. G. Hildrew. Stream hydraulics and the distribution of microcrustacea: A role for refugia? *Freshwater BIol.*, 33:469–484, 1995.

[18] F. J. Rueda. *A three-dimensional hydrodynamic and transport model for lake environments*. PhD thesis, University of California, Davis, 2001.

[19] P. E. Smith. *A three-dimensional, finite-difference model for estuarine circulation*. PhD thesis, University of California, Davis, 1997.

[20] D. C. Speirs and W. S. C. Gurney. Population persistence in rivers and estuaries. *Ecology*, 82(5):1219–1237, 2001.

[21] R. Waters. The drift of stream insects. *Ann. Rev. Entomol.*, 17:253–272, 1972.

[22] J. H. Winterbottom, S. E. Orton, and A. G. Hildrew. Field experiments on the mobility of benthic invertebrates in a southern English stream. *Freshwater Biol.*, 38:37–47, 1997.

[23] J. H. Winterbottom, S. E. Orton, A. G. Hildrew, and J. Lancaster. Field experiments on flow refugia in streams. *Freshwater BIol.*, 37:569–580, 1997.